Description of document: **AD-B069354 (AFWL·TR·81·223) Summary of Trapped Electron Data, Final Report, October 1982**

Requested date: 12-August-2008

Released date: 05-November-2008

Posted date: 24-December-2008

Source of document: 377 MSG/SCBIF (FOIA Manager)
1952 First Street
Kirtland AFB, NM 87117-5666.
Email foia.kirtland@kirtland.af.mil

Note: The 377th Mission Support Group (388 MSG) is the FOIA processing activity for Kirtland AFB including for records of the Air Force Weapons Laboratory (AFWL)

FREEDOM OF INFORMATION ACT *(FOIA)* RESPONSE AND INVOICE

REQUEST DATE	REQUEST NUMBER
20080812	

TO	FROM
	377 MSG/SCBF (FOIA Analyst) 2051 Wyoming Blvd., S.E. Kirtland AFB NM 87117-5607

1. REQUESTED RECORDS

- [X] COMPLETELY RELEASED
- [ ] PARTIALLY RELEASABLE
- [X] DOCUMENTS ARE ATTACHED
- [ ] DOCUMENTS WILL BE FORWARDED ON RECEIPT OF PAYMENT
- [ ] DOCUMENTS MAY BE VIEWED AT THIS LOCATION *(Please call for an appointment)*
- [ ] TIME EXTENSION IS REQUIRED BECAUSE
- [ ] ALL OR PART OF THE REQUESTED RECORDS ARE NOT AT THIS LOCATION
- [ ] VOLUMINOUS RECORDS MUST BE COLLECTED AND REVIEWED
- [ ] RECORDS ARE BEING REVIEWED BY ANOTHER AGENCY FOR POSSIBLE RELEASE
- [ ] WE HOPE TO PROVIDE A FINAL DECISION BY

2. THE COSTS OF PROVIDING THESE DOCUMENTS ARE INDICATED BELOW

REQUEST ACTIONS	RATE	MATERIAL	TIME	COST
SEARCH *(Hourly)*				
REVIEW *(Hourly)*				
COPY *(Page)*				
COMPUTER MACHINE TIME *(Hourly)*				
COMPUTER OPERATOR TIME *(Hourly)*				
COMPUTER TAPES				
OTHER				
			TOTAL AMOUNT DUE	

3.Send your check or money order payable to "US DEPARTMENT OF TREASURY " with a copy of this invoice within 30 days. *(Future requests will not be processed until payment is received.)*	3A. MAIL TC

4. THIS ACKNOWLEDGES RECEIPT OF YOUR CHECK OR MONEY ORDER FOR PAYMENT OF REQUESTED DOCUMENTS

NUMBER	DATE	AMOUNT

5. ALL OR PART OF THE INFORMATION YOU REQUESTED IS NOT AVAILABLE AT THIS INSTALLATION. WE HAVE FORWARDED YOUR REQUEST TO THE FOLLOWING LOCATION FOR ACTION WITH DIRECT RESPONSE TO YOU.

6. COMMENTS

This is in response to your 12 August 2008, Freedom of Information Act (FOIA) request for AD-B069354 - Summary of Trapped Electron Data. The cost is waived.

7. FREEDOM OF INFORMATION ACT MANAGER

NAME AND PHONE	SIGNATURE	DATE
MARVIN L. EVANS (505) 846-7717	Marvin L. Evans	5 Nov 08

AFMC FORM 556, 19950201 *(IMT-V1)* **REPLACES AFMC 556, JUL 92 WHICH IS OBSOLETE**

Summary of Trapped Electron Data

MCDONNELL DOUGLAS ASTRONAUTICS CO HUNTINGTON BEACH CA

OCT 1982

Encl 2

UNCLASSIFIED / LIMITED

AFWL-TR-81-223

AFWL-TR-81-223

AD B069354

SUMMARY OF TRAPPED ELECTRON DATA

K. A. Pfitzer

McDonnell Douglas Corporation
5301 Bolsa Avenue
Huntington Beach, CA 92647

October 1982

Final Report

Distribution limited to US Government agencies only; test and evaluation ~~of military systems/equipment are discussed in the report~~; Oct 82. Other requests for this document must be referred to AFWL (NTY), Kirtland AFB, NM 87117.

SUBJECT TO EXPORT CONTROL LAWS: This document contains information for manufacturing or using munitions of war. Exporting this information or releasing it to foreign nationals living in the United States without first obtaining an export license violates the International Traffic in Arms Regulations. Under 22 USC 2778, such a violation is punishable by up to 2 years in prison and by a fine of $100,000.

AIR FORCE WEAPONS LABORATORY
Air Force Systems Command
Kirtland Air Force Base, NM 87117

The following notice applies to any unclassified (including originally classified and now declassified) technical reports released to "qualified U.S. contractors" under the provisions of DoD Directive 5230.25, Withholding of Unclassified Technical Data From Public Disclosure.

NOTICE TO ACCOMPANY THE DISSEMINATION OF EXPORT-CONTROLLED TECHNICAL DATA

1. Export of information contained herein, which includes, in some circumstances, release to foreign nationals within the United States, without first obtaining approval or license from the Department of State for items controlled by the International Traffic in Arms Regulations (ITAR), or the Department of Commerce for items controlled by the Export Administration Regulations (EAR), may constitute a violation of law.

2. Under 22 U.S.C. 2778 the penalty for unlawful export of items or information controlled under the ITAR is up to ten years imprisonment, or a fine of $1,000,000, or both. Under 50 U.S.C., Appendix 2410, the penalty for unlawful export of items or information controlled under the EAR is a fine of up to $1,000,000, or five times the value of the exports, whichever is greater; or for an individual, imprisonment of up to 10 years, or a fine of up to $250,000, or both.

3. In accordance with your certification that establishes you as a "qualified U.S. Contractor", unauthorized dissemination of this information is prohibited and may result in disqualification as a qualified U.S. contractor, and may be considered in determining your eligibility for future contracts with the Department of Defense.

4. The U.S. Government assumes no liability for direct patent infringement, or contributory patent infringement or misuse of technical data.

5. The U.S. Government does not warrant the adequacy, accuracy, currency, or completeness of the technical data.

6. The U.S. Government assumes no liability for loss, damage, or injury resulting from manufacture or use for any purpose of any product, article, system, or material involving reliance upon any or all technical data furnished in response to the request for technical data.

7. If the technical data furnished by the Government will be used for commercial manufacturing or other profit potential, a license for such use may be necessary. Any payments made in support of the request for data do not include or involve any license rights.

8. A copy of this notice shall be provided with any partial or complete reproduction of these data that are provided to qualified U.S. contractors.

DESTRUCTION NOTICE

For classified documents, follow the procedure in DoD 5220.22-M, National Industrial Security Program, Operating Manual, Chapter 5, Section 7, or DoD 5200.1-R, Information Security Program Regulation, Chapter 6, Section 7. For unclassified, limited documents, destroy by any method that will prevent disclosure of contents or reconstruction of the document.

This final report was prepared by McDonnell Douglas Corporation, Huntington Beach, California, under Contract F29601-78-C-0015, Job Order 88091902, with the Air Force Weapons Laboratory, Kirtland Air Force Base, New Mexico. Capt Robert J. Greaves (NTY) was the Laboratory Project Officer-in-Charge.

This technical report has been reviewed and is approved for publication.

Robert J. Greaves

ROBERT J. GREAVES
Captain, USAF
Project Officer

FOR THE COMMANDER

Marion F. Schneider

MARION F. SCHNEIDER
Lt Colonel, USAF
Chief, Satellite and C³ Branch

Norman K. Blocker

NORMAN K. BLOCKER
Colonel, USAF
Chief, Applied Physics Division

UNCLASSIFIED

SECURITY CLASSIFICATION OF THIS PAGE (When Data Entered)

REPORT DOCUMENTATION PAGE

READ INSTRUCTIONS BEFORE COMPLETING FORM

1. REPORT NUMBER: AFWL-TR-81-223
2. GOVT ACCESSION NO.: AD-B069354L
3. RECIPIENT'S CATALOG NUMBER:
4. TITLE (and Subtitle): SUMMARY OF TRAPPED ELECTRON DATA
5. TYPE OF REPORT & PERIOD COVERED: Final Report
6. PERFORMING ORG. REPORT NUMBER:
7. AUTHOR(s): K. A. Pfitzer
8. CONTRACT OR GRANT NUMBER(s): F29601-78-C-0015
9. PERFORMING ORGANIZATION NAME AND ADDRESS: McDonnell Douglas Corporation, 5301 Bolsa Avenue, Huntington Beach, California 92647
10. PROGRAM ELEMENT, PROJECT, TASK AREA & WORK UNIT NUMBERS: 62601F/88091902
11. CONTROLLING OFFICE NAME AND ADDRESS: Air Force Weapons Laboratory (NTY), Kirtland Air Force Base, New Mexico 87117
12. REPORT DATE: October 1982
13. NUMBER OF PAGES: 204
14. MONITORING AGENCY NAME & ADDRESS (if different from Controlling Office):
15. SECURITY CLASS. (of this report): UNCLASSIFIED

15a. DECLASSIFICATION/DOWNGRADING SCHEDULE:

16. DISTRIBUTION STATEMENT (of this Report)

Distribution limited to US Government agencies only; test and evaluation ~~of military systems/equipment are discussed in the report~~; Oct 82. Other requests for this document must be referred to AFWL (NTY), Kirtland AFB, NM 87117.

17. DISTRIBUTION STATEMENT (of the abstract entered in Block 20, if different from Report)

18. SUPPLEMENTARY NOTES

19. KEY WORDS (Continue on reverse side if necessary and identify by block number)

Argus	Radiation Belts
Teak	Nuclear Environment
Orange	Electron Injection
Starfish	Electron Environment
Russian	

20. ABSTRACT (Continue on reverse side if necessary and identify by block number)

This report summarizes the analysis of artificially injected electron data. Data from Teak, Orange, Argus, and Starfish are included. The calibrations of various satellite detectors are reviewed and in some cases modified, and the detectors from the various satellites are compared. Error analyses are performed and the accuracy of the various satellite experiments is discussed.

TABLE OF CONTENTS

SECTION PAGE

LIST OF FIGURES

LIST OF FIGURES

(continued)

LIST OF FIGURES

(continued)

LIST OF FIGURES

(continued)

LIST OF FIGURES

(continued)

LIST OF TABLES

Section 1

INTRODUCTION

The objective of this analysis was to assemble a data base for artificially trapped radiation. The effort was directed toward producing a computer oriented data base complete with error estimates. The data base was to cover data containing information on artificially injected electrons from the nuclear events, Starfish, Teak, Orange, Argus I, II, III, and Russian I, II, III. If possible, the data were to be presented as the number of electrons/cm^2/sec greater than a given energy as a function of time and B and L space.

The requirement that the data be put into isotropic integral spectral form as a function of position and time was soon found to be inconsistent with the published data sets. For example, the published data for Explorer IV for the Argus events showed only an isolated case of flux versus position as the satellite crossed through the Argus shells. Most of the data had only the amplitude of the Argus shell peak as a function of time. For many of the other satellites the published data were presented in terms of total fission electrons. In very few cases were time, B and L available as required.

Thus a redirection of the effort from the analysis of published documents to an analysis of data from experimenter data tapes was begun early in the program. Prior to this effort the principal investigator had successfully worked with several data sets obtained from the National Space Sciences Data Center (NSSDC). This work was in connection with data from more recent satellites. The use of the more recent NSSDC tapes was quite favorable and straightforward. The use of the much older NSSDC tapes for this effort proved to be a difficult task. Documentation of the old data sets was often completely inadequate and so much time had passed that very few of the principal investigators were able to help in decoding the tapes.

The Explorer IV Argus data set is a classic case of some of the frustrations experienced in this program. The Explorer IV tape analysis algorithms were developed for the Teak and Orange bursts because the Explorer data for Teak and Orange were well documented in several theses. The analysis of the data tapes for Teak and Orange proved to be extremely useful. At the completion of the Teak and Orange effort an easy Argus effort was expected. However, it was found that the entire Argus I, II and III time period was missing from the NSSDC tapes. During a call to Dr. James Vette at NSSDC it was suggested that since Argus interferred with the analysis of natural radiation environment, the NSSDC had probably removed the Argus data from the tapes. Dr. Vette said he knew of several additional tapes that should contain the entire data set. These were obtained after some delay. The tapes had a different format and a new computer program had to be written. The best of these tapes contained data during the Argus I, II, III time period; however, every single Argus crossing was missing. At this point a visit was made to Dr. Carl McIlwain at the University of California at San Diego (UCSD). He remembered that the Argus data were initially classified and thus was not submitted to the NSSDC. He retrieved three different data tapes from the UCSD archive storage. These tapes had Explorer IV data in various forms. These were brought to MDAC for analysis. All three data sets were dumped to the printer and portions hand decoded. None had any Argus data. Additional calls to various people produced no Explorer IV Argus data. It was finally decided that the Argus data simply did not exist. Well over a year later the Air Force Weapons Laboratory (AFWL) was able to produce a number of additional classified documents concerning the various nuclear bursts. Among these was a confidential document containing hundreds of confidential plots of Argus Explorer IV data. A security review determined that the document had been downgraded and was no longer classified. Thus after many false starts and wasted manhours, the Argus data were finally available.

The analysis of so many different computer tapes of various formats required an extensive programming effort. A large number of programs had to be written. Some of the tapes were written in packed format, and assembly

The remainder of this report is organized on a satellite by satellite basis. The key to the analysis was the understanding of the instrument, its calibration and the ability to read the NSSDC data tapes. Section 10.0 addresses the intercalibration of the various instruments.

Section 2

THE JASON PROGRAM

The Jason program consisted of nineteen solid propellant rockets launched from a number of launch sites. For this effort, the study of the Argus nuclear explosions, only five rockets launched from Wallops Island were usable.

The Jason data and instrumentation are very wel. described in the report "Analysis of Jason Data" (Reference 1). This report is one of the most complete and useful documents encountered in our entire study. The report contains all pertinent experiment and data information. The document was complete and the other documents were found to be a subset of it. A brief description of the experiment is presented in Section 2.1. This description is reproduced from Reference

2.1 Experiment Description

"The radiation-detection instruments consisted of eight Geiger tubes with various absorbers and collimators. A diagram of the instrumentation package is shown in Figure 2-1. The detectors in Channels 1, 5, 7, 3, and 6 are referred to as the long detectors. Each of these detectors utilized the same type of Geiger tube, an Anton 106-C. Of these, only the detectors in Channels 1 and 5 were rather highly collimated. The detectors in Channels 2, 8 and 4 are referred to as the short detectors. These also utilized a single Geiger tube type, but it was an end-window Anton 222R. All of the 222R detectors were highly collimated. The absorbers were selected such that the detectors in Channels 7 and 8 had thresholds at about 440 keV; the detectors in 3 and 4 had threshold energies of about 1 MeV, and the detector in Channel 6 was alone with a threshold energy of 4.3 MeV.

---

1. Analysis of Jason Data, AFSWC-TR-61-82, Air Force Special Weapons Center, Kirtland AFB, NM, October 1961. (AD 268400)

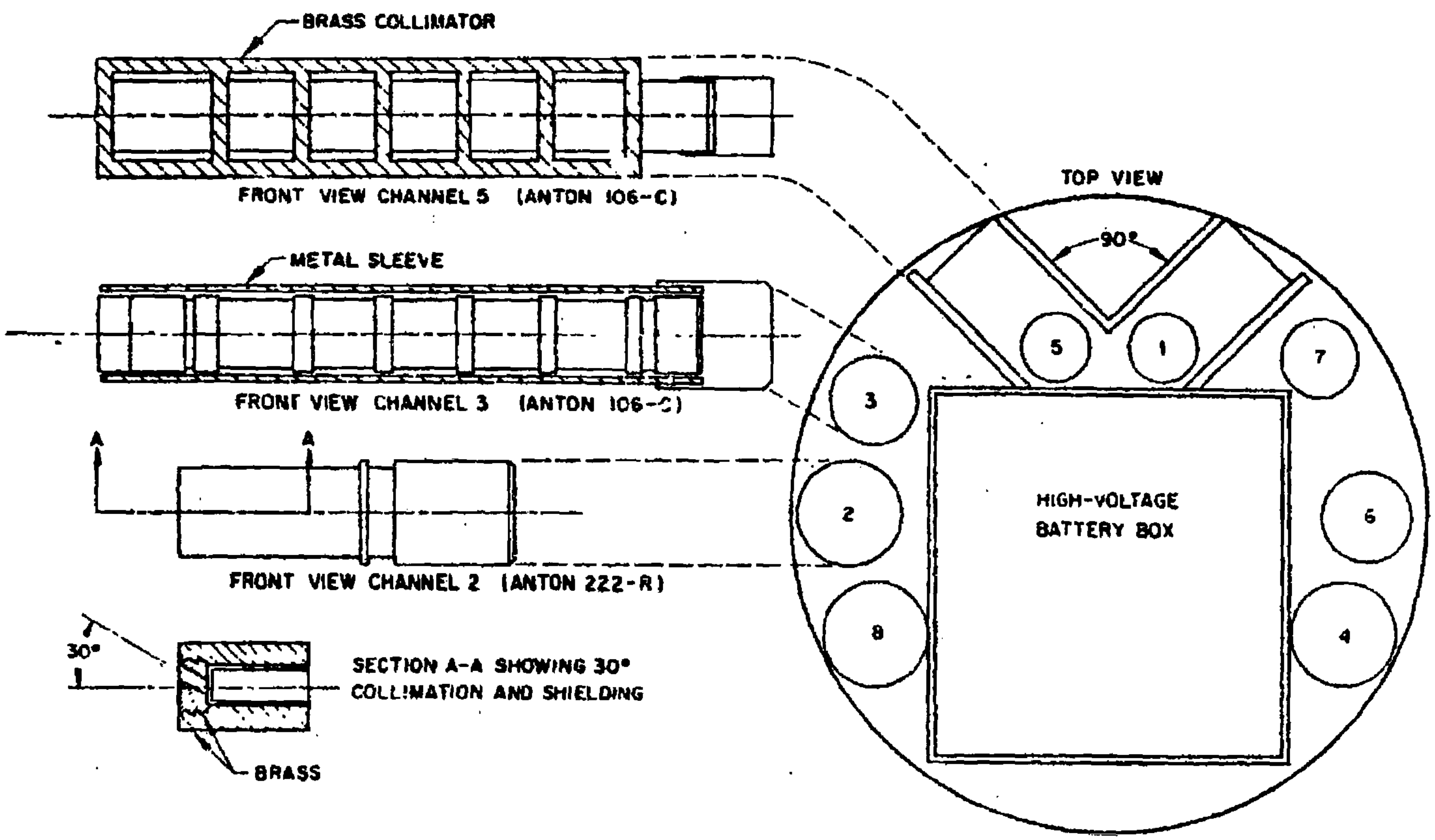

Figure 2-1. Diagram of the Jason Instrument Package (from Reference 1)

The output pulses of the Geiger tubes were sequentially sampled for a time duration of about 1/75 sec with a multi-segment commutator, and the pulses were transmitted directly to ground stations. In the telemetry records, regularly spaced synchronization pulses appeared, followed by pedestal-shaped signals, each of which corresponded to a sampling of the output of a particular detector. The Geiger tube pulses appeared at the top of the pedestals. For each Channel, the counts per pedestal were determined visually by personnel of the Air Force Special Weapons Center and recorded as a function of time.

These data, together with the trajectories of the rockets and the telemetry signal strength records received by the six ground stations of the Air Force Missile Test Center range, were used in this study.

2.2 Instrumentation Calibration

The entire data analysis effort was quite straightforward. All calibration and data information was contained in the Lockheed Jason report. The Jason instruments were well calibrated and the results are believed to be quite accurate. The entire Jason payload was placed in a fixture and electrons of various discrete energies were used to test the response of the detectors to the electron beam. The payload was rotated through all possible angles and ultimately an effective isotropic geometry factor was derived which can be used to evaluate the flux levels. The details of the analysis of this rather tedious, but well-done, calibration will not be repeated here. Figure 2-2 summarizes the geometry factors of all of the Jason Channels. These curves were obtained from the published tables in Reference 1 (see Table 2-1).

One thus has an energy dependent geometry factor. This data analysis effort required finding the flux, F, greater than a certain energy, E_i.

The electron flux/cm^2/sec greater than a specified energy can be written as

$$F\ (E > E_i) = \int_{E_i}^{\infty} f(E)\,dE \qquad (1)$$

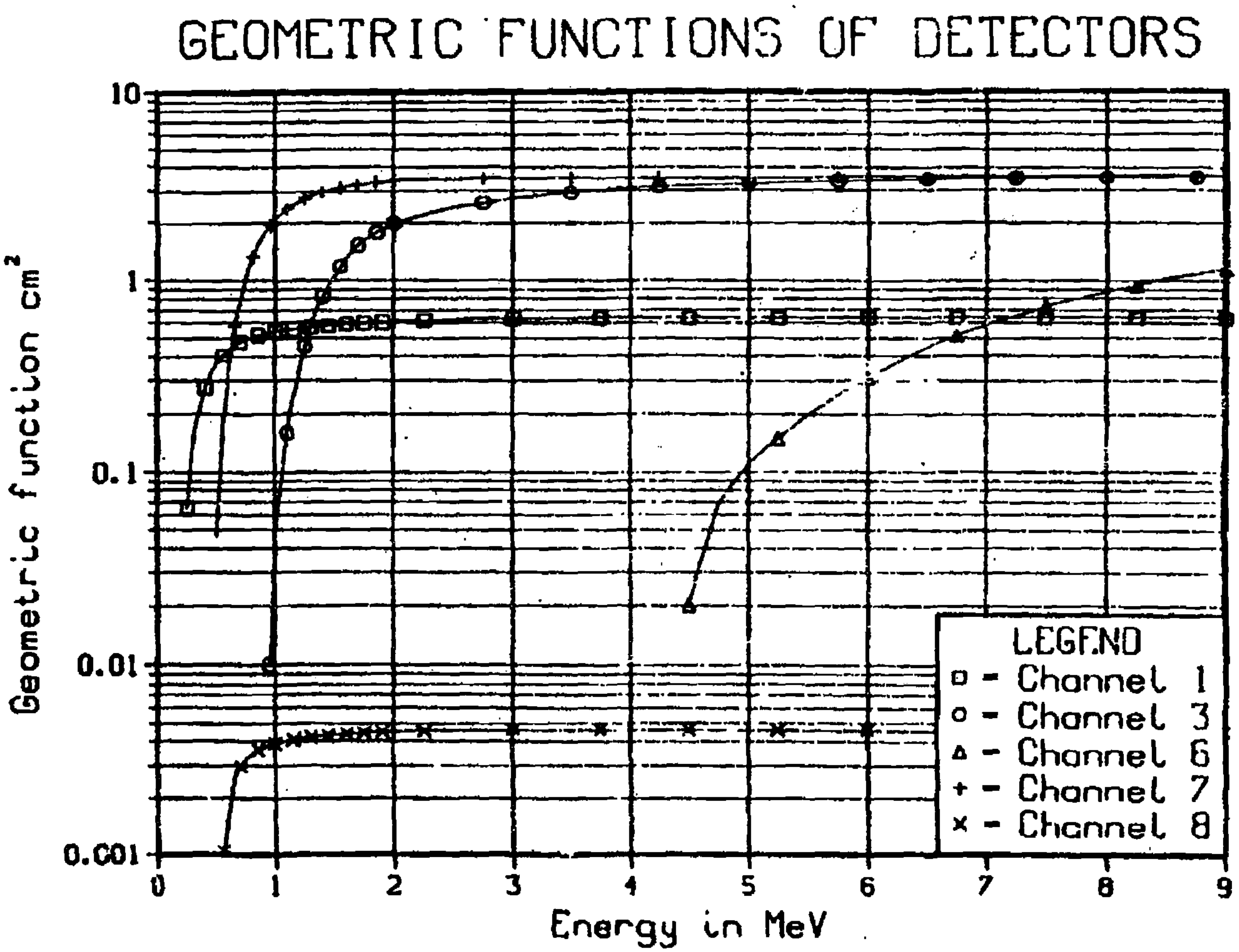

Figure 2-2. Geometric Functions of the Jason Detectors

Table 2-1

GEOMETRIC FACTORS IN cm^2

Electron Energy (MeV)	G1	G7	G3	G6	G2	G8	G4
0.15	0	0	0	0	0	0	0
0.2	0	0	0	0	0.001	0	0
0.25	0.0652	0	0	0	0.00232	0	0
0.3	0.151	0	0	0	0.0028	0	0
0.35	0.212	0	0	0	0.00309	0	0
0.4	0.275	0	0	0	0.00326	0	0
0.450	0.330	0	0	0	0.00341	0	0
0.5	0.374	0.05	0	0	0.00354	0.00045	0
0.55	0.405	0.17	0	0	0.00366	0.00104	0
0.6	0.434	0.35	0	0	0.00375	0.00174	0
0.65	0.455	0.57	0	0	0.00384	0.00264	0
0.7	0.474	0.82	0	0	0.00391	0.00298	0
0.75	0.489	1.07	0	0	0.00397	0.00324	0
0.8	0.501	1.31	0	0	0.00403	0.00344	0
0.85	0.513	1.55	0	0	0.00408	0.00361	0
0.9	0.523	1.76	0	0	0.00412	0.00374	0
0.95	0.531	1.94	0.01	0	0.00416	0.00383	0.00006
1.0	0.536	2.10	0.05	0	0.00420	0.00391	0.00022
1.05	0.543	2.24	0.09	0	0.00423	0.00398	0.00038
1.1	0.547	2.36	0.16	0	0.00426	0.00404	0.00055
1.15	0.554	2.47	0.25	0	0.00429	0.00409	0.00074
1.2	0.559	2.58	0.34	0	0.00432	0.00413	0.00092
1.25	0.562	2.68	0.45	0	0.00434	0.00418	0.00113
1.3	0.566	2.76	0.57	0	0.00437	0.00421	0.00133
1.35	0.571	2.84	0.70	0	0.00439	0.00424	0.00154
1.4	0.575	2.92	0.82	0	0.00441	0.00428	0.00174
1.45	0.578	2.98	0.94	0	0.00443	0.00430	0.00195
1.5	0.581	3.04	1.05	0	0.00444	0.00433	0.00213
1.55	0.585	3.08	1.17	0	0.00446	0.00436	0.00234
1.6	0.587	3.13	1.29	0	0.00447	0.00438	0.00252
1.65	0.590	3.17	1.40	0	0.00448	0.00440	0.00269
1.7	0.593	3.21	1.51	0	0.00449	0.00442	0.00284

Table 2-1
(continued)

Electron Energy (MeV)	G1	G7	G3	G6	G2	G8	G4
1.75	0.595	3.24	1.6	0	0.00450	0.00444	0.00298
1.8	0.598	3.27	1.69	0	0.00451	0.00446	0.00312
1.85	0.6	3.3	1.77	0	0.00452	0.00447	0.00325
1.9	0.601	3.32	1.85	0	0.00452	0.00448	0.00336
1.95	0.603	3.34	1.92	0	0.00453	0.00449	0.00345
2	0.605	3.36	1.98	0	0.00453	0.00450	0.00353
2.25	0.612	3.42	2.21	0	0.00455	0.00453	0.00377
2.5	0.619	3.45	2.39	0	0.00457	0.00456	0.00389
2.75	0.624	3.47	2.54	0	0.00458	0.00457	0.00396
3.0	0.626	3.48	2.67	0	0.00458	0.00458	0.00403
3.25	0.629	3.49	2.79	0	0.00458	0.00458	0.00410
3.5	0.631	3.49	2.89	0	0.00458	0.00458	0.00415
3.75	0.634	3.50	2.98	0	0.00458	0.00458	0.00420
4.0	0.634	3.50	3.06	0	0.00458	0.00458	0.00425
4.25	0.635	3.5	3.12	0	0.00458	0.00458	0.00429
4.5	0.635	3.51	3.17	0.020	0.00458	0.00458	0.00433
4.75	0.635	3.51	3.21	0.068	0.00458	0.00458	0.00437
5.0	0.635	3.51	3.25	0.110	0.00458	0.00458	0.00440
5.25	0.635	3.51	3.28	0.150	0.00458	0.00458	0.00443
5.5	0.635	3.51	3.31	0.198	0.00458	0.00458	0.00445
5.75	0.635	3.52	3.34	0.25	0.00458	0.00458	0.00447
6.0	0.635	3.52	3.36	0.310	0.00458	0.00458	0.00451
6.25	0.635	3.52	3.38	0.370	0.00458	0.00458	0.00451
6.5	0.635	3.52	3.4	0.440	0.00458	0.00458	0.00453
6.75	0.635	3.52	3.42	0.510	0.00458	0.00458	0.00453
7.0	0.635	3.52	3.43	0.580	0.00458	0.00458	0.00454
7.25	0.635	3.52	3.44	0.650	0.00458	0.00458	0.00455
7.5	0.635	3.52	3.45	0.720	0.00458	0.00458	0.00456

Table 2-1
(Concluded)

Electron Energy (MeV)	G1	G7	G3	G6	G2	G8	G4
7.75	0.635	3.52	3.46	0.793	0.00458	0.00458	0.00457
8.0	0.635	3.52	3.47	0.862	0.00458	0.00458	0.00458
8.25	0.635	3.52	3.48	0.933	0.00458	0.00458	0.00458
8.5	0.635	3.52	3.48	1.008	0.00458	0.00458	0.00458
8.75	0.635	3.52	3.48	1.078	0.00458	0.00458	0.00458
9.0	0.635	3.52	3.49	1.149	0.00458	0.00458	0.00458
10.0	0.635	3.52	3.49	1.4	0.00458	0.00458	0.00458
11.0	0.635	3.52	3.49	1.6	0.00458	0.00458	0.00458

where $f(E)$ is the differential flux in electrons/cm^2/sec/keV. (The upper limit of ∞ is mathematically correct; however, when the equations were numerically integrated on a computer an upper limit of 20 MeV was used; ∞ will be used in the text to maintain mathematical correctness.) With a detector whose geometry factor is given as a function of energy the number of counts/sec, C_i, that the detector will see can be written as

$$C_i = \int_0^\infty G_i(E)\ f(E)\ dE \tag{2}$$

where $G_i(E)$ is the energy dependent geometry factor for the ith detector, and C_i is the count rate of the ith detector. Given C_i for a number of energy channels it is then theoretically possible to invert the integral and determine $f(E)$. This is, however, very tedious and is seldom used. A simpler and also more accurate procedure can be used if the spectral shape does not vary rapidly from point to point.

For the ith detector which has a response to electrons above energy E_i, an average geometry factor, $\bar{G}_i$, can be determined such that the count rate, C_i, for this ith detector is represented as

$$C_i = \bar{G}_i \int_{E_i}^\infty f(E)\ dE \tag{3}$$

$$= \bar{G}_i\ F(E > E_i) \tag{4}$$

Combining the above equation for C_i with the exact equation, $\bar{G}_i$ can be evaluated for a given channel.

$$\bar{G}_i = \frac{\int_0^\infty G_i(E_i)\ f(E)\ dE}{\int_{E_i}^\infty f(E)\ dE} \tag{5}$$

and

$$F\ (E > E_i) = \frac{C_i}{\bar{G}_i} \tag{6}$$

$\bar{G}_i$ is, of course, sensitive to the form of $f(E)$. For ultimate accuracy an $f(E)$ is assumed and the $\bar{G}_i$ are calculated. $\bar{G}_i$ is then used to evaluate $F(E > E_i)$, which can then be used to find the $f(E)$ and if the new $f(E)$ is substantially different from the initial $f(E)$, then an iteration process is used to find $\bar{G}_i$. In this study an approximate fission shape was used to determine the $\bar{G}_i$ for each of the detectors and an iteration procedure was not necessary. The fission spectrum used for this analysis was a best fit to the spectrum given in Reference 1. (See Equation 7).

The energy cutoffs of the channel given in the initial Lockheed report were also used in this analysis. These energies are the thresholds where the counters first start counting. The energy labels assigned to the channel are somewhat arbitrary because the procedure evaluating $\bar{G}_i$ uses whatever assumption is made for the energy channel labels and determines the appropriate $\bar{G}_i$ for the assigned E_i that is consistent with the assumed spectrum.

The spectrum used to determine $\bar{G}_i$ is

$$\begin{aligned} f(E) &= 4 \times 20^6\ e^{(-2.38E)} && E < 1\ \text{MeV} \\ f(E) &= 1.14 \times 10^6\ e^{(-1.11\ E)} && E > 1\ \text{MeV} \end{aligned} \tag{7}$$

The G_i for the Channels used in the analysis are given in Table 2-2.

Table 2-2
GEOMETRIC FACTOR FOR JASON

Channel Number	E	$\frac{1}{G}$
1	0.21 MeV	2.62
3	1.0 MeV	0.719
6	4.3 MeV	6.09
7	0.44 MeV	0.582
8	0.44 MeV	286.0

2.3 Data Analysis

Data from the five flights were available in Appendix A of the Lockheed report. Table 2-3 is a sample of one of the tables. The tables list the counts/second for the various energy Channels as a function of time since the start of the flight. The center of the time interval and the counts were entered into the computer. A function dependent on counts was used to enter the errors.

A second set of tables (see Table 2-4 as an example) listed the trajectory parameters as a function of time. The time, magnetic field strength, B, and the logarithm of the invariant, J, were entered into the computer. J and B were converted into B and L using a simple conversion program and Hilton's L program. The logarithm of the invariant, J, given in Table 2-4 is given in a strange set of units. To convert the J from Table 2-4 into the I required by Hilton's or McIlwain's program the following conversion was used:

$$I = \frac{e^J}{6371} \tag{8}$$

Table 2-3

COUNTING RATES OF DETECTORS ON FLIGHT 2019

Flight Time Interval (sec) From	To	Average of Channels 1 & 5	Channel 7	Channel 3	Channel 6	Channel 2	Channel 8	Channel 4
177	184	3850 ± 147	2300 ± 160	1010 ± 100	10 ± 10	307 ± 68	0	0
192	199	4900	2960 ± 140	1570 ± 100	18 ± 10	386 ± 62	0	18 ± 13
208	216	6590	3520 ± 150	2010 ± 115	25 ± 12	383 ± 62	0	12 ± 12
221	234	7360 ± 131	3250 ± 110	1910 ± 88	17 ± 9	666 ± 70	18 ± 10	6 ± 6
241	254	9560	4350 ± 136	3440 ± 150	25 ± 9	1820 ± 122	17 ± 12	0
261	273	12,100	4750 ± 140	2420 ± 100	26 ± 10	1030 ± 76	0	17 ± 10
281	294	13,100 ± 170	5200 ± 140	2750 ± 103	44 ± 12	1220 ± 85	26 ± 12	0
300	313	14,500	5810	2900 ± 104	29 ± 11	1350 ± 82	30 ± 12	16 ± 9
321	328	14,900	6180 ± 200	3360 ± 115	66 ± 23	1540 ± 97	18 ± 10	9 ± 9
341	348	18.400	6960	3680 ± 160	18 ± 13	1710 ± 130	18 ± 13	0
362	373	17,500	6870 ± 180	3960 ± 128	44 ± 14	2080 ± 123	13 ± 9	24 ± 12
281	394	18.000 ± 210	7190 ± 163	3860 ± 125	22 ± 9	2100 ± 102	26 ± 12	16 ± 9
401	414	20,400 ± 220	7760	3890 ± 120	8 ± 5	2120 ± 116	6 ± 6	24 ± 12
421	433	20,500 ± 220	7740	3890 ± 128	36 ± 13	1830 ± 101	45 ± 16	5 ± 5
441	453	20,100 ± 210	8350 ± 180	4120 ± 126	86 ± 19	2100 ± 115	32 ± 13	6 ± 6
461	474	24,300 ± 240	8640	4260 ± 120	46 ± 13	2170 ± 110	35 ± 13	16 ± 9
501	508	19,900 ± 280	8950 ± 237	4520 ± 174	42 ± 16	2220 ± 156	52 ± 20	0
516	524	18,500 ± 284	9120	4360 ± 165	68 ± 21	2270 ± 141	29 ± 17	13 ± 13
533	540	18,100 ± 270	9810	4440 ± 182	49 ± 18	2280 ± 151	27 ± 16	0
549	556	17,400 ± 270	9500	4250 ± [illegible]	48 ± 18	2250 ± 148	16 ± 11	13 ± 13
565	571	19,300 ± 290	9630 ± 246	4390 ± 187	64 ± 23	2240 ± 141	39 ± 22	13 ± 13
581	588	22,100 ± 290	10,900	4680 ± 180	62 ± 20	2690 ± 170	39 ± 19	11 ± 11
596	604	18,800 ± 280	10,700	4720 ± 184	58 ± 20	2060 ± 149	9 ± 9	10 ± 10
629	636	18,500 ± 260	11,100	4960 ± 182	61 ± 60	1840 ± 133	20 ± 14	
645	652	10,500 ± 200	9100 ± 250	4640 ± 170	38 ± 15	1230 ± 109	49 ± 22	10 ± 10
655	667	13,300 ± 170	11,900 ± 222	5280 ± 145	48 ± 13	1320 ± 88	61 ± 18	15 ± 9
681	694	11,800 ± 160	13,000	5710 ± 145	63 ± 14	838 ± 70	34 ± 14	0
701	714	8720 ± 140	12,900 ± 223	6100 ± 147	86 ± 17	511 ± 53	55 ± 16	23 ± 10
714	727	9380 ± 140	18,600 ± 273	8080 ± 172	52 ± 14	448 ± 51	24 ± 12	23 ± 10
721	734	9200 ± 140	18,700	8180 ± 166	85 ± 17	411 ± 51	33 ± 13	26 ± 12

Table 2-4

JASON FLIGHT 2019

Flight Time (min)	West Longitude (deg)	North Latitude (deg)	Rocket Altitude (KM)	Magnetic Intensity (Gauss)	Log I	Altitude* 75° West (KM)	Altitude** S. Hemis. (KM)
2.00	75.41	52.60	282				
2.50	75.39	52.89	367				
3.00	75.36	53.17	444				
3.50	75.33	53.45	513	0.4300	10.228	510	139
4.00	75.31	53.72	576	0.4169	10.218	573	259
4.50	75.28	53.99	631	0.4054	10.206	628	318
5.00	75.26	54.25	679	0.3954	10.195	676	366
5.50	75.24	54.51	719	0.3872	10.182	717	409
6.00	75.21	54.77	753	0.3806	10.170	751	443
6.50	75.19	55.03	780	0.3753	10.156	778	468
7.00	75.17	55.28	800	0.3710	10.142	799	486
7.50	75.15	55.53	813	0.3680	10.128	812	501
8.00	75.13	55.79	820	0.3660	10.112	819	508
8.50	75.11	56.04	819	0.3651	10.096	819	510
9.00	75.08	56.29	812	0.3654	10.080	812	503
9.50	75.06	56.54	798	0.3667	10.062	796	487
10.00	75.04	56.80	778	0.3691	10.043	777	463
10.50	75.02	57.05	750	0.3726	10.022	750	444
11.00	75.00	57.31	716	0.3772	9.999	716	412
11.50	74.98	57.57	674	0.3833	9.976	675	372
12.00	74.96	57.83	626	0.3910	9.953	626	325
12.50	74.93	58.10	570	0.4001	9.929	571	274
13.00	74.91	58.38	507	0.4108	9.903	508	228
13.50	74.89	58.65	444				
14.00	74.87	58.94	359				

NOTE: Single and double asterisks refer to last two columns of Tables 7 through 12

*Rocket altitude transformed along lines of constant B_o and I values to the meridian plane at 75° West longitude.

**Altitude in southern hemisphere where magnetic field intensity (along local magnetic line of force) is same as that at the position of the rocket.

2.4 Background Determination

A considerable effort is made in the Lockheed report to identify the background. Various contributions and effects of the various backgrounds are included in Reference 1. Additional data from a Javelin rocket (included in Reference 1) were also used to evaluate the background. The Javelin data set were not available for this effort and thus a simpler, although quite reliable, approach was used.

The fifth flight, Flight No. 2042, was launched much later than the four earlier flights. The first four flights were launched within 19 hours of the burst. Flight 2042 was launched 88 hours after the burst. The analysis in the Jason report showed that by this time the flux had decayed to preburst levels. Thus flight 2042 was used to evaluate the background. Fortunately, flight 2042 cuts across all of the pertinent L shells and also gives a variation in B over a limited L space. The B dependence of closely adjacent L shells during undisturbed times is expected to be very similar and thus a least squares fit in B, L space was used to evaluate the background measured by flight 2042. The background function is

$$BK_i\ (B,\ L) = a_i + b_i B + c_i\ L + d_i\ B\ L \tag{9}$$

Where BK_i gives the background in counts per second for the ith channel, a_i, b_i, c_i, and d_i are coefficients for the ith channel and B and are the McIlwain B, L. The coefficients for the channels that were used in the final analysis are given in Table 2-5.

2.5 Error Analysis

A number of errors were possible for the Jason experiments. The four errors that were found significant are: 1) statistical uncertainties, 2) dead time correction, 3) uncertainty in knowing the background, and 4) uncertainty in knowing the calibration.

Table 2-5

BACKGROUND COEFFICIENTS FOR JASON

CHAN	a	b	c	d
1	-.18645724E+05	-.33241116E+05	.19674592E+05	-.11503467E+05
7	.13225681E+05	-.43587219E+05	-.10899943E+04	.78067239E+04
3	-.97265572E+03	.23142711E+04	.43185220E+03	-.99867263E+03
6	.57948358E+03	-.13721005E+04	-.21212237E+03	.52182959E+03
2	.93666545E+04	-.33228643E+05	-.16638987E+04	.87487088E+04
8	.31203721E+04	-.79988845E+04	-.12398078E+04	.31920189E+04

Since the raw counts used to determine the counts/second were not given in the data listing, the standard $\sqrt{N}$ method could not be used for the statistical errors. The data listings did, however, give many examples of counts $\pm$ statistical errors. A graph of counts versus errors was made and the curve

$$E_S = 2.23\ (N_D)^{.519} \tag{10}$$

was fit to the data set. E_S is the statistical error and N_D is the data counts/second.

The error due to dead time of the geiger tube circuit became very large at high count rates. The Lockheed report gives the error due to dead time as a table.

The function

$$E_D = 1.93 \times 10^{-5}\ (N_D)^2 \tag{11}$$

was found to fit the dead time error data very well. E_D is the error due to uncertainty in the dead time and N_D is the data counts/sec.

The uncertainty in the background represents a sizable portion of the error and was difficult to estimate. It included the uncertainty that the fit to flight 2042 over a very limited region of space adequately represents the background over the entire region of interest and the uncertainty of the intercalibration between flight 2042 and the other flights. The intercalibration uncertainties were determined to be small. The fit uncertainties were estimated to be no larger than 50 percent. The background fight gave data points along a single trajectory through B, L space. The up and down legs of the flight were separated in L and thus gave an L dependence for the background fit. Both legs (up and down) gave a B dependence. Since there were at best two data points for each L, an assumption of smoothness (i.e., slowly varying in space) had to be made. Differences larger than 50 percent from these results were inconsistent with our understanding of the variation of radiation during quiet times over a very limited region of space. Thus

$$E_B = 0.5\ BK_i \tag{12}$$

where E_B is the error in the background count rate and BK_i (see Equation 9) is the background count rate as determined from the fit.

The error in the calibration is also difficult to estimate since the accuracy of geometry factor evaluations are not included in the Lockheed document. In evaluating the G_i for the various channels (Section 2.2) a sensitivity to spectral form was evident. It was assumed that this error was more important than any procedural errors during laboratory geometry factor determinations. The slopes of the fission spectrum, Equation 7, were changed by 0.5. That is, in Equation 7 the $e^{-2.38E}$ term was varied from $e^{-1.98E}$ to $e^{-2.88E}$. This changed the calibration values by no more than 30 percent. Thus

$$E_R = 0.3\ N_D \tag{13}$$

where E_R is the error in the data rate and N_D is the data count rate. The most probable total, E_T, the error in the count rate for a given channel due to electrons injected by Argus, was determined to be

$$E_T = \sqrt{E_S^2 + E_D^2 + E_B^2 + E_R^2} \tag{14}$$

The flux and error estimates for each channel was calculated using

$$F\ (E > E_i,\ B,\ L) = \frac{1}{G_i}\ (N_D \pm E_T) \tag{15}$$

Section 3

EXPLORER IV

The Explorer IV satellite was the only detector available for the Teak and Orange series and the only satellite measurement of the Argus series. The Argus series was supplemented using the Jason sounding rockets. However, the JASON measurements occurred near the top of the atmosphere and the Argus electrons observed by the Jason rockets were quickly (in several days) removed by the atmosphere. Thus Explorer IV is the principal data set for Teak, Orange and Argus.

A substantial amount of published data was available for Teak in Reference 2. The data is presented as a function of L with only approximate values of time and B available. The Orange data set listed only the peak amplitudes. For Argus only a few isolated passes of data were available using the thesis of Manson (Reference 3), Paikeday (Reference 4), and George (Reference 5).

Additional Argus data consisted of such information as peak flux at the center of the shell as a function of time. However, no B, L dependent values showing the structure of the Argus band were available. Thus a decision was made to order the Explorer IV data set from the NSSDC. This tape recorded data set

---

2. D. J., Fennell, J. F. George, J. A., Hickerson, J. L., Maldonado, G. V., Webber, A. H., Review of Artificial Radiation Belts, Explorer 4; Unidirectional Trapped Radiation, Injun I, DASA-2309, 1969.

3. Manson, D. J., Van Allen Radiation Belt and Argus Directional Flux Density Distributions, Explorer IV Satellite Data, (Thesis) Saint Louis University, Saint Louis, Illinois, 1967.

4. Paikeday, J. M., Interpretation of Directional Flux Densities in Argus Shells, Explorer IV Satellite Data, (Thesis) Saint Louis University, Saint Louis, Illinois, 1966.

5. George, J. A., Omnidirectional Fluxes; Explorer 4 Satellite Data, Argus Events 1 and 2, (Thesis) St. Louis University, St. Louis, Illinois, 1967.

proved very valuable in verifying the calibration of Explorer IV by comparing the non-burst data with the Vette environments. It also provided accurate and easy to use data for Teak and Orange. However, as described in the introduction, six different data sets (three from NSSDC and three from UCSD) failed to locate the required Argus data. The Argus data were finally found in a report that was originally classified and then was subsequently declassified (Reference 6).

The Explorer IV data consisted of data from three different detectors. These detectors are described in Reference 7. A portion of this description is reproduced below.

3.1 Experiment Description

"Channel 2 is a circular disc of plastic scintillator (National Radiac Scintilon), thickness 0.178 cm, diameter 0.762 cm cemented on the face of an RCA photomultiplier tube, type 6199. The PM tube was mounted with its axis orthogonal to the longitudinal axis of the payload and with the scintillator near an open hole in the wall of the payload shell. The unidirectional geometrical factor (defined by $G = R/\epsilon j$, where j is the unidirectional intensity in particles/cm^2 sec steradian) of the scintillator was $G = 0.040$ cm^2 steradian through an aperture covered by 0.14 g/cm^2 of aluminum. The geometrical factor as a function of stopping power rose rapidly for stopping power greater than 1.6 g/cm^2 to an asymptotic value of $G = 4.2$ cm^2 steradian (or $G_0 = 0.334$ cm^2) for stopping powers greater than 5 g/cm^2. The collimating apertures were such that the area of the scintillator 'visible' through the foil had its full value for a cone of half angle 6^0 and fell linearly to zero at a half angle of 19^0. The

---

6. Argus I, II and III Observations with Explorer IV Satellite (Supplement Report) Department of Physics and Astronomy, State University of Iowa.

7. Van Allen, J. A., McIlwain, C. E., Ludwig, G. H., Satellite Observations of Electrons Artificially Injected into the Geomagnetic Field, Journal of Geophysical Research, 64, 877-891, 1959.

electronic bias was selected so that about five per cent of the β-rays from a Tl^{204} source on the outside of the stopping foil were recorded. The upper limit of the β-ray spectrum of Tl^{204} is 780 keV. A weak Tl^{204} source was permanently deposited on the foil of the flight instrument to provide an overall check on performance of the system: it gave an average background rate of 0.50 counts/sec, with slight but known dependence on temperature of the amplifier. Overall response of the system was well represented by the following equation:

$$R = \frac{r}{1 - r\tau} \tag{16}$$

in which r = apparent counting rate, τ = 91 μsec, R = true counting rate. Two scaling factors were provided in order to extend the dynamic range of the system: Channel 2 with a scaling factor of 2048 and Channel 5 with a scaling factor of 16.

For channel 3 the basic detector was an Anton Type 302 Geiger tube. It was not deliberately shielded but was more or less surrounded by a miscellany of electronic components and mechanical structure such that the omnidirectional geometric factor G_0 was 0.14 cm^2 for a stopping power of 1.2 g/cm^2 and rose to its full value of 0.705 cm^2 for stopping power of 5 g/cm^2. The material in the low stopping power case was mainly stainless steel. The performance of the overall circuit was found in detailed calibrations to be well represented by the following equation:

$$r = Re^{-R\tau} \tag{17}$$

where r is the apparent rate, R the true rate and τ = 62.5 ± 1.3 μsecs. The useful dynamic range for filtered 50 keV X rays, for example, extended up to about 20 roentgens/hr. The maximum value of r was 5900 counts/sec, and the value of r was very nearly proportional to radiation intensity at rates below 1000 counts/sec. No difficulty was experienced in practice in resolving the ambiguity presented by the fact that r was a double valued function of radiation intensity. The maximum value of r was easily read on the telemetered record due to the large scaling factor, namely 2048.

For Channel 1, the basic detector was again an Anton type 302 Geiger tube. The tube was surrounded by a lead cylinder of 1.6 g/cm^2 thickness and was further shielded on the ends by lead plugs of somewhat greater thickness. $G_o = 0.14$ cm^2 for a total stopping power (lead + stainless steel) of 2.8 g/cm^2, and G_o has substantially its full value of 0.823 cm^2 for stopping powers greater than 6 g/cm^2. Channels 1 and 3 were located side by side with center line separation of 3.6 cm. The maximum observable counting rate of Channel 1 was determined by the information-band-width of the telemetering system. It was about 1500 counts/sec under favorable conditions. The low scaling factor, 64 was selected in order to get a determination of radiation intensities at low altitudes during the often-brief periods of satisfactory telemetering reception by a given station on a given pass. Periods as brief as one or two minutes were anticipated and did indeed occur not uncommonly, though many of the stations were successful in receiving workable signals for up to 15 minutes and in rare cases for longer.

The lower powered transmitter and Channels 2 and 5 'died' about September 3. Channels 1, 3, and 4 continued to operate properly until September 19. The higher powered transmitter ceased sending signals on October 5. There is no reason to believe that the demise of the apparatus was due to any other cause than simple exhaustion of the batteries.

3.2 Calibration

The Explorer IV instrumentation consisted of two separate detector setups. Channels 1 and 3 are Geiger-Muller counters. Channel 2 is a plastic scintillator.

3.2.1 Geiger Tube Calibration

Channels 1 and 3 consist of two Anton 302 Geiger tubes. These tubes have reasonably isotropic response. The geometry factor varies with energy and is given in Figure 3-1. An average efficiency factor for these detectors can be developed using the same equations as in Section 2.

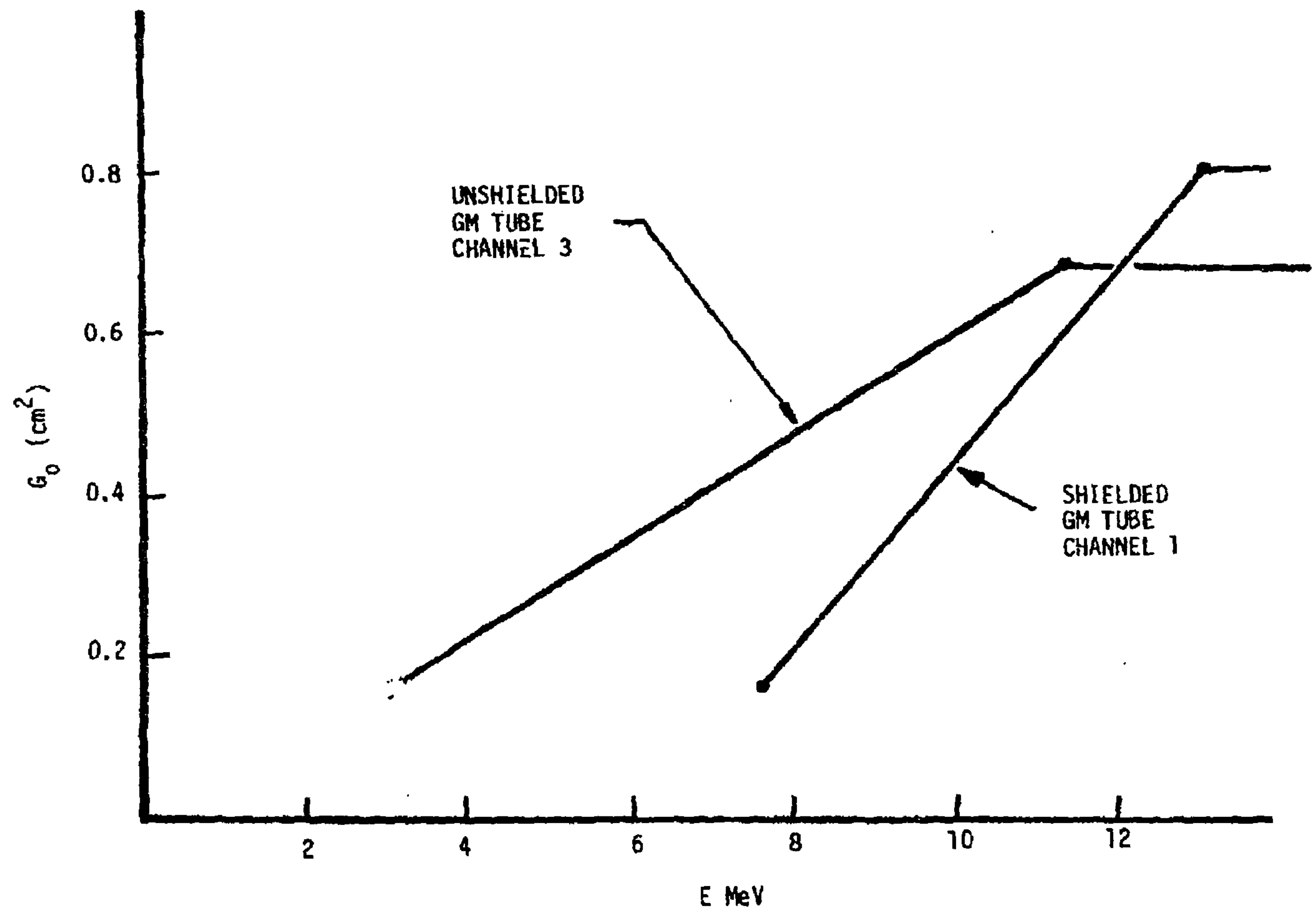

Figure 3-1. Response Curves of the Explorer IV Geiger Counters

$$\bar{G}_i = \frac{\int_0^\infty G_i(E)\ f(E)\ dE}{\int_{E_i}^\infty f(E)\ dE} \tag{18}$$

where $\bar{G}_i$ is the average efficiency for converting counts to the electron flux, $F\ (E > E_i)$, greater than energy E_i. $G_i(E)$ is the energy dependent geometry factor (Figure 3-1); $f(E)$ is the differential fission spectrum (see Equation 7). Thus

$$F\ (E > E_i) = \frac{C_i}{\bar{G}_i} \tag{19}$$

where C_i is the counts/sec. The pertinent constants are given in Table 3-1.

Table 3-1

AVERAGE EXPLORER IV GEOMETRY FACTOR

Channel No.	E_i	$\frac{1}{\bar{G}_i}$
1	6.2 MeV	5.1
3	3.0 MeV	5.1

The geometry factor for Channel 3, the 3 MeV channel was verified by comparing data obtained before the Teak burst against the predictions of the Vette environments. To facilitate this comparison, an iso-intensity contour plot of the Explorer IV calculated electron fluxes was prepared in B, L space (see Figure 3-2). Table 3-2 lists these fluxes as well as the associated raw counts from the Explorer IV data and the counts that would be obtained if the Explorer IV detector were flown through the Vette AE-5 environment (i.e., the calibration curves were folded into the AE-5 flux model). The two count rates do not agree! Thus Explorer IV should not be used to determine the natural electron fluxes. Therefore an attempt was made to see if protons can account for the observed count rate. The average geometry factor using the technique in Equation 18 for AP 8 proton spectrum gives an average geometry factor for protons of about $\sim$ 3. When this proton geometry factor is used one gets the

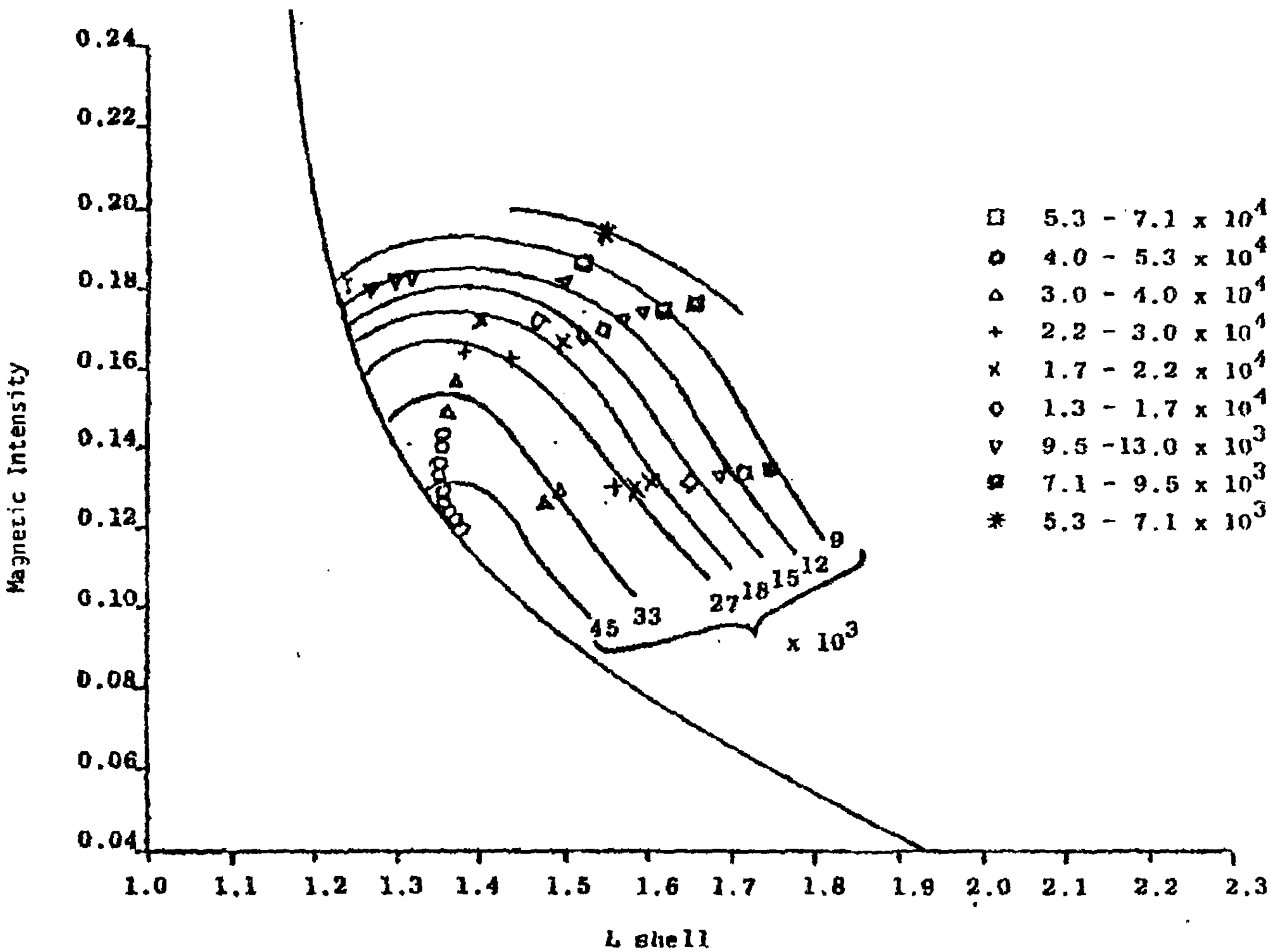

Figure 3-2. MeV Iso-Intensity Electron Flux Contours in the Natural Electron Environment as determined from the Explorer IV Calibration. NOTE: These contours are not correct since Explorer IV measurements are heavily proton contaminated.

proton counts in Table 3-2. From Table 3-2 it is apparent that the Explorer count rate in the absence of a nuclear-burst-induced flux is produced primarily by protons. Thus the natural electron flux values shown in Figure 3-2 and Table 3-2 are not correct; they are heavily proton contaminated. Since the Vette Protons can account for the observed count rate, we believe that the calibration of Explorer IV is correct.

A similar comparison for the 6.2 MeV channel was not possible because the count rates were too low. However, since the two detectors are similar, no special problems are expected.

Table 3-2

VERIFICATION OF CHANNEL 3 CALIBRATION

L	B	Explorer IV Flux	Explorer IV Counts	Counts from Vette Electrons	Counts from Vette Protons
1.3	.18	1.3×10^4	2500	39	2000
1.4	.18	1.5×10^4	2900	235	2300
1.5	.16	3×10^4	5800	400	3000
1.6	.16	1.3×10^4	2500	680	2000
1.6	.12	2.7×10^4	5300	390	4000
1.7	.16	9×10^3	1800	39	1300

3.2.2 Calibration of Plastic Scintillator

The plastic scintillator is a directional instrument and was strongly affected by the tumble of the spacecraft. The theses of Paikeday (Reference 4) and Manson (Reference 3) work out in great detail how the observed counts were to be converted to true counts and how these true counts were then converted to omnidirectional flux because of its complexity. No attempt is made to reproduce any portion of this work here. Using the numbers from the publications (References 3 and 4) and verifying these by checking against published results, this relationship follows:

$$C_{TRUE} = 349 \frac{C_{obs}}{1 - \tau C_{obs}} \qquad (20)$$

where C_{TRUE} is the true omnidirectional count rate, C_{obs} is the observed directional count rate and τ is the dead time (91 μsec). Figures 3-3 and 3-4 from the publication verify this conversion. To convert the true count rate to omnidirectional electrons/cm^2/sec greater than 700 keV, the following relationship (Reference 5) was used

$$F\ (E > 700\ \text{keV}) = 28\ C_{TRUE} \qquad (21)$$

As in the case of Channel 3, the Explorer IV measured electron fluxes (the maximum fluxes from the data tape were used) are compared with the fluxes from the Vette environment. Figure 3-5 is an iso-intensity contour plot in B-L space. Values from this contour plot are used to construct the comparison table (Table 3-3). Protons are not an important contribution to the 700-keV channel count rate. The comparison between the Explorer IV determined fluxes and the Vette inner zone fluxes shows a reasonable agreement indicating that our understanding of the conversion from observed counts on the data tape to isotropic fluxes is correct.

Table 3-3

700 keV ELECTRON COMPARISONS

L	B	Explorer IV Fluxes	Vette Electron Environment
1.4	0.18	1.5×10^5	2×10^5
1.4	0.14	3×10^5	5×10^5
1.6	0.14	1.5×10^5	1.8×10^5
1.5	0.13	2×10^5	3×10^5

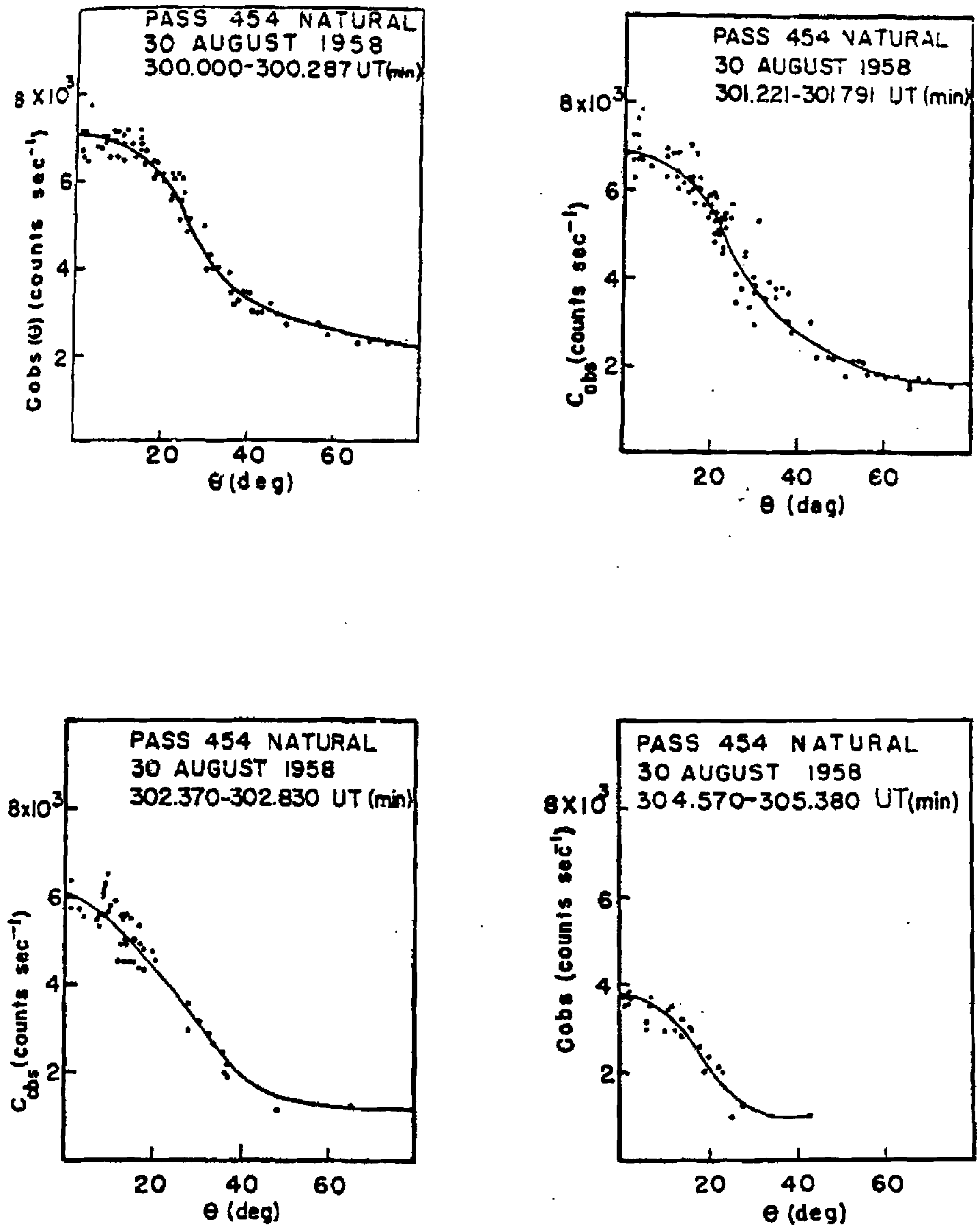

Figure 3-3. Observed Explorer IV Channel 2 Count Rate

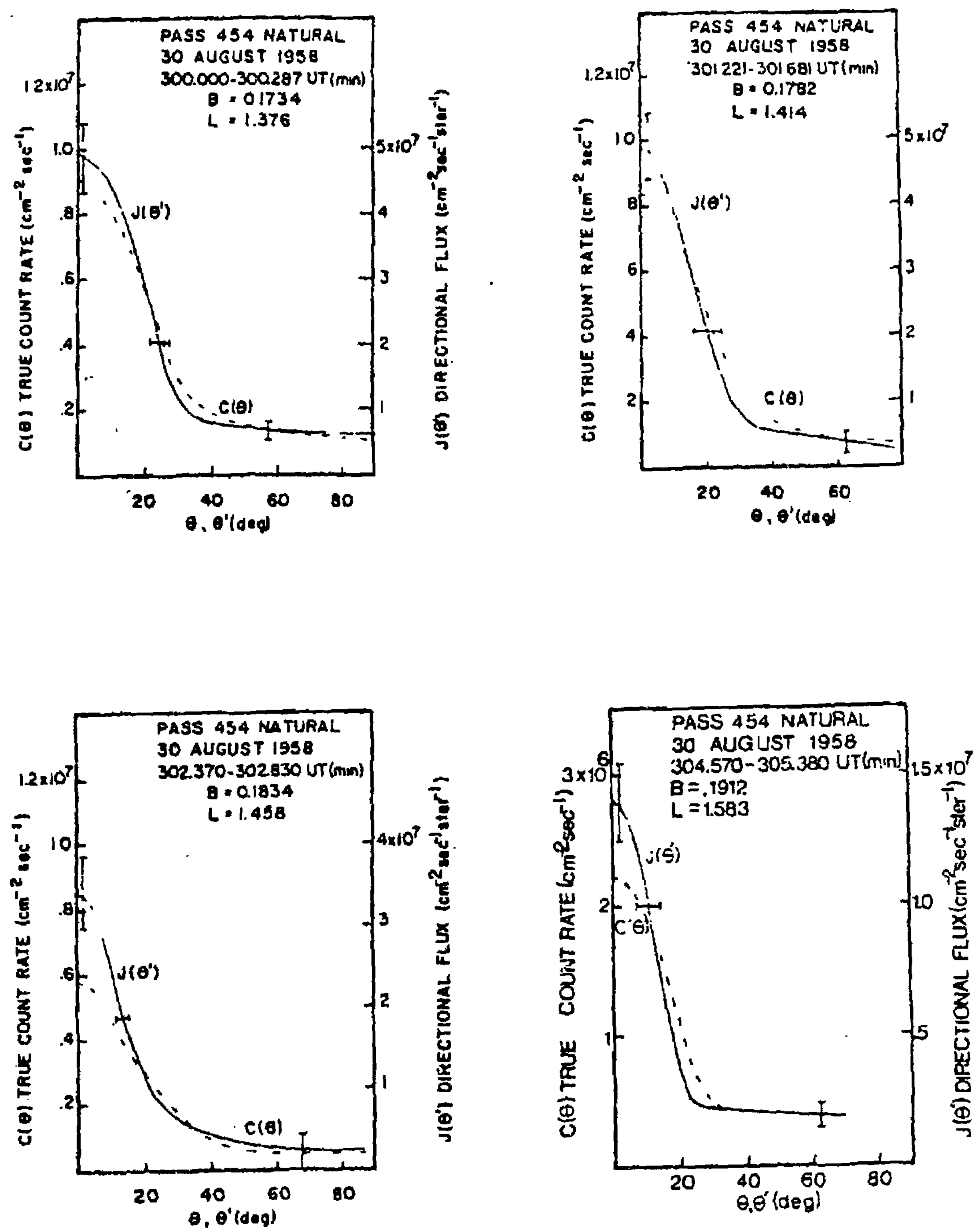

Figure 3-4. True Explorer IV Channel 2 Count Rate

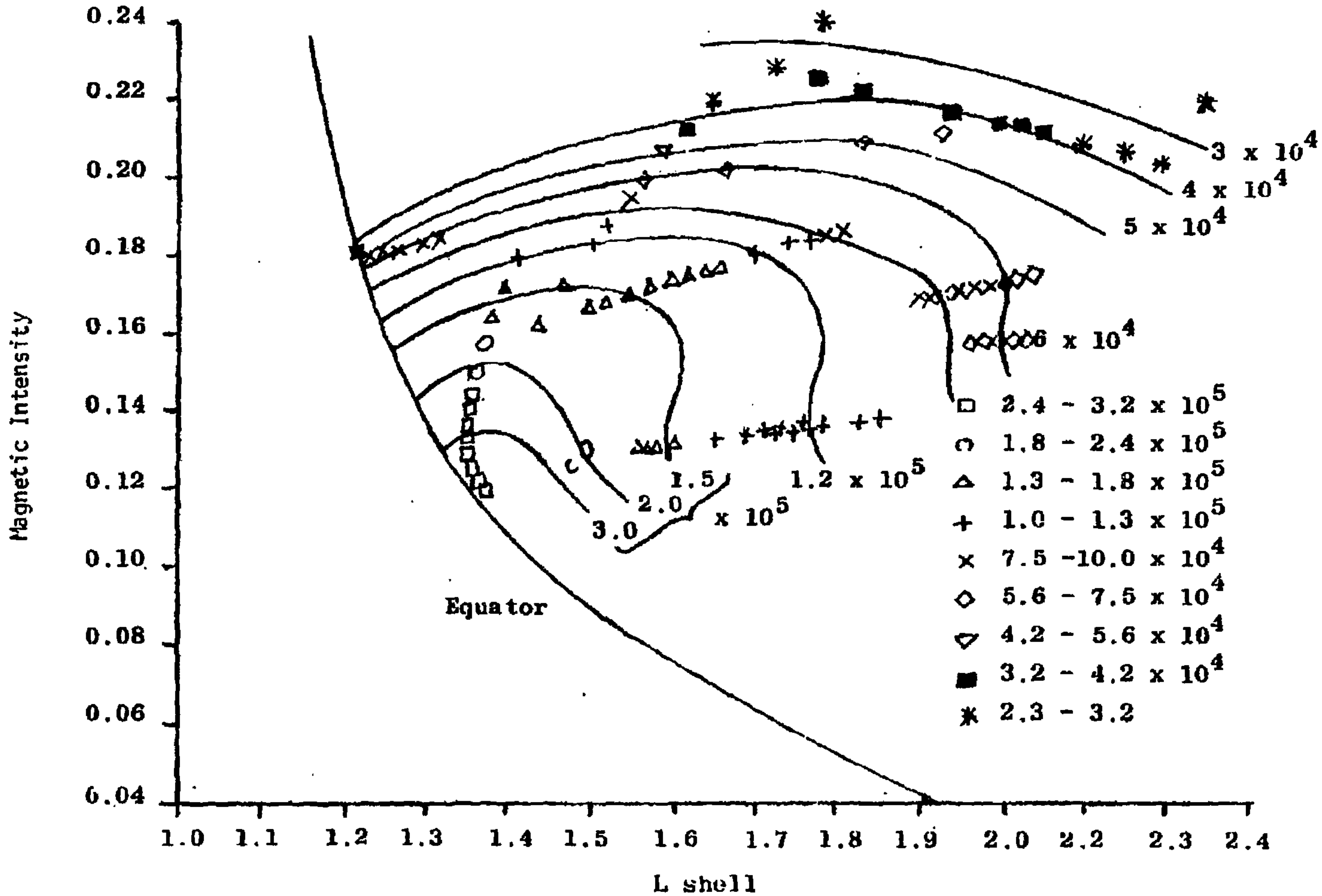

Figure 3-5. Explorer 4 700 keV Iso-Intensity Flux Contours in Natural Electron Environment

3.3 Data Analysis

The data analysis of the Explorer IV satellite can be broken into two very distinct phases. The Teak and Orange data analysis used the NSSDC data tape and the Argus analysis used the declassified plots of the University of Iowa report (1959).

3.3.1 Teak and Orange Data Analysis

The NSSDC data tape gave the data for omnidirectional counts for Channels 1 and 3 and the maximum, minimum and average directional count rates for Channel 2. The conversion of the omnidirectional data to fluxes was straightforward. The counts were dead time corrected and then multiplied by 1/G to give electrons/cm^2/sec. The directional maximum counts from Channel 2 were dead time corrected and multiplied by the factor 349 to give the true counts/sec. Several passes were compared to the published data. Figure 3-6 shows a typical pass for Teak.

The above data analysis from the tape presented no problems. Plots for Channels 2 and 3 were made versus L for all values of B. Figures 3-7 through 3-10 show the flux distributions for 700 keV and 3 MeV electrons during non-burst conditions before each of the bursts. Figures 3-11 and 3-12 show the flux distributions after the Orange burst and Figures 3-13 and 3-14 show the flux distribution after the Teak burst. From these figures it is apparent most of the data points for both Teak and Orange are well above background. For Orange the flux is either due to Orange or too low to measure, and thus for Orange the background fluxes were set to zero. For Teak the background in most cases was quite small; however, background values were entered into the computer if the fluxes were near the natural background levels. This background consisted primarily of protons for the 3 MeV channel and natural electrons for the 700 keV channel.

3.3.2 Argus Data Analysis

The Argus data analysis consisted of analyzing the graphs from Reference 6. These graphs contained the true count rates for the 3 MeV and the 6.2 MeV

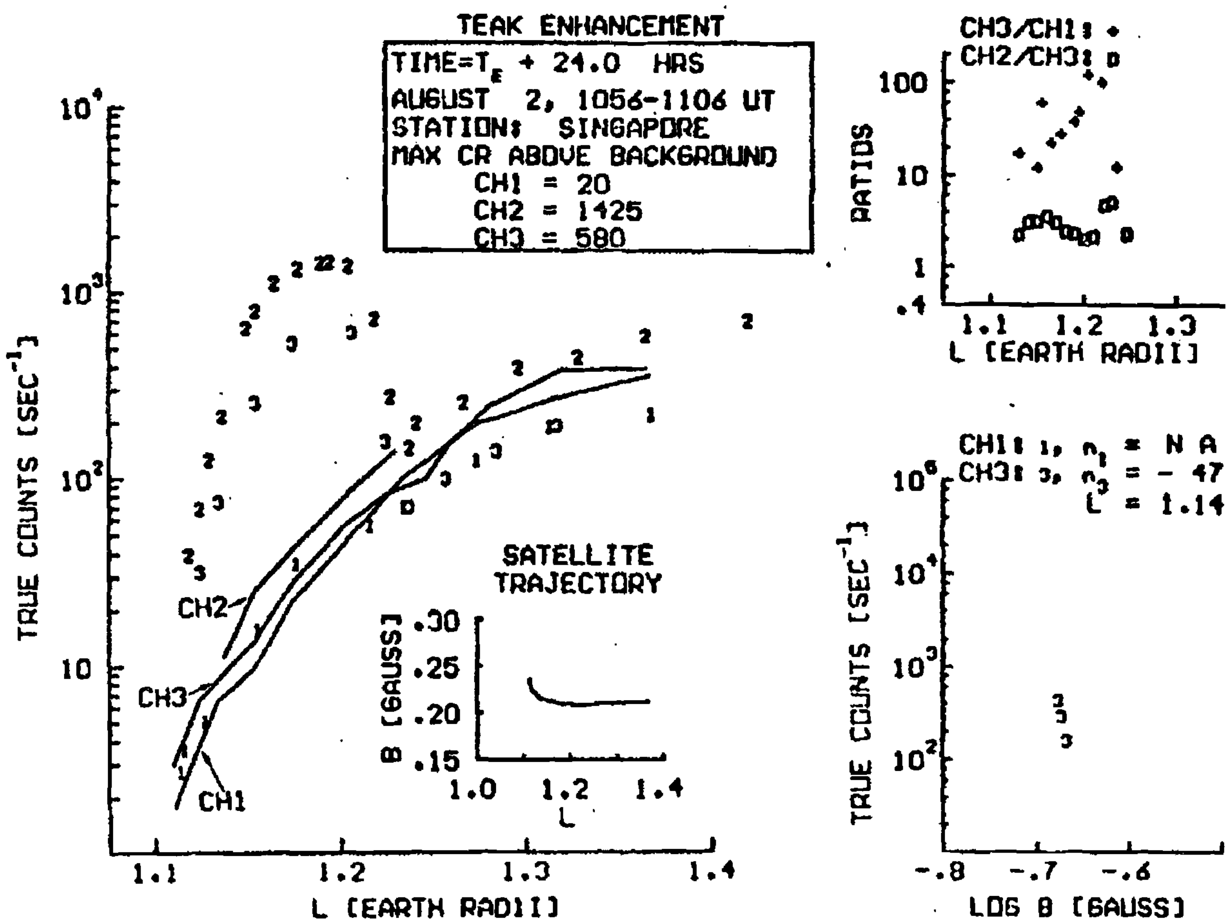

Figure 3-6. Typical Teak Data Pass

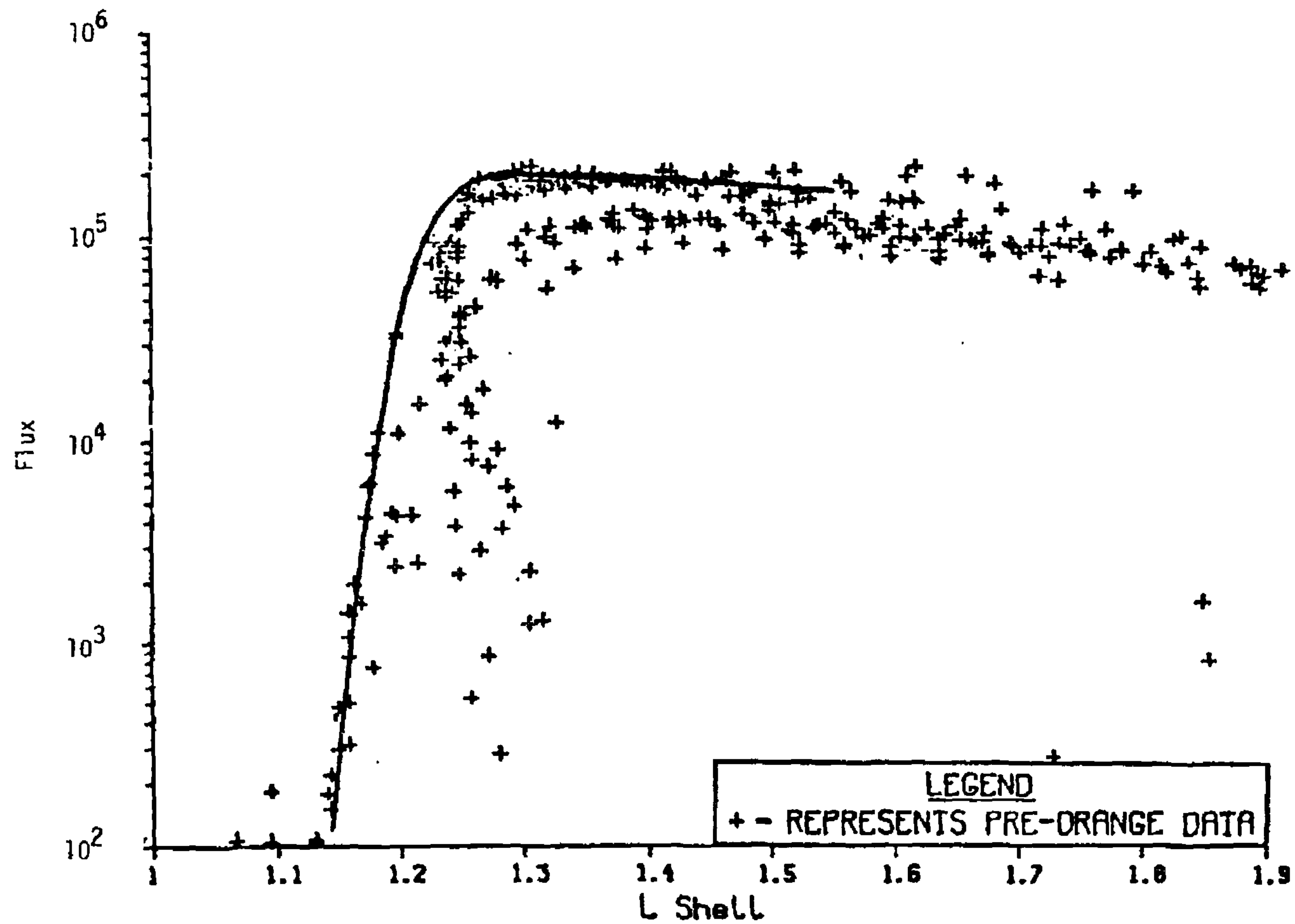

Figure 3-7. Explorer 4 Channel 2 Flux Versus L for Pre-Orange Days

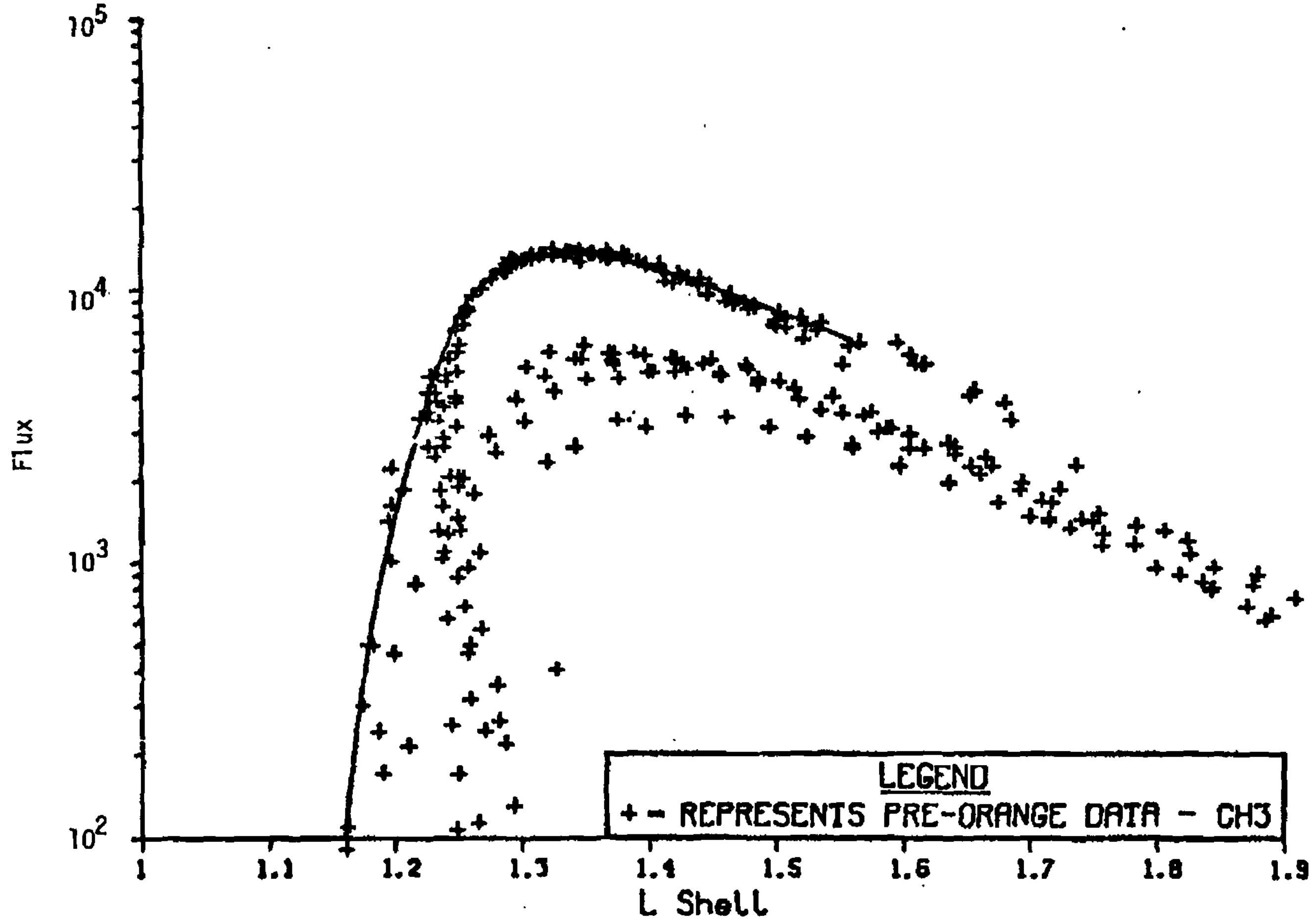

Figure 3-8. Explorer 4 Channel 3 Flux Versus L for Pre-Orange Days

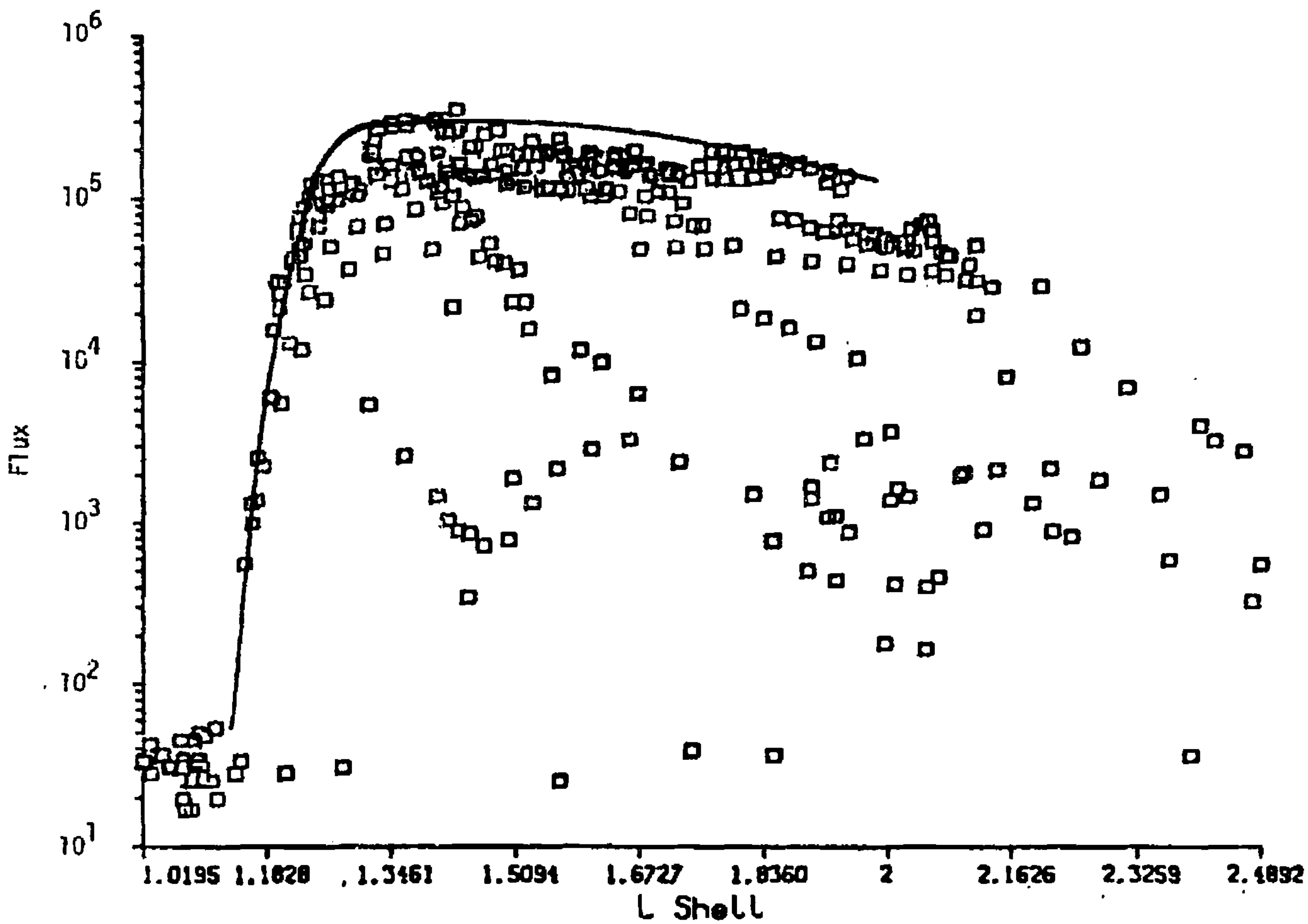

Figure 3-9. Explorer 4 Channel 2 Flux Versus L for Pre-Teak Days

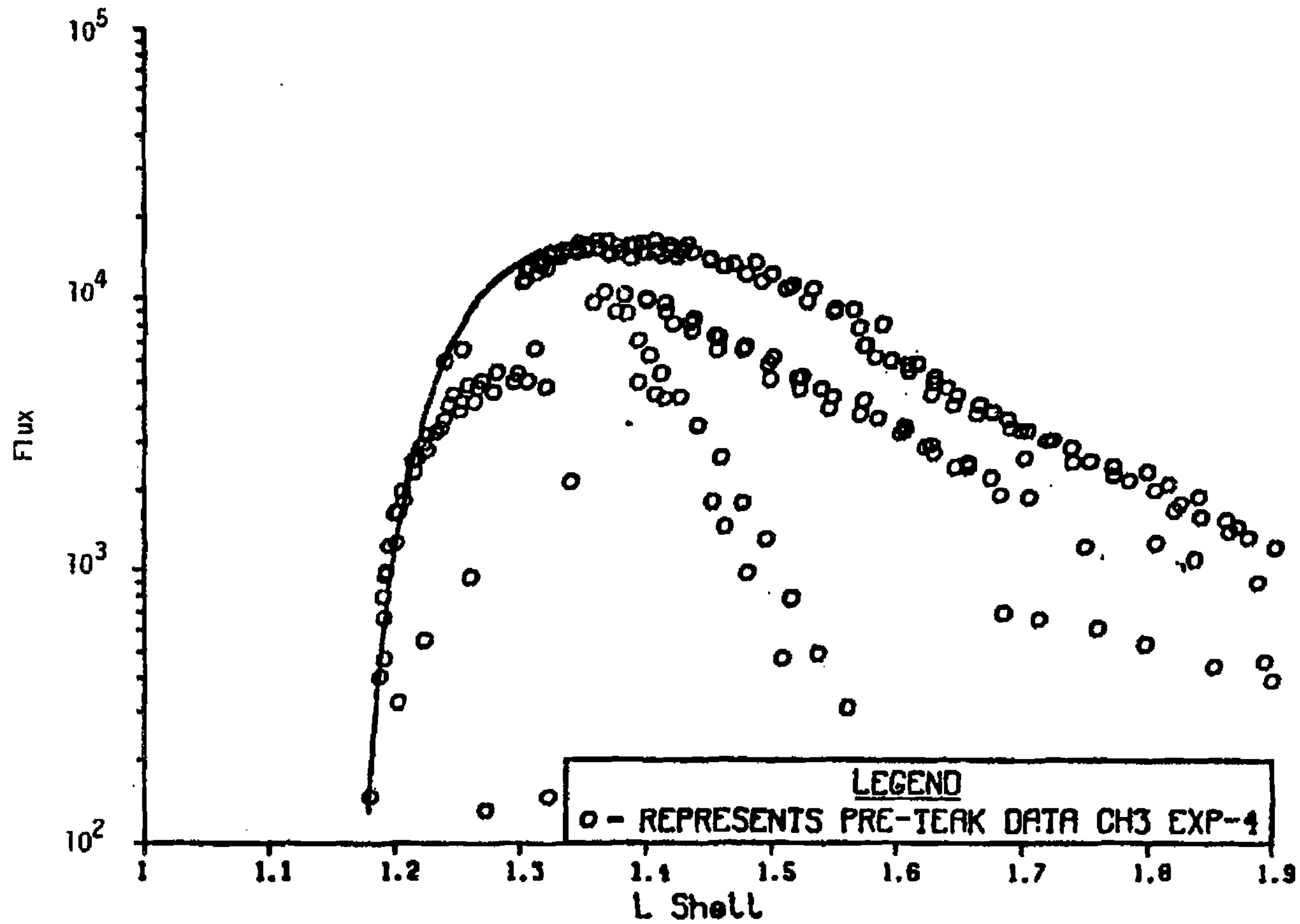

Figure 3-10. Explorer 4 Channel 3 Flux Versus L for Pre-Teak Days

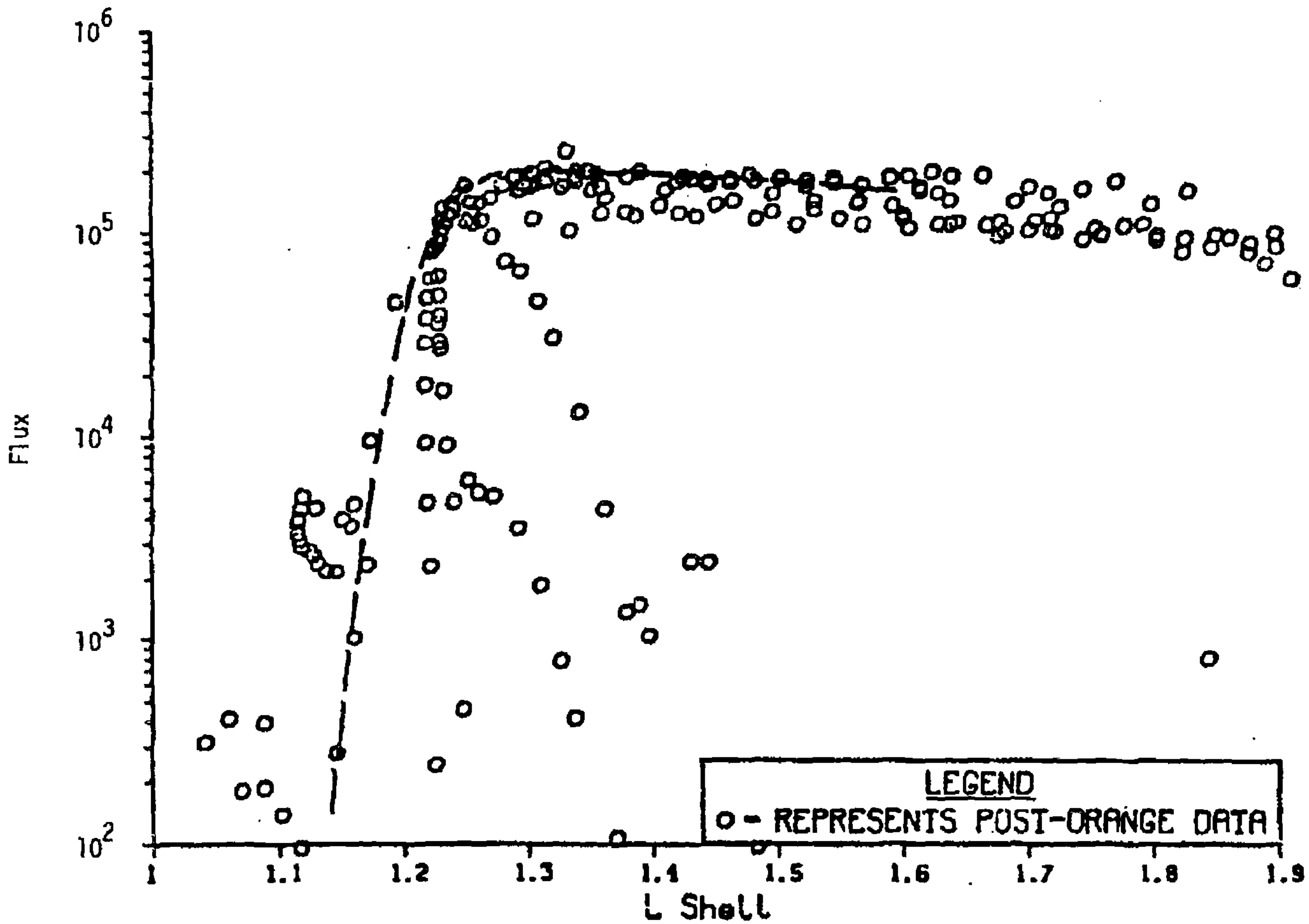

Figure 3-11. Explorer 4 Channel 2 Flux Versus L after the Orange Burst

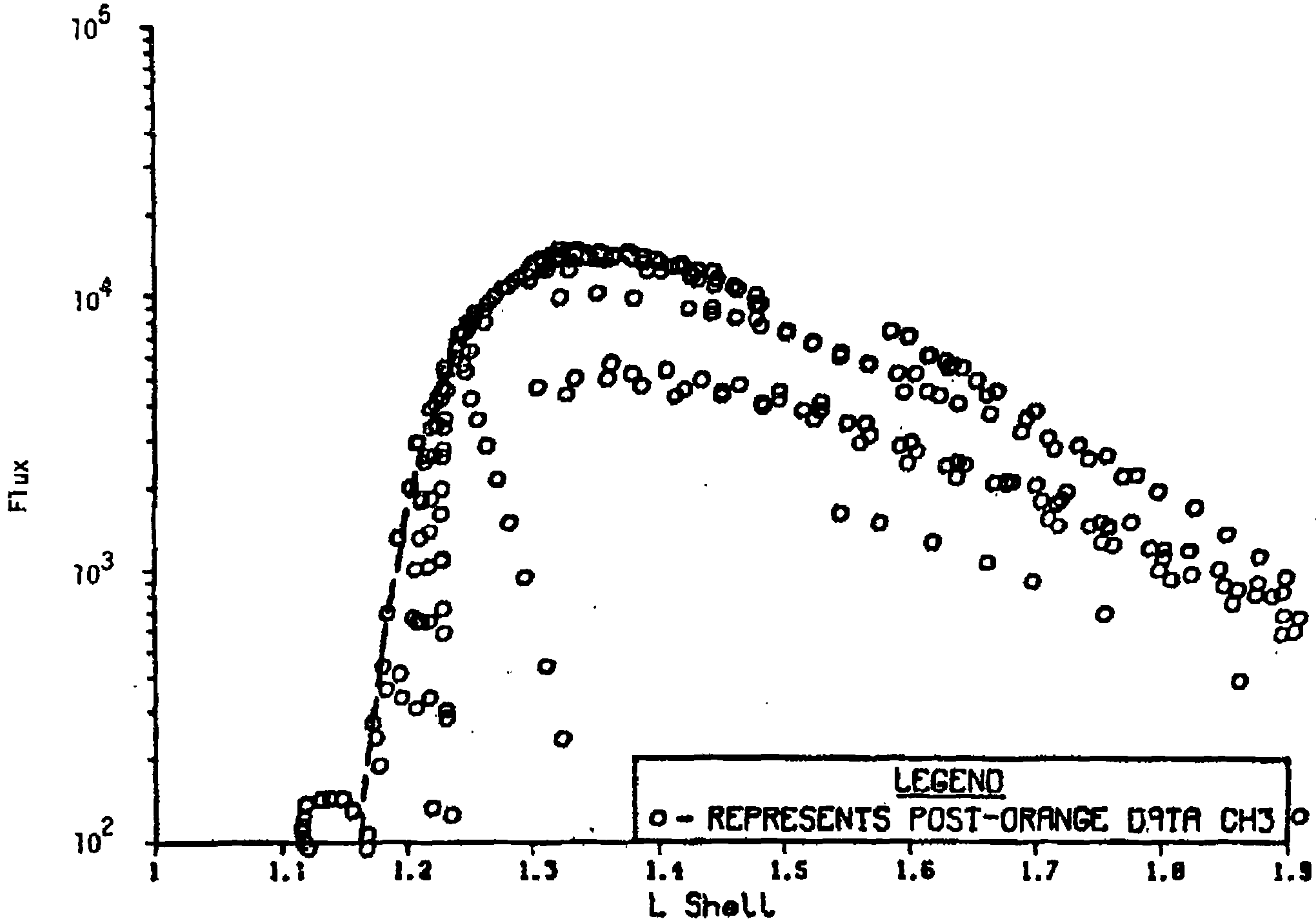

Figure 3-12. Explorer 4 Channel 3 Flux Versus L after the Orange Burst

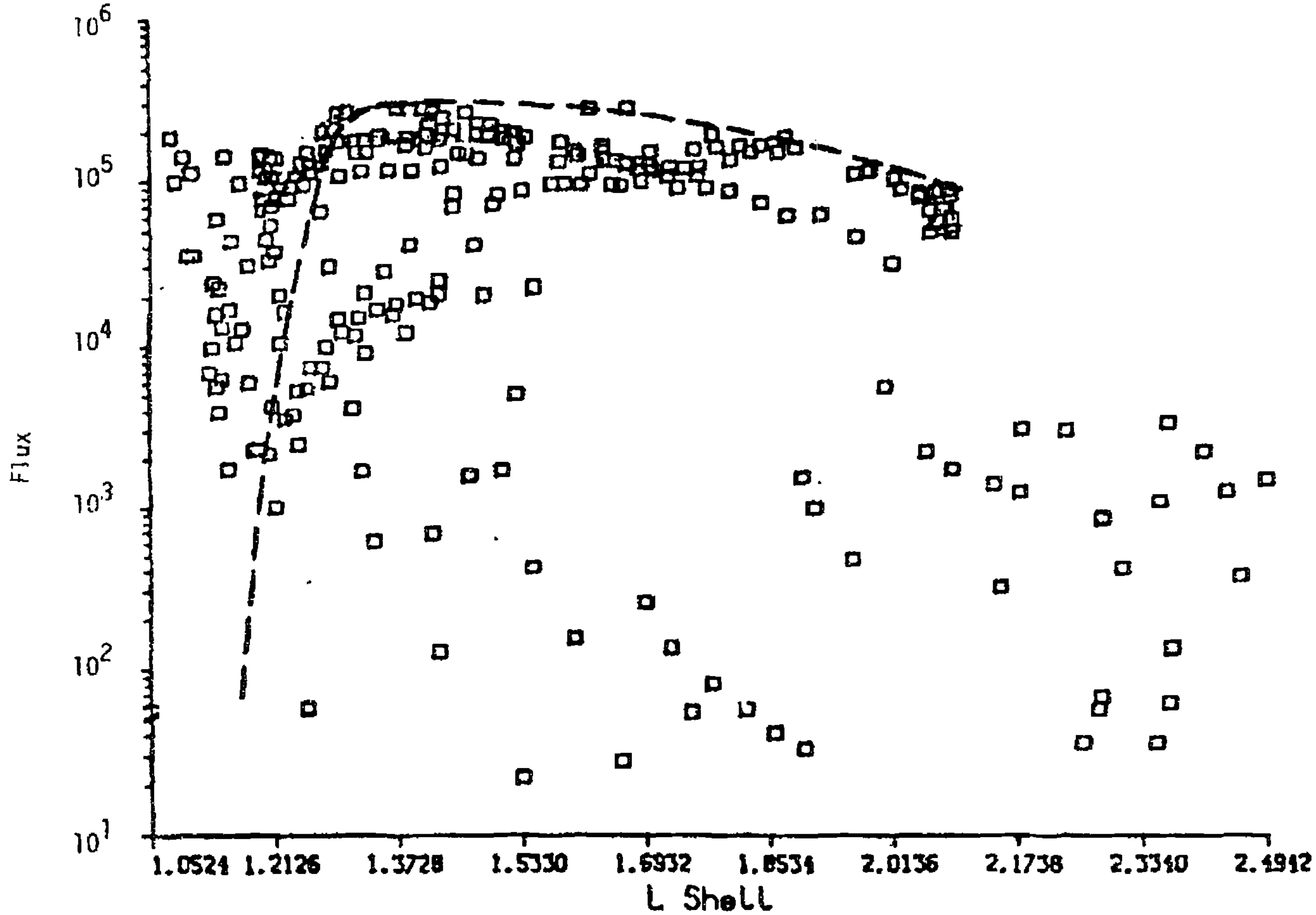

Figure 3-13. Explorer 4 Channel 2 Flux Versus L after the Teak Burst

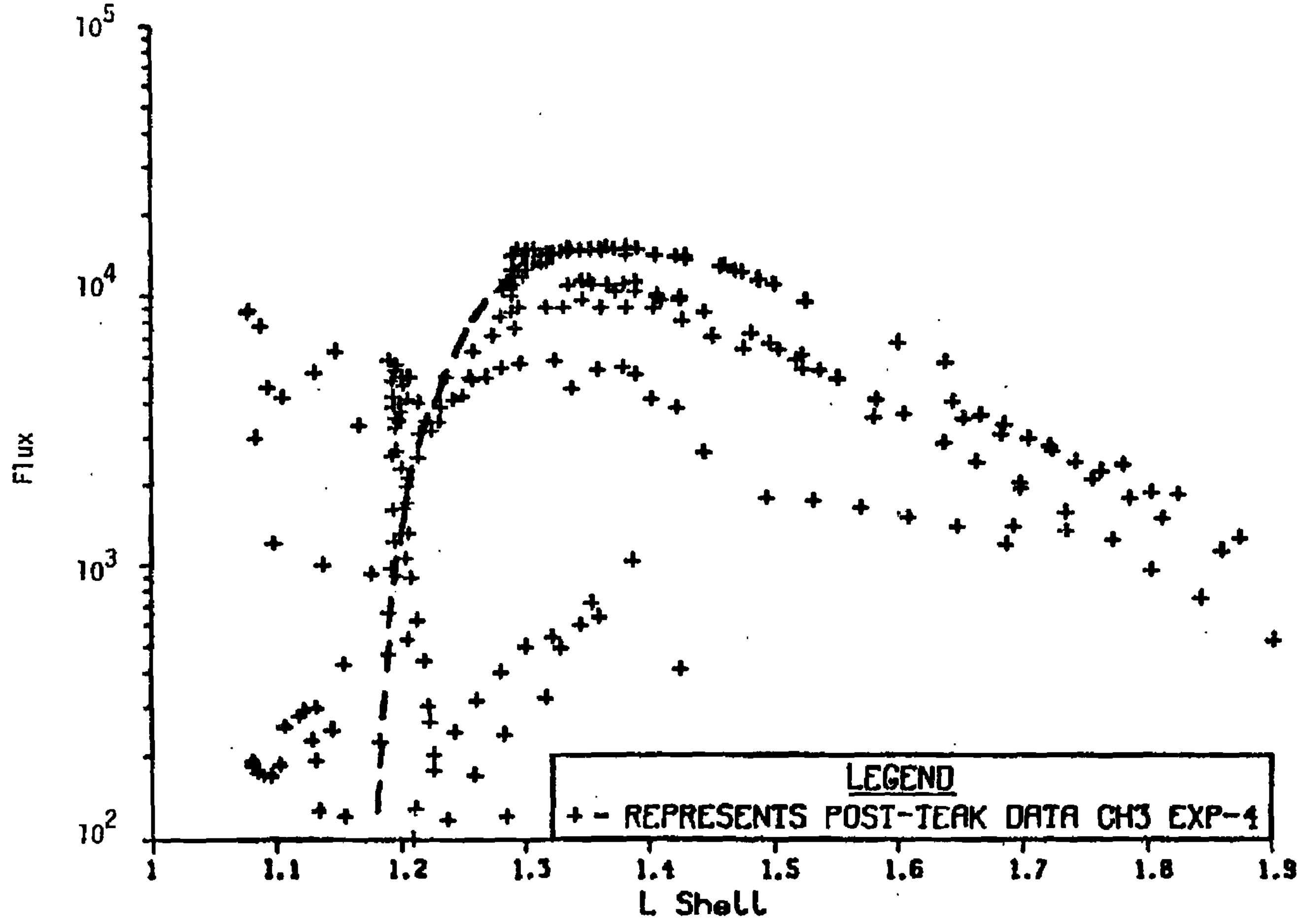

Figure 3-14. Explorer 4 Channel 3 Flux Versus L after the Teak Burst

detector. Many of the graphs also contained the background levels. If the background levels were not available, the background level was added to the graph using the tabulated background at the peak as a data point. Figure 3-15 is an example of a tabulated summary from the report which lists the pertinent flux levels for a given Argus shell crossing. Figures 3-16 and 3-17 give an example of the working data set.

Points from the graph were digitized using a Tektronix 4956 digitizing tablet and a Tektronix 4051 stand-alone computer. A cassette tape containing time and true count rates was made for each graph. The contents of this tape were then read directly into the AFWL computer using the 4051 in the terminal mode.

The above described digitization procedure produced only counts versus time. The plots did not have any position information. The University of Iowa report also contained several tables listing the altitude, latitude, longitude and time of the center of each shell crossing. The AFWL Environments Section (NYTCE) used these coordinate positions along with the known orbital parameters of Explorer IV to regenerate an ephemeris for Explorer IV. The ephemeris was forced to match at each shell crossing coordinate point. Thus B-L coordinates were made available as a function of time in the vicinity of each Argus shell crossing. These reconstructed B-L values were merged with the digitized data set. The final data tape was then produced with relative ease.

3.4 Error Analysis

Error analysis of the Explorer IV data presented no special problems. Statistical errors for the data set presented no special problems. On the tape as well as on the graph, the data were given as counts/sec. This was converted to counts per sample in order to evaluate the statistical error. The largest error of the experiment is the conversion of the directional counts for Channel 2 to omnidirectional fluxes. This can be highly dependent on the pitch angle distribution. Channel 2 was only used for Teak and Orange (no channel 2 Argus data was found) and for that time period extensive work by Manson and Paikeday (References 3 and 4) adequately evaluated the pitch angle distributions. The conversion to isotropic fluxes used the factors developed

Department of Physics — Iowa City, Iowa — Argus II

Date: 3 September 1958
Time (Z): 0842:14 ± 06

Geographic Long.: +144°43'
Geographic Lat.: - 28°49'
Altitude (Km): 2059
Λ_{1000}: - 33.23°
t_E: 101.40 hr
Distance to dipole: 8166 km

Channel 1

Peak Counting Rate	19.0
Background	6.0
Difference	13.0
Δt (1.2)	16 sec
Peak Intensity Time	0842:16±06

Channel 3

Peak Counting Rate	550
Background	30
Difference	520
Δt (1.2)	27 sec
Δt (1.10)	58 sec
Peak Intensity Time	0842:14±06

Channel 2 or 5 — no data

Time of Maximum
Maximum Counting Rate (M)
Max_1
Max_2
$M = \left(\frac{Max_1 + Max_2}{2}\right)$
Time of Minimum
Minimum Counting Rate (m)
min_1
min_2
$m = \left(\frac{min_1 + min_2}{2}\right)$

Channel 4 — noise

Time of Maximum
Maximum Ergs/sec cm^2 ster (M)
Max_1
Max_2
$M = \left(\frac{Max_1 + Max_2}{2}\right)$
Time of Minimum
Minimum Ergs/sec cm^2 ster (m)
min_1
min_2
$m = \left(\frac{min_1 + min_2}{2}\right)$

REMARKS: Average data.

Figure 3-15. Sample Argus Data Summary

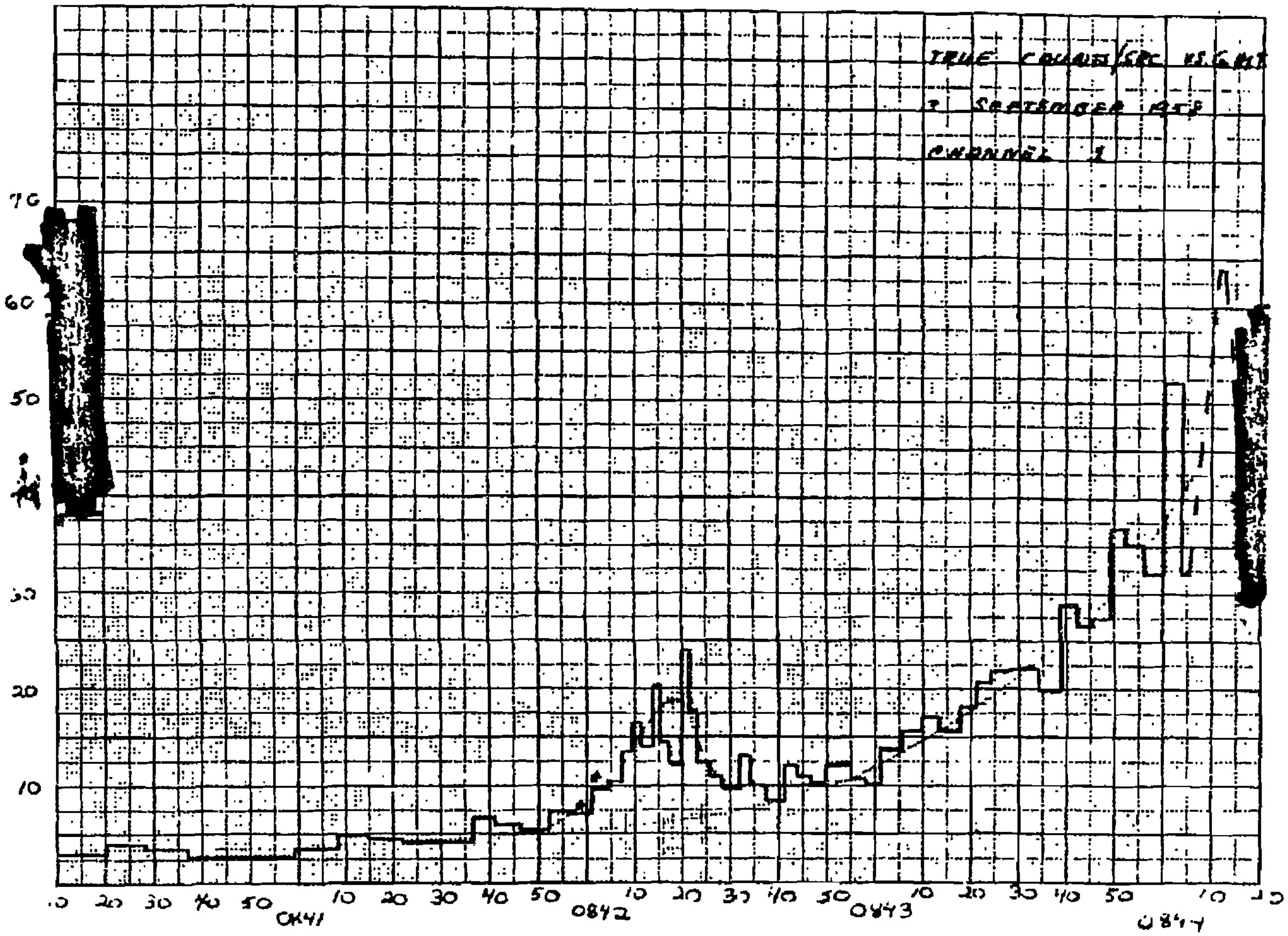

Figure 3-16. Sample Argus Data for Channel 1

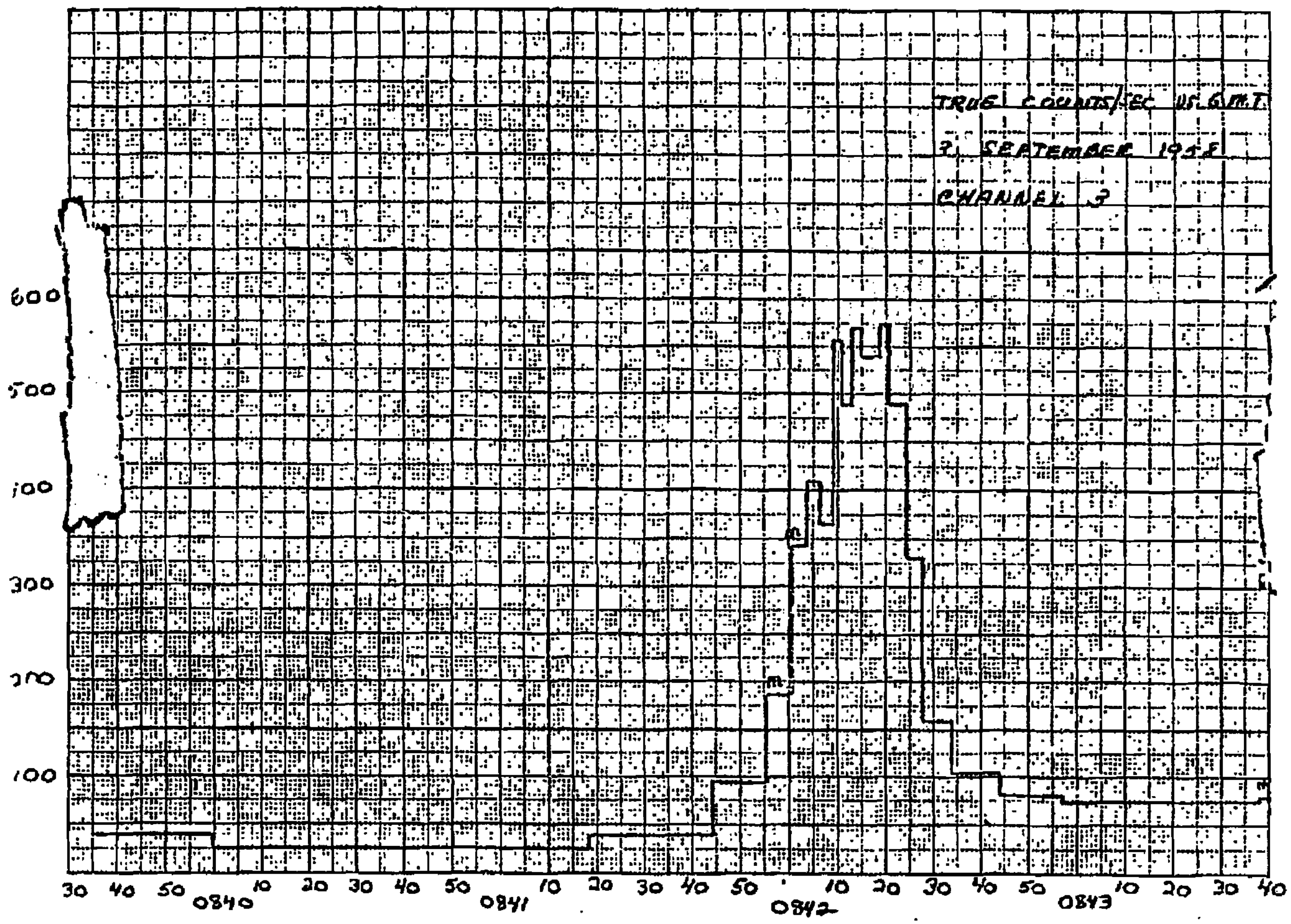

Figure 3-17. Sample Argus Data for Channel 3

during their analysis. It is estimated that the error in this conversion is no worse than 50 percent. Since response of the detector as a function of energy is not given it is not possible to evaluate sensitivity to the shape of the electron spectrum. Thus it was difficult to evaluate the error in the calibration of Channel 2. A 30 percent value was assumed.

Channels 1 and 3 are isotropic and the only errors are errors in calibration and statistics and a possible bremsstrahlung contamination. Calibration uncertainties were evaluated by varying the energy dependent geometry factor and the shape of the electron spectrum. Changes of 30-40 percent in the calibration factors were possible using reasonable changes in geometry factor and energy spectrum. The bremsstrahlung effect was impossible to estimate. It is expected to be small for Channel 3. However, the 6.2 MeV channel may be influenced by bremsstrahlung. A simple calculation is close enough to indicate that a problem is possible. Full evaluation of any bremsstrahlung effect would require a full mock-up of Explorer IV and a complex computer run using electron and X-ray transport in matter. This was outside the scope of this effort. If bremsstrahlung effects were present, the flux above 6.2 MeV would be overestimated. The ratio of the channel 3 MeV channel to the 6.2 MeV channel is consistent with a fission spectrum. Thus bremsstrahlung effects, if they exist, are probably small.

Background errors for Teak and Orange as well as Argus are very small. The effect of the burst is localized in space and limited in time and an excellent background evaluation can be made from adjacent data values. The error in the background is typically no worse than 10 percent and almost always better than 20 percent. The statistical flux error is $E_s = M_2 \sqrt{N_{D2}}$, where M_2 is the multiplier to convert counts/sample to flux and N_{D2} are the data counts in channel 2. The error equations used in this analysis were

for Channel 2

$$E_{T2} = \sqrt{(M_2 \sqrt{N_{D2}})^2 + (0.5F_2)^2 + (0.3F_2)^2 + (0.2F_{B2})^2} \qquad (22)$$

where E_{T2} is the flux error, F_2 is the channel 2 flux, and F_{B2} is the Channel 2 background flux.

for Channels 1 and 3

$$E_{Ti} = \sqrt{(M_i \sqrt{N_{Di}})^2 + (0.35 F_i)^2 + (0.2 F_{Bi})^2} \tag{23}$$

The definition of variables is the same as above, except i represents Channels 1 or 3.

Section 4
TELSTAR PROGRAM

The work with the TELSTAR data was the turning point in the analysis program. Initial attempts to work with the published data sets and rectify some of the known problems with the TELSTAR data were complicated by the lack of sufficient data in the published literature. The Bell Telephone Laboratory (BTL) data tapes were ordered from NSSDC (NSSDC tape No. 62-029-01A). These tapes were written in a BTL packed format generated on an IBM computer. Although decoding the tapes would involve the development of a very complicated assembly language computer program, the discrepancies between the published TELSTAR data and some of the other experiments could not be resolved without use of the data tapes. The analysis proved to be more complex than initially expected. However, the identification of a proton contamination (not reported in any of the literature) is believed to have been well worth the additional effort. It is now believed that the TELSTAR data is reasonably consistent with the other data sets.

4.1 Experiment Description

The experiment is very well described in the BTL journal (Reference 8) and a large number of other published reports. A short summary is reproduced below from Reference 8.

"The BTL electron detector is mounted so that it protrudes through the satellite skin and looks out perpendicular to the spin axis. Particles are accepted in a cone having an angle of 20 degrees with an 82-mil-diameter aperture immediately in front of the junction detector can. The deposition of energy by electrons in the sensitive volume of the detector is much less clearly related to the actual particle energy than is the case for protons. A 600-keV electron may leave all its energy in a sensitive volume 0.43 mm thick

---

8. Brown, W. L., Buck, T. M., Medford, L. V., Thomas, E. W., Gummel, H. K., Miller, G. L., Smits, F. M., The Spacecraft Radiation Experiments, The Bell System Technical Journal, 42, 899-942, 1963.

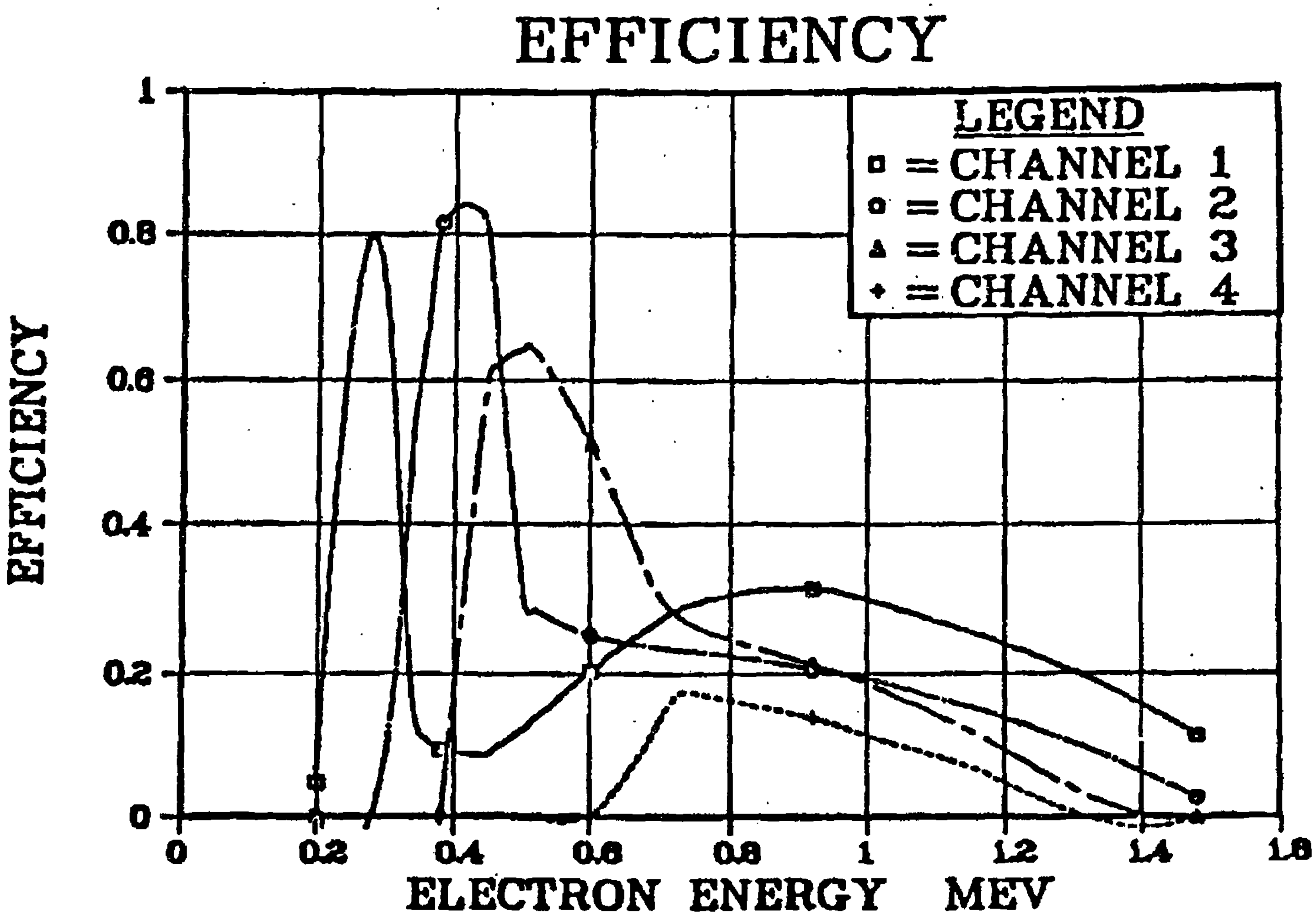

Figure 4-1. Efficiency Versus Energy for the Telstar Detectors

(the thickness of the electron detector on the Telstar satellite); it may back scatter in the first fraction of this thickness and leave only a small part of its total energy; or it may penetrate entirely and leave less than all its energy to be detected. By examining the distribution of pulse heights produced in the detector, only a rough evaluation of the spectrum of incident electrons can be obtained, since the spectrum must be unfolded from the distribution of pulse heights produced by monoenergetic particle groups. The probability that an electron of more than 1 MeV will leave all its energy in the sensitive detector thickness is very small. Such electrons can be detected by the lower energy pulses they produce, but their energy cannot be directly deduced.

In the Telstar electron detector, particle pulses are sorted into four pulse height channels: 180-280, 285-440, 390-615, and 635-900 keV. The bottom edges of these channels correspond to 215, 315, 420, and 660 keV, taking into account the energy lost by electrons in penetrating the 0.3-mil detector can window and an additional 1.6-mil aluminum absorber used to remove protons of less than 2.3 MeV. Pulses from two of the four channels are fed to the 14-bit telemetry register for three seconds each in every other telemetry frame. The second pair of channels, produced by a change in amplifier gain, is measured in the alternate frames.

The efficiency of each of the four channels for counting electrons up to approximately 1 MeV is illustrated Figure 4-1. Each channel starts abruptly as the energy requirement of the channel is met, but retains a substantial efficiency at electron energies above the upper pulse height limit of the channel.

The electron detector is potentially susceptible to background problems from protons. The addition of the 1.6-mil aluminum absorber eliminates the problem for very low energy protons. In addition, the top pulse height channel is closed. Pulses in excess of 990 keV will not be counted. To be recorded, protons must have energies greater than 2.4 MeV to penetrate the entrance window and leave at least 180 keV in the detector, but energy less than 2.7 MeV, so they do not leave more than 990 keV (a shield that stops 2.3-MeV protons will extract less than 2.3 MeV from 2.7-MeV protons). This very narrow energy range for proton acceptance makes the proton contribution to the counting rate small except when the electron flux nears the minimum values that it has in the Telstar satellite's portion of space.

Direct calibration of the particle detectors was carried out with electrons from a 1-MeV Van de Graaff generator and also with 17-MeV protons from the Princeton cyclotron (these calibrations were carried out with the kind cooperation of Professor R. Scheer of the Princeton University Physics Department).

Detector noise is an extremely important characteristic of the junction detector, particularly in the case of the electron detector, where pulses corresponding to particle energy losses in the detector of less than 200 keV are to be measured. Spurious noise pulses which even approach this threshold level are serious because of the distortion they produce in the pulse height distribution. The noise in low-noise devices can be examined most easily, not in terms of the probability of finding a spurious pulse equivalent to 200 keV, but as a broadening in the distribution of pulse heights produced in response to a series of uniform electrical pulses artificially introduced in the detector. The full width at half height of this pulse height distribution is measured and expressed in terms of an equivalent particle energy. Such noise linewidth measurements were obtained in all detectors under standard conditions, and in a number of cases whole sequences of noise measurements were made through a series of environmental tests."

4.2 Telstar Calibration

The Telstar calibration used in the literature converts the counts to total fission electrons greater than 0 keV. The Telstar experiment was designed to study electrons in discrete energy bands; however, this capability was not used very much in the literature. This lack of use of Telstar to determine the spectrum of the observed electron fluxes led us to a complete review of the Telstar calibration. It is this review that ultimately determined the proton contribution to the higher energy Telstar channels.

The Telstar electron detector was designed as a differential instrument. The characteristics of the instrument were adequately described in Reference 8. Of principal interest in this publication is the response of the detector to electrons of differing energies. Figure 4-1 shows the efficiency of the solid state detector to electrons of differing energies. The most noteworthy aspect of these curves is that, although Channels 1, 2 and 3 have an enhanced response over a limited energy band, there is a large response at much higher energies. To check the effect of this high energy tail in the efficiency curve, the response functions were folded into a fission spectrum, $f(E) \propto e^{-1.1 E}$. The counts seen by the 1-MeV detector at the various energies when exposed to a fission spectrum is shown in Figure 4-2. Figure 4-3 is the integral of Figure 4-2. This integral curve shows the counts in the various channels due to electrons having an energy less than E. The low energy, high response region of Channel 1 accounts for less than 25 percent of the observed total count rate. This indicates that the Telstar detector is not a very good differential instrument, and that although it does have an enhanced low energy efficiency, its response to high energy electrons dominates the total count rate.

Various schemes were attempted at this time to remove the high energy tail of this response function and create a detector response that is limited to the specified energy. Since the response of Channel 4 looked similar to the high energy tail, various percentages of Channel 4 were subtracted from Channels 1, 2 and 3 in order to make the response of the detectors more specific. Although this effort made the response functions look more like true differential detectors, this technique produced spectra which were inconsistent and could not be interpreted (the correction was too energy dependent).

It was finally decided that although BTL had declared the detector response differential, its response in the presence of a fission spectrum made it appear to have an integral response. Thus the entire BTL calibration was reworked beginning with the published response curves (Figure 4-1). Figure 4-1 gives the efficiency as a function of energy for the four detectors. The counts/sec measured by the instrument's ith channel can be written as

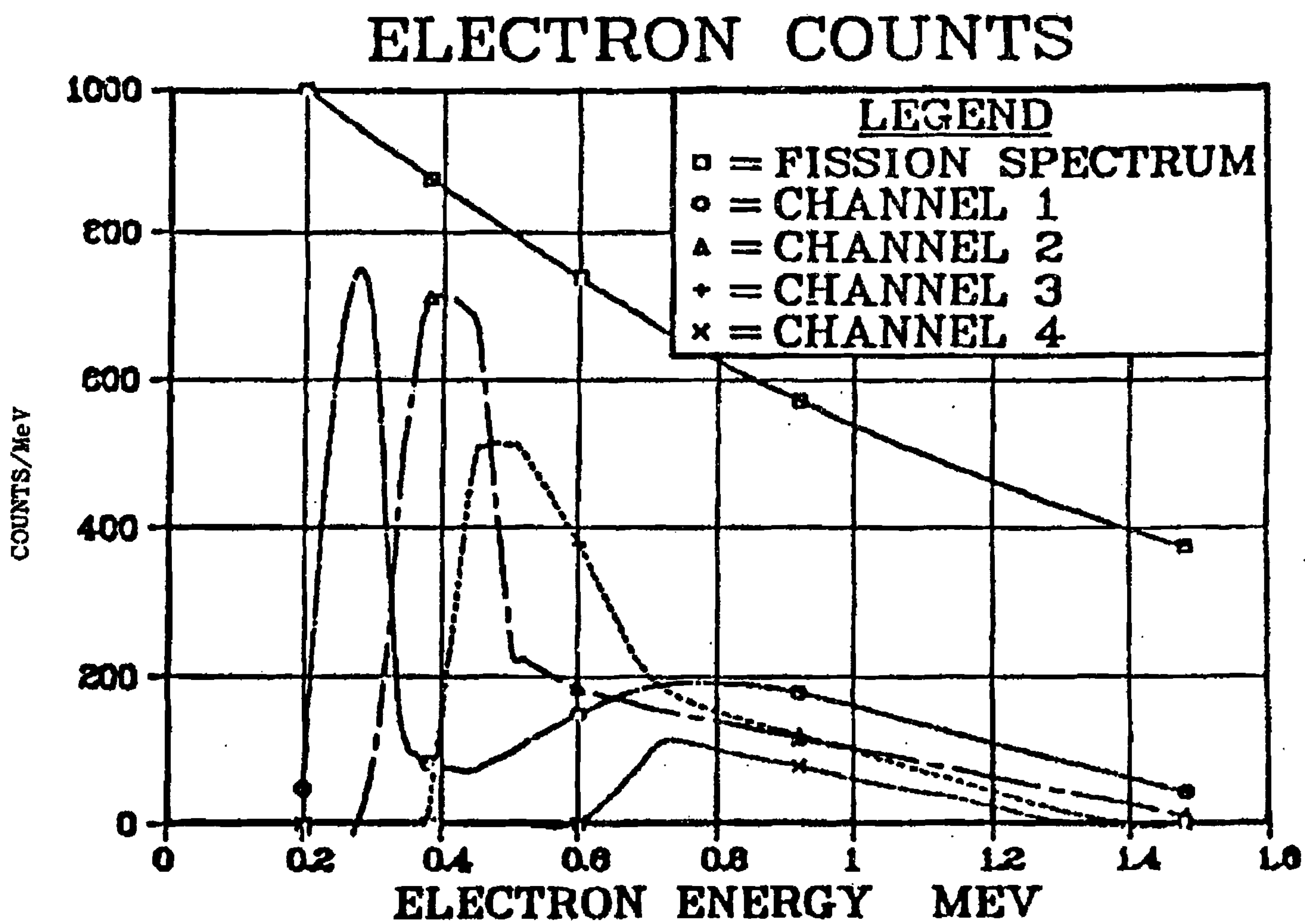

Figure 4-2. Counts/MeV as a Function of Energy in Each of the Telstar Channels in the Presence of a Fission Spectrum

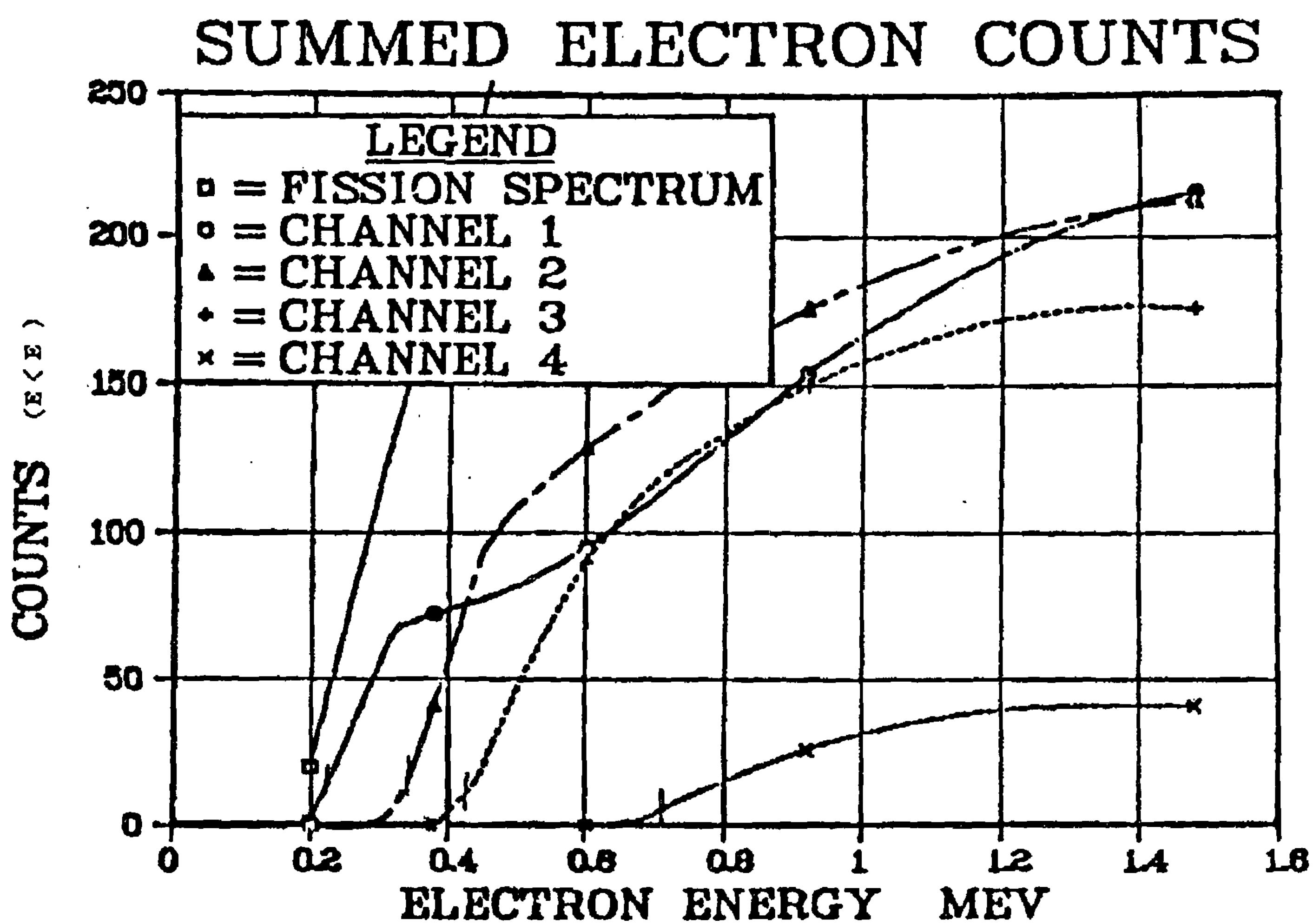

Figure 4-3. Counts in the Four Electron Channels due to Electrons Having Energy Less Than E

$$C_i = G \int_0^{\infty} \varepsilon_i(E)\, f(E)\, dE \tag{24}$$

where C_i is the counts/sec of the ith channel, G is the geometry factor of the fixed acceptance cone, $\varepsilon_i(E)$ is the energy dependent efficiency curve, f(E) is the electron spectrum in electrons/cm^2/sec/keV.

The integral flux, the flux of electron above some energy E_i is given by

$$F\ (E \quad E_i) = \int_{E_i}^{\infty} f(E)\, dE \tag{25}$$

To simplify the conversion of counts/sec to integral flux, we need to determine an average efficiency-geometry factor such that

$$C_i = \bar{G}\, \bar{\varepsilon}_i\, F\ (E > E_i)$$

$$\bar{G}\, \bar{\varepsilon}_i = \frac{C_i}{F\ (E > E_i)}$$

$$= \frac{G \int_0^{\infty} \varepsilon_i(E) f(E)\, dE}{\int_{E_i}^{\infty} f(E)\, dE} \tag{26}$$

The above integrals were initially evaluated using the fission spectrum. However the resultant $\overline{G}_i\ \overline{\varepsilon}_i$ produced spectra steeper than the fission spectra. Thus the $\overline{G}_i\ \overline{\varepsilon}_i$ were reevaluated using a spectrum of the form $e^{-1.6E}$ and the resultant $\overline{G}_i\ \overline{\varepsilon}_i$ were used to determine the integral flux as seen by Telstar.

These integral efficiencies were applied to a large body of Telstar data and provided results that were totally inconsistent with reality. The results obtained gave an integral spectrum with a positive slope (Figure 4-4). Channel 4 was consistently higher than Channel 3 and Channel 3 occasionally was higher than Channel 2. An integral spectrum must have a negative slope. Considerable effort was expended at this point checking the calculations and reevaluating the efficiency values for many differing exponential and power law spectra. Nothing helped very much. The spectra continued to have a positive slope. We began to doubt our ability to decode the tapes properly and the validity of treating Telstar as an integral detector.

At this point it was noticed that the positive slopes were worse at later times, times much past Starfish and worse at larger L's. This began to suggest that, many claims to the contrary, Telstar was responding to something other than electrons. The first effort evaluated the Telstar response to bremsstrahlung. This was a very crude back of the envelope exercise but it proved that Telstar did not have a bremsstrahlung problem.

The BTL journal states that the Telstar detector is sensitive to protons only in the range of 2.3-2.7 MeV and that the number of protons in this range is insufficient to produce any contamination of the observed count rate. However, the Vette AP8 environment was used to determine the number of protons in the specified energy range; this was then combined with detector size and geometry factor and was found to produce counts comparable to the observed count rate in the vicinity of $L = 2$. The result was checked many times and in each case gave the same answer, <u>the Telstar channels 3 and 4 were responding to protons</u>. Since the exact response to protons is obviously not available, the exact proton correction was difficult to determine. The proton spectrum between 2.3-2.7 MeV is flat to within 15 percent (i.e., the change in intensity over such a small energy interval is small). Thus an energy independent proton flux was used on one side of an absorber such that the

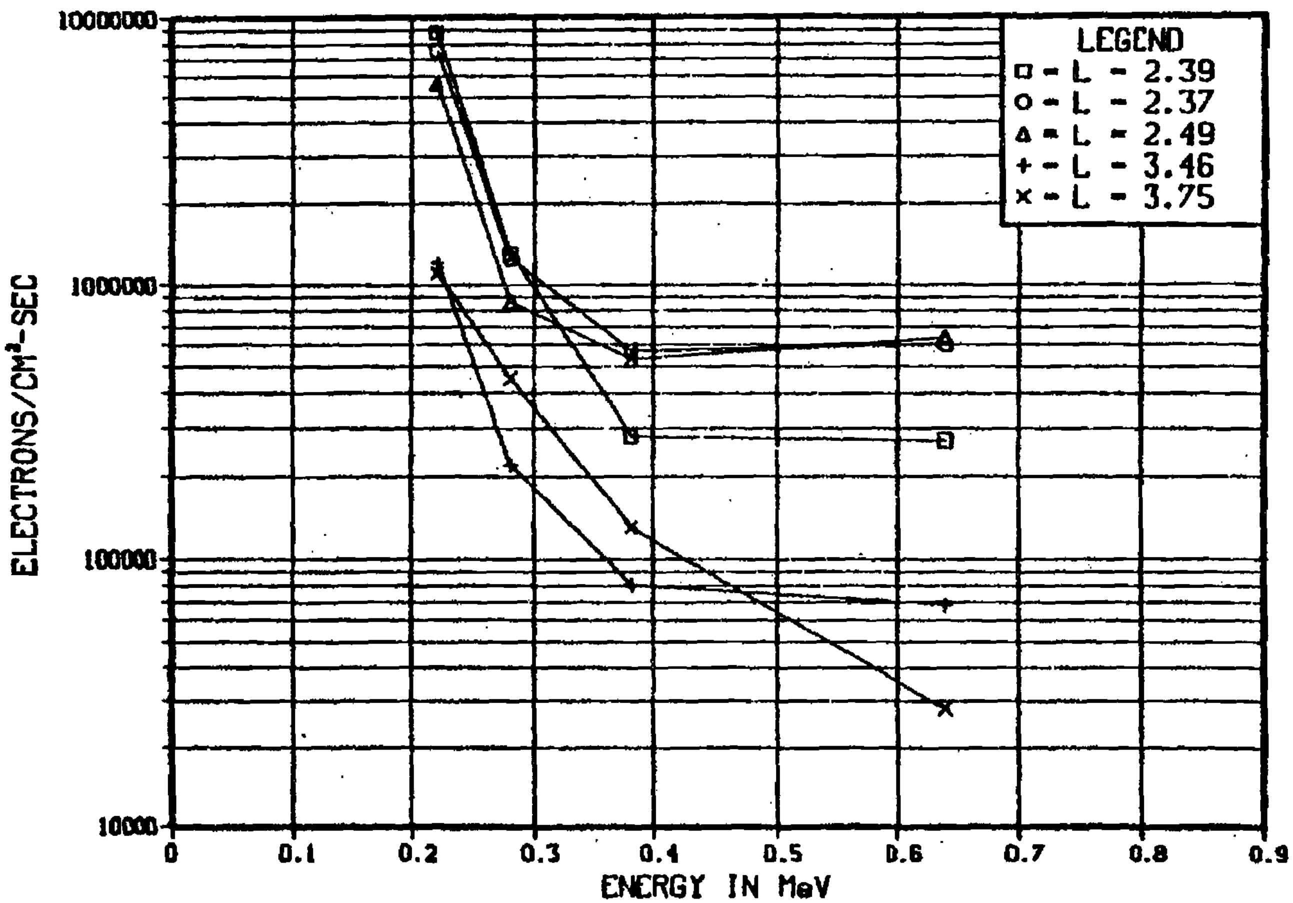

Figure 4-4. Telstar Integral Spectra Uncorrected for Protons

protons had a residual energy of 0.4-1.0 MeV after passing through the absorber (the amount of energy required to trip the channel 3 and channel 4 discriminators). The proton energy distribution on the other side of the absorber was increased and the residual calculated. This crude hand calculation determined that the proton contamination to channels 3 and 4 were very similar in magnitude.

The proton correction was implemented by entering the AP8 2 MeV-proton curves into the computer and using a linear interpolation routine to evaluate the 2-MeV flux values at a given B and L. Figure 4-5a and 4-5b are copies of the AP8 curves used to evaluate the proton background. The AP-8 curves gives B and L a dependence of the proton flux. The geometric conversion factor for protons could not be calculated. However, since there were places later in the post Starfish period when the proton contamination accounted for over 90 percent of the channel 4 count rate, the proton geometry factor could be experimentally determined. The factor for converting the 2 MeV AP-8 flux curves to proton counts was found to be ~ 2.0. Multiplying the Vette AP8 2 MeV protons/cm^2/sec by the factor 2 produced a correction to the Telstar counts such that the integral spectrum (derived using the newly determined integral response values), gave consistent results (negative slope) over all B and L space.

This proton correction has been applied to all Telstar results. The Telstar proton effect is strongly believed to account for many of the discrepancies in the literature.

The calibration constants which were used to convert counts/sec to flux greater than the specified energy are given in the Table 4-1 below.

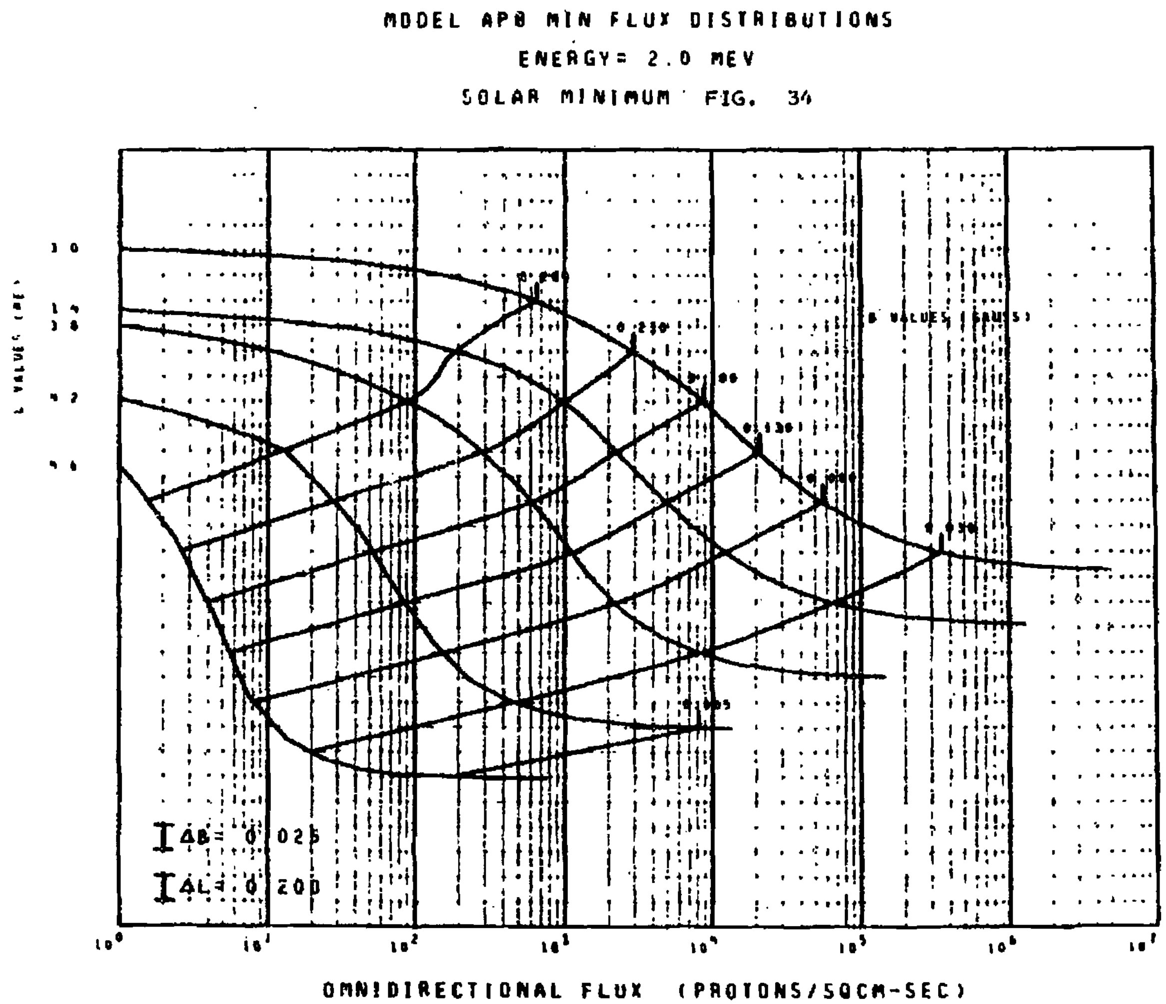

Figure 4-5a. AP8 Model Flux Distribution

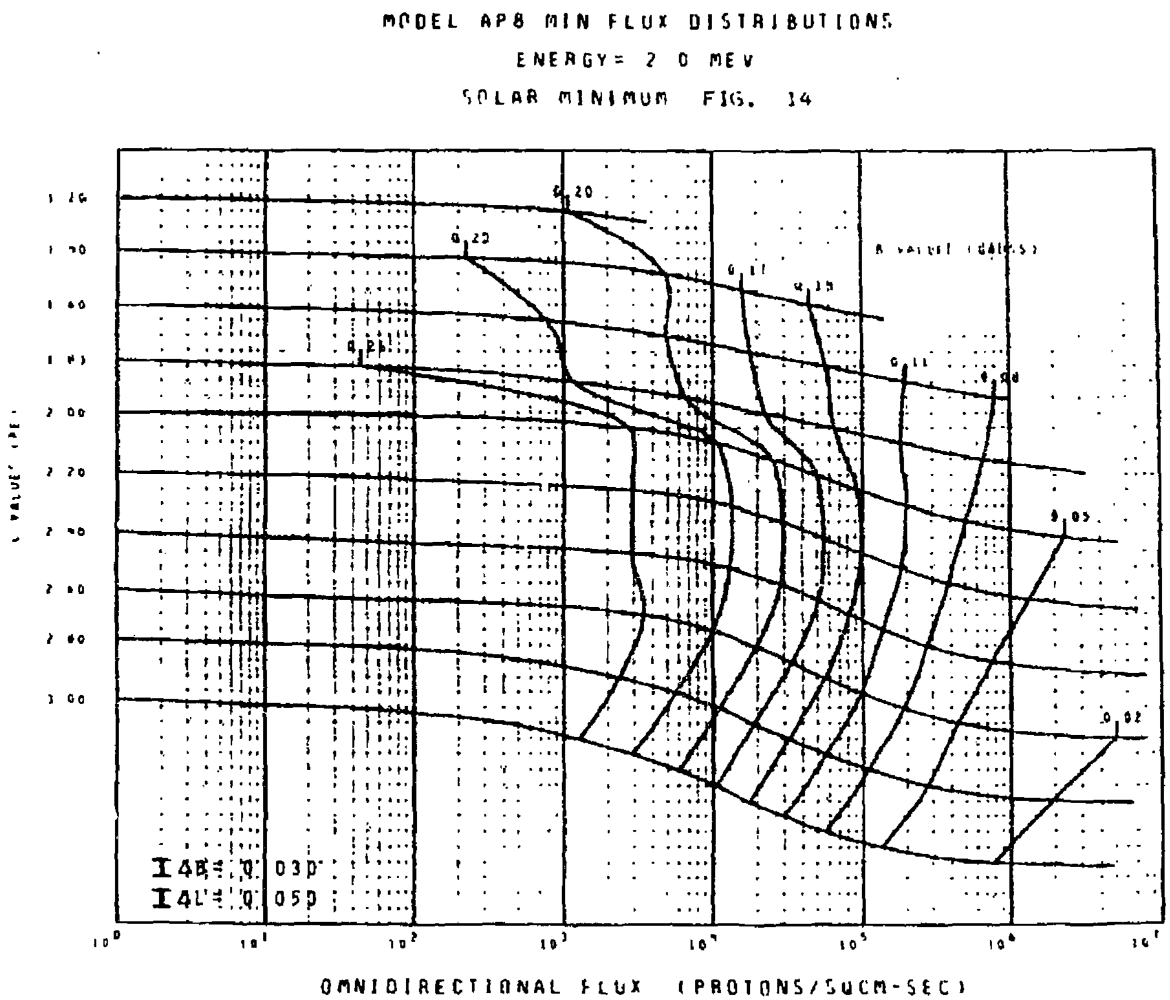

Figure 4-5b. AP8 Model Flux Distribution

Table 4-1

TELSTAR EFFICIENCY VALUES

Channel Number	Energy	$\frac{1}{\bar{G}\,\bar{\varepsilon}}$
1	220 keV	7.3×10^3
2	320 keV	6.6×10^3
3	420 keV	6.5×10^3
4	660 keV	1.3×10^4

4.3 Telstar Data Analysis

Initial work using published data was unable to produce the integral flux values required by AFWL. Telstar was the first data set ordered from the NSSDC to try to improve the data results. As indicated in the last section, considerable difficulties were encountered due to proton contamination. The proton contamination would not have been discovered if only published results were used.

The Telstar data tapes were written in IBM packed format and an assembly language program for the CDC Cyber computers was developed to read the tape. After the tapes were finally read and converted to CDC useable numbers, the published geometry and correction factors were applied and comparisons between tape derived data and the published data sets were attempted. This unfortunately was not a simple task. Initially there was some confusion as to the meaning of the geometry and solid angle factors but after several weeks it was still impossible to rectify published and calculated data. Finally, iso-intensity contour plots in B, L space covering the same time interval as iso-intensity contour plots in the literature were generated. It was assumed that both the channel identification as well as the calibration information was unknown. This technique solved the mystery. The four channels had different B, L behavior, and the B, L dependence between the tape data and the published data could be matched within a uniform multiplier only if the channel identifications were reversed from the tape documentation. The tape recorded data contained a bit indicating high and low amplifier bias. If the sense of this bit was changed, the B, L dependence matched the published data within a multiplicative constant. This multiplicative constant was calculated and found to agree with the published geometry factor.

Earlier attempts had been made to reverse the channel identification but these always lead to positive slope integral spectra, and thus were ruled out. The existence of two unknown problems complicated the analysis task and consumed a great deal of effort and time.

Once the channel identifications were unambiguously defined, the data set was ready for processing. If the data quality control bit (contained on the NSSDC tape) was used, random noise was not a problem. The positive integral spectra discovered earlier became a fact of life. The discovery and removal of the proton contamination described in the last section was then implemented for all of the data. An intermediate tape containing time, B, L, look direction and data were generated.

4.4 Background Evaluation

For the Starfish burst, the most important background source was the above described proton contamination. The electron fluxes observed by Telstar were well above what is now our current understanding of the natural flux electron levels. The only exception to this may have been during the first few hours of Telstar, before a complete electron rearrangement took place. In this case the natural electron flux is the background level.

The channels 1 and 2 background levels are set to zero. The proton flux contamination for channels 1 and 2 is smaller than the uncertainty in determining the proton effects and thus the background was set to zero for these channels prior to the Russian event. The Channels 3 and 4 background prior to the Russian burst was set to the AP8 proton determined levels. (Figures 4-5a and 4-5b show the AP8 curves used for this analysis.)

To isolate the effects of the Russian bursts from the Starfish burst, the uncorrected (not corrected for protons) Telstar data for days 285-294 were fit with a polynomial in B and L. The polynomial defined the Telstar background just prior to the Russian bursts. This background includes the effect of the protons as well as the Telstar electron effect. Figures 4-6 and 4-7 show the Telstar data just before and after the Russian I burst. A separate attempt was made to fit the proton corrected data and subtract the proton and Starfish data as separate functions. It was found that the single correction (a fit to proton plus Starfish) produced a much more consistent data base. Therefore the discrete (proton separate from Starfish correction) was abandoned. Two separate data tapes were generated for Telstar. The first is a proton corrected data tape for the Starfish event; the second is a tape of the Russian series with the Starfish and the proton background removed.

4.5 Error Analysis

The basic errors for the Telstar data are: statistics, uncertainty in the calibration, uncertainty in the background, and conversion to isotropic flux.

The Telstar detector was designed to be a differential instrument. However, sensitivity to high energy electrons permitted its use as an integral instrument. Its non-uniform response over the large energy range can introduce substantial possibilities for error. The efficiency factors were strongly dependent on the electron spectra. Small inaccuracies in the efficiency curves, especially in extending the curves to energies beyond the published energy values, can also introduce errors. It is estimated that these effects can introduce a deterministic (i.e., they can affect all of the data for a given channel the same way) error of approximately a factor of 2.

The statistical error is given simply as the square root of the number of counts/sample. Additional errors such as conversion from the spin-averaged isotropic fluxes, to the true isotropic fluxes, errors in orbit, etc., are quite small and are less than 30 percent. Changing the proton background up by 30 percent produces negative flux values over a substantial space region and decreasing the proton contribution by 30 percent produces a substantial

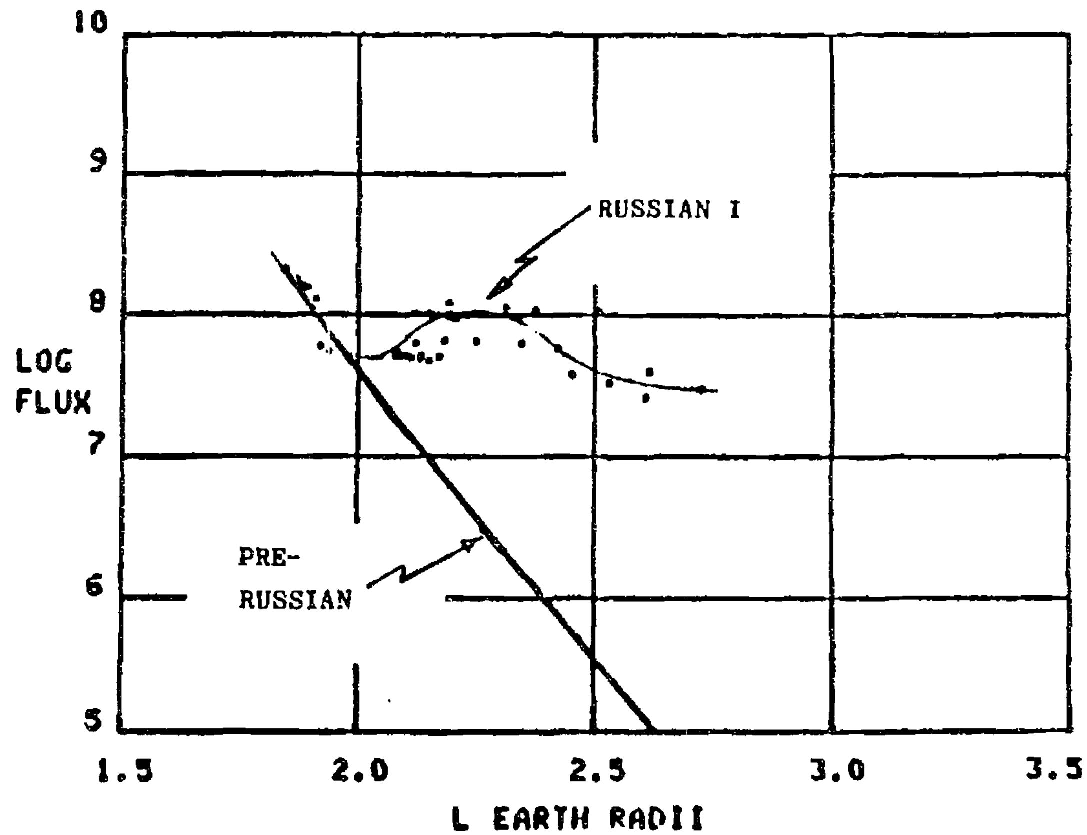

Figure 4-6. Telstar Pre and Post Russian I Flux Values for the 220 keV Telstar Detector

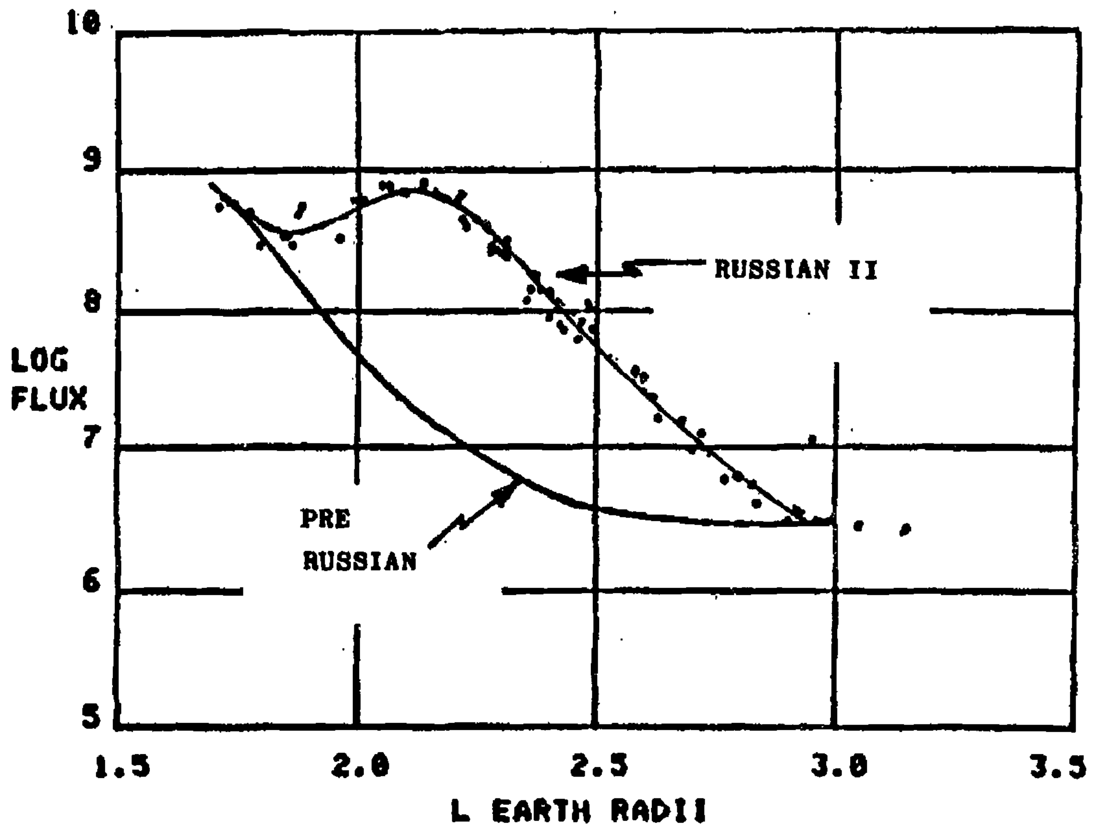

Figure 4-7. Telstar Pre and Post Russian II Flux Values for the 220 keV Relstar Detector

region where the fluxes cause an integral spectrum with a positive slope. For the Russian burst, the root means square (rms) error of the least squares fit was approximately 40 percent.

Thus the total random error for the Telstar count rate is

$$E_T = \sqrt{E_s^2 + E_D^2 + E_B^2} \tag{27}$$

$$E_s = \sqrt{N_D} \tag{28}$$

$$E_D = 0.3\ N_D \tag{29}$$

$$E_B = 0.4\ N_B \tag{30}$$

where N_D is the counts/sample, N_B is the background counts, and E_T is the total counts rate error, E_D is the deterministic error in the channel to channel calibration and E_B is the uncertainty in the background flux.

The deterministic error was not included in the error specified with each data point. The user of the data tape is reminded at the start of the tape that an additional factor-of-two error might apply.

Section 5

EXPLORER XV

Explorer XV was launched just before the Russian II burst. Explorer XV contained a number of instruments designed to measure the effects of the Starfish burst. The spacecraft contained two separate instruments for measuring electrons. One was a BTL instrument measuring electrons in three different energy ranges, and the other an instrument by C. McIlwain measuring electrons in a single energy. The initial analysis was started using the BTL instrumentation because it contained three different energy intervals and, more importantly, many of the data reduction programs developed for the Telstar analysis effort could be used. The tape read program is usually the most complicated part of the analysis effort. For the BTL Explorer XV experiment, the assembly language program developed for Telstar could be used with only minor changes.

5.1 Explorer XV Experiment Description

The best description of the Explorer XV instrumentation was given in the Final Report on the BTL Experiments on Explorer XV (Reference 9). The pertinent information is reproduced here.

"The particle experiments were designed to measure the distribution of electrons in the trapped radiation belts with good spatial and time resolution and to provide information on the spectral characteristics and angular distribution of these particles. The primary intent was to study the injection of new electrons into the trapping region by high altitude nuclear explosions and the subsequent disappearance of these particles by atmospheric scattering and other loss mechanisms. Explorer XV was launched on October 27, 1962, three and one-half months after the U.S. Starfish nuclear test in the

---

9. Documentation of the BTL Satellite Data Tapes, Bell Telephone Laboratories, Murray Hill, N.J.

Pacific and five days after a high altitude nuclear test by the Soviet Union on October 22. On October 28, a few hours after launch, the satellite observed the addition of new particles as a result of a second Soviet high altitude test. Four days later, on November 1, it detected electrons from the third test in the Soviet series. There were thus opportunities to observe transient phenomena associated with impulsive injections of particles at widely different phases of their time history. With its apogee at about 4 earth radii, in the outer Van Allen electron belt, Explorer XV was able to measure the natural fluctuations in the properties of that particle population. It was also possible to carry out measurements on relatively low energy protons whose distribution in space had not previously been determined.

All of the particle experiments by Bell Laboratories on Explorer XV made use of semiconductor p-n junction detectors as their particle-sensitive elements. The p-n junction region of the detector contains a high electric field developed by an applied bias potential. This region is a solid state ionization chamber in which holes and electrons created by a high energy charged particle are collected and produce an output pulse. Holes and electrons are generated in silicon in proportion to the energy lost by incident particles. Thus the output pulse of charge is in magnitude proportional to the amount of energy the particle loses in the active, field containing region of the device. This region is disc shaped in the device, about 2.6 mm in diameter and, at 100 volt bias, about .4 mm thick. By making use of the different energy loss characteristics of electrons and protons and by changing the thickness of the active region by a change in bias, it is possible to distinguish electrons and protons from one another in this type of device. These detectors have output pulse rise times of less than .2 μsec. As a result, they can readily be used to study the particle distribution in the high intensity regions of the inner and outer Van Allen belts.

Particles are intended to reach the detector through an aperture 2 mm in diameter in the lid of the can. This aperture is covered with a 0.3 mil Koval diaphragm which completes the vacuum tight encapsulation of the device to avoid changes in its surface. This window also serves the important function of excluding light and very low energy particles which are heavily damaging to semiconductor devices. In the detectors of Explorer XV, additional absorbers are added in front of the Koval window to make the minimum mass thickness seen by the particles approximately 20 mg/cm^2.

The experiments utilize six detectors of the type described above, mounted in different arrangements of shielding and provided with different thicknesses of absorber for measurements of electrons of different energies. Table 5-1 lists the detectors, their approximate threshold energies, their angular acceptance and their effective geometrical factors. For all six detectors a pulse height discrimination level of approximately 0.4 MeV has been established. Detector A is unique in having a second discrimination level set at 2.7 MeV. The effective geometrical factors given in Table 5-1 apply at a detector bias of 100 volts where the detectors have an active thickness of about 0.4 millimeters. The devices are also supplied a 5 volt bias in part of the experiment. At this lower value, the active thickness is reduced to approximately .12 millimeters. This change reduces the electron detection efficiency by a factor of approximtely 100 because of the low probability that an electron will leave at least 0.4 MeV in such a thin active region. The detection efficiency for low energy protons is essentially unaffected. By comparing the counting rates at 100 volts and 5 volts bias, the proton and electron components of the counting rate can be separated. For the output channel E4 with its high discrimination level, the detection efficiency for electrons is extremely small and the detector counts only low energy protons."

5.2 Calibration

The Explorer XV calibration was adequately described in the BTL document. A brief summary of this calibration is given below.

5.2.1 Calibration of 0.5 MeV Channel

The detection characteristics of this detector have been measured with a Sr^{90} beta source and with monoenergetic electrons up to 2 MeV. The angular response of the detector is shown in Figure 5-1 with the Sr^{90} source. Measurements were made with essentially point source geometry. The detector is displaced behind the truncated end of the entrance cone of the shielding block in order to reduce the probability of electron scatter into the

Table 5-1

EXPLORER XV INSTRUMENT SUMMARY

Detector	Channel	Pulse Height Discrim. MeV†	Absorber g/cm^2	Threshold Energies Electrons MeV	Threshold Energies Protons MeV	Full Angular Aperture	Math. Geometrical Factor cm^2 ster.	Effective Geometrical Factor for Electrons cm^2 ster.
A	E1	0.408	0.020	0.5	2.1	20°	2.9×10^{-3}	6.5×10^{-4}
	E4	2.7	0.020	2.8	4.0	20°	2.9×10^{-3}	
B	E2	0.411	0.42	1.9	15	2π (20°)	*2.9×10^{-3}	5.5×10^{-4}
C	E3	0.408	0.84	2.9	22	2π (30°)	*6.5×10^{-3}	~9×10^{-4}
D	E5	0.402	6.3	background		4π	2×10^{-1}	
E	E6	0.410	0.020	0.5	2.1	10°	4.7×10^{-4}	1.6×10^{-4}
F	E7	0.413	0.41	1.9	15	14°	9.4×10^{-4}	~1.5×10^{-4}

*Assuming uniform scattering over 2π solid angle for electrons penetrating a hemispherical dome.

†Energy equivalent of charge pulse required by the discriminator.

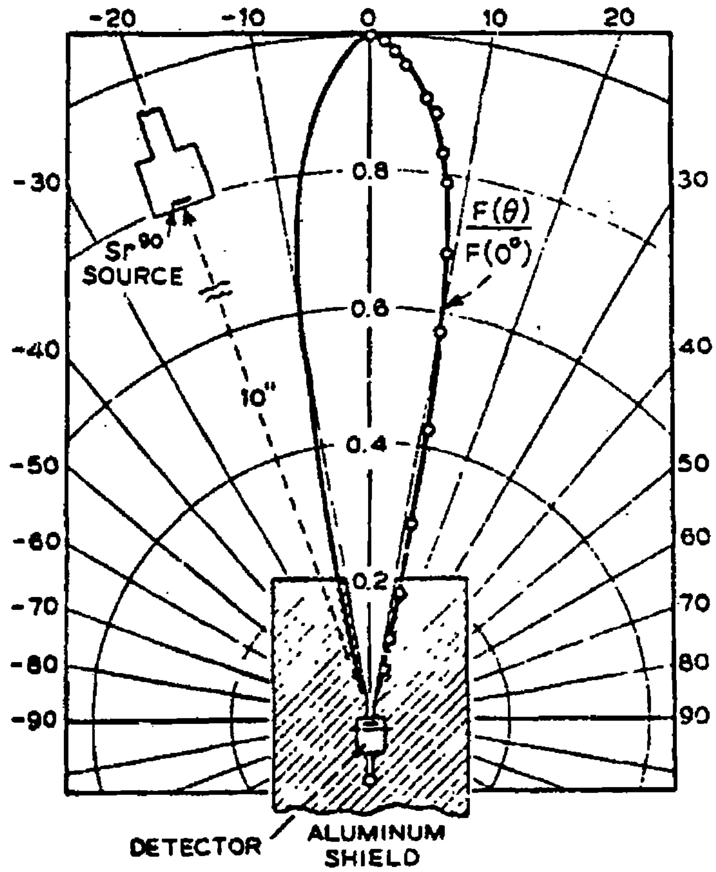

Figure 5-1. Angular Response of 0.5 MeV Channel

detector. The sharpness of the cutoff in the detector response near 10^{o}, the geometrical edge of the detector aperture, indicates the success of this design.

Figure 5-2 shows the geometrical factor of the detector for monoenergetic electrons. For energies up to one MeV, an electron Van deGraaf at BTL, Murray Hill, was used in these measurements, and for the higher energies, a Van deGraaf at MIT. The detector's effective geometrical factor rises steeply at about 0.5 MeV as electrons succeed in penetrating a 20 mg/cm^2 entrance window and satisfying the 0.4-MeV pulse height requirement of the discriminator. The mathematical geometrical factor given in Table 5-1 is approximately 29 x 10^{-4} cm^2 steradian. Thus the peak efficiency of the detector, which occurs at an energy of about 1.7 MeV is between 35 and 40 percent. The active thickness of the silicon p-n proton detector is 0.37 mm and a minimum ionizing electron will, on the average, lose only about 0.15 MeV in passing through it. The discriminator level was set considerably higher than this to avoid possible problems of discrimination. Thus the detector efficiency runs through a maximum for electrons that stop with high probability in the active thickness and slowly increases toward higher energy as the mean energy loss drops below the discrimination level.

The energy dependent geometry efficiency factors were folded into a fission spectrum as described in Section 4.2 and an overall effective average geometry factor for isotropic fission electrons was determined.

$$\bar{G} = \frac{\int_{4\pi} \int_{0}^{\infty} G(E)\ f(E,\Omega)\ dE\ d\Omega}{\int_{4\pi} \int_{0}^{\infty} f(E,\Omega)\ dE\ d\Omega} \qquad (31)$$

where G(E) is the energy dependent geometry efficiency factor in cm^2-steradians, f(E) is the fission flux in electrons/cm^2/sec/ster/keV, and G is average geometry-efficiency factor for converting flux greater than 0.5 MeV to counts/second.

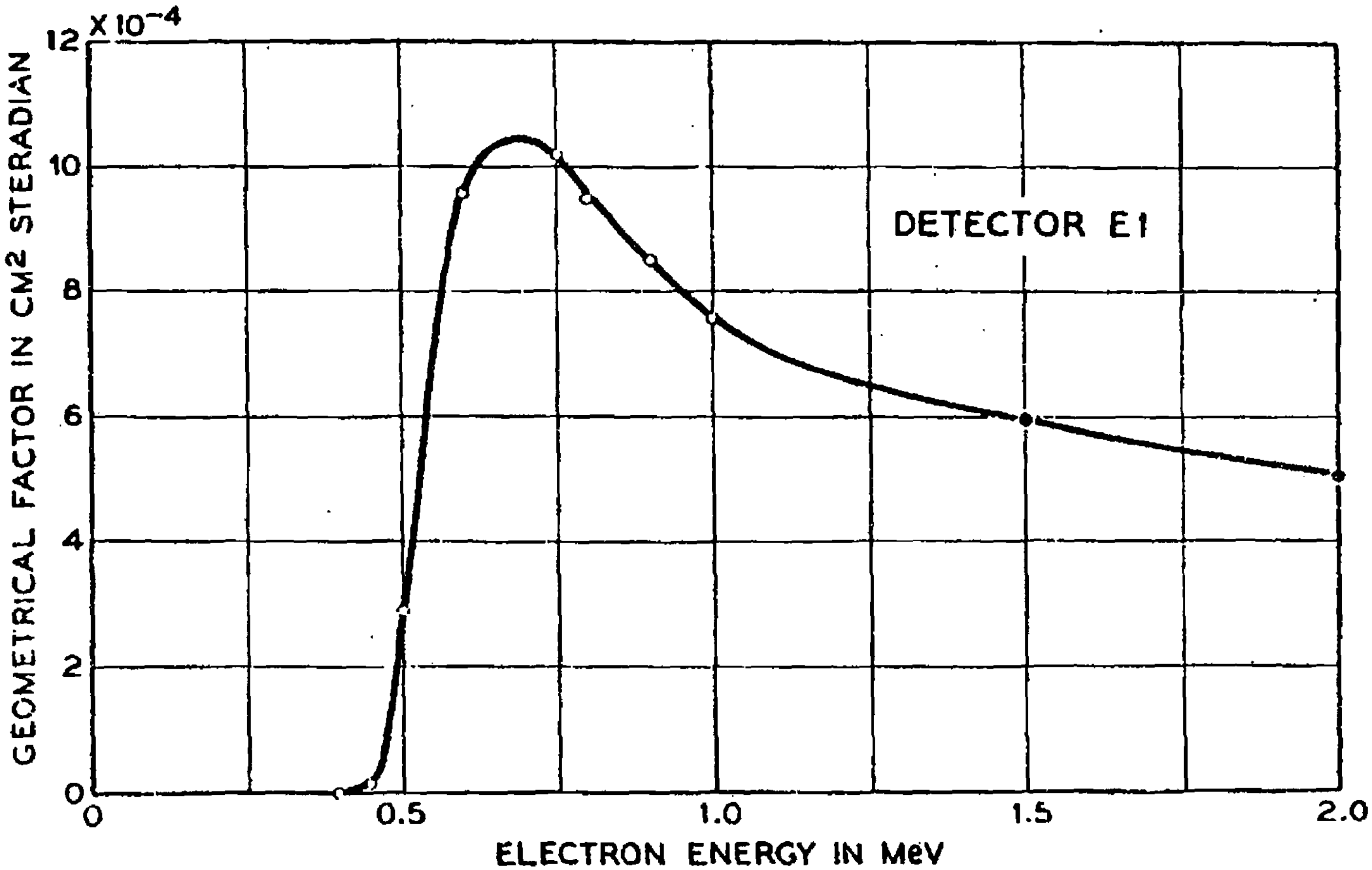

Figure 5-2. Energy Dependent Geometry Factor for 0.5 MeV Channel

5.2.2 Calibration of the 1.9 MeV Channel

The angular response of this detector is shown in Figure 5-3 as measured with a Sr^{90} source. This detector depends on the properties of the trace scattering disc for its wide angle characteristics. The curve 1/2 (1 + cos θ) shown on the figure is the response that would be obtained if the electrons were isotropically distributed in angle when they penetrated a truly hemispherical disc. The actual disc is elongated to compensate for the incompleteness of the scattering, but the detector is nonetheless a factor of approximately 2 down in response at 90^0. From the standpoint of measuring an omnidirectional flux by averaging the counting rate of this detector as the satellite rotates around its spin axis, this discrepancy is undetectable.

Figure 5-4 shows the effective geometrical factor for monoenergetic electrons up to 2.8 MeV. The brass dome, 0.42 g/cm^2 in thickness, broadens the rise of the detector response because of the statistical variability of electron energy loss in penetrating the dome. It was not feasible to extend the measurements above 3 MeV and the dashed line is a reasonable extrapolation to higher energies. Because of the variability of the electron energy loss in this relatively thick absorber, it is likely that the curve will come down at high energies only very slowly if at all.

The effective average efficiency geometry factor to convert total isotropic flux above 1.9 MeV to counts/sec was determined in the same manner as for the 0.5-MeV detector.

5.2.3 Calibration of 2.9 MeV Detector

This detector has a brass scattering dome 0.83 g/cm^2 in thickness. This is too thick to make measurements with a Sr^{90} source and too thick even using the high energy Van deGraaff to see more than the start of its energy dependence. As a result, the geometrical factor and the equivalent threshold energy for this detector have been estimated by analogue with the 1.9-MeV detector.

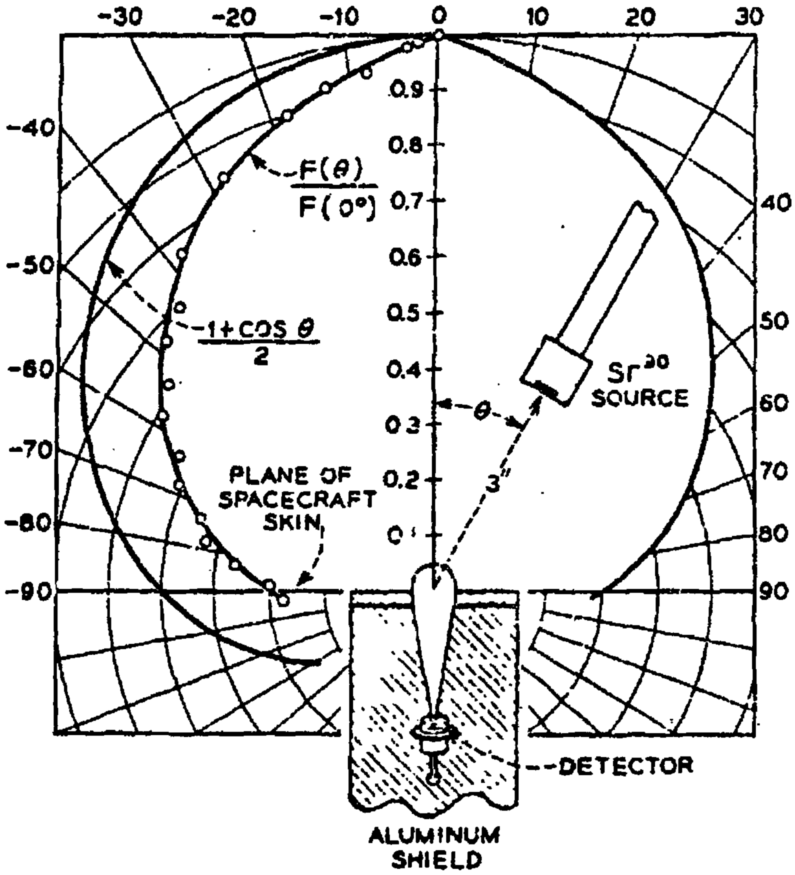

Figure 5-3. Angular Response of the 1.9 MeV Channel

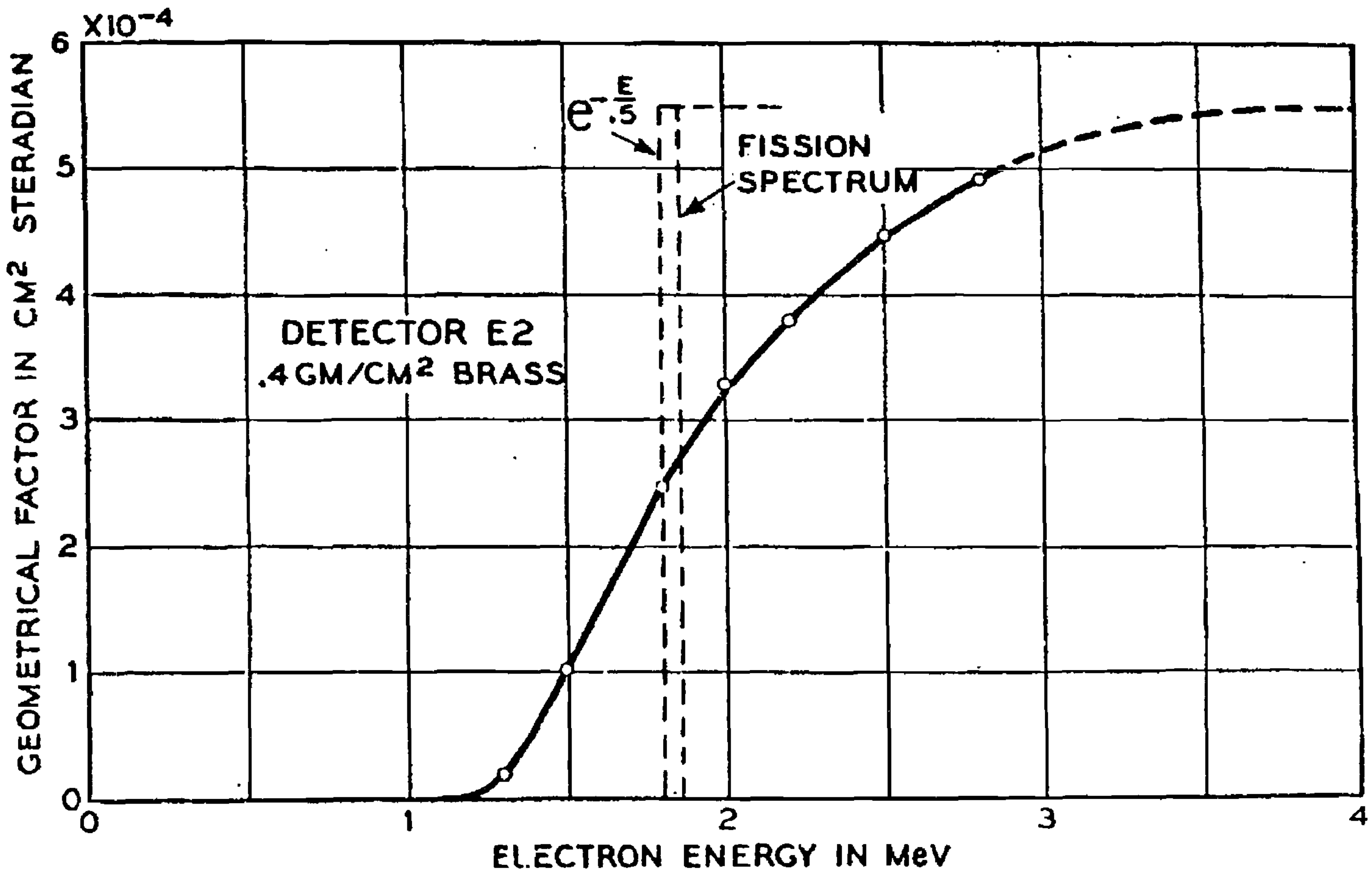

Figure 5-4. Energy Dependent Geometry Factor of the 1.9-MeV Channel

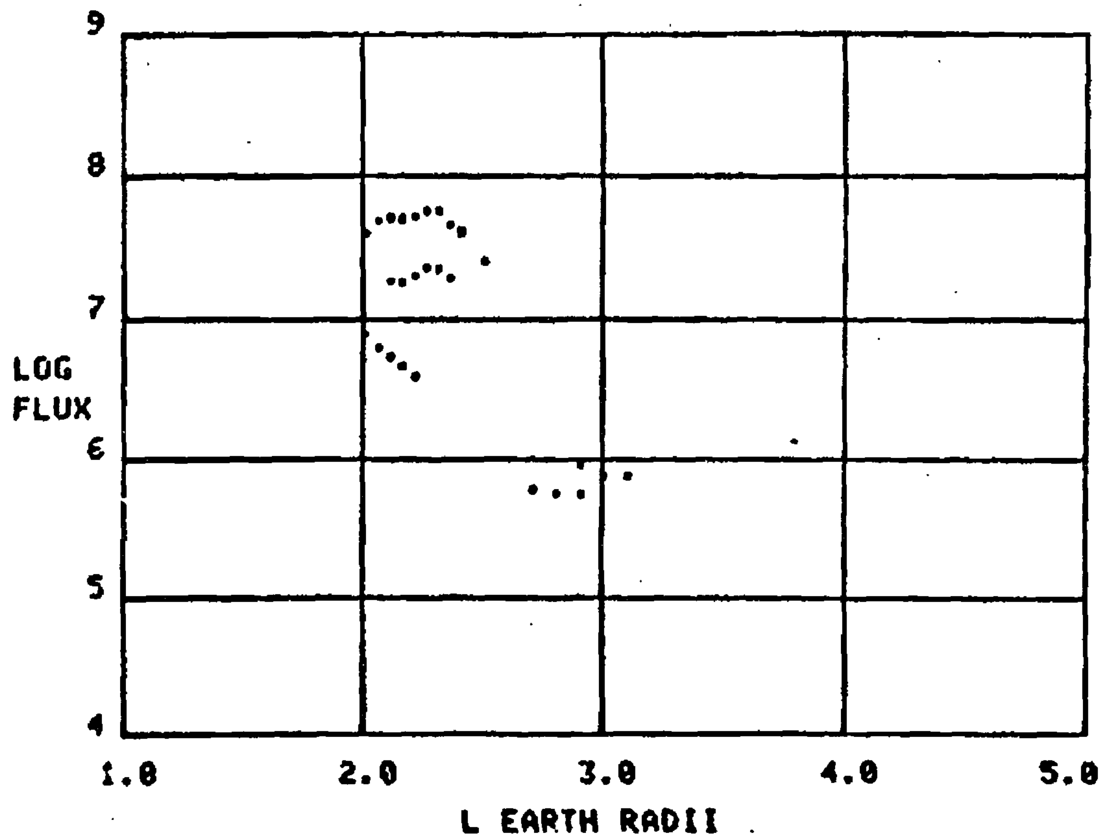

Figure 5-5. 500-keV Flux Versus L on Day 301, the Day of the Russian II Burst

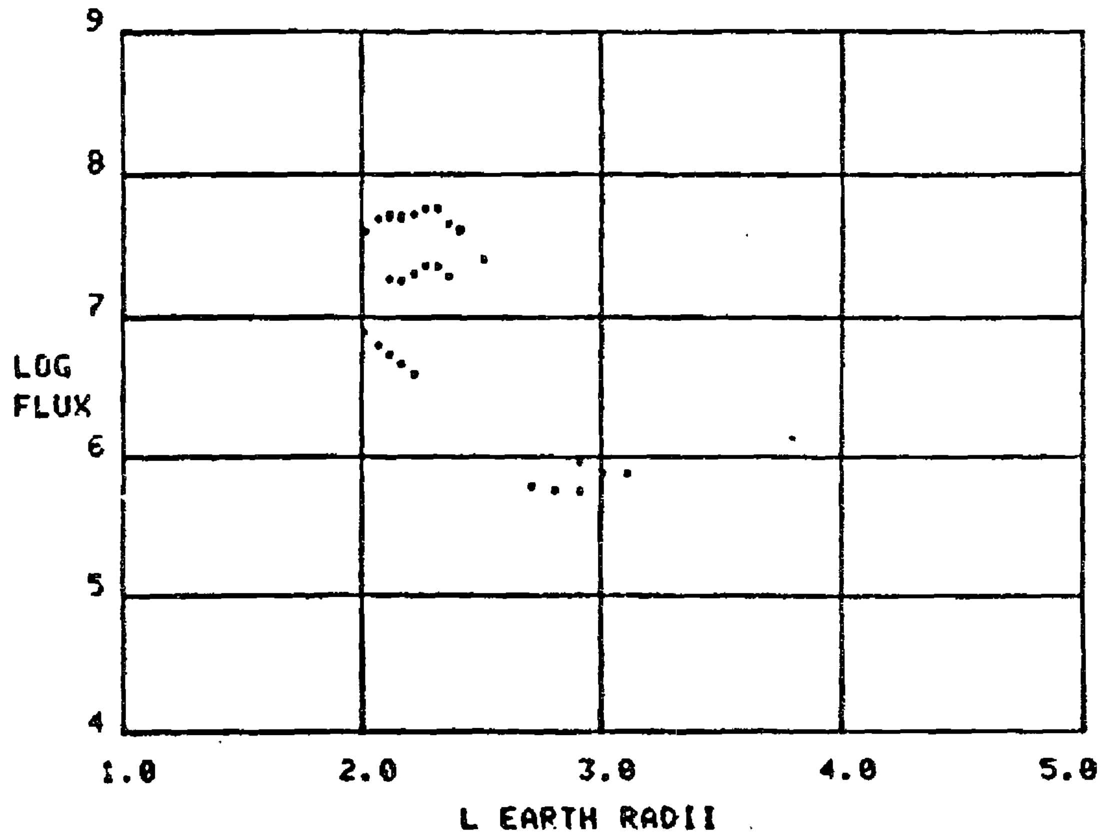

Figure 5-5. 500-keV Flux Versus L on Day 301, the Day of the Russian II Burst

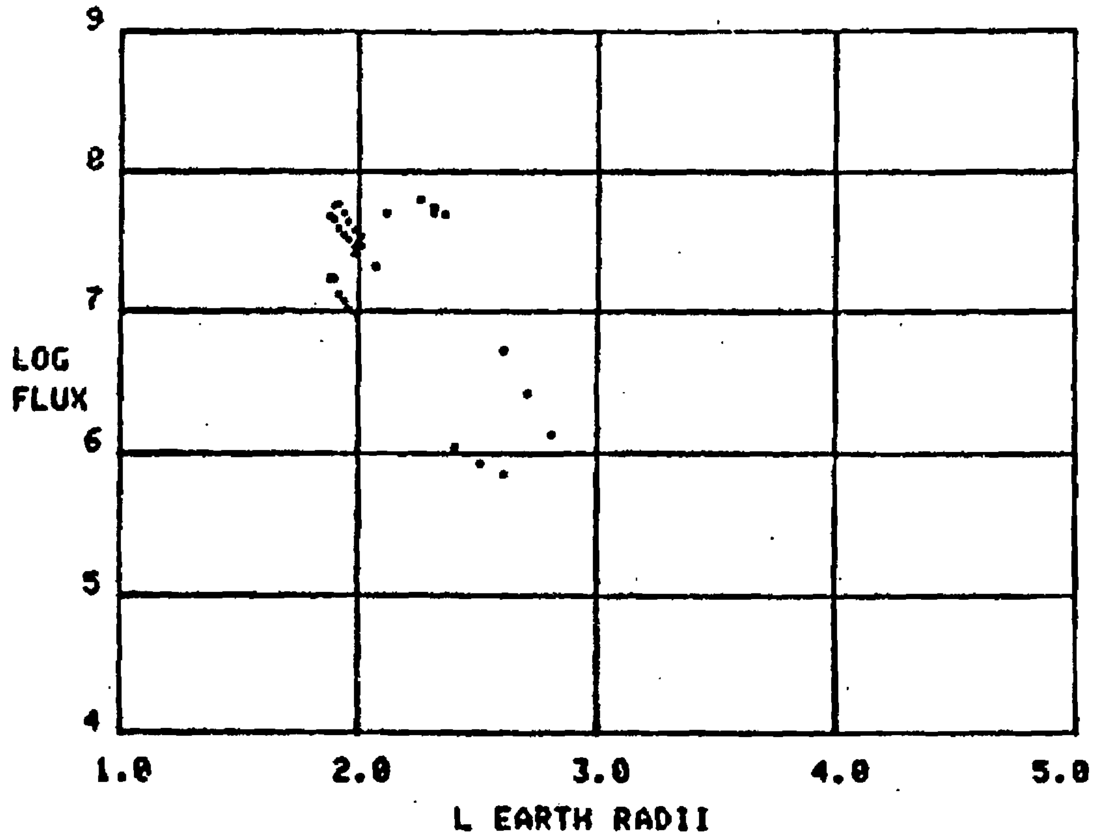

Figure 5-6. 500-keV Flux Versus L on Day 301, the Day of the Russian II Burst

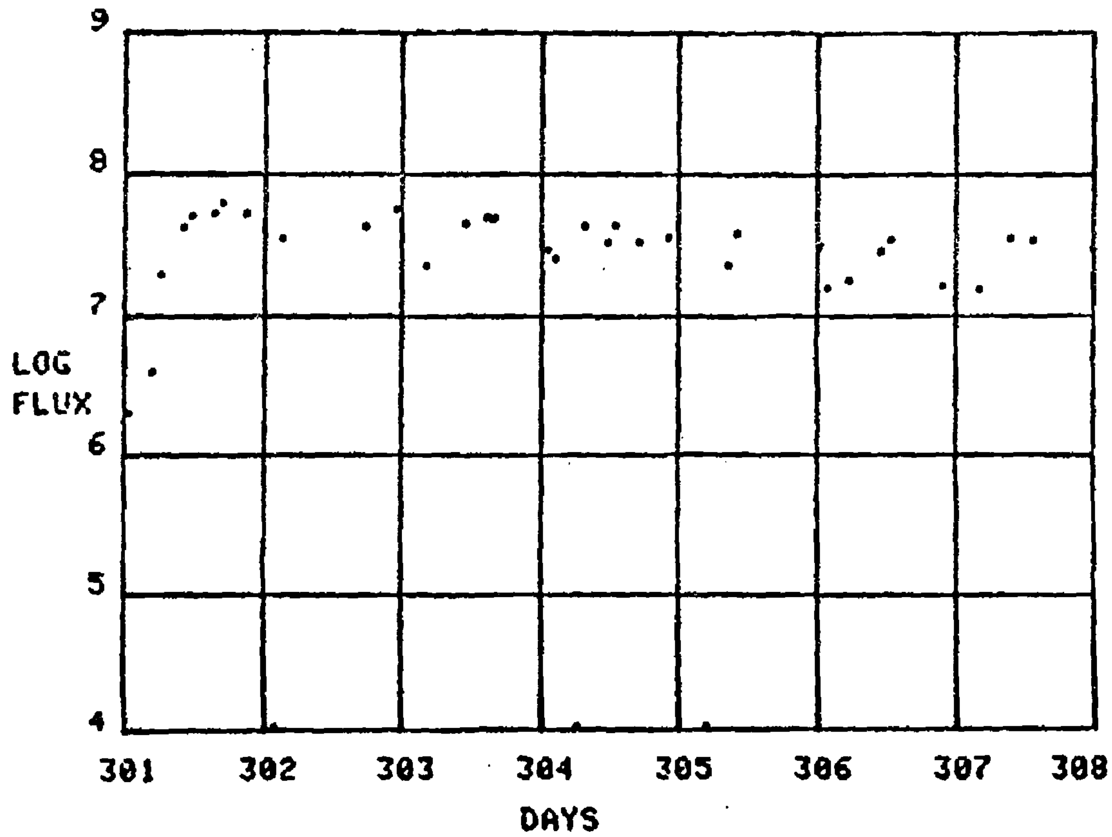

Figure 5-7. Time Dependence of the 500-keV Channel at L = 2.2 and B ∿ 0.05

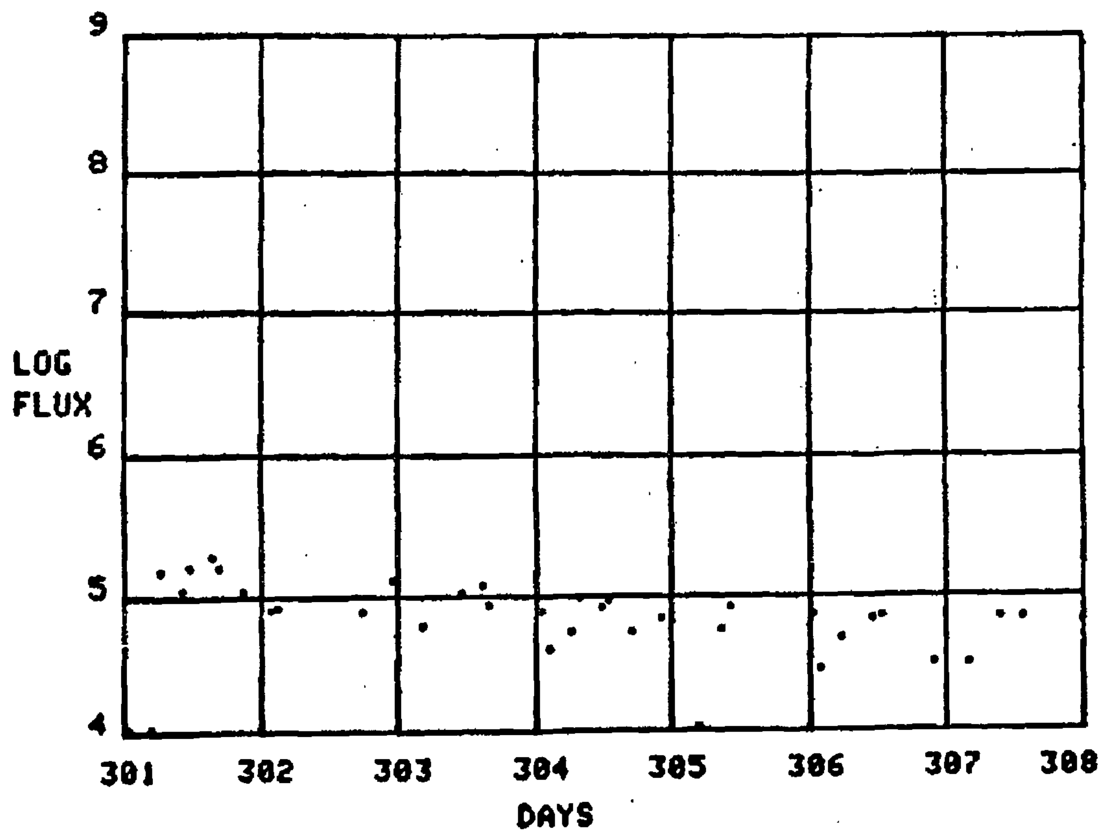

Figure 5-8. Time Dependence of the 1.9-MeV Channel at L = 2.2 and B ~0.05

500 keV and the 1.9 MeV channel. Note the increase on day 301 due to Russian II. Figure 5-9 shows the Russian III peak above the earlier detonations.

5.4 Error Analysis

The detectors for Explorer XV were similar to Telstar. The random errors were more or less the same and the function used to evaluate the errors for Explorer XV were the same as for Telstar. The reader is referred to Section 4.5 for the functions used to evaluate the errors. Since the Explorer XV detectors were evaluated as integral detectors, it is estimated that the factor of 2 deterministic error which was applied to Telstar is much smaller for Explorer XV.

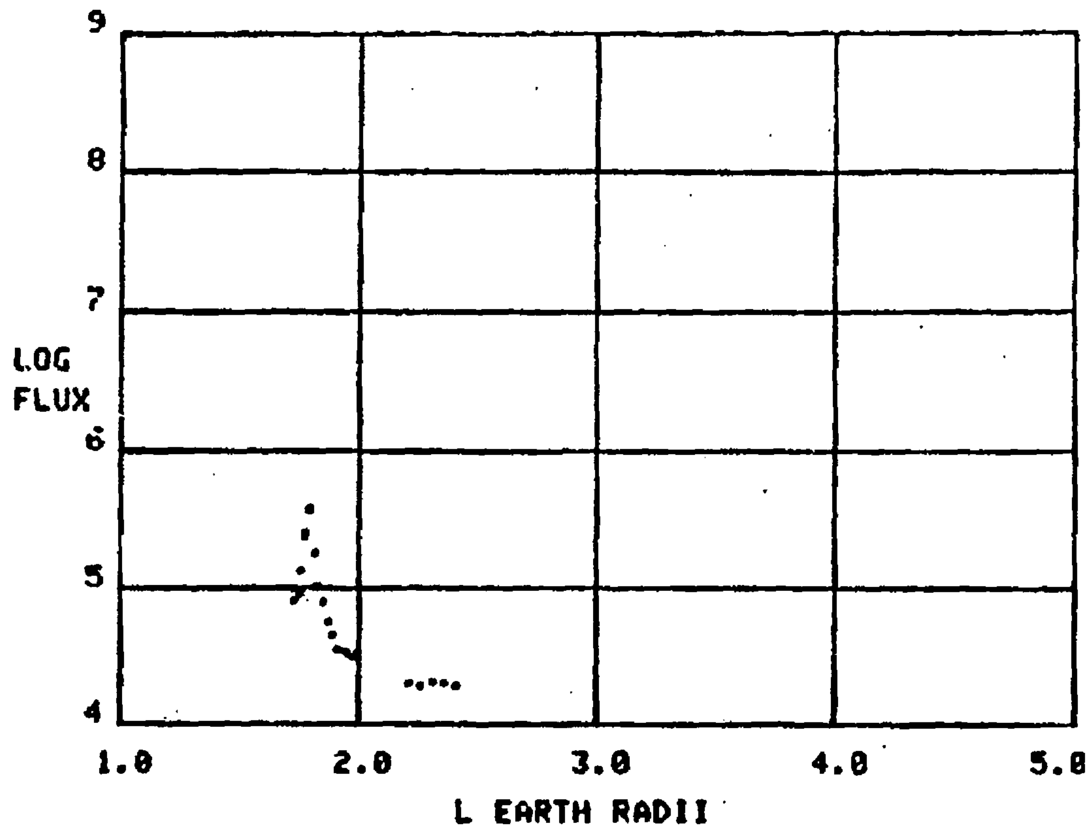

Figure 5-9. The Russian III Enhancement as seen by the Explorer XV 1.9-MeV Channel

Section 6

ALOUETTE SATELLITE

The Alouette satellite contains a cluster of charged particle experiments that were designed to measure electrons and protons in three different energy intervals. The three detectors are summarized below.

6.1 Detector Description

Detector 1 is an Anton 302 Geiger counter whose omnidirectional geometric factor is 0.55 cm^2 for particles capable of penetrating all of the surrounding shielding material. The effective shielding consists of about 1.4 g/cm^2 of medium Z material (Al and Fe) over about 2.4 steradians which extend in a "quadrant" 140^o along the satellite equator and from the equator up to the spin axis. The shielding is much greater over the remaining solid angle. The minimum shielding corresponds to approximately 50 percent transmission for 3.9-MeV electrons.

Detector 2 consists of an Anton 223 thin-window (approximately 1.2 mg/cm^2) Geiger counter placed at the end of a cylindrical brass collimator which is inclined 10^o to the spin axis. The angular aperture of the collimator is 4.5^o. For particles incident outside the angular opening of the collimator the effective shielding is similar to that of detector 1. The minimum shielding extends over a slice, 200^o in the equatorial plane and 35^o above the equator, and it is much greater over the remaining solid angle.

Detector 3 is similar to 2 except that a magnetic field of a few hundred gauss is applied across the collimator in order to exclude electrons with energies less than 250 keV. The angular aperture of the collimator is 6.6^o and its axis is in line with the satellite spin axis.

Detectors 1 and 2 were designed to be omnidirectional. However, the fission spectrum was much too hard (the number of electrons at high energies is too great and more high electrons penetrate the shield than low energies entering the acceptance cone) and the primary response of the three Alouette detectors were due to electrons penetrating the shielding surrounding the detectors. All three detectors had a minimum shielding thickness of 1.4 g/cm^2. This shielding was inadequate and thus the primary response of the Alouette detectors was to electrons having an energy greater than 3.9 MeV. Thus, instead of having three detectors looking at three different energies, the Alouette detectors measured the same electrons with three different detectors.

6.2 Detector Calibration

Very little calibration information is available for the Alouette detectors since they responded in an anomalous manner. The pertinent response characteristics are given in Table 6-1.

Table 6-1

PHYSICAL PROPERTIES OF ALOUETTE DETECTORS

Detector	Geometry (cm^2)	Minimum Shielding (gm/cm^2)	Solid Angle Over Minimum Shielding (sr)
1	0.55	1.4	2.4
2	0.22	1.4	2.0
3	0.22	1.4	0.5

If an approximate response curve is folded into a fission spectrum and allowances are made for detection efficiencies, then within the limits of error which are larger than normal (since the response curves for electrons penetrating the shield are not known), one can derive an approximate geometry factor that does not differ substantially from $\bar{G} = \Omega A$ (the area of the detector times the solid angle over which the minimum shield exists). Thus, in order to keep the analysis simple, the dead time corrected counts/sec were multiplied by the factor $4\pi/\Omega A$. This factor was used to convert counts/sec to the flux of electrons/cm^2/sec greater than 3.9 MeV. This admittedly is very crude; however, any other number could not be justified at this time.

The factors used for the three detectors are given in Table 6-2.

Table 6-2

AVERAGE GEOMETRY FACTORS FOR ALOUETTE

Channel	Energy	$1/\overline{G}$
1	> 3.9 MeV	9.52
2	> 3.9 MeV	28.56
3	> 3.9 MeV	114.24

6.3 Data Analysis

The Alouette tapes were easy to read since they were written in a BCD format. The Alouette data set description was one of the few that unambiguously and uniquely identified the channels. The tape, however, was not in time sequence. Data from separate tracking stations were recorded on separate files.

The initial data analysis effort stripped the pertinent information from the tape and used the CDC SORT/MERGE routines to place the data in time sequence.

The first step in the data analysis was to verify that the three detectors were indeed measuring identical electrons. Figures 6-1 through 6-3 show the flux of electrons greater than 3.9 MeV as measured by the three detectors. The three results are very close, although on the average for Channel 3 reads about a factor of 2 low. Detectors 1 and 2 exhibit special problems for fluxes in excess of 10^5. This is attributed to telemetry and data reduction problems.

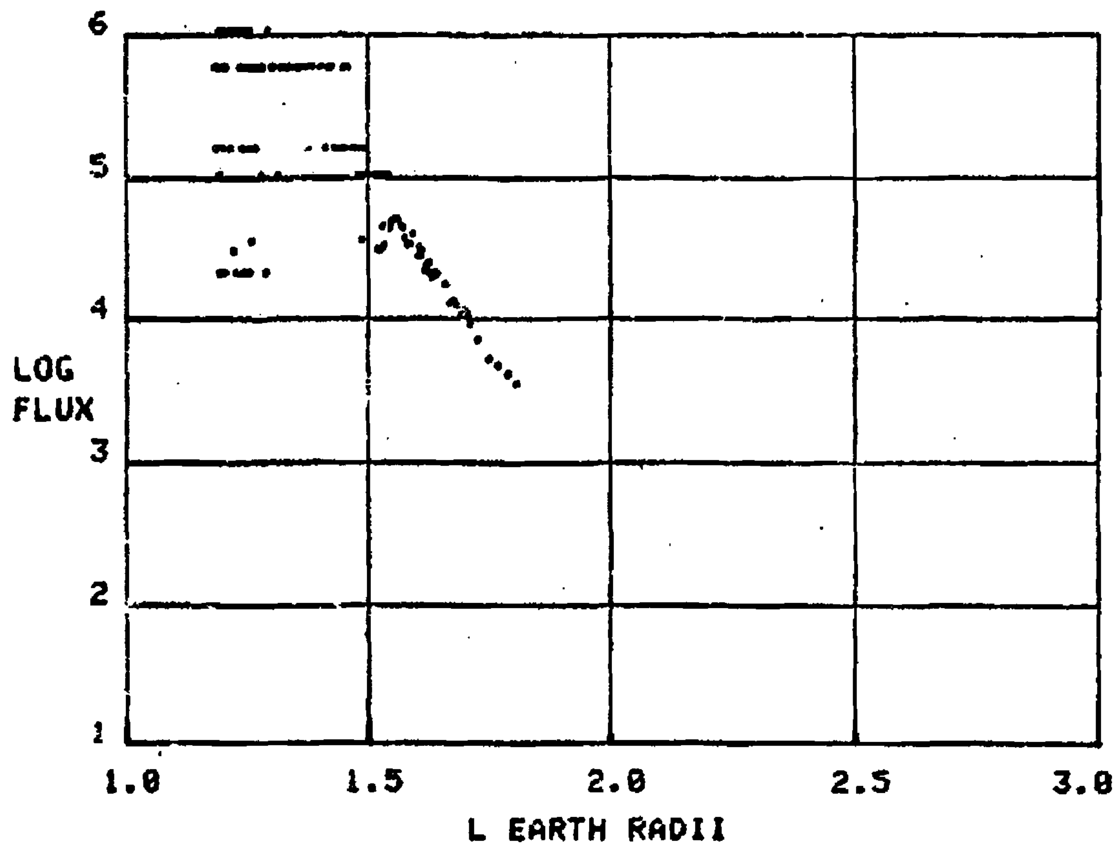

Figure 6-1. Alouette Channel 1 Flux Versus L

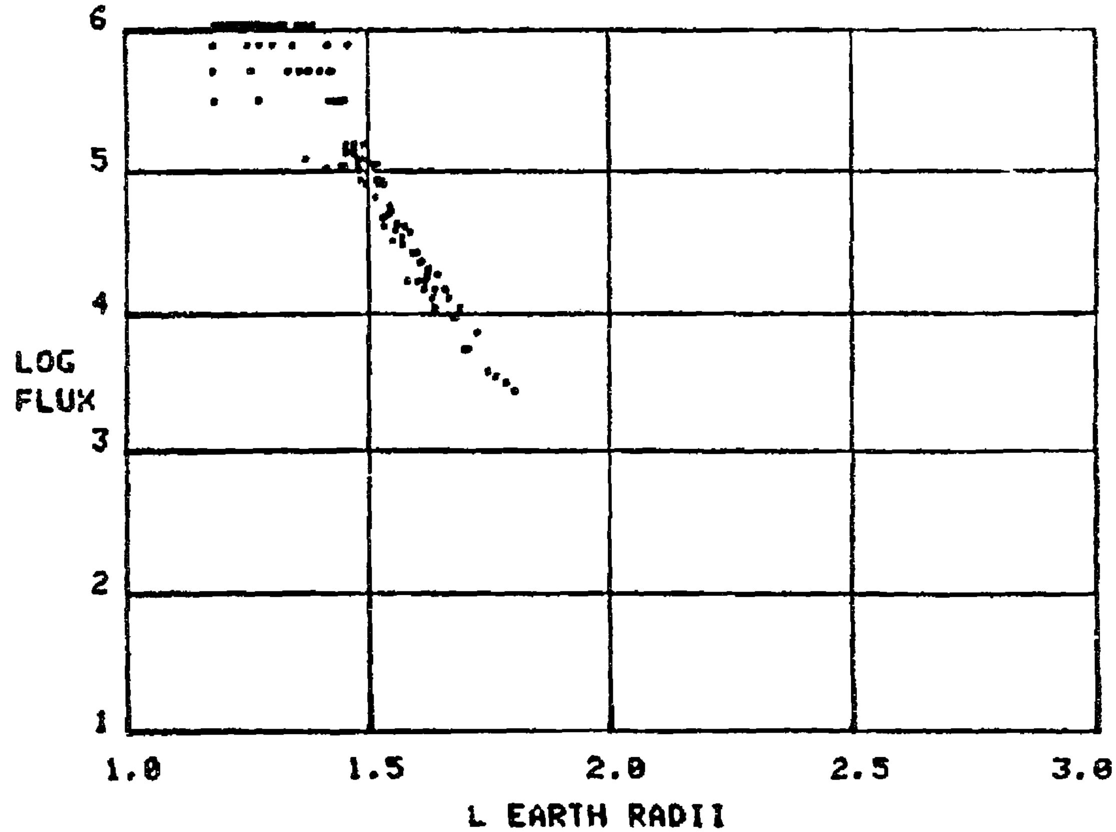

Figure 6-2. Alouette Channel 2 Flux Versus L

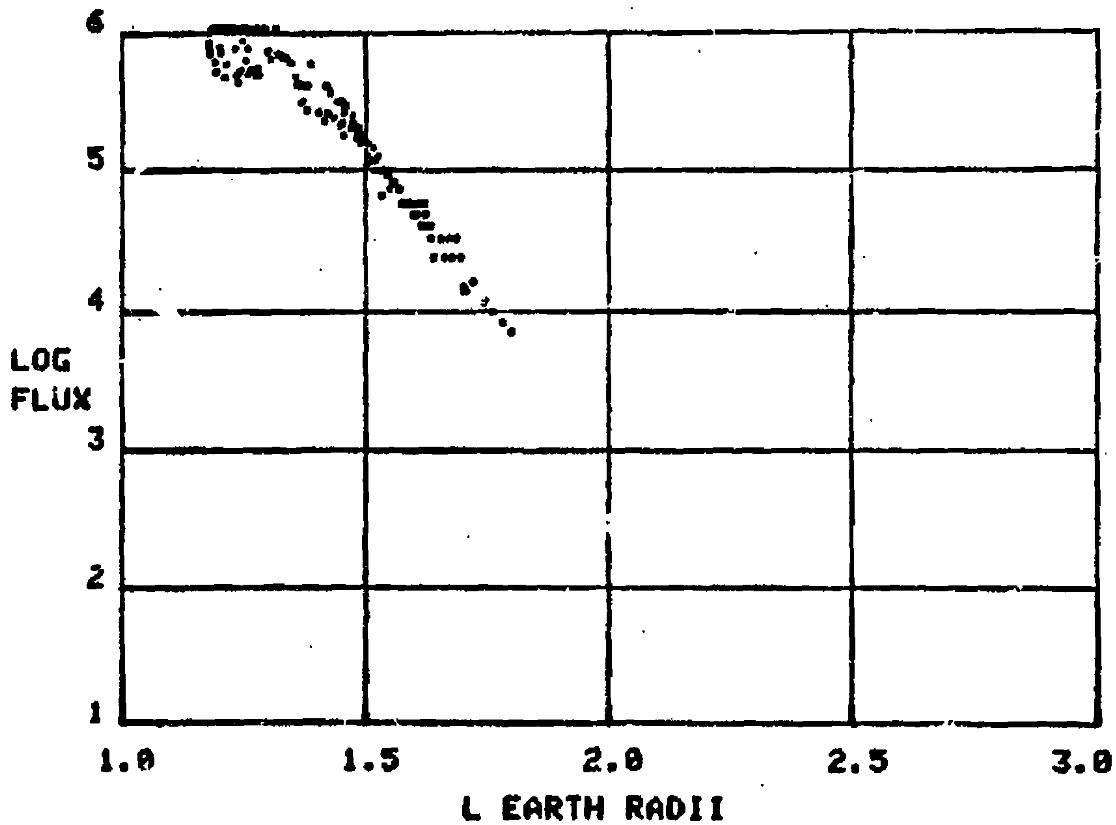

Figure 6-3. Alouette Channel 3 Flux Versus L

6.4 Background

The background for the Russian series could easily be evaluated by fitting the data prior to the Russian I and the Russian II burst with least squares functions in B and L. This fit removes any contamination due to Starfish, natural electrons and protons. As with all other experiments up to this point, this least squares subtraction was very successful. Figures 6-4 to 6-6 show the pre-Russian fluxes. The solid curves represent the fit. Figures 6-7 through 6-9 show the background corrected Alouette flux complete with error bars.

6.5 Error Analysis

Since the calibration information in the literature was incomplete, error analysis is quite difficult. One of the best measures of the uncertainty of the measurement is the variation between the three detectors. The difference between the three detector sets is just over a factor of 2. Channel 2 is consistently high, Channel 3 consistently low. Unfortunately, it was impossible to decide which of the detectors was correct. Thus there exists a systematic error of at least a factor of 2 (this systematic error is not included on the data tape) for the entire data set. Errors due to statistics and uncertainty in converting to isotropic fluxes on a point-to-point basis were treated in the usual manner. In addition, a special error function was introduced when the fluxes were larger than 10^5 for Channels 1 and 2. This function increased the flux errors in the 10^5 to 10^6 range from 0 to an order of magnitude (i.e., the error in the logarithm of the flux was zero at 10^5 and $\pm$ 1 at 10^6).

The total random error, E_T, then was given by

$$E_T = \sqrt{E_S^2 + E_C^2 + E_L^2 + E_B^2} \tag{32}$$

where E_S is the statistical error, E_C is the uncertainty due to spectral shape and conversion to isotropic flux (for Alouette this was set to 50 percent of the flux level); E_L is the special large intensity error function and E_B is the background error. For Alouette, the background error is approximately 40 percent of the background flux levels.

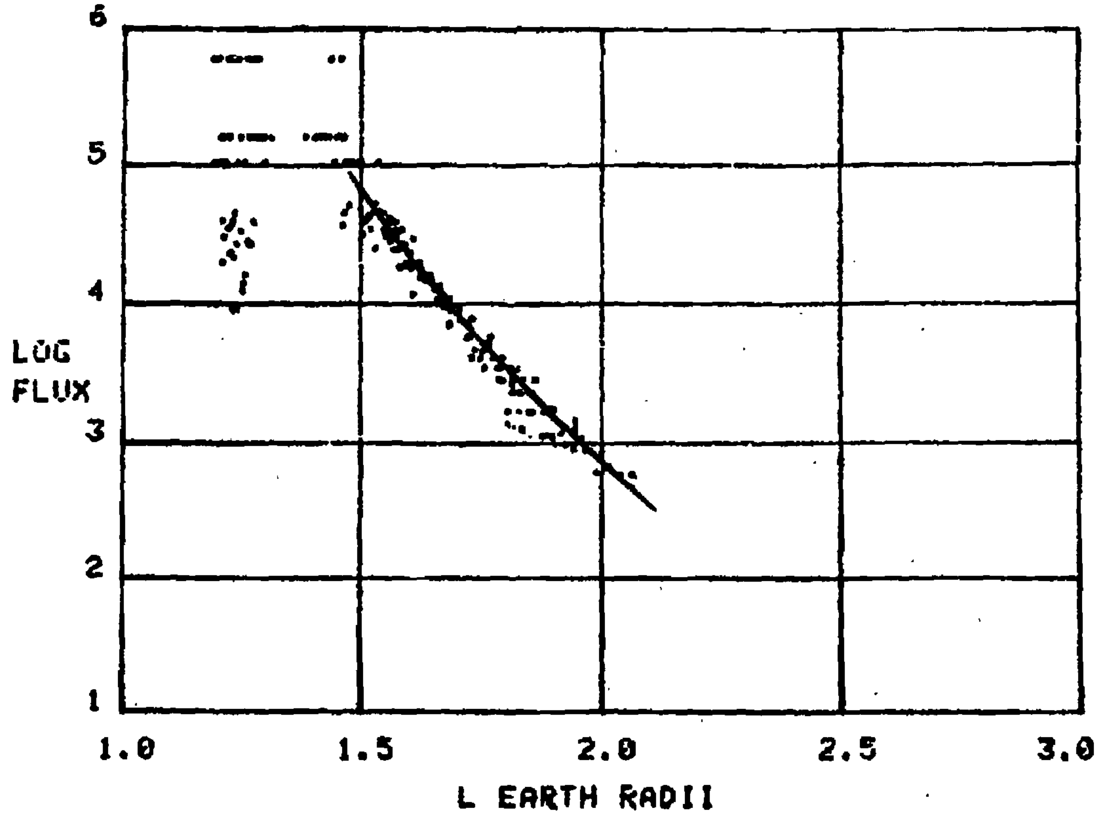

Figure 6-4. Starfish Background Fit for the Alouette Detector (Solid Line is Least Squares Fit).

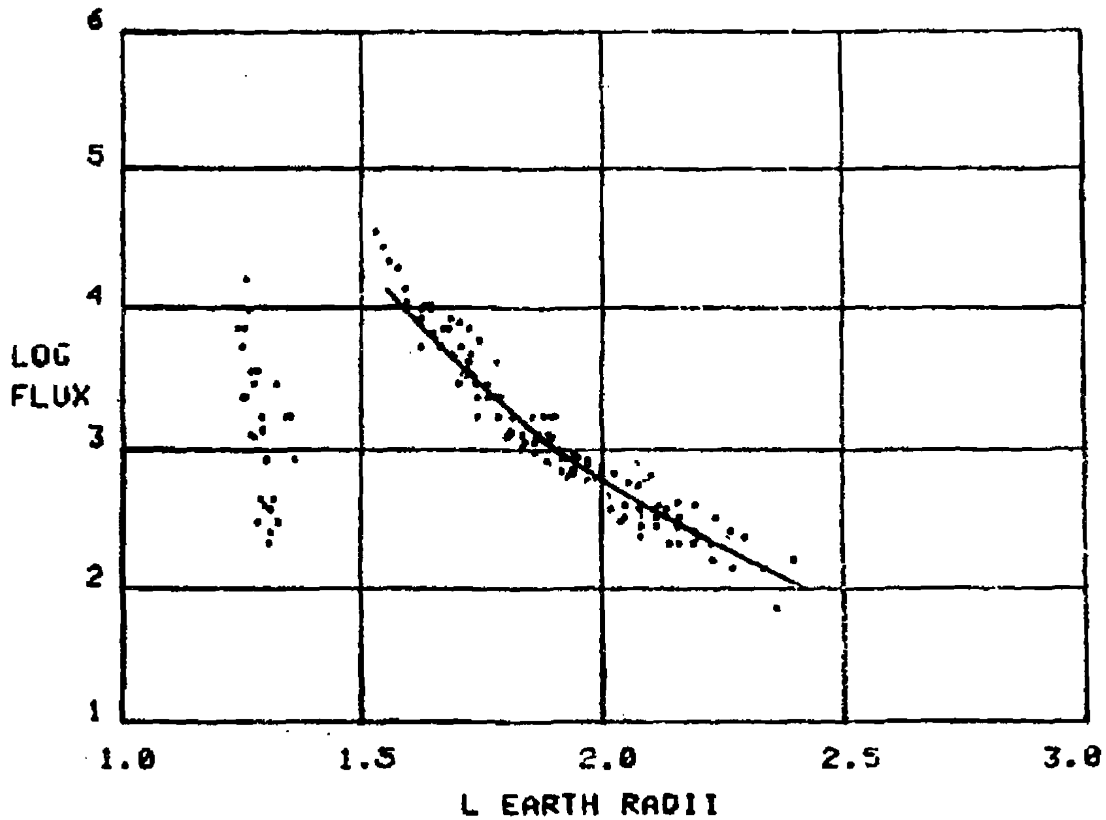

Figure 6-5. Starfish Background Fit for the Alouette Detector (Solid Line is Least Squares Fit).

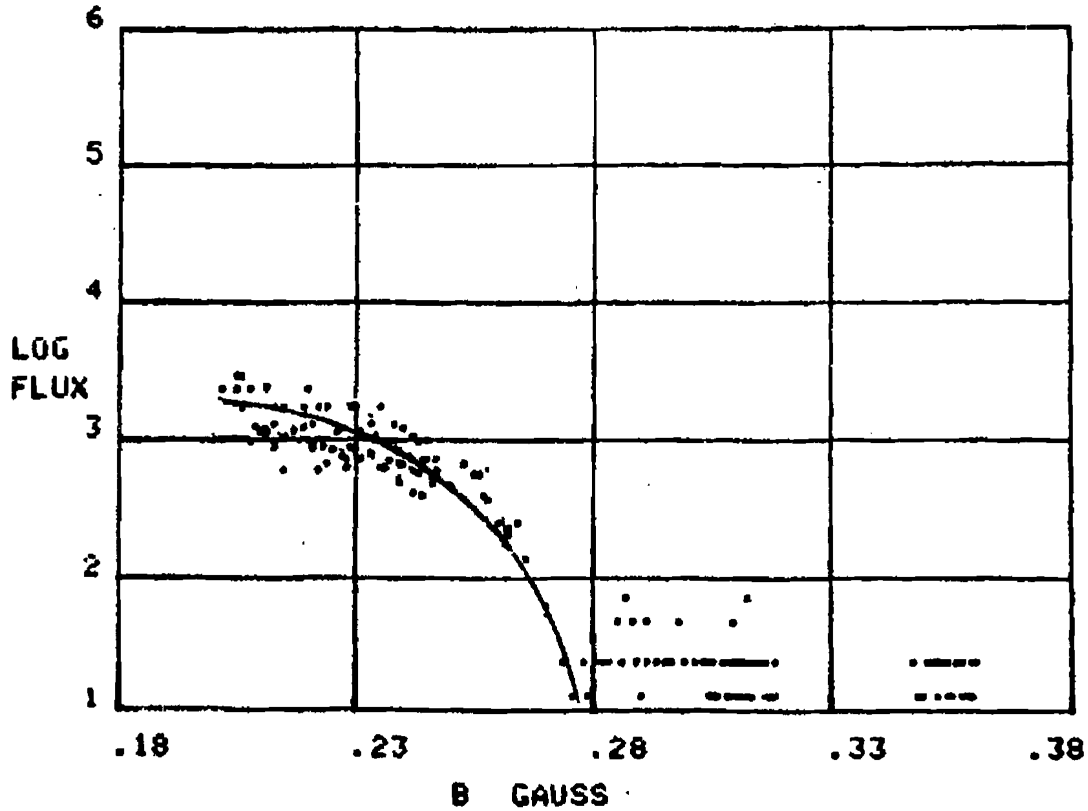

Figure 6-6. Starfish Least Squares Fit Plotted Versus B

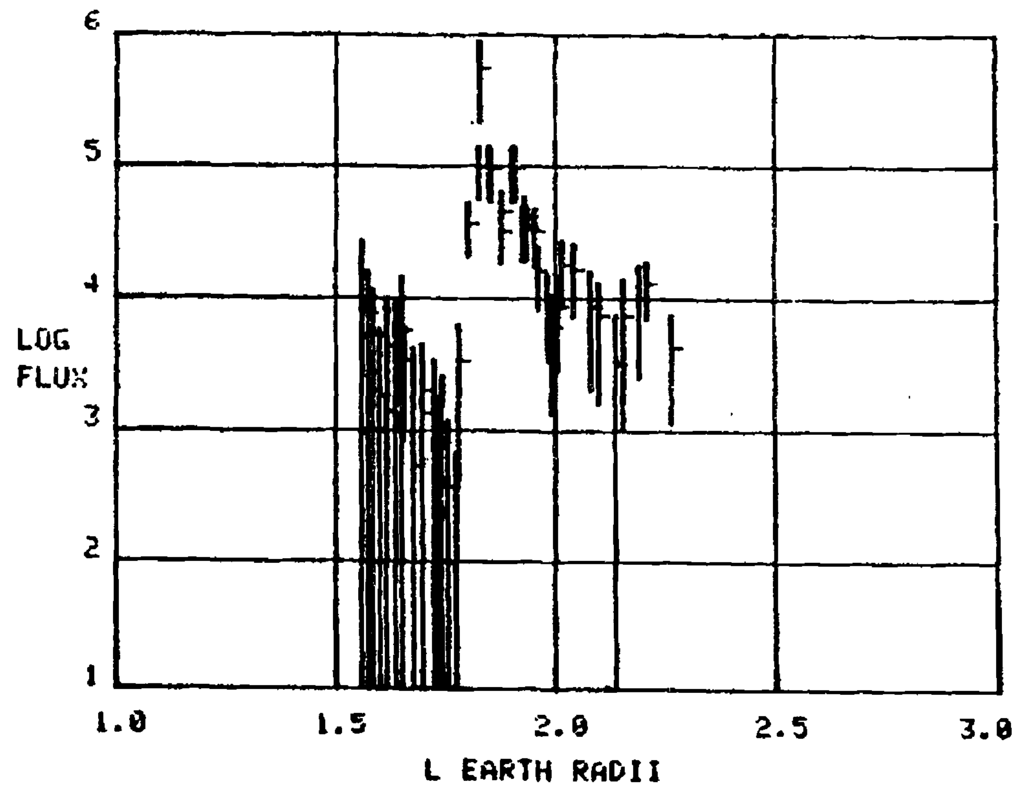

Figure 6-7. Background Corrected Flux with Error Bars for Alouette Channel 1

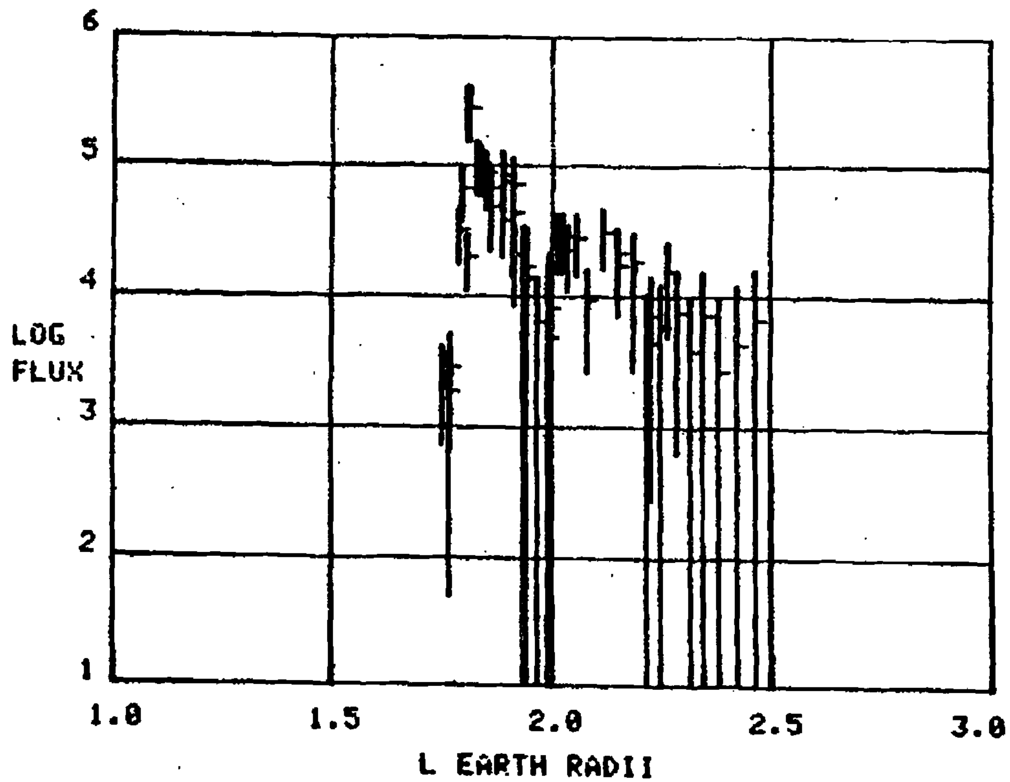

Figure 6-8. Background Corrected Flux with Error Bars for Alouette Channel 2

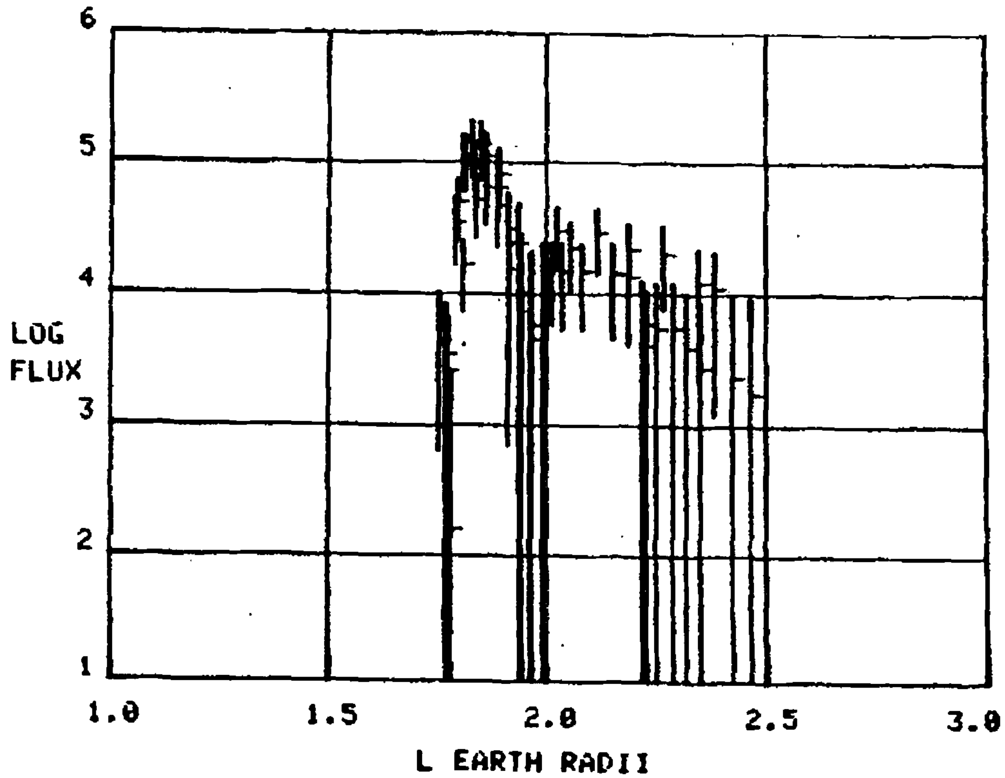

Figure 6-9. B::ckground Corrected Flux with Error Bars for Alouette Channel 3

Section 7

THE TRAAC SATELLITE

There is very little information or data available for the Traac satellite. Furthermore, only a very limited description of the instrumentation exists.

7.1 Experiment Description

The Traac instrument consists of an Anton 302 Geiger counter with a geometric factor of 0.75 cm^2 and subtends a solid angle of 3π steradians (Reference 10). The shielding thickness is ~ 0.66 g/cm^2.

7.2 Instrument Calibration

In Reference 11 there is a curve showing the response of the Traac detector to the fission spectrum (see Figure 7-1). This figure shows that Traac responds primarily to electrons above 1.5 MeV.

The geometric-efficiency factor can be calculated in two ways. First, using the above described geometric constants one can write

$$\bar{G} = \frac{3\pi * 0.75}{4\pi} = 0.56 \qquad (33)$$

A second method can be used to determine $\bar{G}$. The Traac instrument was exposed to a fission spectrum and Hess 1963 and others report that Traac counts 18 percent of the total fission spectrum. This means that

---

10. Pieper, G. F., A Second Radiation Belt from the July 9, 1962, Nuclear Detonation, Journal of Geophysical Research, 68, 651-655, 1963.

11. Hess, W. N., The Artificial Radiation Belt Made on July 9, 1962, Journal of Geophysical Research, 68, 667-683, 1963.

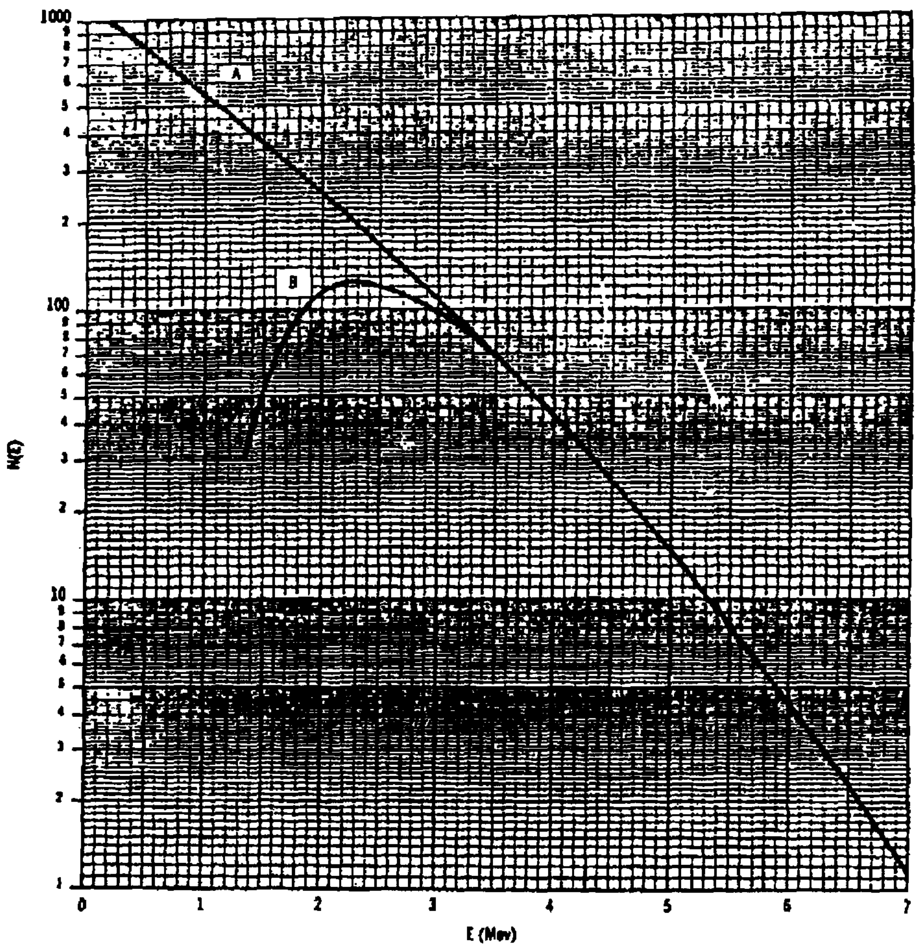

Figure 7-1. Curve A is the Fission Energy Spectrum and Curve B the Transmission Energy Spectrum for the Traac GM Counter (0.66 g/cm^2 Wall Thickness)

$$\frac{{}_0\int^{\infty} G(E)\, f(E)\, dE}{{}_0\int^{\infty} f(E)\, dE} = 0.18 \qquad (34)$$

The fraction of the fission spectrum having an energy $E_0 > 1.5$ MeV is given by

$$\frac{{}_{Eo}\int^{\infty} f(E)\, dE}{{}_0\int^{\infty} f(E)\, dE} = R \qquad (35)$$

This ratio was calculated by numerical means and was found to have the value 0.298 (i.e., R = 0.298). By definition one can write that

$$\bar{G} = \frac{{}_0\int^{\infty} G(E)\, f(E)\, dE}{\int_{E_0}^{\infty} f(E)\, dE} \qquad (36)$$

Substitutions into the above equation give

$$\bar{G} = \frac{0.18 \int_0^{\infty} f(E)\, dE}{0.298 \int_0^{\infty} f(E)\, dE} \qquad (37)$$

$$= \frac{0.18}{0.298} = 0.6$$

This method yields a result almost identical to the previous geometric values.

The value $\frac{1}{\bar{G}} = 1.66$ was used so that

$$F\ (E > E_0) = 1.66 * C \tag{38}$$

where C is the counts/second.

7.3 Data Analysis

The data analysis was very primitive. It consisted of digitizing the almost microscopic plots in Reference 10. These plots are given as the total fission electrons/cm^2/sec and thus the numbers scaled from the graph were multiplied by 0.298 (see Equation 34) to convert for flux above 1.5 MeV. Figure 7-2 is an example of the working data set. We were unable to locate any tapes or other larger plots.

7.4 Background Analysis

No background evaluations were possible with such a limited, poorly defined data set. Similar instruments on Alouette indicate that bremsstrahlung is not a problem. Proton contamination was not evaluated for the Traac detector.

7.5 Error Analysis

The largest error in this effort was the result of digitizing these exceptionally small graphs. The results are uncertain by at least a factor of 2. The error on the data tape is set to zero.

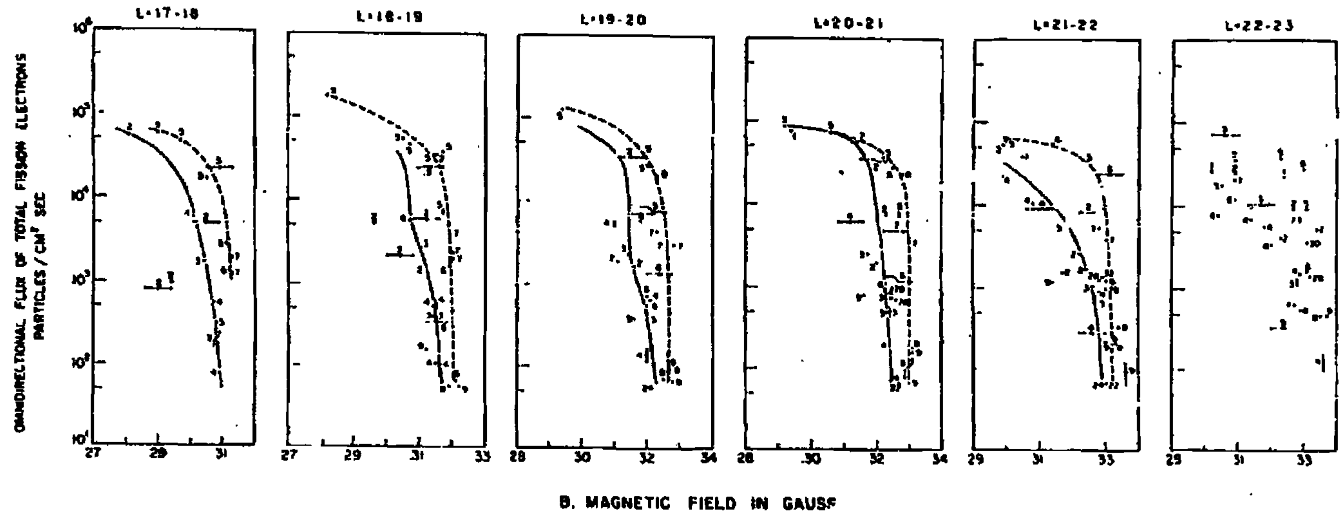

Fig. 2 Flux of 'total fission electrons' as a function of B (magnetic field strength in gauss) for finer graduations in the magnetic shell parameter L than are shown in Figure 1 at higher L values. The solid curves connect points taken before day 195, and the dashed curves connect points taken after day 195. Each point is labeled by a numeral that denotes the day on which the observation was made, 0 being taken as July 9, 1962 (day 190)

Figure 7-2. Traac Data from Pieper (Reference 10)

Section 8

STARAD EXPERIMENT

The description of the Starad experiment calibration, including accuracies of the calibration, are best described in Reference 12. Part of this description is reproduceo in Section 8.1 below.

8.1 Experiment Description

"The pertinent parameters of the satellite orbit at early times were as follows: apogee 5580 km, perigee 198 km, orbital inclination 71^{0}, orbital period 148 minutes, apsidal rate 0.8^{0} per day. The pitch period was 127 seconds and the roll period 53 seconds. The pitch and roll periods, coupled with the data acquisition rate of once per second for each data channel, were ideal for obtaining angular distributions. A three-axis magnetometer provided aspect information. Real-time data transmission was provided throughout the useful life of the satellite. Tape-recorded data were available during about the first week in orbit. The spectrometer sorted electrons according to energy by means of a uniform field using the principle of 180^{0} focussing. The magnetic field (about 1800 gauss) was produced by the ferroceramic Indox V.

The electrons were detected by solid state detectors of 4.5 x 4.5 mm and of various depletion depths from 0.2 to 2.5 mm, depending on the electron energy to be detected. High electronic energy bias was used on each detector in order to minimize bremsstrahlung detection. Bremsstrahlung in the vicinity of the spectrometer was reduced by surrounding the instrument with 1/4 inch of iron and 3/8 inch of Indox V. These materials attenuated the bremsstrahlung as well as stopping protons below about 100 MeV.

---

12. West, H. I., Jr., Some Observations of the Trapped Electrons Produced by the Russian High Altitude Nuclear Detonation of October 28, 1962, Radiation Trapped in the Earth's Magnetic Field, edited by B. M. McCormac, 634-662, D. Reidel Publishing Company, Dordrecht, Holland, Gordon and Breach Science Publishers, New York, 1966.

For stability purposes the signal from each detector was amplified by charge-sensitive preamplifiers. The signal was further amplified and passed to integral discriminators. (Differential discriminators are planned for all future flights.) These pulses went to four logarithmic rate meters of overlapping range and graduated response times covering counting rates of 2 to 150000 Hz. The rate meter in use at any given time was indicated on a separate telemetry channel. The data sampling rate was once per second. A diagram of the electronics and spectrometer are given in Figure 8-1.

The spectrometer was calibrated with extended uniform radioactive sources placed in front of the aperture of the spectrometer. These sources accurately simulated a field of isotropic radiation in which we knew the number of electrons per cm^2 sec keV as a function of energy. The principal radioactive sources used were Sr^{90}-Y^{90} and K^{42}. For the highest energy channel a cross comparison was made with its lower neighbor using Cl^{35}. If $F(E)_c$ denotes the electrons/cm^2/sec/keV coming from the calibration source, then the geometrical factor $A\,\Delta E\,\Omega$ is given by $4\pi\ \Delta N(E)_c/F(E)_c$ in which $\Delta N(E)_c$ is the counting rate of a given channel. The measured space fluxes $F(E,\theta)_s$ are then $F(E,\theta)_s = [\Delta N(E,\theta)_s/4\pi\ \Delta N(E)_c]F(E)_c$ electrons/cm^2/sec/keV/str.

The properties of the spectrometer are given in Table 8-1.

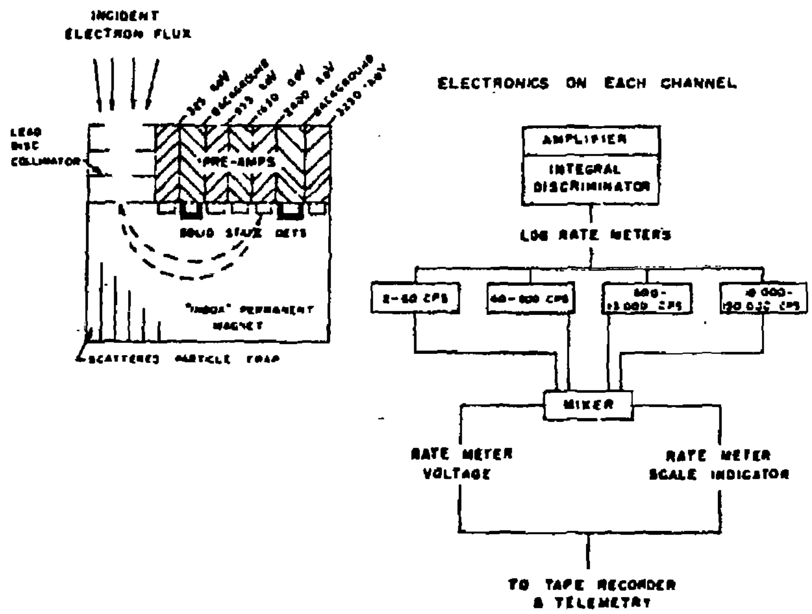

Figure 8-1. The Starad Electron Spectrometer and a Diagram of the Electronics

Table 8-1

PROPERTIES OF THE STARAD ELECTRON SPECTROMETER

Energy (keV	Effective Channel Width (keV)	Discriminator Bias (keV)	Detector Type	Depletion Depth	Geometrical Factor (cm^2 keV Str)
325	137	213	PN	~ 0.2	$1.76 \times 10^{-2} \times 4\pi$
955	162	680	PN	~ 1.2	$3.60 \times 10^{-3} \times 4\pi$
1630	184	1120	PN	~ 2.5	$3.30 \times 10^{-2} \times 4\pi$
2400	214	850	PN	~ 2.5	$4.30 \times 10^{-2} \times 4\pi$
(2590)*	219	850	PN	~ 2.5	$(3.72 \times 10^{-2}) \times 4\pi$
3250	224	850	PN	~ 2.5	$4.50 \times 10^{-2} \times 4\pi$

*Background channel

The energy of the channels was determined using detectors calibrated in a thin-lens beta-ray spectrometer. These energies should be correct to $\pm$ 4 percent. The count rates determined from telemetry data should be correct to about $\pm$ 10 percent when the contribution due to statistics is small. The relative accuracy of the fluxes reported should be better than $\pm$ 20 percent when statistics are reasonably good. Position uncertainties increase the error for absolute intensities to about $\pm$ 30 percent. Error bars are shown on the spectra only when the relative error was greater than $\pm$ 20 percent.
A high modulation of the counting rates was observed due to the tumbling of the satellite. When the minima in the counting rates coincided with low pitch angles they were used as background or used in establishing normalization factors for applying the background channels to the data channels. The three lowest energy channels were not accurately matched to a background channel and hence the normalization factor varied slowly from place to place depending on the relative contributions of protons and bremsstrahlung to the background. The two highest energy channels were well matched for sensitive volume and

energy threshold to the background channels and hence the normalization was fairly constant and consistent with expectations from the relative volumes of the respective detectors. The 325 keV channel always gave excellent signal-to-background ratios (often 100/1) whereas the 3250 keV channel data were often lost in background. In the high-background Starfish region, however, the signal-to-background ratio of the 3250-keV channel was about 5 to 1.

Timing errors in the tape-recorded data were apparent. Errors of $\pm$ 15 seconds, and sometimes more, usually occurred even when the satellite orbit was accurately known. These errors were evident in one prominent feature of the data which was most apparent in the background occurring at an L = 1.84 and caused by the USSR high-altitude nuclear detonations. This was a well-defined peak which in our data appeared to shift slightly in L-value as a function of B. A suitable time shift invariably brings the three peaks we observed in a given data acquisition into good alignment. This correction was made on all tape-recorded data.

Errors in pitch angle of about $\pm$ 5 degrees occurred due to magnetometer error and possible error in the transformation connecting the look angle of the spectrometer to the magnetometer axes."

8.2 Data Analysis

The Starad analysis effort proved to be the most difficult and frustrating. Even though many difficulties were encountered with the Data Center tapes, the problems with the Starad data tapes were many orders of magnitude more severe. Some of the basic problems encountered with this data set were:

1. The data tapes were not labeled as to content and format.
2. No documentation of any form existed on the tapes.
3 Description of instrument calibration functions did not exist.

The working Starad data set consisted of a stack of computer listings from AFWL, 27 unmarked 7-track tapes and a set of working notes from Reference 13. A discussion with the author who last used the computer program and the data introduced enough clues to permit the analysis to begin.

The keys to successfully analyzing the data tapes were contained in the comment cards at the beginning of the AFWL Starad computer program. These comment cards contained information on the array location of some of the important variables for the data analysis. This identified array was an array internal to the program; however, decoding of the program permitted identification of the data locations on the tapes. The tapes were written using an unformatted WRITE statement and contain the following information per data record:

NPOINT, NFRAME, ((DATA(I, J), J = 1, NPOINT), I = 1, NFRAME)

Each tape record thus had several data frames (NFRAME) and each data frame is NPOINT long.

Because of the age and uniqueness of the tapes, AFWL attempted to duplicate the tapes before turning them over to MDAC for analysis. This effort was unsuccessful. The tapes were then physically transferred to MDAC. MDAC's computer equipment differs from AFWL's equipment and thus it was hoped that the tapes could be copied at MDAC. We at MDAC were also unsuccessful in using the standard tape copy routines in making duplicate copies. A data analysis routine was thus written to study the contents of each tape and determine the format of each tape. The tapes proved to be a very interesting lot indeed. None of the tapes were free from parity errors. Some of the tapes were readable at 556 bpi and some at 800 bpi, some were written in CDC S format and some in CDC SI format, some had Starad data matching the above described WRITE

---

13. Kuck, G. A., Pitch Angle Diffusion on Relativistic Electrons in the Plasmosphere (PhD Thesis), AFWL-TR-73-116, Air Force Weapons Laboratory, Kirtland Air Force Base, NM, 1973.

statement and some had a totally undecipherable format and one tape was blank. Table 8-2 lists the tapes, the specified density, the density at which the tape was readable, the format of the tape and the content of the tape. During the tape read operation a full hardware inhibit was invoked (all data was accepted regardless of error). All records that had errors on the first read attempt were ignored and not used in the analysis. Any other form of error recovery proved futile. Table 8-3 is a copy of the header information of each of the useable data files. A total of 25 data files were retrieved from the data tapes. This retrieved data set covered the period 27 October 1962 to 4 November 1962, and thus covered the Russian II and III time period.

Because of the complexity and the many tape problems, no duplicate data tapes were made. Instead, the information pertinent to this effort was transferred to permanent files on the computer system. Since the time resolution of the Starad data set was very high, only one-fifth of the data was transferred to the data files. This produced a manageable data base with adequate resolution. The intermediate files had the following format.

Record 1	Copy of the header record
Records 2-N	Data records.

Each data record had the following format.

Word	1	day of month
	2	time of day in seconds
	3-5	data channels for an experiment not used in this effort
	6-8	B_x, B_y, B_z magnetometer voltages
	9-11	B_x, B_y, B_z alternate magnetometer voltages
	12	McIlwain L parameter
	13	local magnetic field value in gamma
	14-19	West experiment counts/sec
	20	spare

Table 8-2

STARAD DATA TAPES

Tape No.	Density	Format	Comments
XDA55			Not Starad
BF95	800	S	
FF66			Not Starad
NF145			Not Starad
DB12			Not Starad
DE116			Not Starad
EI109			Not Starad
EF45	800	S	
AD104	800	S	
AF33	800	S	
AF34	—	—	Not Starad
BA58	800	S	
BD24	556	SI	Bad Tape
BF116	800	S	
CA126	556	S	
CG89	556	S	
CI9			Blank Tape
DA15			Bad Tape
DB92			Not Starad
DI79			Not Starad
EB105			Not Starad
FD82	556	S	
FD111	556	S	
FD112	556	S	
FD123	556	S	
FE33	556	SI	
FE34	556	SI	

Table 8-3

STARAD TAPE HEADER INFORMATION

```
1 VDH. 1401 ORBIT  04/1  PBK  05   271062STIMD=  6399.0
1 VDH. 1401 ORBIT  05/1  PBK  06   271062STIMD= 36499.0
1 VDH. 1401 ORBIT   6/1  PBK   7   271062STIMD= 24000.0
1 VDH. 1401 ORBIT   7/1  PBK   8   271062STIMD= 33536.0
1 VDH. 1401 ORBIT   8/1  PBK   9   271062STIMD= 43426.0
1 VDH. 1401 ORBIT  10/1  PBK  11   271062STIMD=061770.
1 VDH. 1401 ORBIT  15/1  PBK  16   281062STIMD=018018.0
1 VDH. 1401 ORBIT  17/1  PBK  18   281062STIMD= 36000.0
1 VDH. 1401 ORBIT  18/1  PBK  19   281062STIMD= 45984.
1 VDH. 1401 ORBIT  23/1  PBK  24   291062STIMD=  2434.
1 VDH. 1401 ORBIT  24/1  PBK  25   291062STIMD= 11330.0
1 VDH. 1401 ORBIT  25/1  PBK  26   291062STIMD= 20003.0
1 VDH. 1401 ORBIT  26/1  PBK  27   291062STIMD= 29411.0
1 VDH. 1401 ORBIT  30/1  PBK  34   291062STIMD= 75236.
1 VDH. 1401 ORBIT  35/1  PBK  36   301062STIMD=022548.0
1 VDH. 1401 ORBIT  36/1  PBK  37   301062STIMD=031719.0
1 VDH. 1401 ORBIT  43/1  PBK  44   311062STIMD=  7238.0
1 VDH. 1401 ORBIT  49/1  PBK  52   311062STIMD= 61291.0
1 VDH. 1401 ORBIT  56/1  PBK  57   011162STIMD= 19233.0
1 VDH. 1401 ORBIT  58/1  PBK  59   011162STIMD=055661.0
1 VDH. 1401 ORBIT  63/1  PBK  64   021162STIMD=011566.0
    J     A1 VEH. 1401 ORBIT  65/1  PBK  66   021162STIME=
    J     A1 VEH. 1401 ORBIT  66/1  PBK  67   021162STIME=
    J     A1 VEH. 1401 ORBIT  73/1  PBK  74   031162STIME=
```

The AFWL data tapes contained the data for the electron spectrometer in terms of analog voltages. The only description of the translation of these voltages to counts was given in the AFWL computer listings. The Kuck notes did not include the transformation information. A call to Dr. H. West at Lawrence Livermore failed to produce any corroboration. Dr. West said that it would be foolhardy and futile to attempt to work with the data set. Thus the subroutine transferring voltages to counts was used without comment or verification. A listing of this routine is given in Appendix C. Use of this routine gives count rates which are continuous over the voltage ranges encountered and indicate that this subroutine is the valid conversion routine for the spectrometer data.

Since the spectrometer is highly directional, the look direction of the instrument must be obtained. This once again proved to be a major detective job. No description of the look information was found in any published article or in any of the notes. Thus, it was once again necessary to decode the undocumented uncommented portion of the computer code. The AFWL program contained extensive B smoothing algorithms and other B field baseline correction elements. The pertinent lines of code were discovered only after considerable effort. Verification of correctness is not available; however, the results give reasonable pitch angle distributions and are thus thought to be correct. The following algorithms were used:

1. Convert magnetometer voltages V_x, V_Y and V_z to B_x, B_y, B_z.
   $B_x = 0.219027 * (V_x - 2\ 54256)$
   $B_y = 0.221356 * (V_y - 2.587481)$
   $B_z = 0.216310 * (V_z - 2.517688)$

2. Determine the local pitch angle α $\cos(\alpha) = (B_x * 0.86603 - B_y * 0.5 * 0.57736 - B_z * 0.5 * 0.8192)/B_{mag}$

   where $B_{mag} = \sqrt{B_x^2 + B_y^2 + B_z^2}$

3. The equatorial pitch angle, α_0, is then given by

$$\cos(\alpha_0) = 1. - 0.315\ (1-\cos^2 \alpha)/(L^3 * B)$$

where L is the local McIlwain L parameter and B is the local calculated magnetic field strength.

Figure 8-2 is a figure of counts versus equatorial pitch angle.

This study effort required the development of omnidirectional fluxes and thus conversion from directional to omnidirectional was required. If the local look angle was found to be in or close to the electron loss cone, the data must be ignored. The following approximate algorithm was used to determine the equatorial pitch angle of the loss cone, α_L.

$$\sin \alpha_L = [L^3 \sqrt{4 - 3/L}]^{-1/2} \tag{39}$$

Any measurement within 10 degrees of the equatorial loss cone was ignored. Data further from the loss cone is reasonably constant with pitch angle. Corrections for the pitch angle effect were attempted but the magnetometer data was sufficiently noisy and thus the pitch angle information was not very reliable.

The corrected data scattered more than the uncorrected data. Thus the pitch angle dependent data were multiplied by a local loss cone dependent solid angle factor to convert the data to isotropic fluxes.

Because of the narrow energy width in the Starad electron channels it was impossible to convert the Starad data into integral channels. Thus Starad is the only data set in differential form. The calibration constants of West (Reference 12) were used to convert counts to flux. A reasonably noisy data set must be integrated over the proper energy channels to obtain an integral data set. To do this routinely at each data point would have introduced unreasonably large errors.

There are five electron channels and a background channel. The highest three energy channels are strongly contaminated by bremsstrahlung and protons. Figures 8-3 to 8-8 show the six uncorrected data channels versus L. The peak at L = 1.84 is due to Russian I bremsstrahlung and not due to electron fluxes directly. When the data are corrected for the background observed by Channel 6, the peak disappears. Figures 8-9 through 8-11 show the background corrected rates before the Russian II event. Figures 8-12 to 8-16 show the data during October 29-30, 1981, just after Russian II. The lowest 4 energy channels show a distinct Russian II enhancement, however, the enhancement appears lost in the noise for the highest energy channel. The data before Russian II can be fitted by a polynomial in L and equatorial pitch and (a polynomial with order 4 in L and order 2 in pitch angle was used) used as a background function for determining the true injected flux component for the Russian II and Russian II, III data set.

8.3 Error Analysis

H. West (Reference 12) indicates that the basic errors are on the order of 30 percent. Pitch angle uncertainties, as well as noise in the pitch angle data, substantially increase the size of the errors. The total errors of the raw data corrected by the measured background channel consists of the statistical error, the uncertainty in knowing the exact intercalibration between the data channel and the background channel (a 25 percent uncertainty was assumed) and the error due to position uncertainties. Once the fluxes are to be converted to isotropic fluxes, additional errors occur. There is at least a 5-degree pitch angle uncertainty, the exact shape of the pitch angle function is unknown and a single directional point measurement must be converted to an isotropic flux. The errors in this conversion can be as large as 50 percent to a factor of 2.

Thus if N_B is the number of counts in the background channel, the error in the background count rate, E_B, is

$$E_B = \sqrt{(\sqrt{N_B})^2 + (0.25\ N_B)^2} \qquad (40)$$

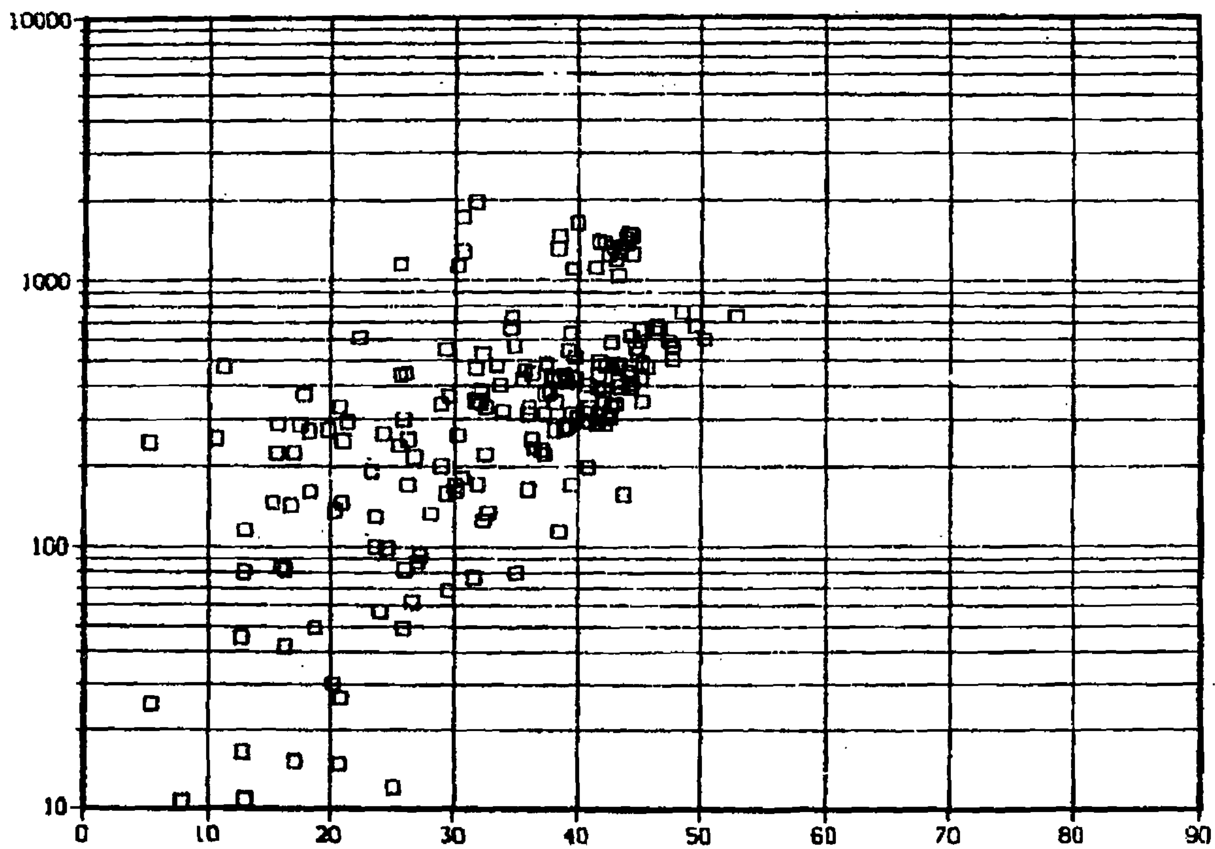

Figure 8-2. Equatorial Pitch Angle for Starad Channel 3 at L = 2.1 to 2.3

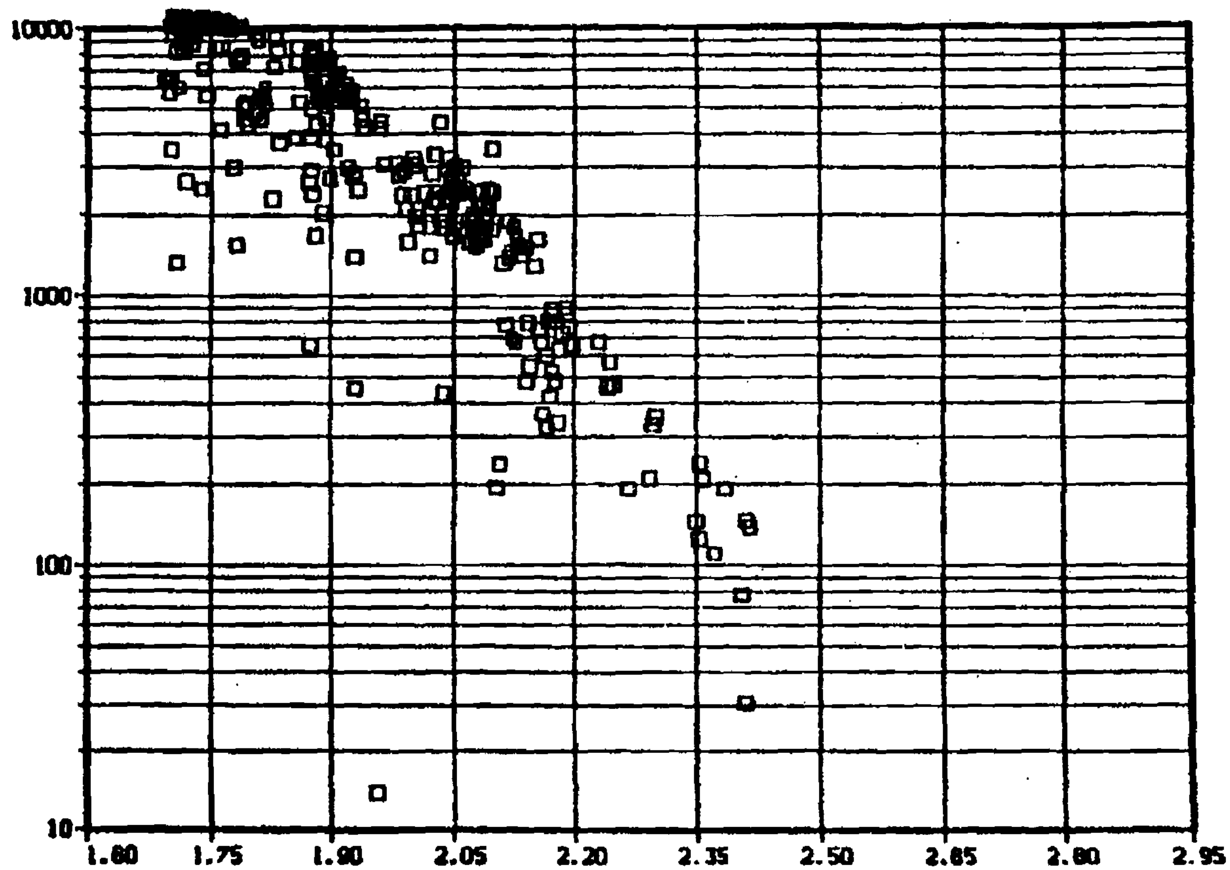

Figure 8-3. Uncorrected Starad 325-keV Channel Versus L Prior to Russion II

127

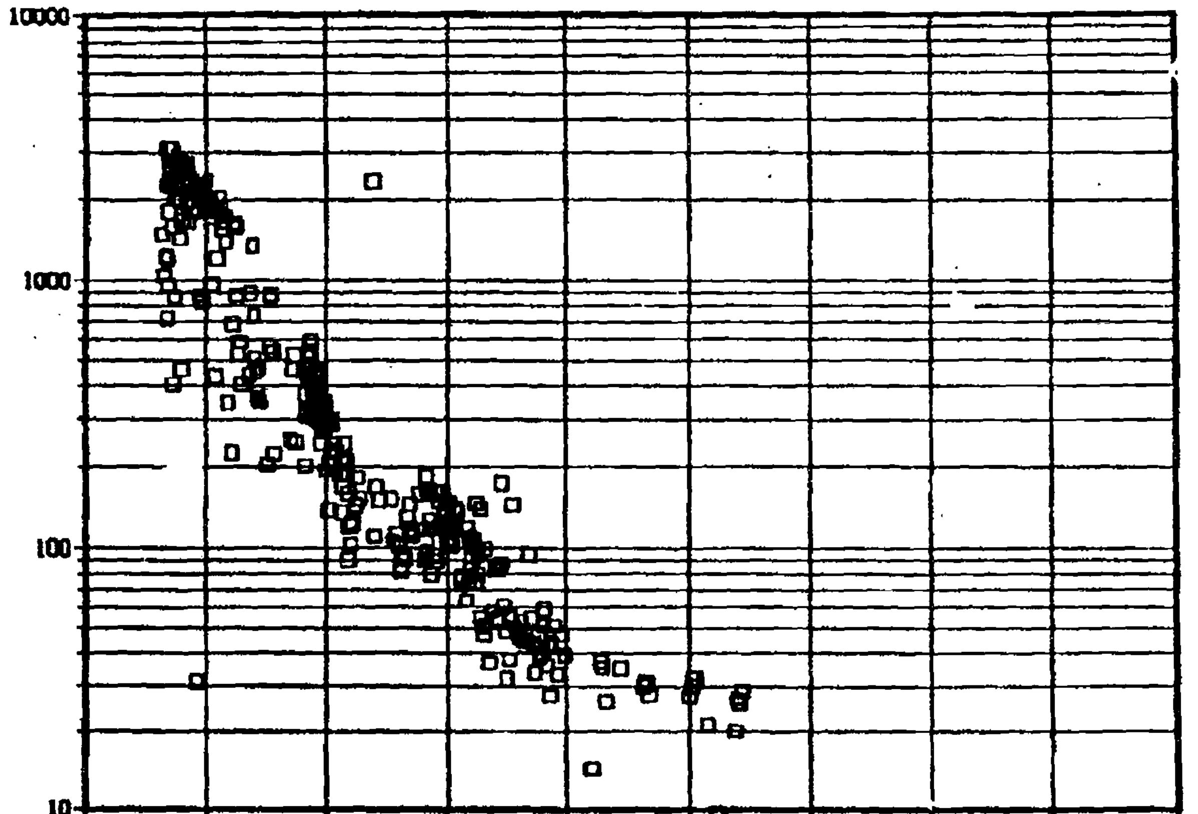

Figure 8-4. Uncorrected Starad 955-keV Channel Versus L Prior to Russian II

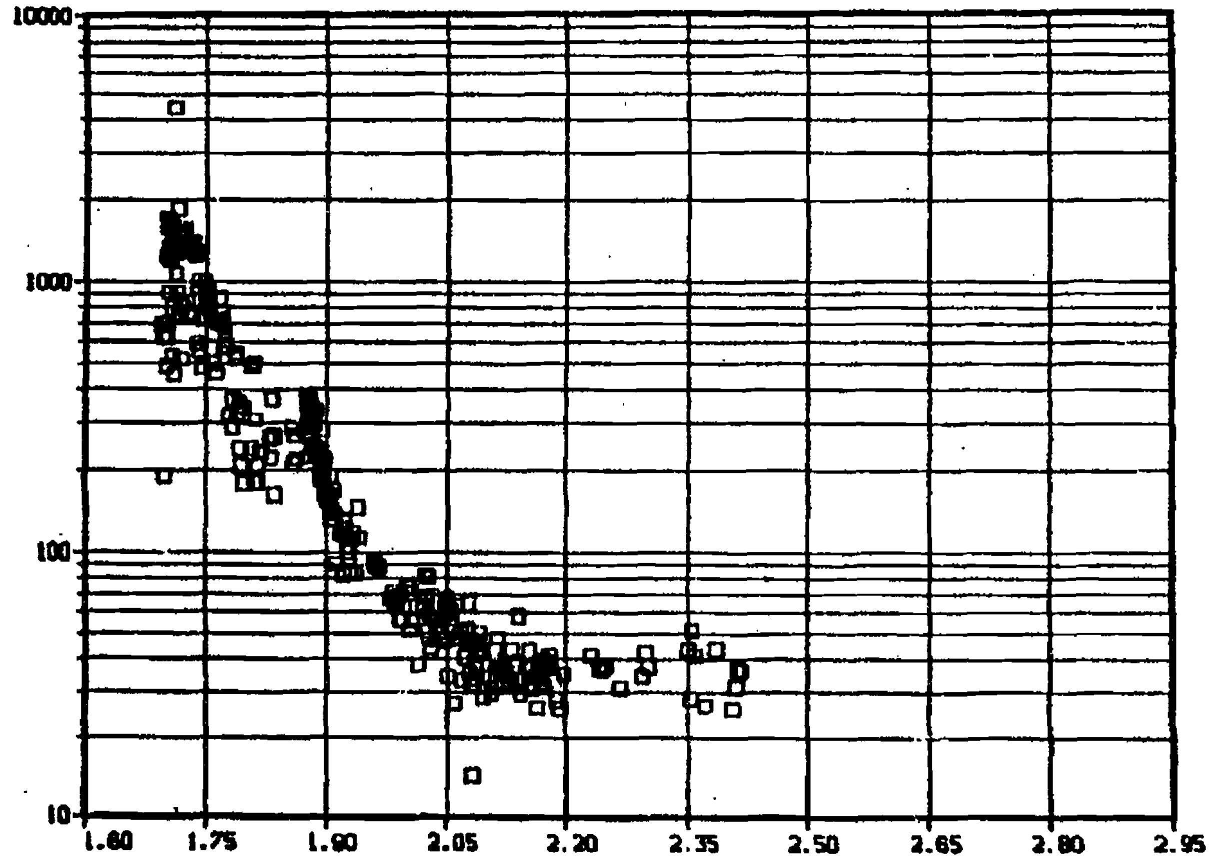

Figure 8-5. Uncorrected Starad 1630-keV Channel Versus L Prior to Russian II

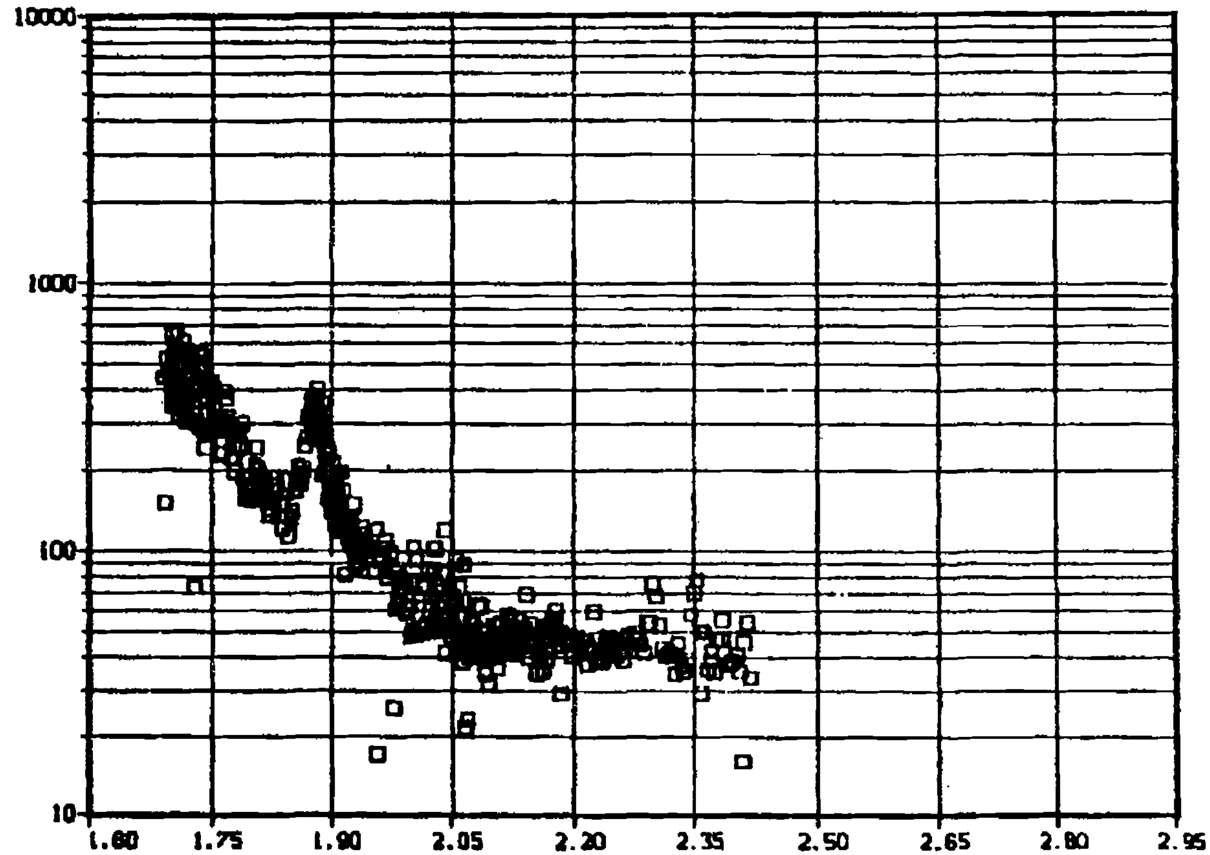

Figure 8-6. Uncorrected Starad 2400-keV Channel Versus L Prior to Russian II

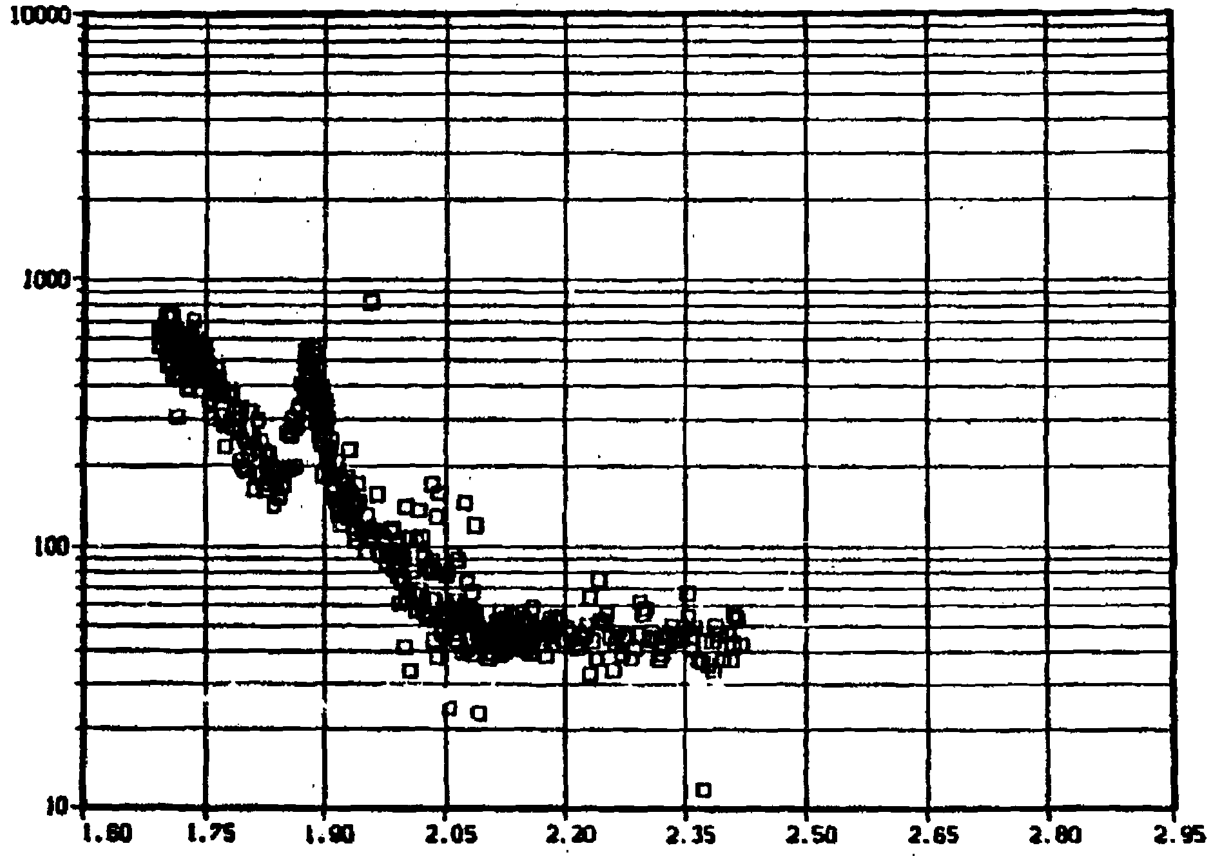

Figure 8-7. Uncorrected Starad 3250-keV Channel Versus L Prior to Russian II

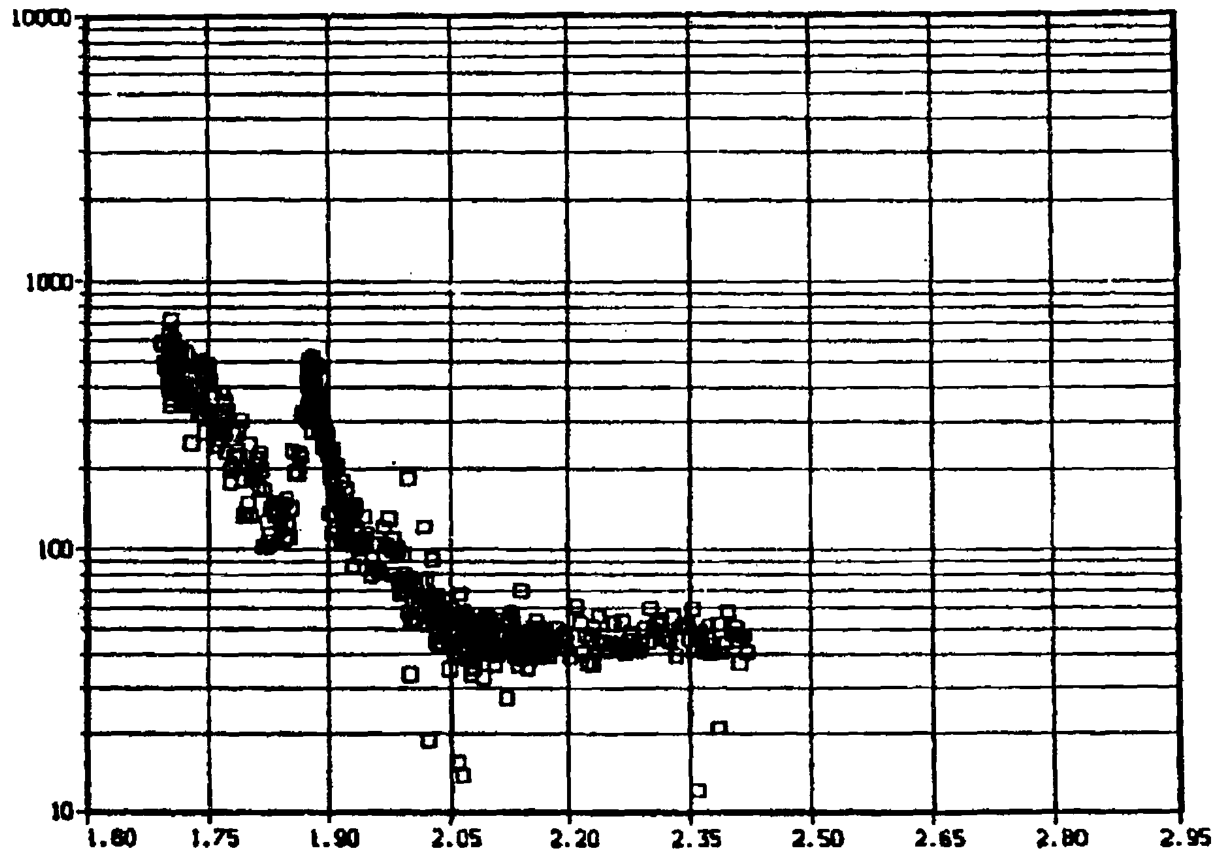

Figure 8-8. Uncorrected Starad Background Channel Versus L Prior to Russian II

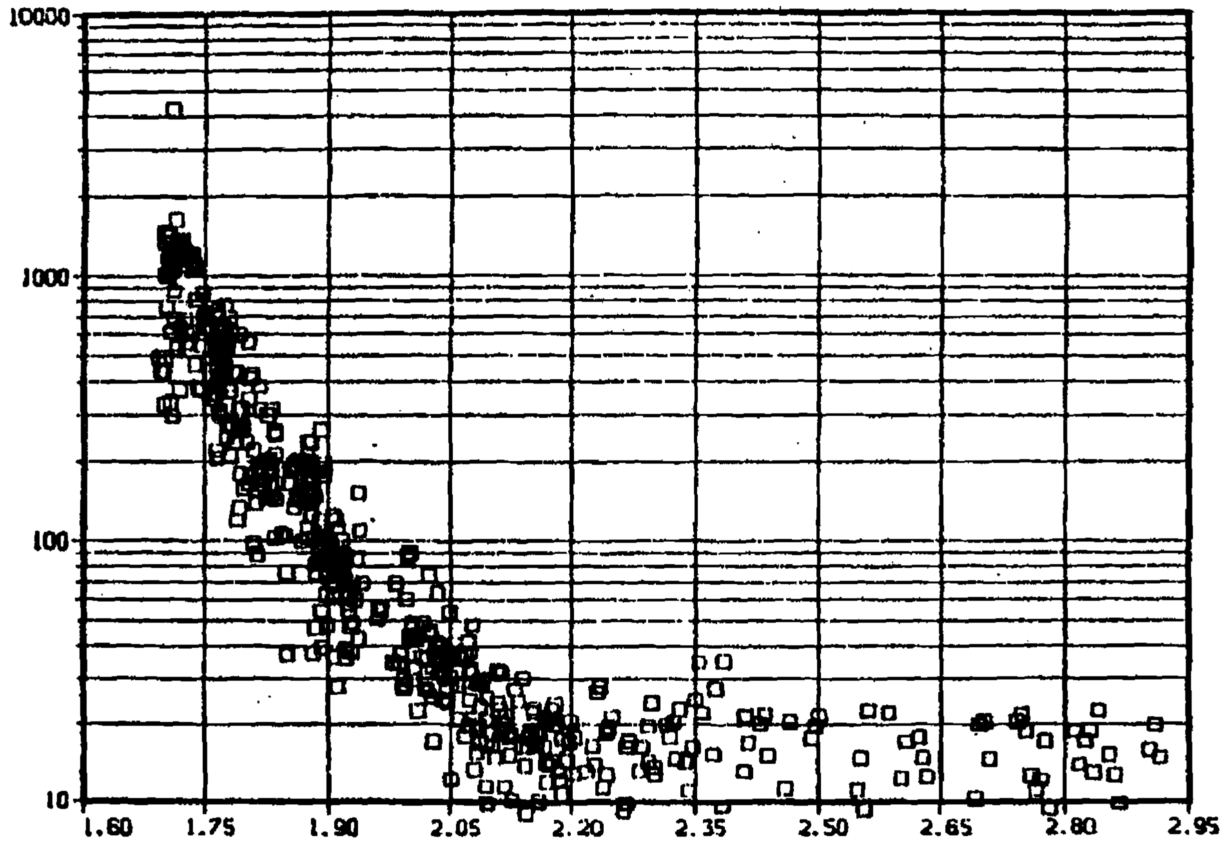

Figure 8-9. 1630-keV Starad Channel Prior to Russian II Corrected by the Counts in the Background Channel

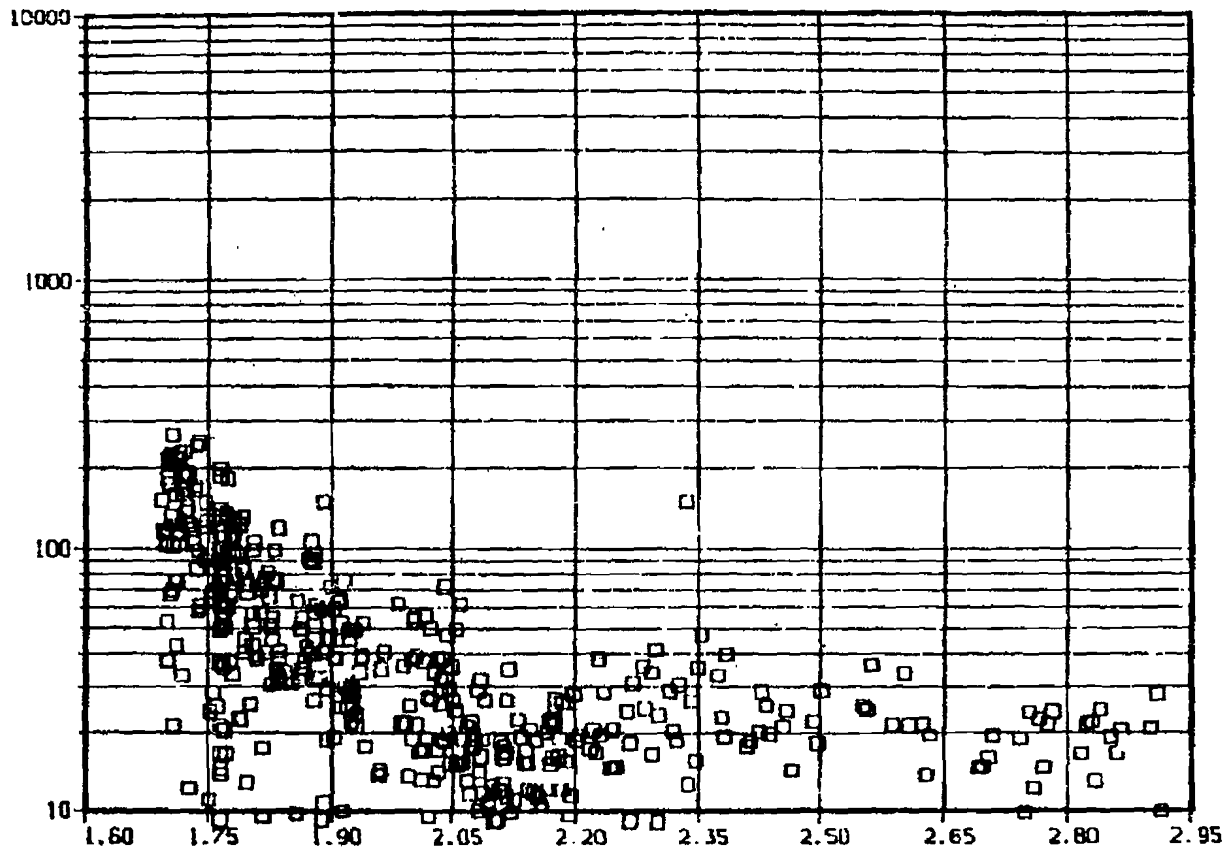

Figure 8-10. 2400-keV Starad Channel Prior to Russian II Corrected by the Counts in the Background Channel

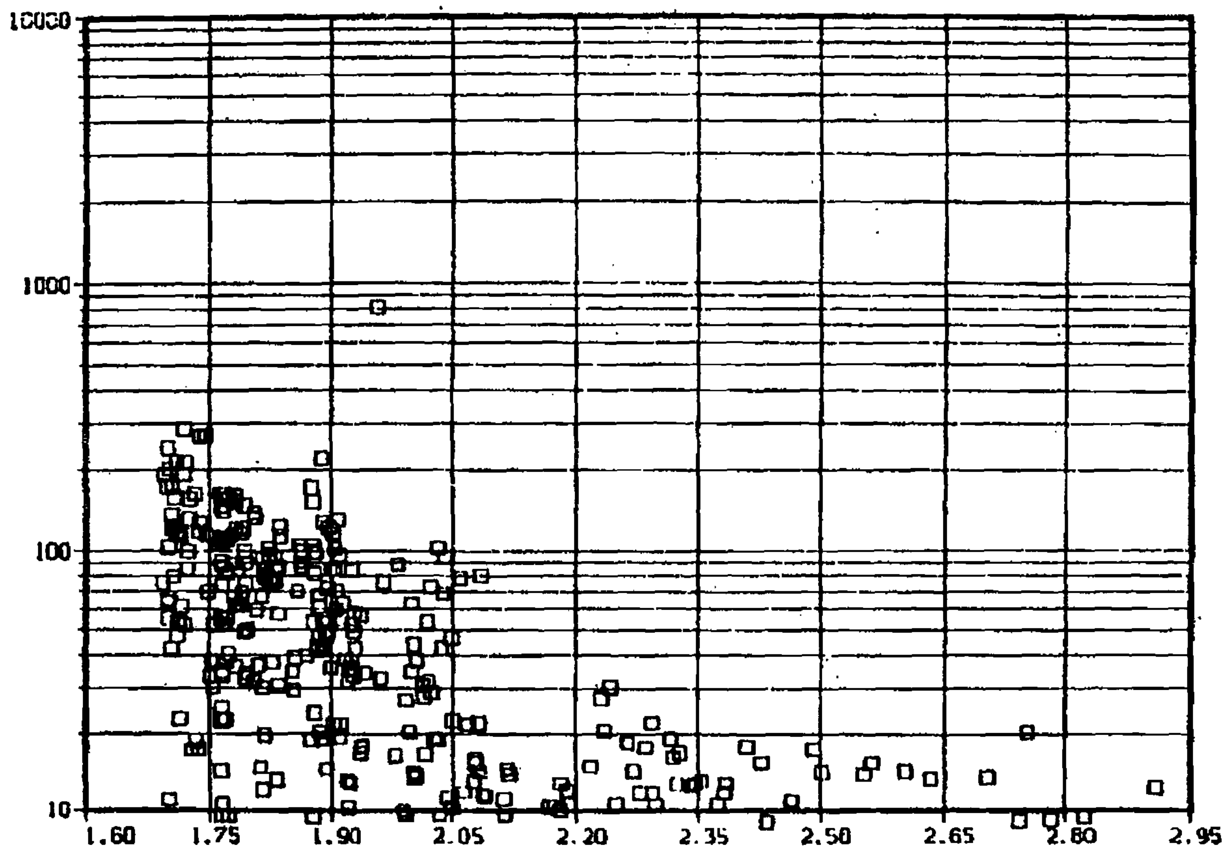

Figure 8-11. 3250-keV Starad Channel Prior to Russian II Corrected by the Counts in the Background Channel

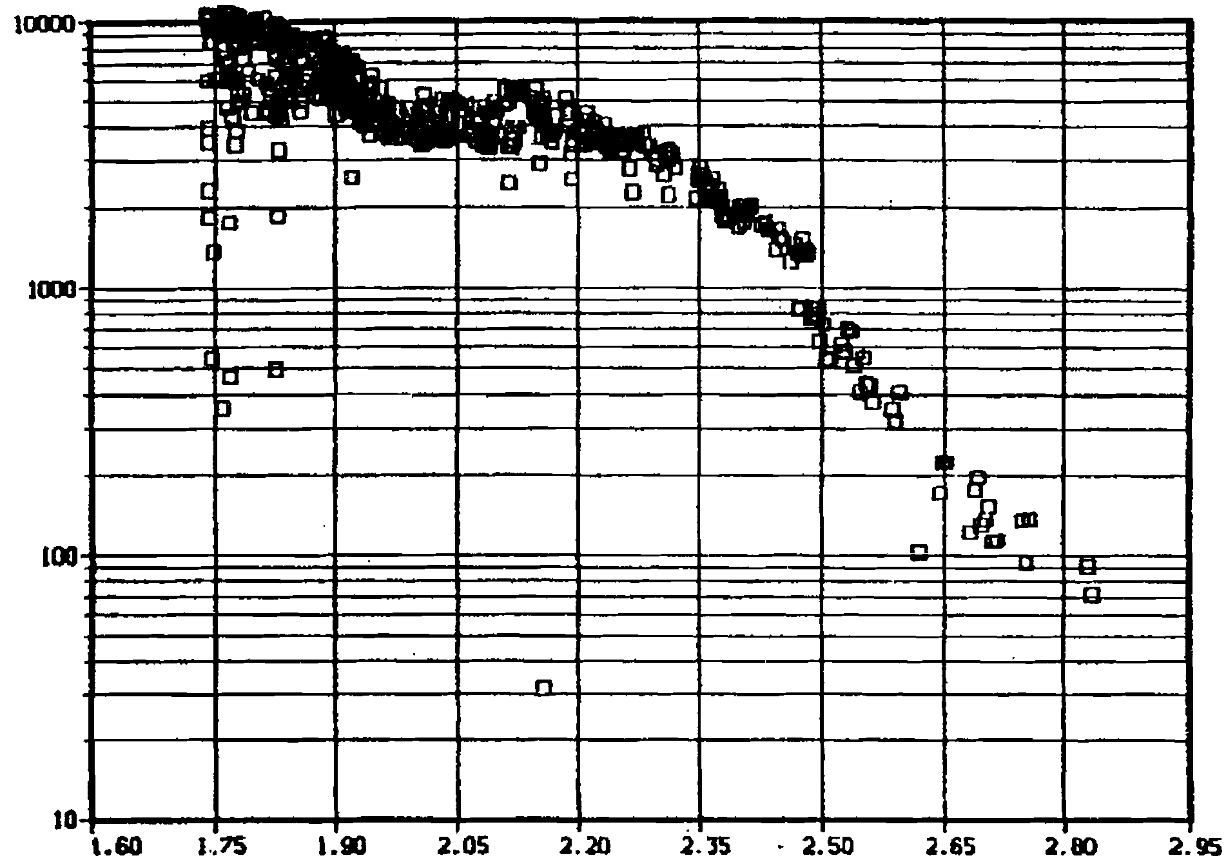

Figure 8-12. Background Channel Corrected 325-keV Channel After Russian II

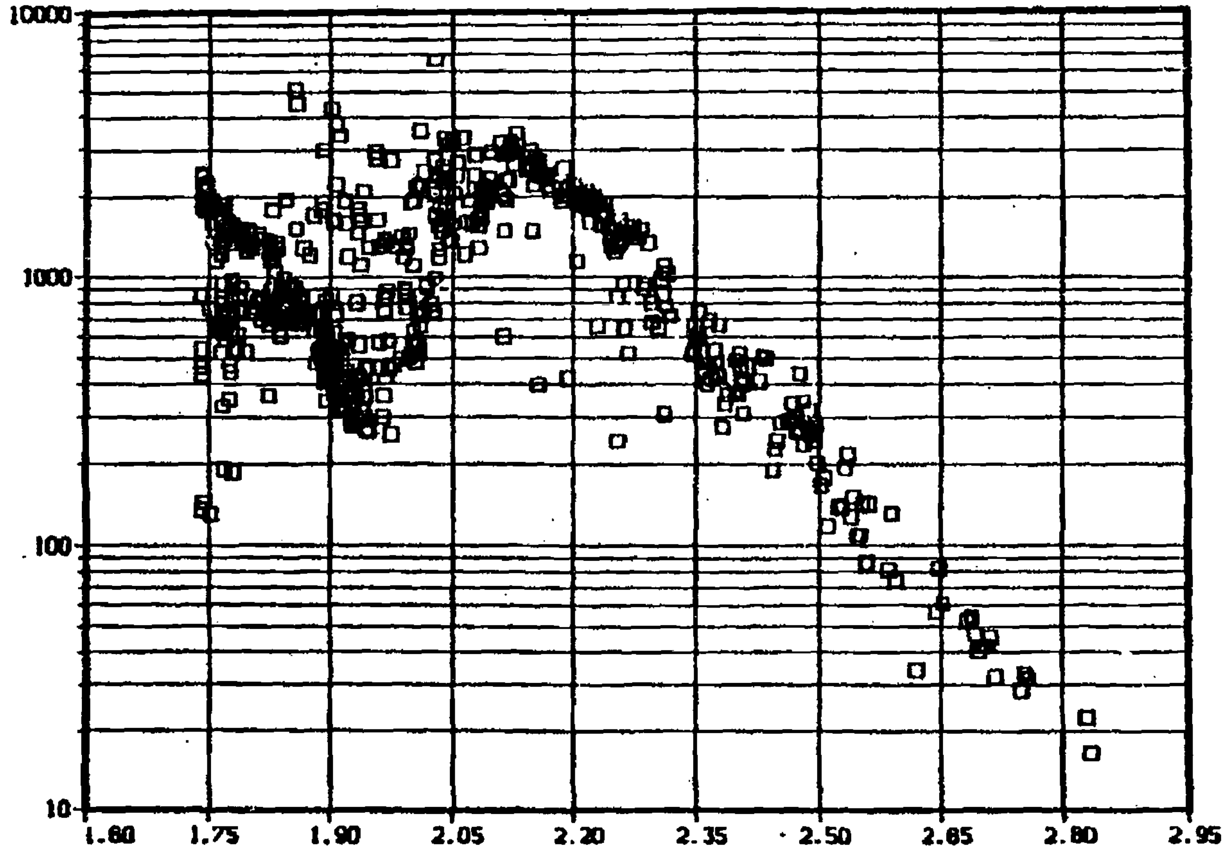

Figure 8-13. Background Channel Corrected 955-keV Channel After Russian II

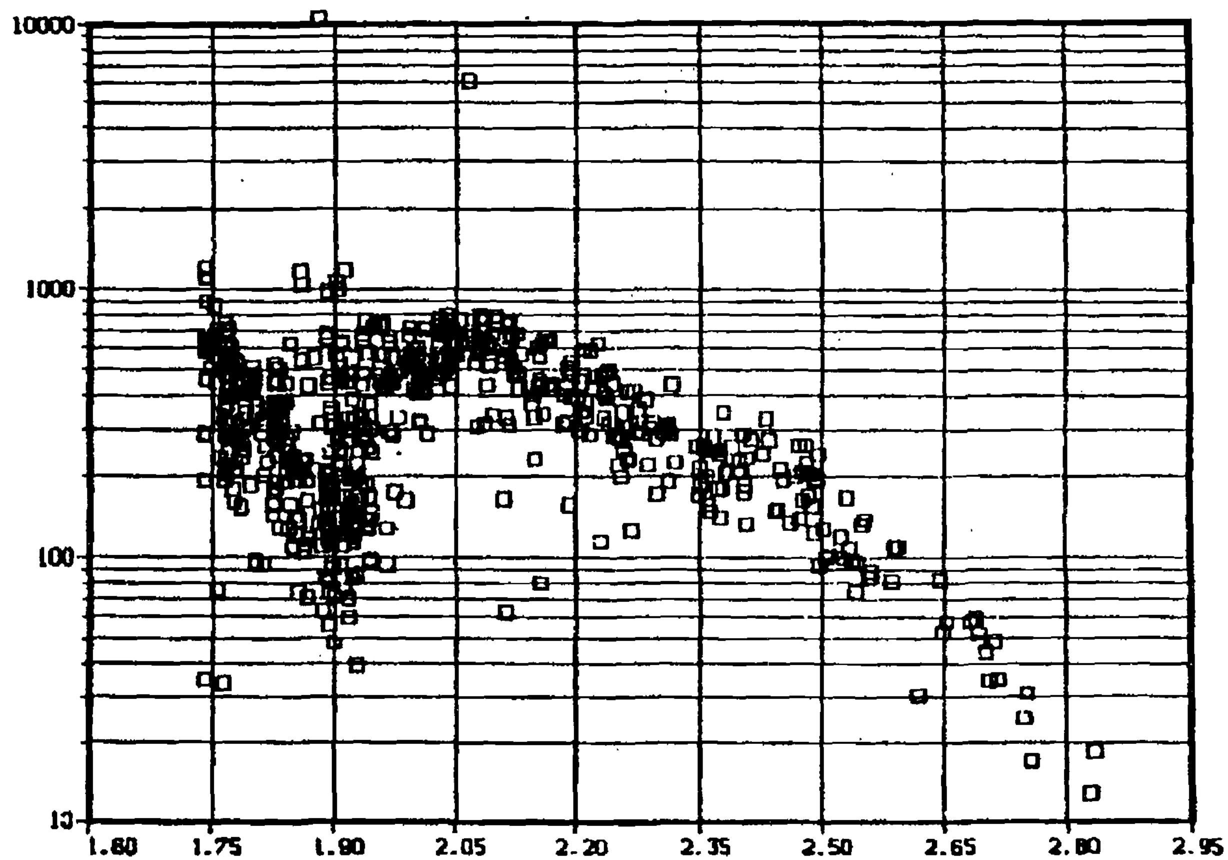

Figure 8-14. Background Channel Corrected 1630-keV Channel After Russian II

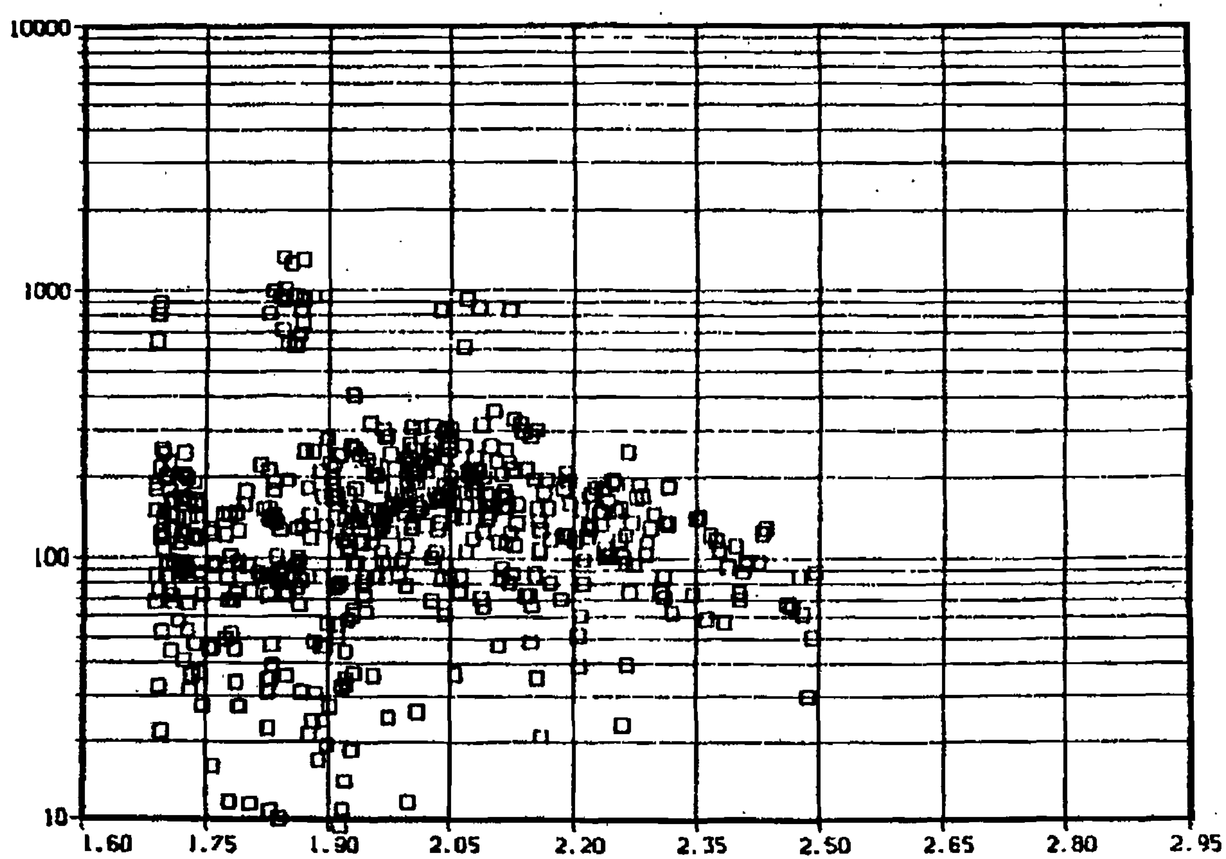

Figure 8-15. Background Channel Corrected 2400-keV Channel After Russian II

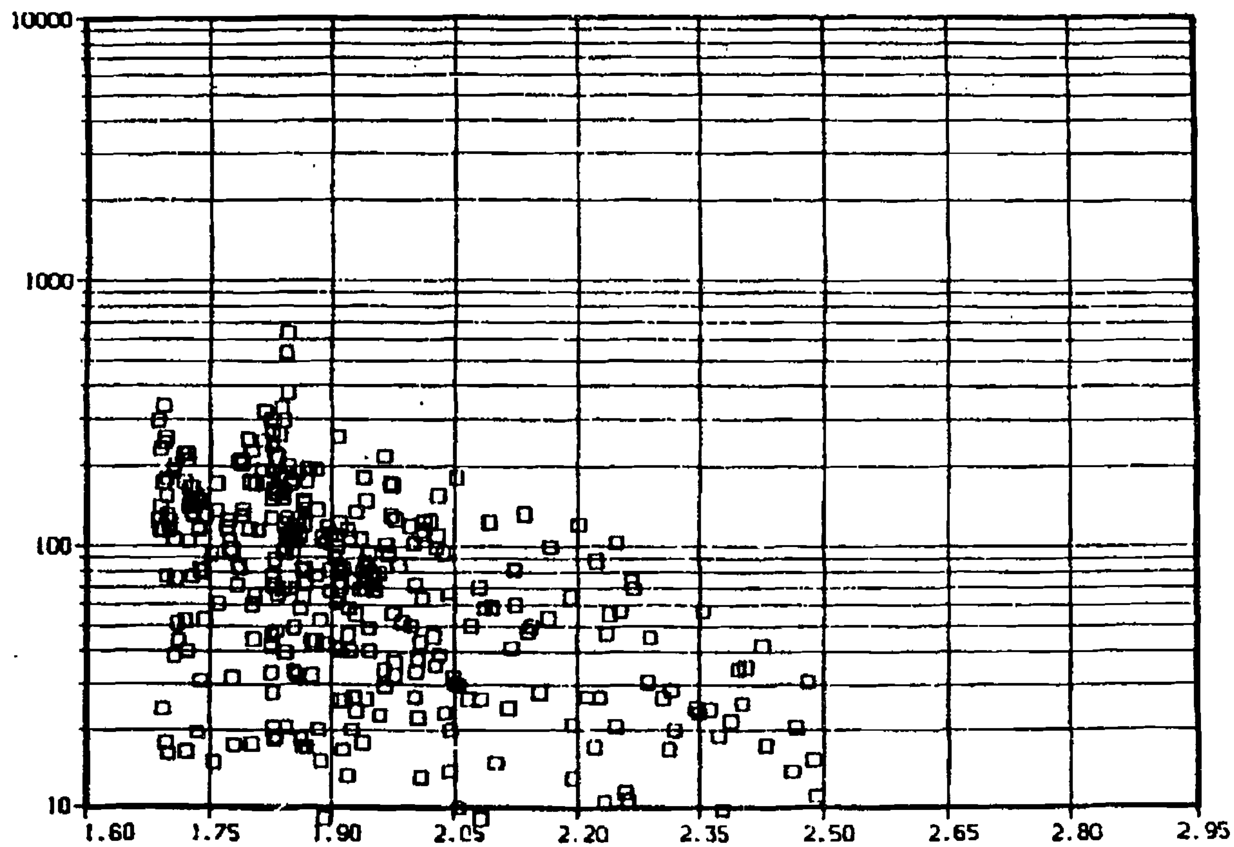

Figure 8-16. Background Channel Corrected 325-keV Channel After Russian II

If N_D is the number of counts in one of the data channels. The error in the data channel directional counts, E_D, is

$$E_D = \sqrt{(\sqrt{N_D})^2 + (0.30\ N_D)^2} \tag{41}$$

The error F_{error} in the flux, F, of a channel is then

$$F_{error} = \sqrt{(0.5\ F)^2 + (N_B\ (0.25\ N_B)^2 + N_D + 0.30\ N_D^2)\ G} \tag{42}$$

where G is the geometry factor.

Thus from Equation 42 one can see the uncertainty in the electron flux is always worse than 50 percent and for the higher channels where the background corrections due to bremsstrahlung and protons is large. The error very often approaches a factor of two. Additional errors are introduced when the Russian I/Starfish background is subtracted out of the data set. The r.m.s. error of the least squares fit to the data was 45 percent. Thus the total probable flux error

$$(F_{error})_{Total} = \sqrt{(F_{error})^2 + (.45\ F_{fit})^2} \tag{43}$$

where F_{fit} is determined from the polynomial function for the Russian I/Starfish background evaluated at the observation point.

The above described errors are believed to include all errors. Calibration errors for the spectrometer in excess of those discussed are small. Energy ambiguities are also expected to be small. It is felt that no additional errors are present. Furthermore, agreement between Telstar, Explorer XV, and Alouette is such that the above described errors include all known effects (see Section 10). The steep spectral slope observed by the low energy Starad channels agree with the Telstar observations.

Section 9

THE INJUN I SATELLITE

Injun I carried several detectors. Among these were Geiger tubes and a spectrometer. However, the intense proton and bremsstrahlung background prevented these instruments from accurately measuring the electron flux. The only detector that was ever used in the analysis of the Starfish burst is the heavily shielded background detector.

9.1 Detector Description

The detector is an Anton type 213 Geiger tube encased in 3.5 g/cm^2 of lead. This detector has an approximate geometry factor of 0.2 cm^2. The detector shielding is adequate to stop the penetration of electrons with energies of less than 10 MeV.

9.2 Instrument Calibration

The Injun I spacecraft was calibrated in a flux of fission electrons at Los Alamos. The Injun detector measured 1/4000 of the total fission flux. These calibration tests showed that the detector responded primarily to bremsstrahlung from several MeV electrons. A slight improvement can be made in defining the response of Injun I to electrons. Very little of the response of the Injun I detector is to electrons less than 1 MeV. An energy above 1 MeV can be used and the conversion factor for that energy can then be defined as was done for the Traac instruments in Section 7. A parametric analysis of the response of the heavily shielded background detector to a range of reasonable spectral shapes was performed using electron and bremsstrahlung transport computer codes. The analysis shows that the response of this detector is not particularly sensitive to spectral shapes for electron response thresholds from 1.5 to 3.0 MeV. Although the minimum sensitivity to spectral shape occurred at 2.5 MeV, a threshold value of 1.5 MeV was used primarily for the sake of comparisons. This is the same value as Traac. Thus we define a $\bar{G}$ such that $1/\bar{G}$ can be multiplied by counts/sec to obtain the number of electrons/cm^2/sec greater than 1.5 MeV. Using the equations from Traac,

$$\frac{\int_0^\infty G(E)\, f(E)\, dE}{\int_0^\infty f(E)\, dE} = \frac{1}{4000} = 2.5 \times 10^{-4} \tag{44}$$

it can be shown that $\overline{G} = \frac{2.5 \times 10^{-4}}{0.298}$ and thus that $\overline{G} = 8.4 \times 10^{-4}$ when f(E) is a fission spectrum.

9.3 Data Analysis

The Injun I data were available on a NSSDC data tape in BCD format. The tape was of physically poor quality (many parity errors) but otherwise presented no special problems. A period before Starfish and a period just after Starfish was analyzed.

9.4 Background

Figures 9-1 to 9-18 show pre-Starfish plots followed by Starfish plots. It can be seen that in all cases where the counts/second are greater than the noise level of about 1 count/sec the Starfish flux is at least an order of magnitude above the background level.

9.5 Error Analysis

Use of Injun I to specify a measurement of electrons above 1.5 MeV is arbitrary. If the spectrum is an exact fission spectrum then the results are valid to within a factor of 2 or better. However, deviation from a fission spectrum can produce large errors in the calibration. The changes are not calculable, since no response curves are available for the Injun detector. For the tape generation a simple statistical error and a factor of 2 deterministic error was used. This factor of 2 error is not included on the tape. The total error specified on the tape is $E_T = 1/G \sqrt{N_D}$, where $\sqrt{N_D}$ is the statistical error.

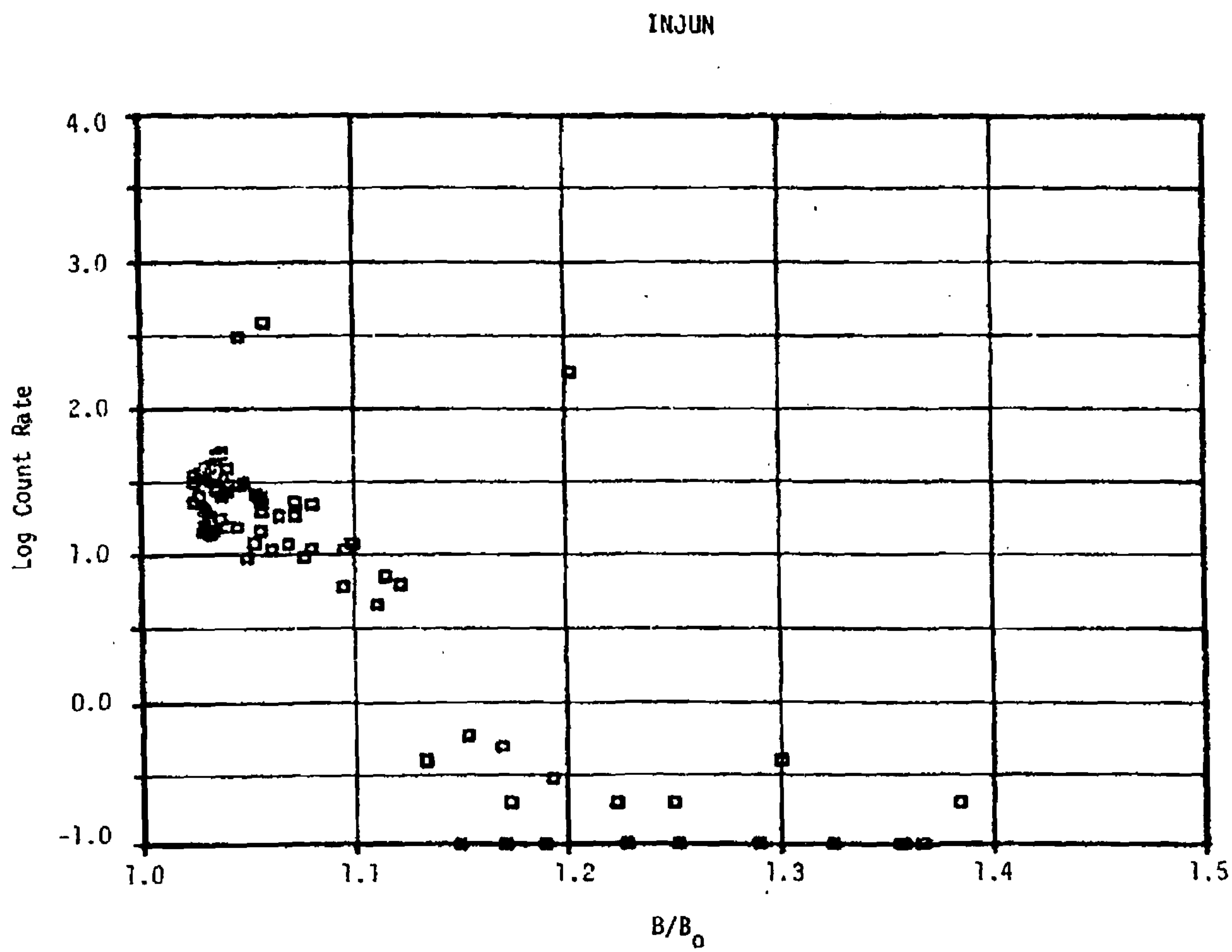

Figure 9-1. Pre-Starfish Cout Rate Versus B/B_0 at $1.16 < L < 1.17$

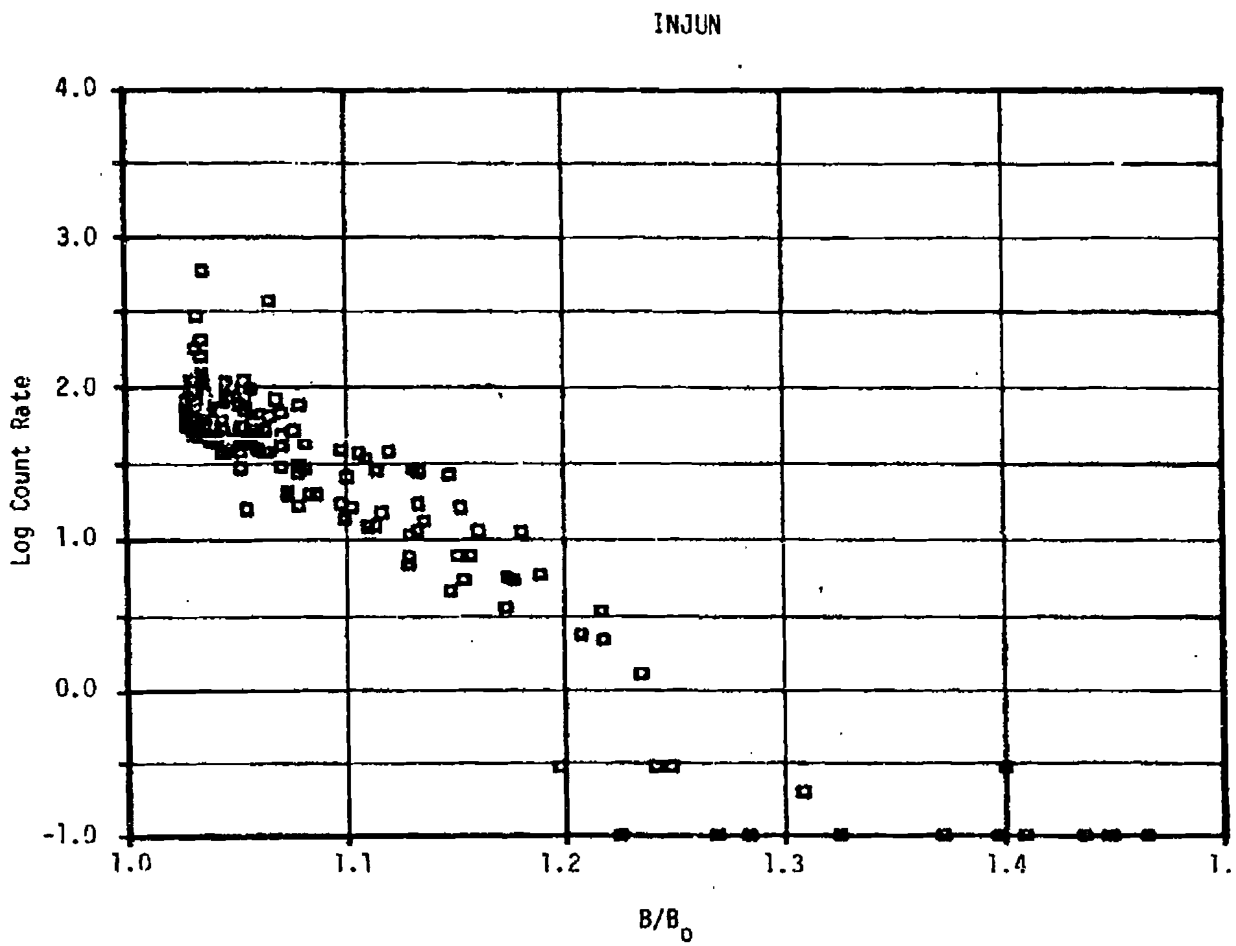

Figure 9-3. Pre-Starfish Count Rate versus B/B_0 at $1.18 < L < 1.20$

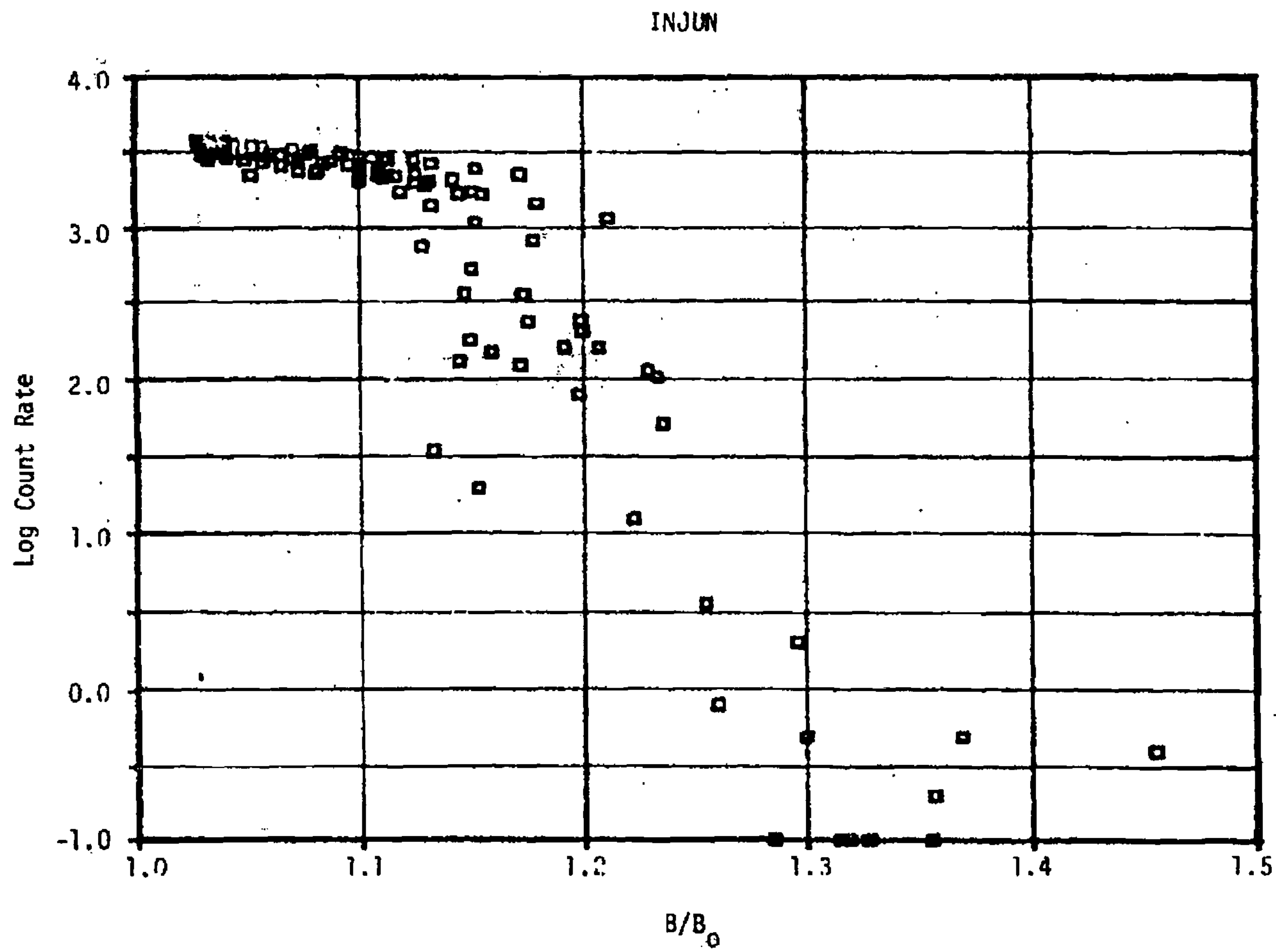

Figure 9-4. Starfish Count Rate Versus B/B_o at $1.18 < L < 1.20$

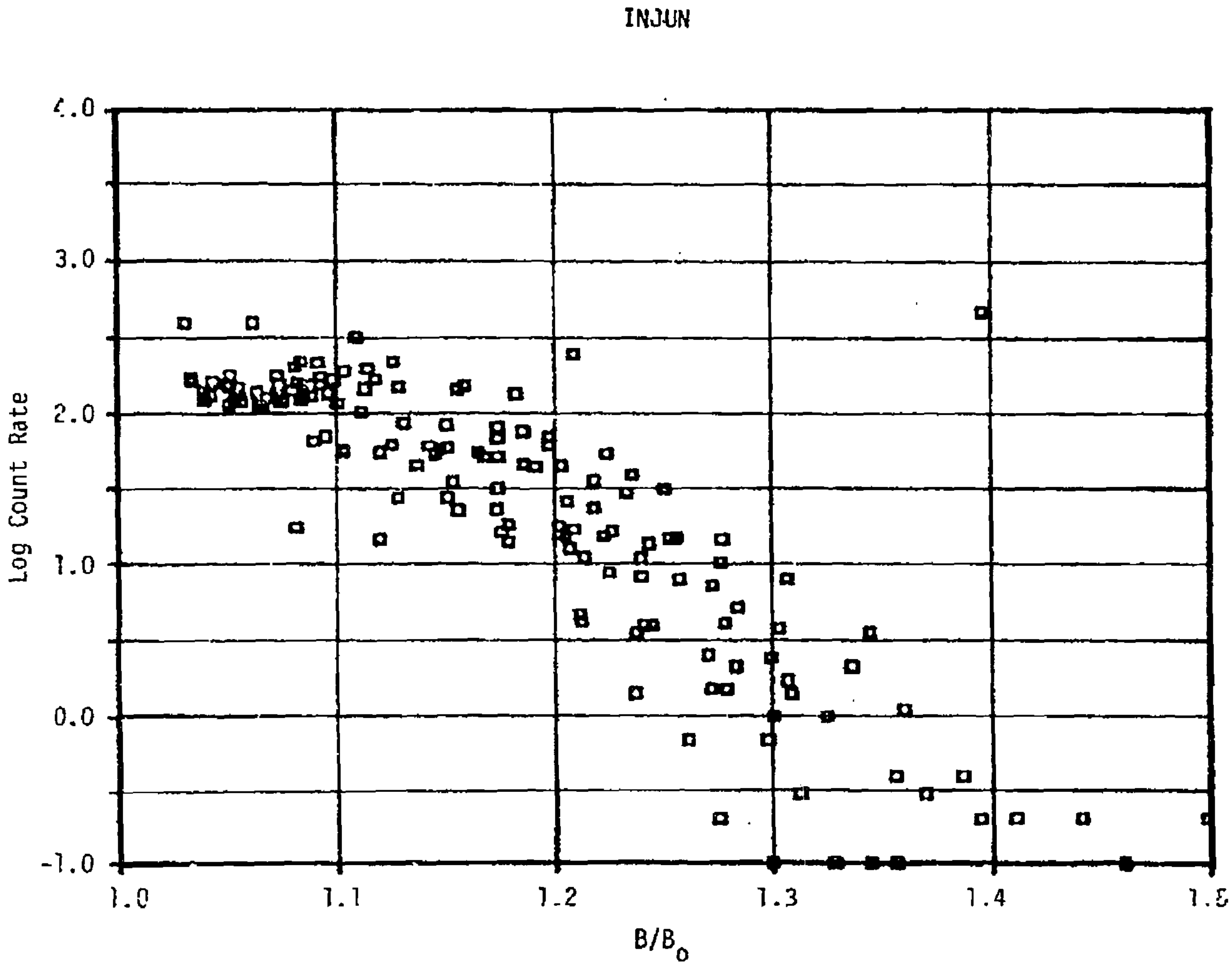

Figure 9-5. Pre-Starfish Count Rate Versus B/B_o at $1.20 < L < 1.23$

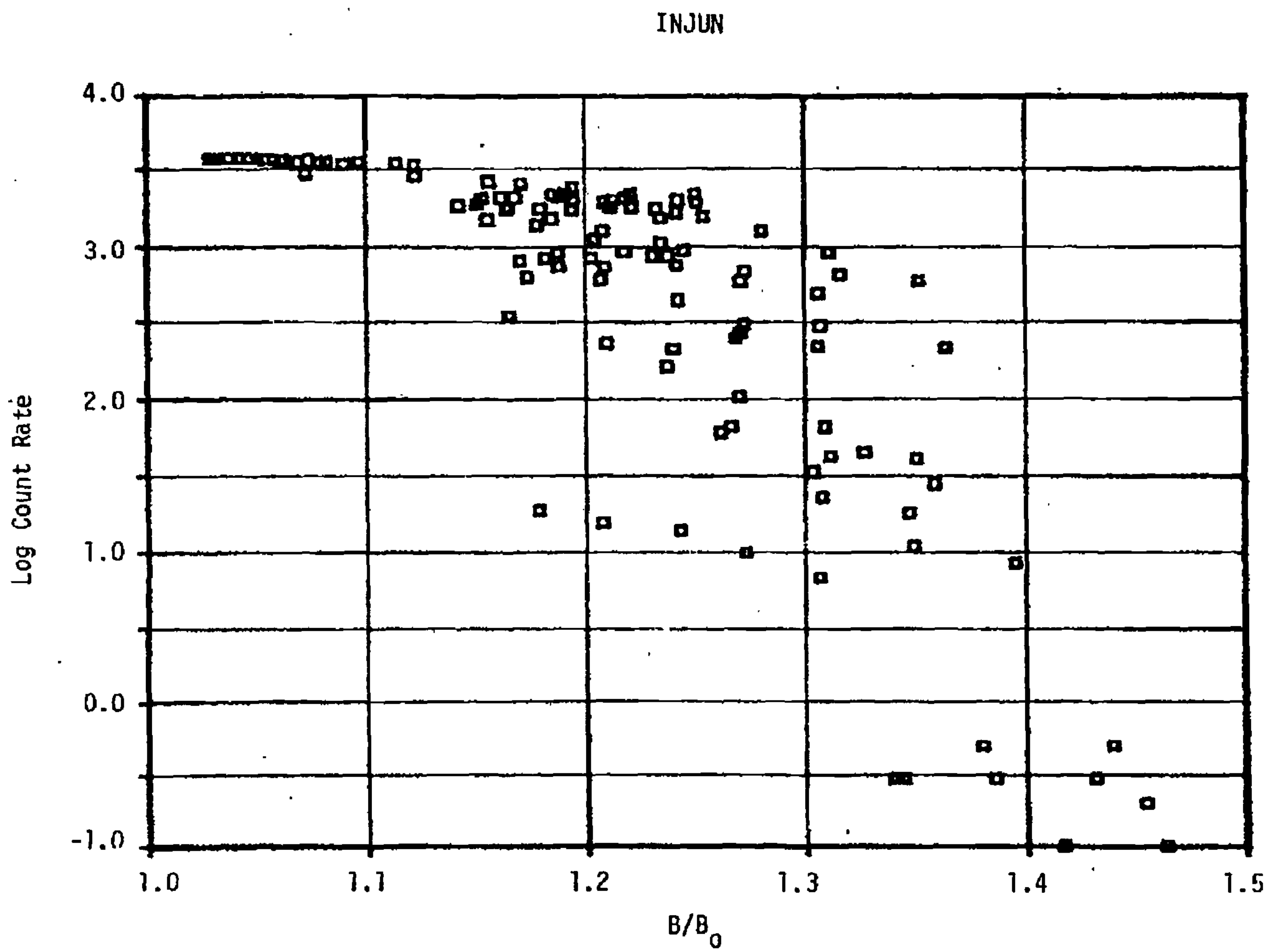

Figure 9-6. Starfish Count Rate Versus B/B_0 at $1.20 < L < 1.23$

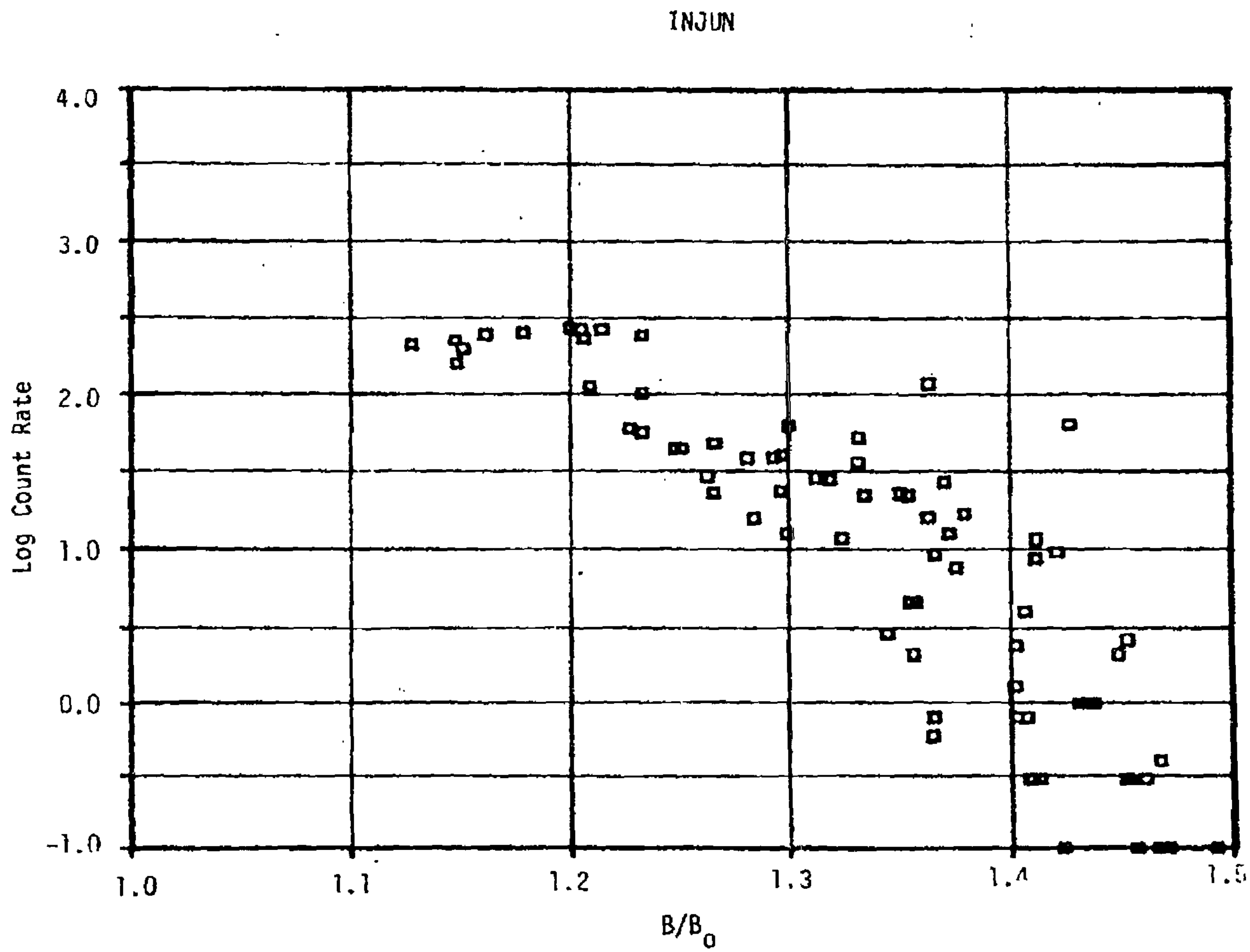

Figure 9-7. Pre-Starfish Count Rate Versus B/B_0 at $1.23 < L < 1.26$

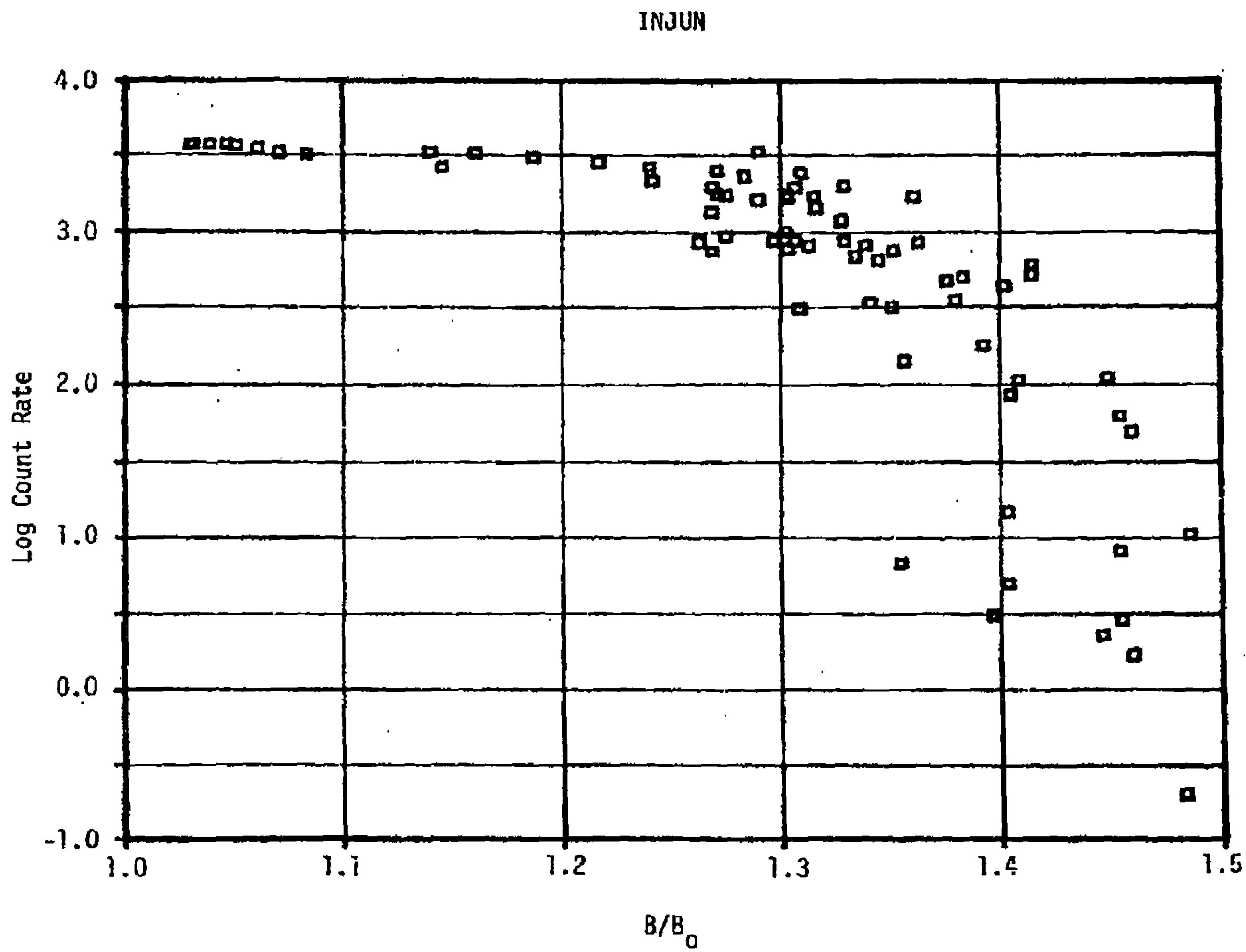

Figure 9-8. Starfish Count Rate Versus B/B_o at $1.23 < L < 1.26$

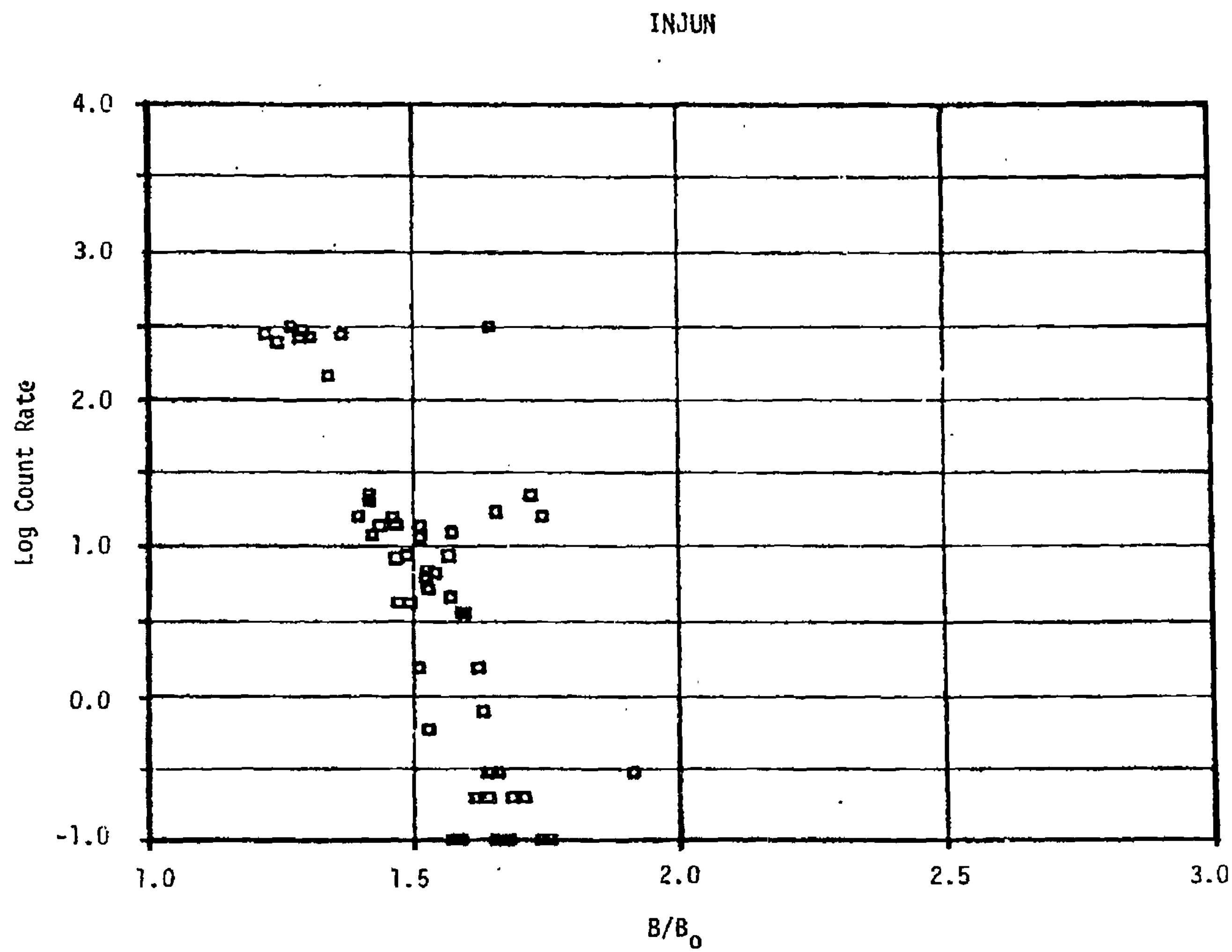

Figure 9-9. Pre-Starfish Count Rate Versus B/B_0 at $1.26 < L < 1.30$

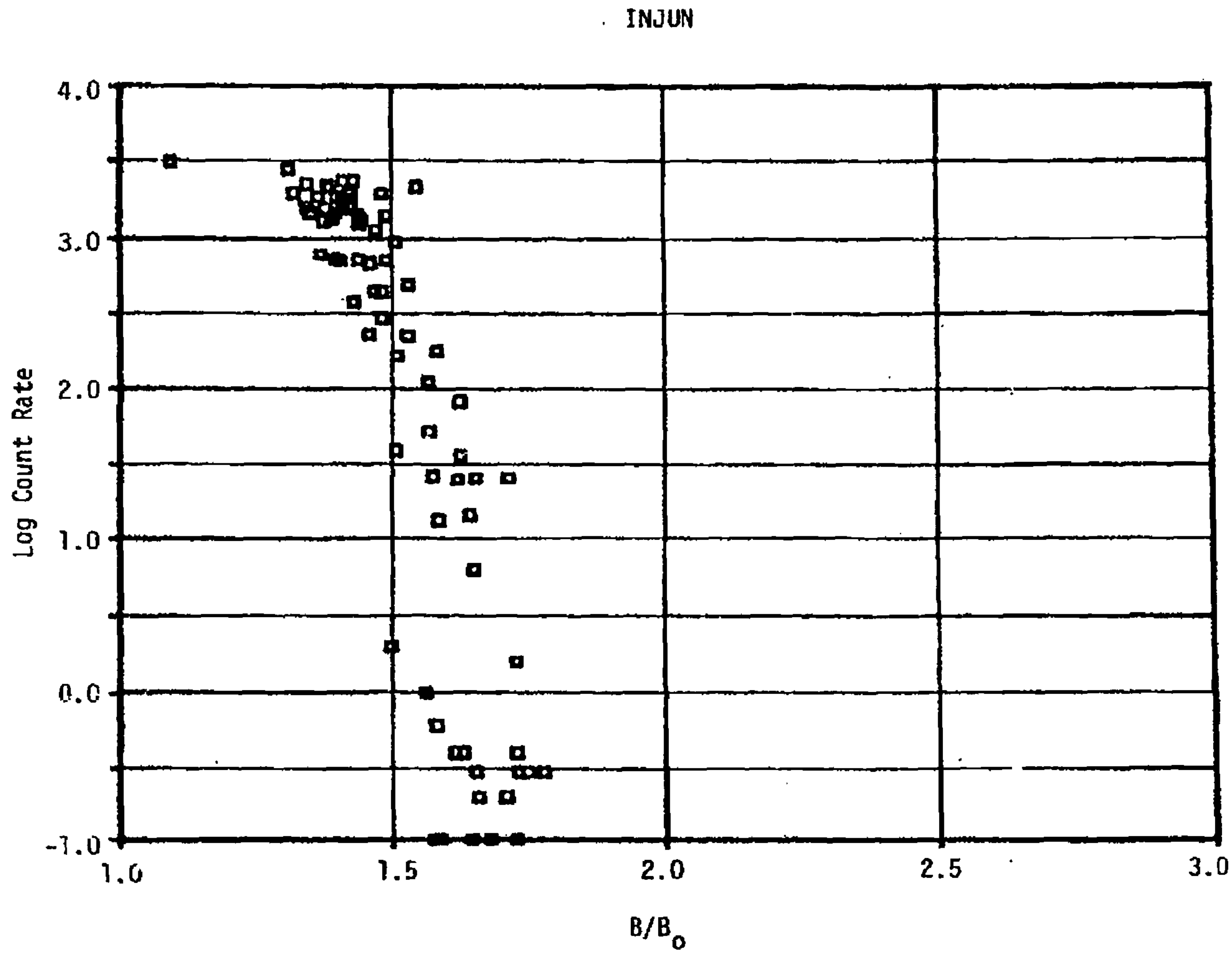

Figure 9-10. Starfish Count Rate Versus B/B_0 at $1.26 < L < 1.30$

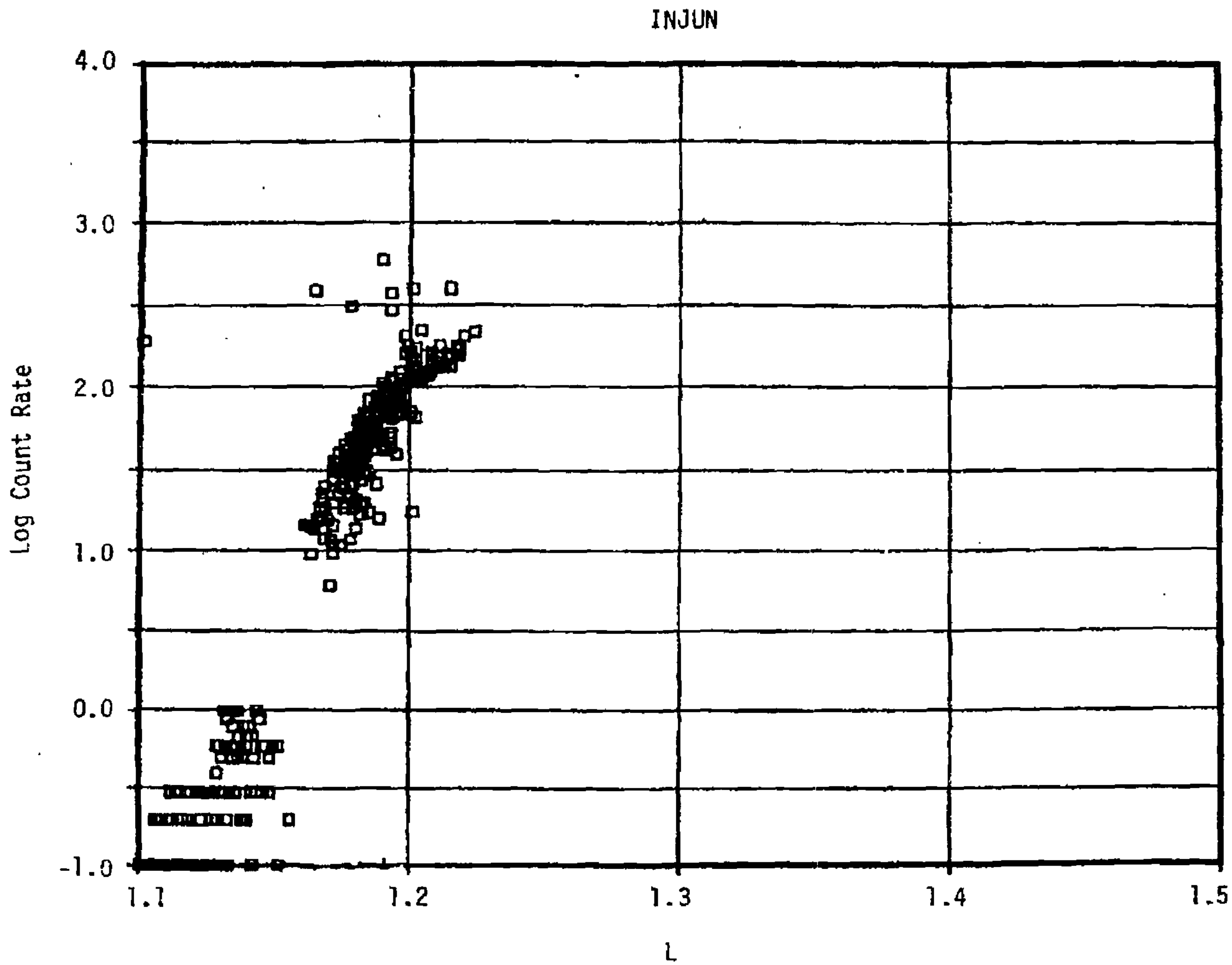

Figure 9-11. Pre-Starfish Count Rate Versus L at $1.0 < B/B_0 < 1.1$

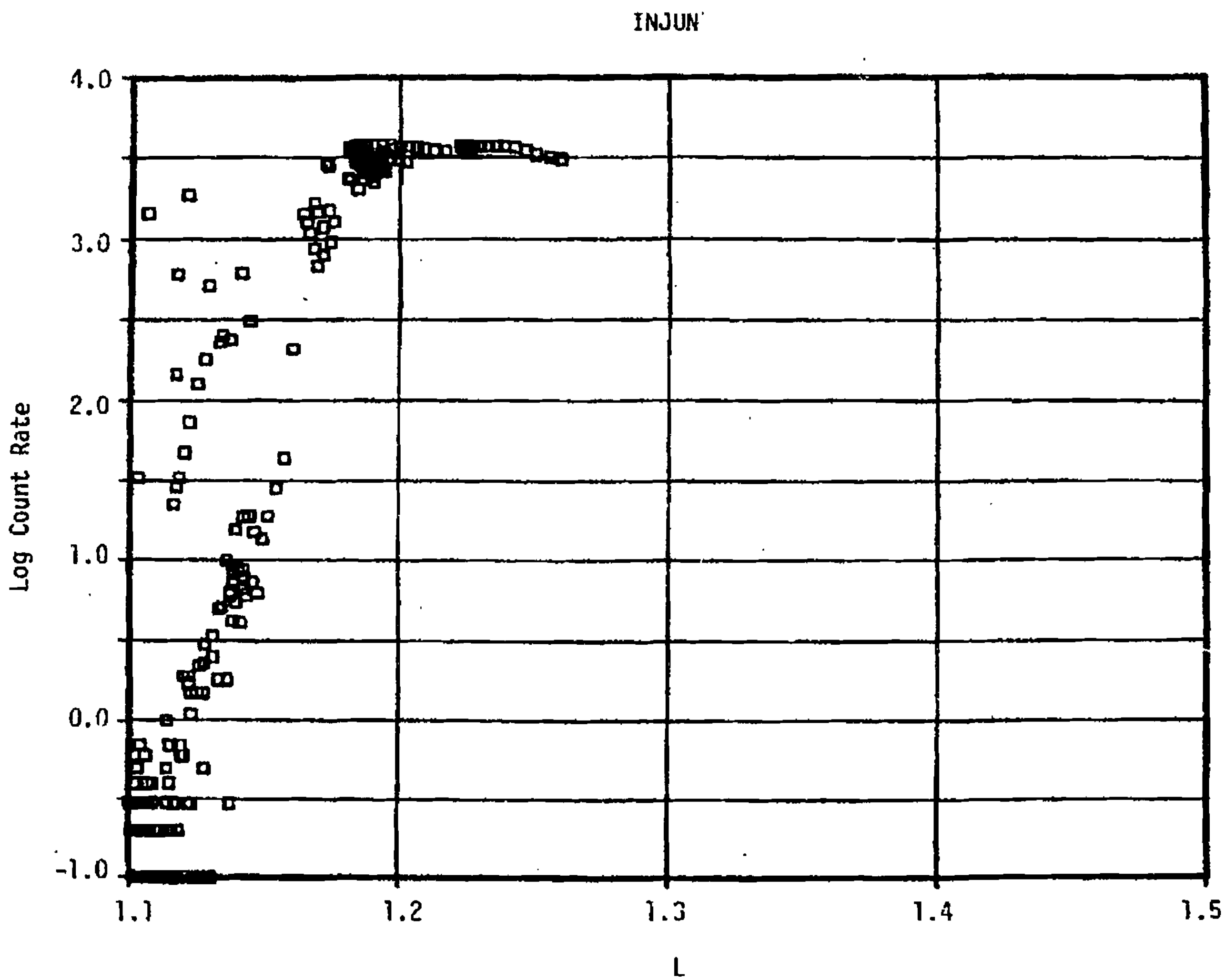

Figure 9-12. Starfish Count Rate Versus L at $1.0 < B/B_0 < 1.1$

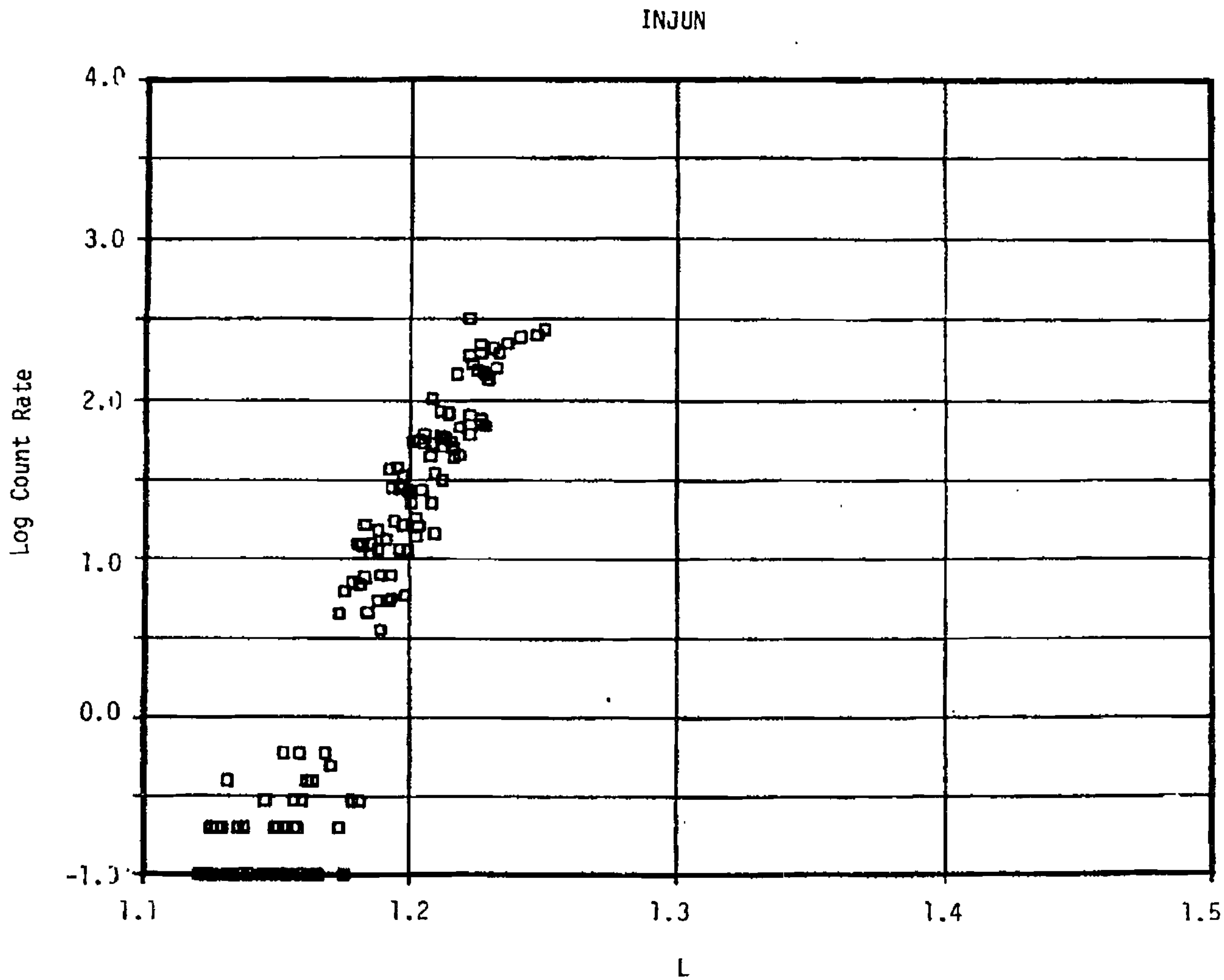

Figure 9-13. Pre-Starfish Count Rate Versus L at $1.1 < B/B_o < 1.2$

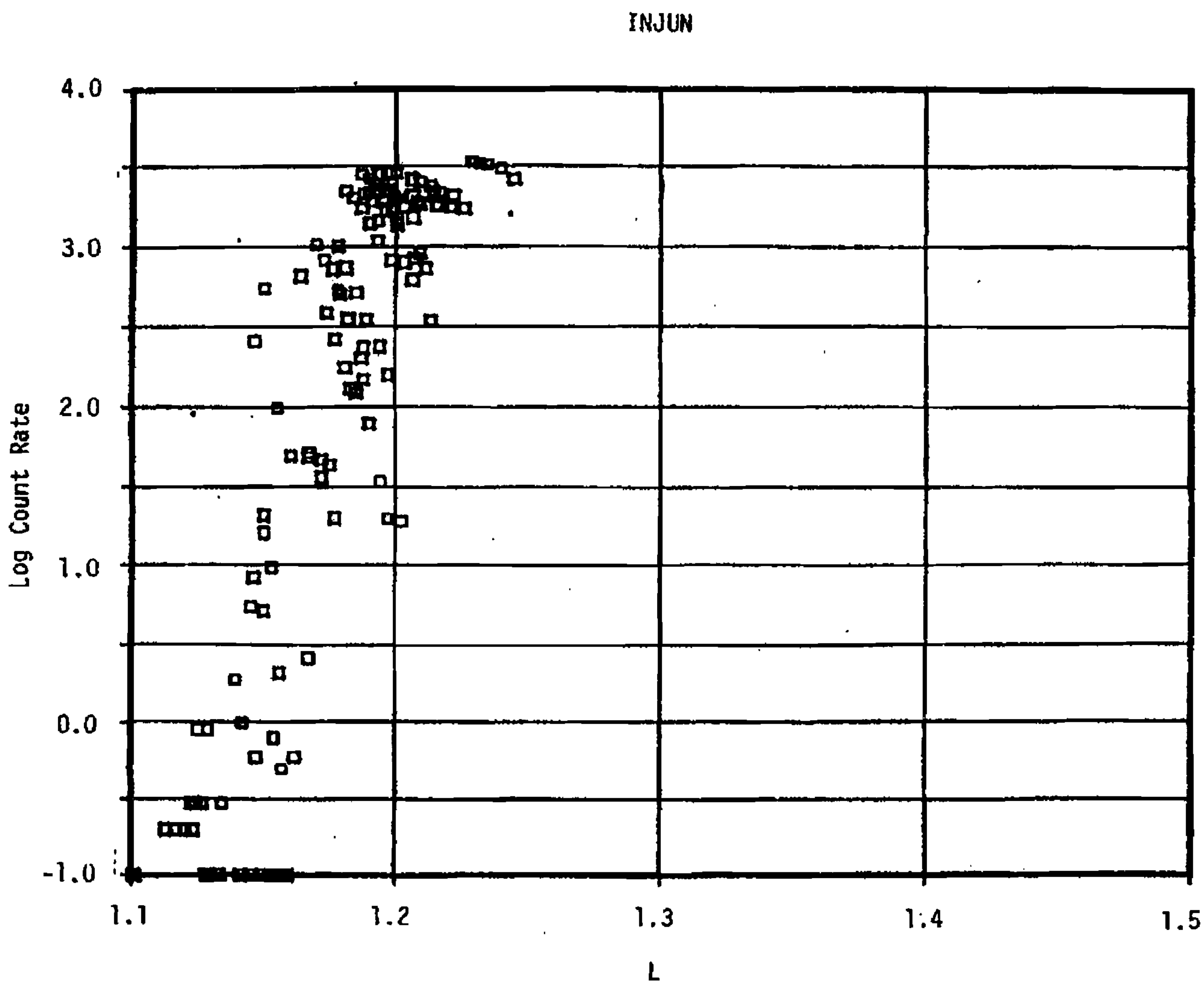

Figure 9-14. Starfish Count Rate Versus L at $1.1 < B/B_0 < 1.2$

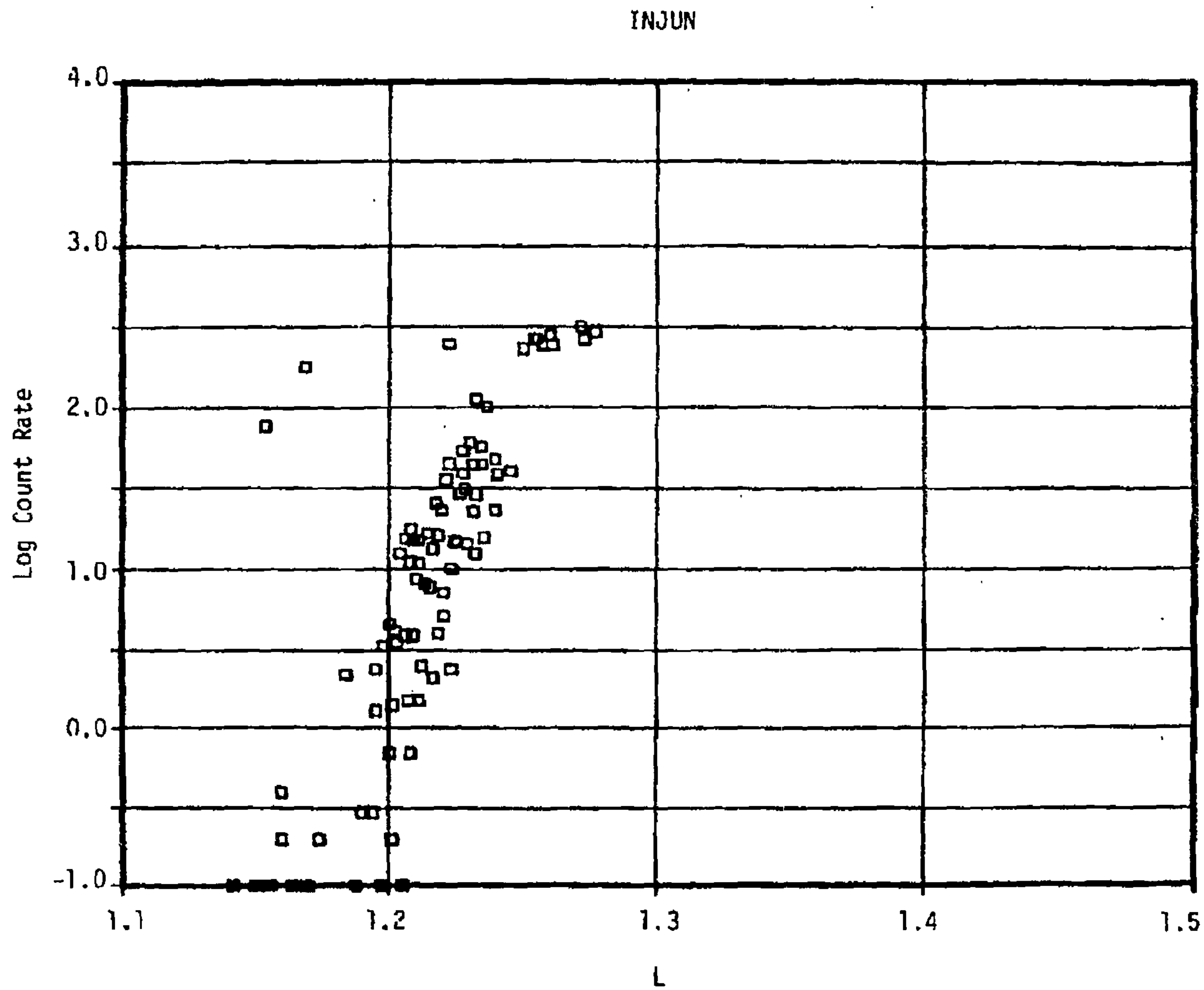

Figure 9-15. Pre-Starfish Count Rate Versus L at $1.2 < B/B_o < 1.3$

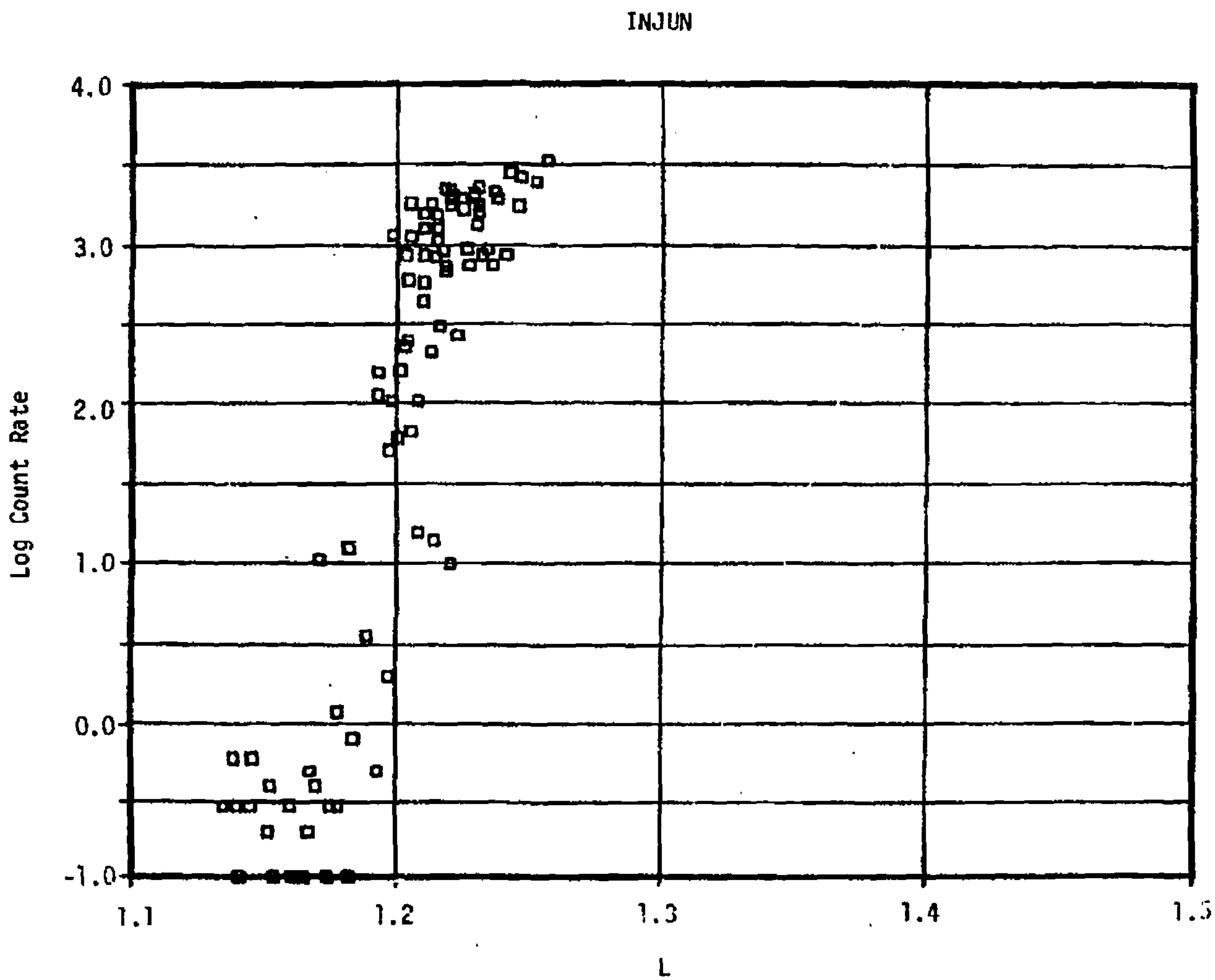

Figure 9-16. Starfish Count Rate Versus L at 1.2 < B/B_0 < 1.3

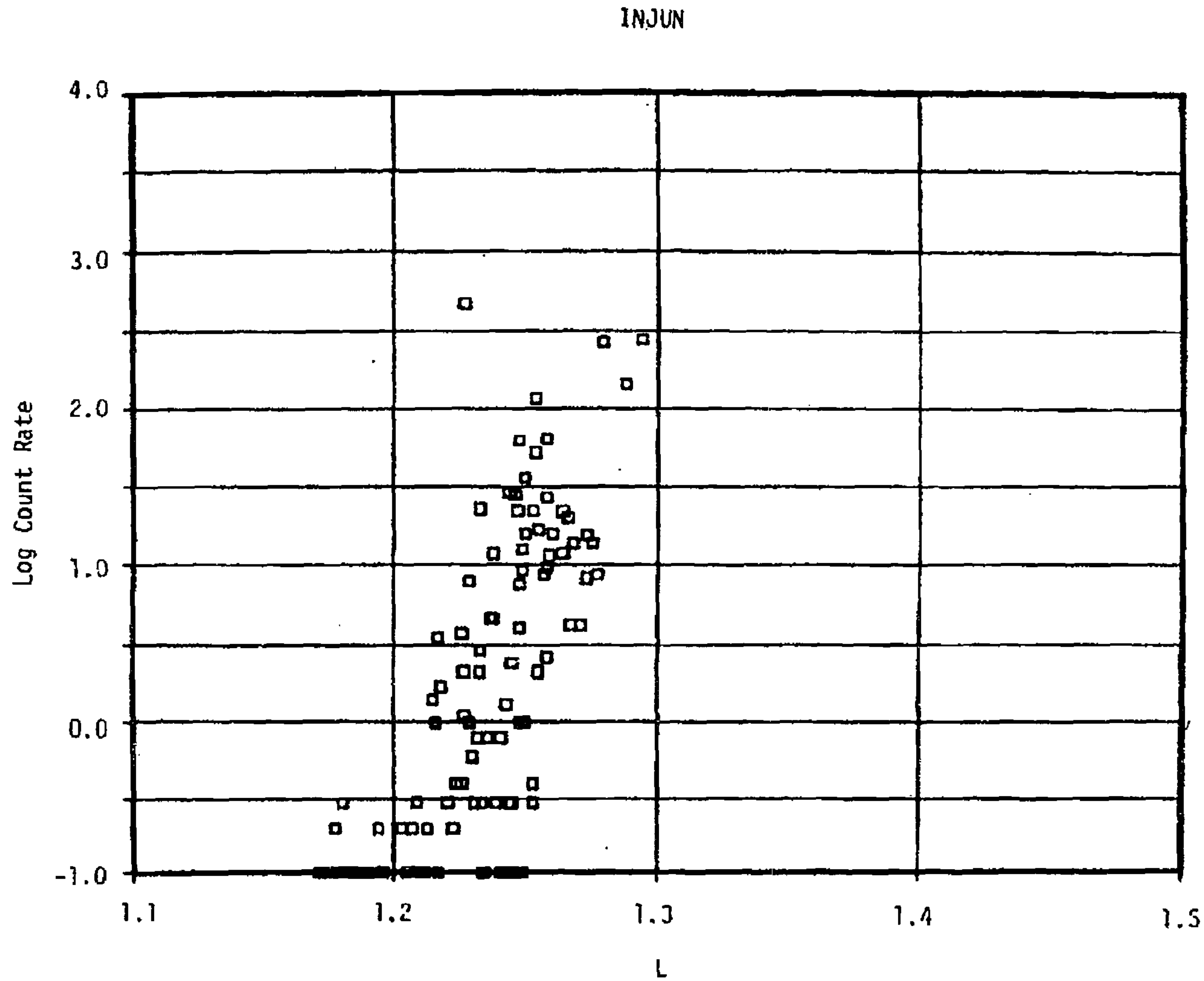

Figure 9-17. Pre-Starfish Count Rate Versus L at $1.3 < B/B_0 < 1.5$

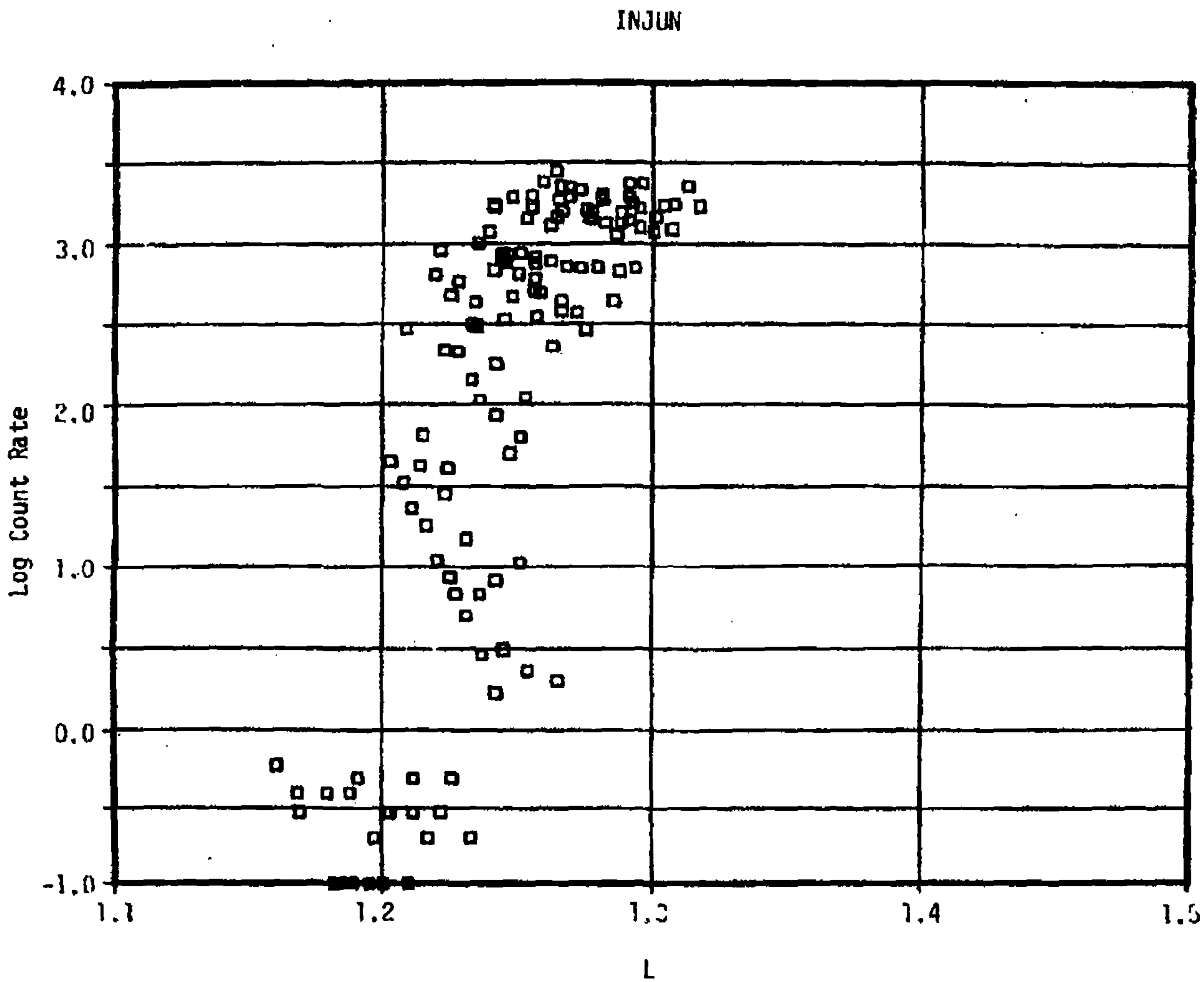

Figure 9-18. Starfish Count Rate Versus L at $1.3 < B/B_0 < 1.5$

Section 10

INTERCALIBRATION

A number of comparisons were performed to check the results of our analysis. Hess et al (Reference 11) also extensively compared Injun, Traac, and Telstar. In that analysis it was shown that Injun and Traac agree quite well (Hess compared total fission electrons; in this report > 1.5 MeV was used; however, the overall calibration was not changed); whereas the Telstar results are high by a factor of 2 to 3. Figure 10-1 is a copy of the Hess comparisons.

A comparison between Telstar, Starad, Explorer XV and Alouette was performed as a part of this effort. Intercomparisons between the various satellites is difficult at best since the satellite is moving through different regions of B, L space. Figure 10-2 is a sample comparison. The data are at an L of 1.6 and B of 0.2. At this L the data are from the Starfish burst and the time decay is very slow. Thus data separated by several days can be used. The data from the four satellites are graphed to form a composite spectrum. A number of conclusions can be drawn from this and other similar curves.

1. The spectrum is much steeper than the fission spectrum, $f(E) \alpha\ e^{-1.0E}$. Above 600 keV the spectrum is only slightly steeper than the fission spectrum.

2. Below 600 keV there is an abrupt rise in the slope of the spectrum. This increase in the spectral slope at low energies is seen by both Telstar and Starad. Furthermore, in the Jason analysis performed by Lockheed (1961) it was also shown that the best fit spectrum had a steeper slope at low energies (see Figure 10-3).

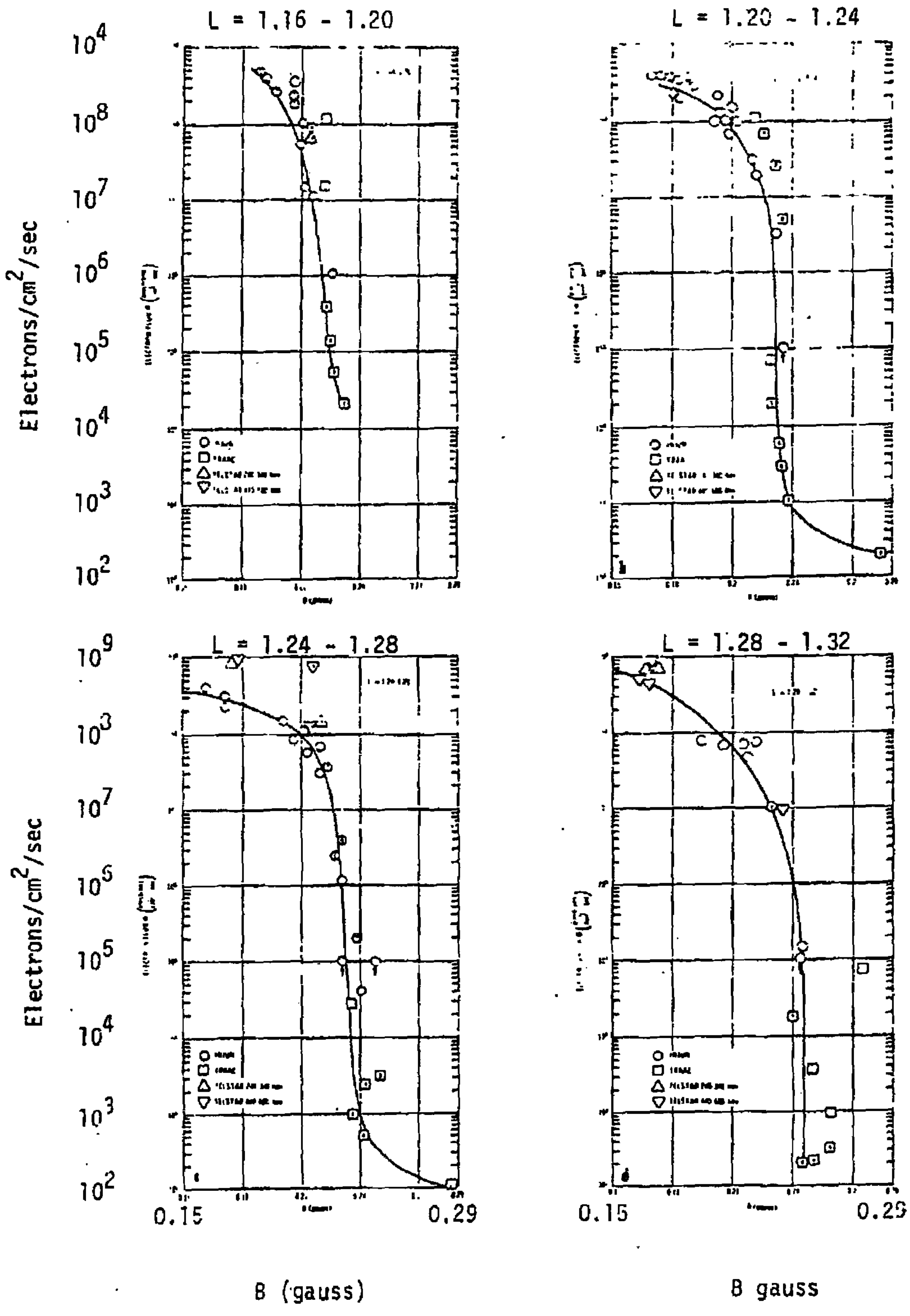

Figure 10-1. Comparison of Injun, Traac and Telstar (Reference 11)

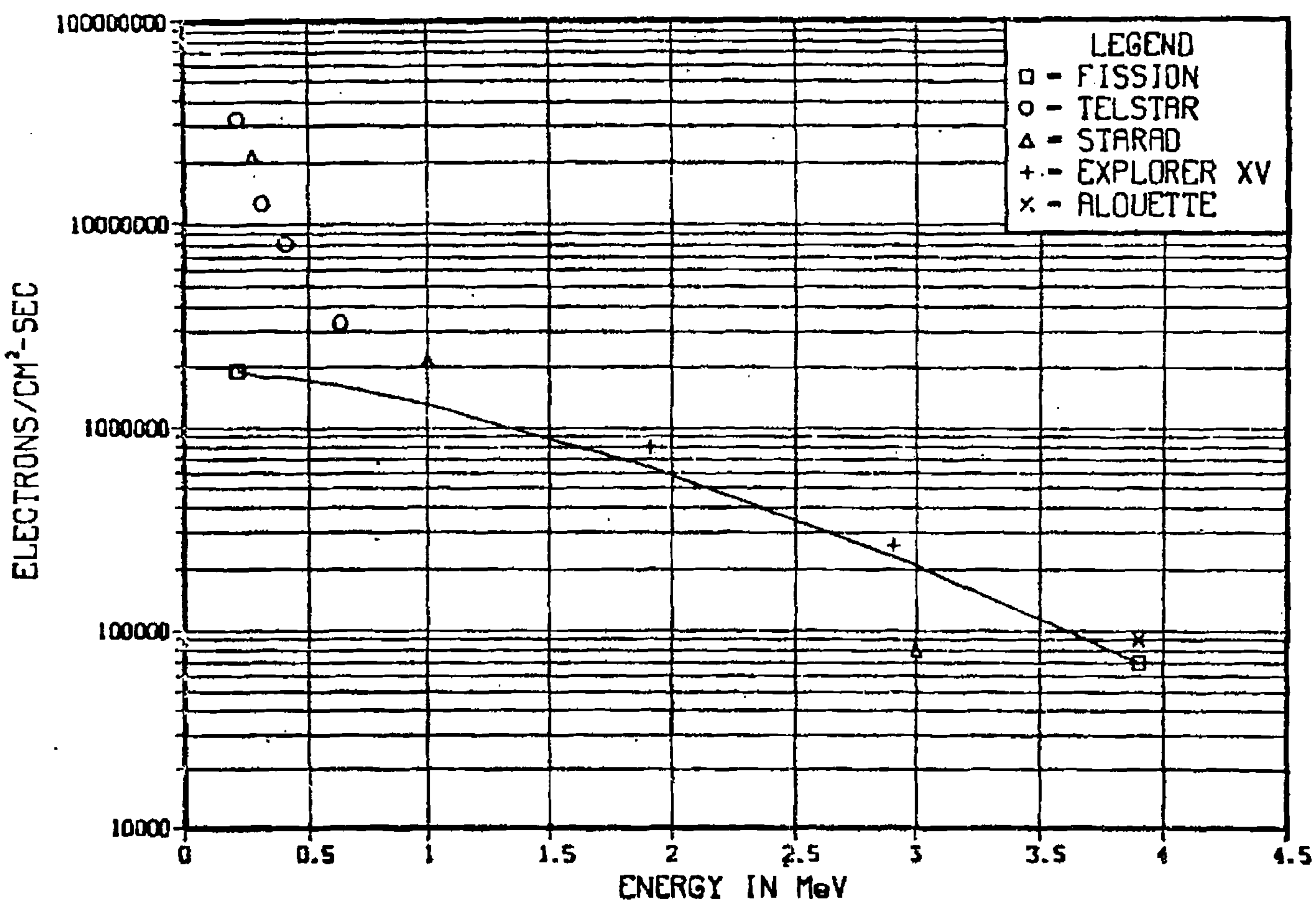

Figure 10-2. Comparison of Telstar, Explorer XV, Alouette and Starad to the Fission Spectrum

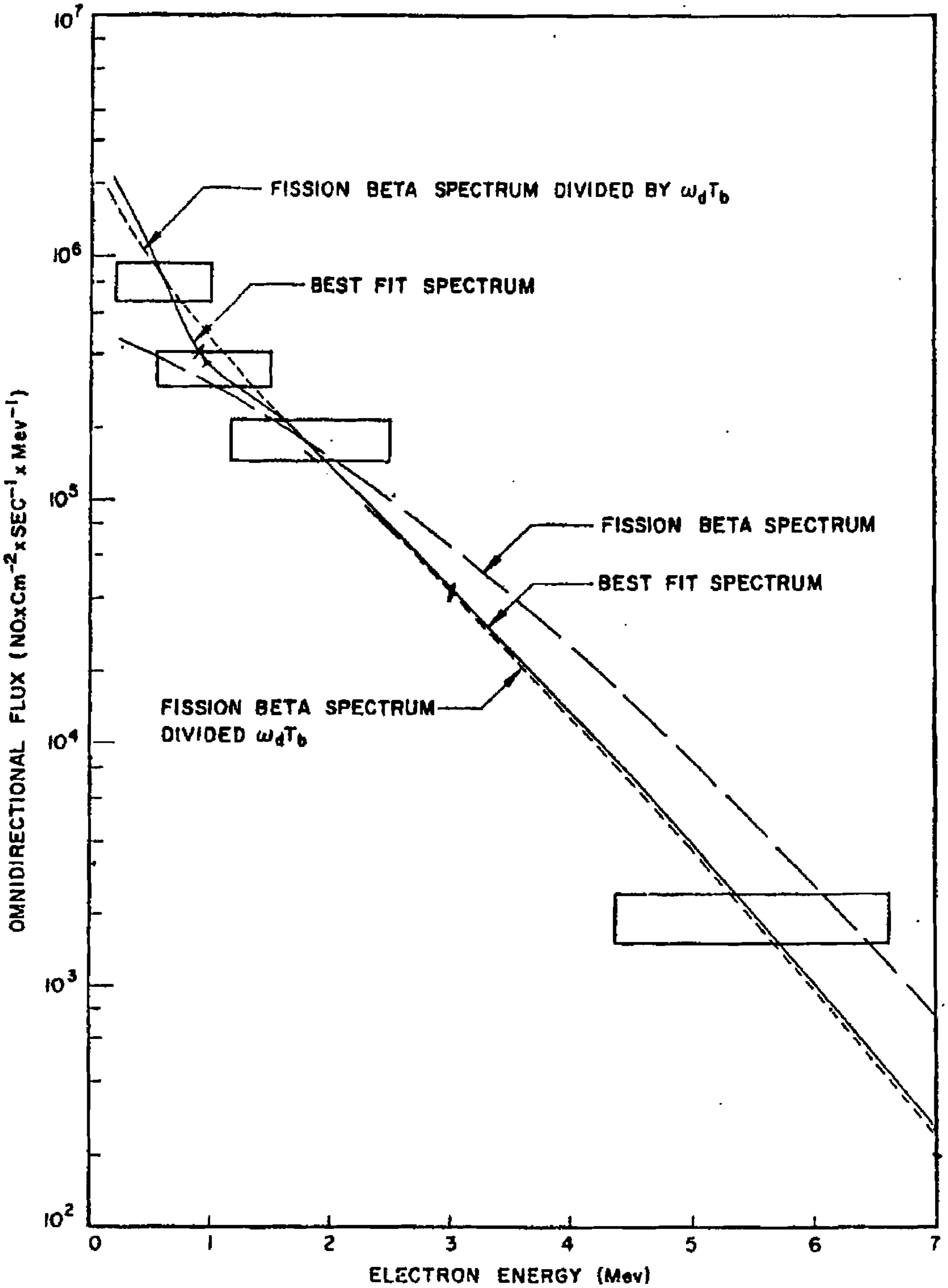

Figure 10-3. Omnidirectional Flux at the Center of the Argus Shell as Determined by the Jason Rockets (Reference 1)

3. If the Telstar channels 1 and 2 were to be used to estimate the number of fission electrons (i.e., a $e^{-1.0E}$ slope curve were fit through these data points and the area under the curve were integrated to obtain a total fission spectrum), then the predicted flux would be high by a factor of 2 to 4. Furthermore, if the proton component were added back into the third and fourth channels, the total number of fission electrons would also be overestimated.

It is now reasonably certain that the Telstar measurements agree quite well with the rest of the data set. At low energies the spectrum is <u>not</u> fission like. This non-fission component is <u>not</u> a natural component.

An attempt was also made to compare Explorer IV and the Jason experiments. This comparison is quite difficult because the measurements by Jason were in the loss region at a totally different B and L than Explorer IV. The Jason flux is over an order of magnitude less than the Explorer IV flux. This is in the right direction; however, no firm conclusion can be drawn from this analysis.

Section 11

RESULTS AND CONCLUSIONS

A computerized data base has been established. The data base has data for Teak, Orange, Argus I, II, and III, Starfish, and Russian I, II, and III. Data from the following instruments have been included in the data base; the Jason rockets, Explorer IV, Injun I, Traac, Telstar, Explorer XV, Alouette and Starad.

The data have been evaluated using our present understanding of the radiation environment. For Explorer IV it has been shown that if the Explorer IV detector were flown through the Vette AP8 and AE5 environments the counts observed by Explorer IV during non-burst times match those predicted using AP8 and AE5. This calibration check increases the confidence level for the Explorer IV data.

The Telstar detectors were found to be proton contaminated. When the proton corrected data are compared with data from Explorer XV and Alouette, the resultant spectrum closely approximates the Starad spectrum. The Telstar data are now in excellent agreement with the measurements of Injun, Traac, Explorer XV, and Alouette. The spectrum, however, does not have a fission spectral slope. This conclusion can be made with high confidence.

The data base consists of a series of tapes in the AFWL computer library. Information for each satellite is on a separate tape (several satellites, especially Telstar, occupy several tapes). The tapes are time ordered and contain, in addition to the fluxes and time, the B, L, and the satellite position. The structure and data tape identifications can be found in Appendix A.

Although most of the available data have been included in the data base, there are several exceptions. This effort was a level of effort attempt and not all efforts were complctely successful. Additional work would probably be able to retrieve extra data. The initial tapes received for Explore· ıV were not the right tapes and the Explorer XIV data could not have been included in this work. Explorer XV has been used extensively in this effort using the BTL detectors. Additional tapes containing the McIlwain single channel detector were obtained but could not be included. The McIlwain tapes contain data at a much higher energy and would be a valuable addition.

The analysis effort was a very complex programming effort. A large number of (in excess of 100) separate analysis programs were written to separate from the tapes, compare, graph analyze, sequence or in some other manner manipulate the data.

A number of major "breakthroughs" were made during this analysis. The most important is the reevaluation of the Telstar data in integral spectral form and the determination of the proton contribution to the Telstar count rate. When Telstar is combined with the data from Starad, Explorer XV, and Alouette, a complete spectrum from 220 keV to 4.0 MeV is generated. This spectrum is steeper than a fission spectrum at all energies. The deviation from a fission spectrum at low energies is considerably larger.

This analysis effort and the data base produced by it should assist AFWL in its understanding of the post-nuclear-burst-environment.

BIBLIOGRAPHY

The following is a list of all documents which contain information on the nuclear burst environment or contain information which is useful for interpreting the results.

Ackerson, L. L., Frank, L. A., Explorer 12 Observations of Charged Particle in the Inner Radiation Zone, Journal of Geophysical Research, 72, 951-957, 1967.

Air Force Weapons Laboratory, Argus Data and Report Bibliography - Volume I, 1978.

Air Force Weapons Laboratory, Argus Data and Report Bibliography - Volume II, 1978.

Allen, L., Jr., Measurement of Geomagnetically Trapped Particles of Natural and Artificial Origin, in The Upper Atmosphere Above F-2 Maximum, papers presented at the Symposium of the Ionospheric Research Committee Agard Avionics Panel, Paris, France (AGARDograph 42), edited by H. Poeverlein, pp. 67-82, NATO-AGARD, Paris, (May 1959).

Allen, L., Jr., Blue Scout Experiments for Vela Hotel, Air Force Special Weapons Center, Kirtland Air Force Base, New Mexico, TN61 10, 1961.

Allen, L., Beavbers, J. L., Whitaker, W. A., Welch, J. A., Walton, R. B., Project Jason Measurement of Trapped Electrons from a Nuclear Device by Sounding Rockets, Journal of Geophysical Research, 64, 893-907, 1959.

Anderson, A. D., Crane, G. E., Francis, W. E., Newkirk, L. L., Walt, M., Theoretical Investigation of Geomagnetically Trapped Electrons from High-Altitude Nuclear Explosions, DASA 1480 (LMSC 895355), June 1964.

Argus I, II and III Observations with Explorer IV Satellite (Supplement Report) Department of Physics and Astronomy, State University of Iowa.

Bame, S. J., Felthauser, H. E., Hundhausen, A. J., Strong, I. B., Asbridge, J. R., Gilbert, H. E., Smith, D. M., Sydoriak, S. J., A Compilation of Vela 3 Solar Wind Observations 1965 to 1967, LA-4536, Vol I, October 1970.

Bangert, J. T., Engelbrecht, R. S., Harkless, E. T., Sperry, R. V., Walsh, E. J., The Spacecraft Antennas, The Bell System Technical Journal, 42, 869-898, 1963.

Beall, D. S., Bostrom, C. O., Structure and Decay of the Starfish Radiation Belt, October 1963 to December 1965, Journal of Geophysical Resarch, 72, 3403-3424, 1967.

Documentation of the BTL Satellite Data Tapes, Bell Telephone Laboratories, Murray Hill, N.J.

Bernstein, M., Goldblatt, S. L., Kalstein, S., Zeller, G., Bibliography of Open and Unclassified Literature Pertaining to the Effects of High Altitude Nuclear Explosions: part V, DASA Report No. 1795-V, 1969.

Bleuler, E., Goldsmith, G. J, Experimental Nucleonics, Rinehart and Company, Inc., New York, 1952.

Bolyunova, A. D., Radioactivity of the Satellite Cosmos 3 after the Explosion of July 9, 1962, Cosmic Research, 4, 167-169, 1966, English Translation of Kosmicheskie Issledovaniya.

Bolyunova, A. D., Role of the "Fountain Effect" in the Equatorial Ionosphere in the Prolonged Retention of Radioactive Products of the "Starfish" Explosion at F-Region Altitudes, Kosmicheskie Issledovaniia, 13, 723-729, 1975, Cosmic Research, 13, 646-650, 1976.

Bolyunova, A. D., Vaisberg, O. L., Galperin, Yu, I., Potapov, B. P., Temny, V. V., Shuiskaya, F. K., Preliminary Results of the Studies of Corpuscles on the Electron-I Satellite, paper presented at Cospar Eighth Plenary Meeting and Sixth International Space Science Symposium, Mar Del Plata, Argentina, May 10-21, 1965, to be published by Spartan Books, Inc., Washington, D.C.

Bomberger, D. C., Moose, L. F., Nickel-Cadmium Cells for the Spacecraft Battery, The Bell System Technical Journal, 42, 1687-1702, 1963.

Bostrom, C. O., Williams, D. J., Time Decay of the Artificial Radiation Belt, Journal of Geophysical Research, 70, 240-242, 1965.

Brown, W. L., Studies of Trapped Radiation by the Telstar I and Explorer XV Satellites, Proceedings of the Plasma Space Science Symposium, edited by C. C. Chang and S. S. Huang, 189-211, D. Reidel Publishing Company, Dordrect, Holland, 1965.

Brown, W. L., Observations of the Transient Behavior of Electrons in the Artificial Radiation Belts, Radiation Trapped in the Earth's Magnetic Field, edited by B. M. McCormac, 610-633, D. Reidel Publishing Company, Dordrect, Holland, Gordon and Breach Science Publishers, New York, 1966.

Brown, W. L., Reduction and Analysis of Particle Data from Explorer 15 and Explorer 26 Final Report, September 1962 - August 1970, NASA-CR-119286, 1971.

Brown, W. L., Studies of Trapped Radiation by the Telstar and Explorer 15 Satellites, N71-30919 18-29, 1971.

Brown, W. L., Buck, T. M., Medford, L. V., Thomas, E. W., Gummel, H. K., Miller, G. L., Smits, F. M., The Spacecraft Radiation Experiments, The Bell System Technical Journal, 42, 899-942, 1963.

Brown, W. L., Gabbe, J. D., The Electron Distribution in the Earth's Radiation Belts During July 1962 as Measured by Telstar, Journal of Geophysical Research, 68, 607-618, 1963.

Brown, W. L., Gabbe, J. D., Rosenweig, W., Results of the Telstar Radiation Experiments, The Bell System Technical Journal, 42, 1505-1556, 1963.

Brown, W. L., Hess, W. N., Van Allen, J. A., Collected Papers on the Artificial Radiation Belt from the July 9, 1962, Nuclear Detonation, Journal of Geophysical Research, 68, 605-606, 1963.

Buck, T. M., Wheatley, G. H., Rodgers, J. W., Silicon P-N Junction Radiation Detectors for the Telstar Satellite, IEEE Transactions of Nuclear Science, II, 294-3-1, 1964.

Burrows, J. R., McDiarmid, I. B., A Study of Electrons Artificially Injected into the Geomagnetic Field in October, 1962, Canadian Journal Physics, 42, 1529-1547, 1964.

Burrows, J. R., McDiarmid, I. B., Wilson, M. D., On the High-Latitude Limit of Closed Geomagnetic Field Lines, Proceedings of the IEEE, 57, 1051-1053, 1969.

Center for Radio Astronomy, Stanford University, The Interplanetary Electron Number Density from Preliminary Analysis of the Pioneer 6 Radio Propagation experiment, Journal of Geophysical Research, 71, 3325-3327, 1966.

Chapman, M. C., Farley, T. A., Absolute Electron Fluxes and Energies in the Inner Radiation Zone in 1965, Journal of Geophysical Research, Space Physics, 73, 6825-6834, 1968.

Christofilos, N. C., The Argus Experiment, Journal of Geophysical Research, 64, 869-875, 1959.

Christofilos, N. C., Sources of Artificial Radiation Belts, Radiation Trapped in the Earth's Magnetic Field, proceedings of the Advanced Study Institute held at the Chr. Michelsen Institute, Bergen, Norway, August 16-September 3, 1965, edited by B. M. McCormac, 565-574, D. Reidel Publishing Company, Dordrecht, Holland, Gordon and Breach Science Publishers, New York, 1966.

Clark, B., Adams, D. A., Ion Chamber Observations of Trapped Electrons, paper presented at AGU, 44th Annual Meeting, Washington, D.C., April 17-20, 1963.

Clark, B. C., Adams, D. A., Experimental Measurements of the Radiation Hazards Associated with Manned Space Flights, Life Sciences and Space Research III, edited by M. Florkin, 29-47, North-Holland Publishing Company, Amsterdam, Holland, 1965.

Claudis, J. B., Walt, M., Behavior of Geomagnetically Trapped Electrons Injected by High-Altitude Nuclear Detonations, Journal of Geophysical Research, 67, 5035-5054, 1962.

Colgate, S. A., The Phenomenology of the Mass Portion of a High Altitude Nuclear Explosion, Journal of Geophysical Research, 70, 3161-3173, 1965.

Coon, J. H., Vela Satellite Measurements, Radiation Trapped in the Earth's Magnetic Field, edited by B. M. McCormac, 231-255, D. Reidel Publishing Company, Dordrect, Holland, Gordon and Breach Science Publishers, New York, 1966.

Craven, J. D., Temporal Variations of Electron Intensities at Low Altitudes in the Outer Radiation Zone as Observed with Satellite Injun 3, Journal of Geophysical Research, 71, 5643-5663, 1966.

D'Arcy, R. G., Colgate, S. A., The Space Distribution of Trapped Fission Debris from the High Altitude Nuclear Test of July 9, 1962, paper presented at NASA-DASA Symposium, Goddard Space Flight Center, Greenbelt, Maryland, September 10-11, 1962.

Davis, L. R., Low Energy Trapped Protons and Electrons, Proceedings of the Plasma Space Science Symposium, edited by C. C. Chang and S. S. Huang, 212-226, D. Reidel Publishing Company, Dordrecht, Holland, Gordon and Breach Science Publishers, New York, 1965.

Davis, C. G., Hutchison, P. T., Witt, F. J., Maunsell, H. I., The Spacecraft Communications Repeater, The Bell System Technical Journal, 42, 831-868, 1963.

Durney, A. C., Elliot, H., Hynds, R. J., Quenby, J. J., Satellite Observations of the Energetic Particle Flux Produced by the High-Altitude Nuclear Explosion of July 9, 1962, Nature, 195, 1245-1248, 1962.

Durney, A. C., Elliot, H., Hynds, R. J., Quenby, J. J., The Artificial Radiation Belt produced by the Starfish nuclear explosion, Proceedings of the Royal Society of London, Series A, 281, 565-583, 1964.

Durney, A. C., Elliot, H., Hynds, R. J., Quenby, J. J., The Energy Spectrum of the Heavy Primary Cosmic Rays, Proceedings of the Royal Society of London, Series A, 281, 553-564, 1964.

Dyce, R. B., High Altitude Nuclear Detonations, Satellite Observations, Advances in Upper Atmosphere Research, 29-44, The Macmillan Company, New York, 1963.

Elliot, H., The Van Allen Particles, Reports on Progress in Physics, 26, 1963.

Elliot, H., Some Cosmic Ray and Radiation Belt Observations Based on Data from the Anton 302 G-M Counter in Ariel I, Radiation Trapped in the Earth's Magnetic Field, edited by B. M. McCormac, D. Reidel Publishing Company, Dordrect, Holland, Gordon and Breach Science Publishers, New York, 76-99, 1966.

Fillius, R. W., McIlwain, C. E., Anomalous Energy Spectrum of Protons in the Earth's Radiation Belt, Physical Review Letters, 12, 609-612, 1964.

Filz, R. C., Comparison of the Low-Altitude Inner-Zone 55-MeV Trapped Proton Fluxes Measured in 1965 and 1961-1962, Journal of Geophysical Research, 72, 959-963, 1967.

Filz, R. C., Holeman, E., Time and Altitude Dependence of 55-MeV Trapped Protons, August 1961 to June 1964, Journal of Geophysical Research, 70, 5807-5822, 1965.

Filz, R., Holeman, E., Yagoda, H., Variation of the Directional Flux of Slow Trapped protons, paper presented at AGU, 44th Annual Meeting, Washington, D.C., April 17-20, 1963.

Frank, L. A., Efficiency of a Geiger-Mueller Tube for Non-Penetrating Electrons, Journal of The Franklin Institute, 273, 91-106, 1962.

Frank, L. A., Inward Radial Diffusion of Electrons of Greater than 1.6 Million Electron Volts in the Outer Radiation Zone, Journal of Geophysical Research, 70, 3533-3540, 1965.

Frank, L. A., A Survey of Electrons E (greater than) 40 keV Beyond 5 Earth Radii with Explorer 14, Journal of Geophysical Research, 70, 1593-1626, 1965.

Frank, L. A., On the Extraterrestrial Ring Current During Geomagnetic Storms, Report 67-9, February 1967.

Frank, L. A., Van Allen, J. A., Hills, H. K., A Study of Charged Particles in the Earth's Outer Radiation Zone with Explorer 14, Journal of Geophysical Research, 69, 2171-2191, 1964.

Frank, L. A., Van Allen, J. A., Whelpley, W. A., Craven, J. D., Absolute Intensities of Geomagnetically Trapped Particles with Explorer 14, Journal of Geophysical Research, 68, 1573-1579, 1963.

Freden, S. C., Inner-Belt Van Allen Radiation, Space Science Reviews, 9, 198-242, 1969.

Freden, S. C., Paulikas, G. A., Trapped Protons at Low Altitudes in the South Atlantic Magnetic Anomaly, Journal of Geophysical Research, 69, 1259-1269, 1964.

Freeman, J. W., Jr., The Geomagnetically Trapped Radiation, Second Symposium on Protection Against Radiations in Space, Gatlinburg, Tennessee, October 12-14, 1964, 7-17, Report SP-71, 1965.

Fritz, T. A., Study of the High-Latitude, Outer Zone Boundary Region for (greater than or equal to) 40-keV Electrons with Satellite Injun 3, Journal of Geophysical Research, Space Physics, 75, 5387-5400, 1970.

Fritz, T. A., Gurnett, D. A., Diurnal and Latitude Effects Observed for 10-keV Electrons at Low Satellite Altitudes, Journal of Geophysical Research, 70, 12485-2502, 1965.

Fritz, R., Yagoda, H, Holeman, E., Observations on Trapped Protons in Emulsions Recovered from Satellite Orbits, Space Research IV, Proceedings of the Fourth International Space Science Symposium, Warsaw, Poland, June 4-10, 1963, edited by P. Muller, 642-645, North-Holland Publishing Company, Amsterdam, (Interscience Publishers) John Wiley and Sons, Inc., New York, 1964.

Gaines, E. E., Glass, R. A., Satellite Measurements of th Decay of the Artificial Electron Belt, Journal of Geophysical Research, 69, 1271-1275, 1964.

Gal'perin, Yu. I., Effects of the American High-Altitude Explosion of July 9, 1962 in the Upper Atmosphere, Cosmic Research, 3, 326-331, 1965.

Gal'perin, Yu. I., Bolyunova, A. D., Study of the Drastic Changes of the Radiation in the Upper Atmosphere in July, 1962, Space Research V, Proceedings of the Fifth International Space Science Symposium, Florence, May 12-16, 1964, edited by D. G. King-Hele, P. Muller, G. Righini, 446-457, North-Holland Publishing Company, Amsterdam, (Interscience Publishers), John Wiley and Sons, Inc., New York, 1965.

Gal'perin, Yu., Mulgarch, K. T., Satellites, Atmosphere, and Electrons, Report TT 62, 1547, October 1962.

Gal'perin, Yu. I., Krasovskii, V. I., Upper-Atmosphere Research with the Cosmos 3 and Cosmos 5 Satellites - I. Instrumentation, Cosmic Research, 1, 99-103, 1963, English translation of Kosmicheskie Issledovaniya.

George, J. A., Omnidirectional Fluxes; Explorer 4 Satellite Data, Argus Events 1 and 2, (Thesis) St. Louis University, St. Louis, Illinois, 1967.

Giacconi, R., Paolini, F. R., Hadley, W. C., Talbot, R., Jr., A Research Program to Investigate Artificially Injected Trapped Radiation, Report ASE-759, October 1964.

Goddard Space Flight Center, Greenbelt, Maryland, Ariel I, The First International Satellite: Experimental Results, NASA SP-119, 23-24, 56-57, 1966.

Green, A. E. S., Wyatt, P. J., Nuclear Explosions and Trapped Radiation, Atomic and Space Physics, 229-236, Addison-Wesley Publishing Company, Inc., Reading, Mass., 1965.

Hess, W. N., The Artificial Radiation Belt Made on July 9, 1962, Journal of Geophysical Research, 68, 667-683, 1963.

Hess, W. N., The Bomb Produced Radiation Belt, IEEE Transactions on Nuclear Science, NS-10, 8-11, 1963.

Hess, W. N., Radiation Belts, Transactions, American Geophysical Union, 44, 433-435, 1963.

Hess, W. N., The Effects of High-Altitude Explosions, (lecture) C65N31363, April 14, 1964.

Hess, W. N., Lifetimes and Time Histories of Trapped Radiation Belt Particles, Space Research IV, Proceedings of the Fourth International Space Science Symposium, Warsaw, Poland, June 4-10, 1963, edited by P. Muller, 60-76, North-Holland Publishing Company, Amsterdam, (Interscience Publishers) John Wiley and Sons, Inc., New York 1964.

Hess, W. N., The Radiation Belt and Magnetosphere, Blaisdell Publishing Company, Waltham, 1968.

Hess, W. N., Mead, G. D., Introduction to Space Science, Gordon and Breach Science Publishers, New York, 1965.

Hess, W. N., Nakada, P., Artificial Radiation Belt Produced by Nuclear Explosion and Composed Principally of Electrons, Artificial Radiation Belt Discussed in Symposium at Goddard Space Center, Science, 138, 53-54, 1962.

Heller, G. B., Shelton, R. D., Dozier, J. B., Secondary Measurements by Pegasus, The Meteoroid Satellite Project Pegasus NASA TN D-35-5, 77-111, 1966.

Higgins, P. W., Lill, J. C., White, T. T., Radiation Environment at High Orbital Altitudes, NASA SP-138, 149-157, 1967.

Hittinger, W. C., Components for the Telstar Project, The Bell System Technical Journal, 42, 1659-1664, 1963.

Imhof, W. L., Electron Precipitation in the Radiation Belts, Journal of Geophysical Research, Space Physics, 73, 4167-4184, 1968.

Imhof, W. L., Gaines, E. E., King, D. R., Nakano, G. H., Smith, R. V., Vaughn, F. J., Analysis and Evaluation of Measurements of Geomagnetically Trapped Electrons from High-Altitude Nuclear Explosions, DA49-146-XZ-205, July 1964.

Imhof, W. L., Reagan, J. B., Smith, R. V., Long-Term Study of Electrons Trapped on Low L Shells, Journal of Geophysical Research, 72, 2371-2377, 1967.

Imhof, W. L., Smith, R. V., Proton Intensities and Energy Spectrums in the Inner Van Allen Belt, Journal of Geophysical REsearch, 69, 91-100, 1964.

Imhof, W. L., Smith, R. V., Energy Spectrum of Electrons at Low Altitudes, Journal of Geophysical Research, 70, 2129-2134, 1965.

Imhof, W. L., Smith, R. V., Longitudinal Variations of High Energy Electrons at Low Altitudes, Journal of Geophysical Research, 70, 569-577, 1965.

Imhof, W. L., Smith, R. V., The Behavior of Trapped Electrons and Protons at the Lower Edge of the Inner Radiation Belt, 71, 4157-4171, 1966.

Imhof, W. L., Smith, R. V., Low Altitude Measurements of Trapped Particles, Radiation Trapped in the Earth's Magnetic Field, proceedings of the Advanced Study Institute held at the Chr. Michelsen Institute, Bergen, Norway, August 16-September 3, 1965, edited by B. M. McCormac, 100-111, D. Reidel Publishing Company, Dordrecht, Holland, Gordon and Breach Science Publishers, New York, 1966.

Johnson, G. L., Dyce, R. B., Particle-Counting Satellite Observations made in the Vicinity of the Johnston Island High-Altitude Nuclear Detonations of 1963, AF49(638)-1164, June 1963.

Kane, S. R., Pfitzer, K. A., Winckler, J. R., The Construction, Calibration and Operation of the University of Minnesota Experiments for OGO-I and OGO-III, Report CR-87, September 1966.

Katz, L., Smart, D., Recent Changes in the Artificial Radiation Belts, paper presented at AGU, 44th Annual Meeting, Washington, D.C., April 17-20, 1963.

Katz, L., Smart, D., Paoline, F. R., Giacconi, R., Talbot, R. J., Jr., Measurements of Trapped Particles Injected by Nuclear Detonations, AF19/628/-2799, Space Research IV, International Space Science Symposium 4th, Warsaw, Poland, June 4-10, 1963, Proceedings, Organized by the Committee on Space Research, Cospar and the Polish Academy of Sciences, edited by P. Muller, Amsterdam, North-Holland Publishing Company, New York, Interscience Publishers, 646-664, 1964.

Krasovskiy, V. I., Gal'perin, Yu. I., Temnyy, V. V., Mulyarchik, T. M., Dzhordzhio, N. V., Marov, M. Ya., Bolyunova, A. D., Some New Results of Geophysical Investigations ' Means of the "Cosmos 3" and "Cosmos 5" Satellites, Geomagnetism and Aeronomy, 3, 338-344, English Translation of Geomagnetizm i Aeronomiya.

Krasovskiy, V. I., Gal'perin, Yu. I., Temnyy, V. V., Mulyarchik, T. M., Dzhordzhio, N. V., Marov, M. Ya., Bolyunova, A. D., Vaysberg, O. L., Potapov, B. P., Bragin, M. L., Some Characteristics of Geoactive Particles, Geomagnetism and aeronomy, 3, 333-337, 1963, English Translation of Geomagnetizm i Aeronomiya.

Krasovsky, V. I., Galperin, Yu. I., Jorjio, N. V., Mularchik, T. M., Bolyunova, A. D., Investigations of the Upper Atmosphere Using the Artificial Earth Satellites Cosmos 3 and Cosmos 5, Space Research IV, Proceedings of the Fourth International Space Science Symposium, Warsaw, Poland, June 4-10, 1963, edited by P. Muller, 572-581, North-Holland Publishing Company, Amsterdam, (Interscience Publishers, John Wiley and Sons, Inc., New York, 1964.

Krasovsky, V. I., Kushnir, Yu. M., Bordovski, G. A., Zakharov, G. F., Svetlicki, Ye. M., Detection of Corpuscles by the Third Sputnik, T-340-R, June 1960.

Kuck, G. A., Time Behavior of Charged Particles Injected by 1962 High Altitude Russian Nuclear Tests, (Thesis) Air Force Institute of Technology, Wright Patterson AFB, Ohio, 1964.

Kuck, G. A., Charged Particle Fluxes in the Inner Van Allen Belt Prior to the July 9, 1962, High Altitude Nuclear Test, paper presented at the 12th Annual Air Force Science and Engineering Symposium, Brooks AF Base, Texas, October 12-14, 1965.

Kuck, G. A., Pitch Angle Diffusion on Relativistic Electrons in the Plasmosphere (Ph.D. Thesis), Air Force Weapons Laboratory Technical Report, AFWL-TR-73-116, 1973.

Kukshkin, Yu. V., Strelkov, A. S., Recording of Fragmentary X-Radiation During the High-Level Nuclear Burst Over Johnston Island on July 9, 1962, Cosmic Research, 4, 93-97, 1966.

Leach, E. R., Fairand, B. P., Bettenhausen, L. H., The Space-Radiation Environment and its Interaction with Matter, REIC Report 37, 1965.

Lockheed Aircraft Corporation, Analysis of Jason Data, AFSWC-TR-61-82, Air Force Weapons Laboratory, Kirtland Air Force Base, NM, October 1961. (AD 268400)

Lundquist, C. A., Naumann, R. J., Weber, A. H., Directional Flux Densities and Mirror-Point Distributions of Trapped Particles from Satellite 1958 (epsilon) Measurements, Journal of Geophysical Research, 67, 4125-4133, 1962.

Manley, O. P., Carpenter, J. W., Starfish Debris Measurements from Cosmos 5, Journal of Geophysical Research, 71, 333-334, 1966.

Manson, D. J., Van Allen Radiation Belt and Argus Directional Flux Density Distributions, Explorer IV Satellite Data, (Thesis) Saint Louis University, Saint Louis, Illinois, 1967.

Manson, D. J., Fennell, J. F. George, J. A., Hickerson, J. L., Maldonado, G. V., Webber, A. H., Review of Artificial Radiation Belts, Explorer 4; Unidirectional Trapped Radiation, Injun I, DASA-2309, 1969.

Manson, D. J., Fennell, J. F., Hoverter, R. T., Hickerson, J. L., George, J. A., Maldonado, G. V., Weber, A. H., Artificial Injection of Electrons Into the Geomagnetic Field by Teak and Orange, Low-Altitude Bursts of 1958, Journal of Geophysical Research, Space Physics, 75, 4710-4719, 1970.

Manson, D. J., George, J. A., Paikeday, J. M., Fennell, J. F., Delaney, R. M., Weber, A. H., Unidirectional and Omnidirectional Flux Densities of Trapped Particles in Argus Shells and the Inner Van Allen Belt, Explorer 4 Satellite Data, DASA 2052-1, 1968.

Mayo, J. S., Mann, H., Witt, F. J., Peck, D. S., Gummel, H. K., Brown, W. L., The Command System Malfunction of the Telstar Satellite, The Bell System Technical Journal, 42, 1631-1657, 1963.

McDiarmid, I. B., Burrows, J. R., Budzinski, E. E., Rose, D. C., Satellite Measurements in the "Starfish" Artificial Radiation Zone, Canadian Journal of Physics, 41, 1332-1345, 1963.

McDiarmid, I. B., Burrows, J. R., Budzinski, E. E., Wilson, M. D., Some Average Properties of the Outer Radiation Zone at 1000 km, Canadian Journal of Physics, 41, 2064-2079, 1963.

McDiarmid, I. B., Rose, D. C., Budzinski, E. E., Burrows, J. R., NRC Particle Detectors in Alouette Perform Five Different Experiments, Canadian Electronics Engineering, 6, 37-39, 1962.

McDiarmid, I. B., Rose, D. C., Burrows, J. R., Budzinski, E. H., Satellite Observations of Artificial Radiation Zones in October 1962, paper presented at AGU, 44th Annual Meeting, Washington, D. C., April 17-20, 1963.

McIlwain, C. E., Coordinates for Mapping the Distribution of Magnetically Trapped Particles, Journal of Geophysical Research, 66 3681-3691, 1961.

McIlwain, C. E., The Radiation Belts, Natural and Artificial, Science, 142, 355-361, 1963.

McIlwain, C. E., Measurements of Trapped Electron Intensities Made by the Explorer XV Satellite, Radiation Trapped in the Earth's Magnetic Field, proceedings of the Advanced Study Institute held at Char. Michelsen Institute, Bergen, Norway, August 16-September 3, 1965, edited by B. M. McCormac, 593-609, D. Reidel Publishing Company, Dordrecht, Holland, Gordon and Breach Science Publishers, New York, 1966.

McIlwain, C. E., Fillius, R. W., Valerio, J., Dave, A., Relay I Trapped Radiation Measurements, NASA TN-D-2516, 1964.

Mihalov, J. D., Energetic Trapped Electron Observations During the Fall of 1964, Journal of Geophysical Research, 72, 1081-1094, 1967.

Mihalov, J. D., Mozer, F. S., White, R. S., Artificially Injected Electrons at Low Altitudes, Journal of Geophysical Research, 69, 4003-4013, 1964.

Mihalov, J. D., White, R. S., Low-Energy Proton Radiation Belts, Journal of Geophysical Research, 71, 2207-2216, 1966.

Motz, H. T., Carter, R. E., Artificial Radiation Belt Studies with a Fission Beta-Ray Source, Journal of Geophysical Research, 68, 657-661, 1963

Mozer, F. S., Elliott, D. D., Mihalov, J. D., Paulikas, G. A., Vampola, A. L., Freden, S. C., Preliminary Analysis of the Fluxes and Spectrums of Trapped Particles After the Nuclear Test of July 9, 1962, Journal of Geophysical Research, 68, 641-649, 1963.

Mularchik, T. M., Vaisberg, O. L., Low-Energy Electrons Measured by the Cosmos-3 and Cosmos-5 Satellites, Space Research V, Proceedings of the Fifth International SpaceScience Symposium, Florence, May 12-16, 1964, edited by D. G. King-Hele, P. Muller, G. Righini, 500-510, North-Holland Publishing Company, Amsterdam, (Interscience Publishers) John Wiley and Sons, Inc., New York, 1965.

Nakano, G. H., Heckman, H. H., Evidence for Solar-Cycle Changes in the Inner-Belt Protons, Physical Review Letters, 20, 806-811, 1968.

National Academy of Sciences, Artificial Radiation Belt from the Starfish High-Altitude Nuclear Test, IG Bulletin, 43, 523-527, 1962.

National Bureau of Standards, Handbook of Mathematical Functions, edited by M. Abramowitz and I. A. Stegun, National Bureau of Standards Applied Mathematics Series 55, 1964.

Naumann, R. J., Directional Dependence of Counting Rates from Explorer IV (Satellite 1958 Epsilon), (Thesis) University of Alabama, Alabama, 1961.

Nesterov, V. Ye., Pisarenko, N. F., Savenko, I. A., Tel'tsov, M. V., Shavrin, P. I., Sharvina, K. N., Study of the Inner and Artificial Radiation Zones of the Earth at Low Altitudes in 1960-1964, Transactions of the All-Union Conference on Space Physics, 607-615, June 10-16, 1965, NASA TT-F389.

Newkirk, L. L., Walt, M., Radial Diffusion Coefficient for Electrons at Low L Values, Journal of Geophysical Research, Space Physics, 73, 1013-1017, 1968.

Newman, P., Optical, Electromagnetic, and Satellite Observations of High-Altitudfe Nuclear Detonations, Part I, Journal of Geophysical Research, 64, 923-932, 1959.

O'Brien, B. J., The Injun Satellites, Naval Research Reviews, 16, 15-19, 1963.

O'Brien, B. J., Review of Studies of Trapped Radiation with Satellite-Borne Apparatus, Space Science Reviews, 1, 415-484, D. Riedel Publishing Company, Dordrect, Holland, 1962-1963.

O'Brien, B. J., High-Latitude Geophysical Studies with Satellite Injun 3 3. Precipitation of Electrons into the Atmosphere, Journal of Geophysical Research, 69, 13-43, 1964.

O'Brien, B. J., Laughlin, C. D., Gurnett, D. A., High-Latitude Gerophysical Studies with Satellite Injun 3 1. Description of the Satellite, Journal of Geophysical Research, 69, 1-12, 1964.

O'Brien, B. J., Laughlin, C. D., Van Allen, J. A., Geomagnetically Trapped Radiation Produced by a High-Altitude Nuclear Explosion on July 9, 1962, Nature, 195, 939-943, 1962.

Owens, H. D., Frank, L. A., Electron Omnidirectional Intensity Contours in the Earth's Outer Radiation Zone at the Magnetic Equator, Journal of Geophysical Research, 73, 199-208, 1968.

Paikeday, J. M., Interpretation of Directional Flux Densities in Argus Shells, Explorer IV Satellite Data, (Thesis) Saint Louis University, Saint Louis, Illinois, 1966.

Paolini, F. R., Giacconi, R., Waters, J. R., Katz, L., Smart, D., Measurements in the Radiation Belts from Hitch-Hiker I, AFCRL-65-377, June 1965.

Paolini, F. R., Theodoridis, G. C., A Study of Energetic Electrons in the Radiation Belts with Hitch-Hicker I, Annales de Geophysique, 23, 237-248, 1967.

Paulikas, G. A., Blake, J. B., Freden, S. C., Precipitation of Energetic Electrons at Middle Latitudes, Journal of Geophysical Research, 71, 3165-3172, 1966.

Paulikas, G. A., Freden, S. C., Precipitation of Energetic Electrons into the Atmosphere, Journal of Geophysical Research, 69, 1239-1249, 1964.

Paulikas, G. A., Blake, J. B., Freden, S. C., Inner-Zone Electrons in 1964 and 1965, Journal of Geophysical Research, 71, 2011-2020, 1967.

Peck, D. S., Wooley, M. C., Component Design, Construction and Evaluation for Satellites, The Bell System Technical Journal, 42 1665-1686, 1963.

Peterson, A. M., Optical, Electromagnetic, and Satellite Observations of High-Altitude Nuclear Detonations, Part II, Journal of Geophysical Research, 64, 933-938, 1959.

Petschek, A. G., Interpretation of Satellite Detector Counter Rates, Journal of Geophysical Research, 68, 663-665, 1963.

Pfitzer, K. A., An Experimental Study of Electron Fluxes from 50 keV to 4 MeV in the Inner Radiation Belt, (Thesis) School of Physics and Astronomy, Minnesota University, Minneapolis, August 1968.

Pfitzer, K. A., Winckler, J. R., Experimental Observations of a Large Addition to the Electron Inner Radiation Belt After a Solar Flare Event, Journal of Geophysical Research, Space Physics, 73 5792-5797, 1968.

Pieper, G. F., The artificial Radiation Belt, APL Technical Digest, 2 3-7, 1962.

Pieper, G. F., A Second Radiation Belt from the July 9, 1962, Nuclear Detonation, Journal of Geophysical Research, 68, 651-655, 1963.

Pieper, G. F., Williams, D. J., Frank, L. A., Traac Observations of the Artificial Radiation Belt from the July 9, 1962, Nuclear Detonation, Journal of Geophysical Research, 68, 635-640, 1963.

Pizzella, G., Davis, L. R., Williamson, J. M., Electrons in the Van Allen Zone Measured with a Scintillator on Explorer 14, Journal of Geophysical Research, 71, 5495-5508, 1966.

Porter, R. W., Symposium of Scientific Effects of Artificially Introduced Radiations at High Altitudes (Introductory Remarks), Journal of Geophysical Research, 64, 865-867, 1959.

Rao, C. S. R., Some Observations of Energetic Electrons in the Outer Radiation Zone During Magnetic Bays, Journal of Geophysical Research, 74, 794-801, 1969.

Reagan, J. B., Bakke, J. C., Heinemann, M. A., Imhov, W. L., Smith, R. V., Measurement of Trapped Particle Fluxes and Spectra at Low Altitudes from Gemini 4, paper presented at the AGU, 47th Annual Meeting, Washington, D. C., April 19-22, 1966.

Reagan, J. B., Bakke, J. C., Imhof, W. L., Smith, R. V., Multichannel Spectrometer for the Measurement of Trapped Particles, IEEE Transactions on Nuclear Science, 83-88, 1965.

Roberts, C. S., On the Relationship Between the Unidirectional and Omnidirectional Flux of Trapped Particles on a Magnetic Line of Force, Journal of Geophysical Research, 70, 2517-2527, 1965.

Roberts, C. S., Electron Loss from the Van Allen Zones due to Pitch Angle Scattering by Electromagnetic Disturbances, Radiation Trapped in the Earth's Magnetic Field, proceedings of the Advanced Study Institute held at the Chr. Michelsen Institute, Bergen, Norway, August 16-September 3, 1965, edited by B. M. McCormac, 403-421, D. Reidel Publishing Company, Dordrecht, Holland, Gordon and Breach Science Publishers, New York, 1966.

Rosen, D. J., Kraus, A. F., Bibliography of Open and Unclassified Literature Pertaining to the Effects of High Altitude Nuclear Explosions: Part III, DASA Report No., 1795-3, 1968.

Rosen, D. J., Kraus, A. F., Bibliography of Open and Unclassified Literature Pertaining to the Effects of High Altitude Nuclear Explosions: Part IV, DASA Report no. 1795-4, 1969.

Rosen, D. J., Kraus, A. F., Goldblatt, S. L., Bibliography of Open and Unclassified Literature Pertaining to the Effects of High Altitude Nuclear Explosions: Parts I and II, DASA Report No. 1975, 1966.

Rosen, A., Sanders, N. L., Potter, R., Urban, E., Shelton, R., The Temporal and Spatial Dependence of the "Starfish" Belt Electrons in 1965 and Early 1966, paper presented at the AGU, 48th Annual Meeting, Washington, D.C., April 17-20, 1967.

Rosen, A., Sanders, N. L., Shelton, R., Potter, R., Urban, E., Pegasus I: Observations of the Temporal Behavior of the Inner Zone Electrons, 1965-1966, Journal of Geophysical Research, Space Physics, 73, 1019-1033, 1968.

Savenko, I. A., Shavrin, P. I., Nesterov, V. E., Pisarenko, N. F., Tel'tsov, M. V., Radiation Conditions in Space on the Even of the Flights of the Spaceships Vostok 3 and Vostok 4, Cosmic Research, 1, 140-143, 1963.

Savenko, I. A., Tel'Tsov, M. V., Maduyev, V. L., Savun, O. I., Yuroskiy, A. V., Radiometric Equipment on the Cosmos 41 Satellite, Geomagnetism and Aeronomy, 5, 889-892, 1965.

Sawyer, D. M., Vette, J. I., AP-8 Trapped Proton Environment for Solar Maximum and Solar Minimum, NSSDC/WDC-A-R and S 76-05, 1976.

Sayers, J., The Electron Density Distribution in the Topside Ionosphere II. Effects of the Nuclear Explosion Over Johnston Island and the Ionization Produced by Corpuscular Radiation at High Magnetic Latitudes, Proceedings of the Royal Society of London, Series a, 281, 459-464, 1964.

Shennum, R. H., Haury, P. T., A General Description of the Telstar Satellite, The Bell System Technical Journal, 42, 801-830, 1963.

Shennum, R. H., Reid, E. J., The Design and Construction of the Electronics Package, The Bell System Technical Journal, 42, 1749-1764, 1963.

Singer, S. F., Nuclear Explosions in Space, last of four articles, Missiles and Rockets, 26-30, 1959.

Smalley, V. G., Smart, D. F., Filz, R. C., Corpuscular Radiation Environment of a Low-Altitude Polar-Orbiting Earth Satellite: A Brief Summary, AFCRL-66-540, 1966.

Smith, K. D., Gummel, H. K., Bode, J. D., Cuttriss, D. B., Nielsen, R. J., Rosenzweig, W., The Solar Cells and Their Mounting, The Bell System Technical Journal, 42, 1765-1816, 1963.

Smith, R. V., Imhof, W. L., Bakke, J. C., Reagan, J. B., Rowland, J. H., Measurements of Artificially Injected Electrons from Satellite 1962 Beta Kappa, LMSC30-56-31, 1963.

Space Division, Satellite 1963 38C Launch and Performance in Orbit, 28 September-25 October 1963, Report TG 474, 2, October 1963.

Space Technology Laboratories, Inc., Reduction and Analysis of Explorer VI and Pioneer V Data, Vol. II, TRW 8626-6006-RU-000, November 1962.

Space Physics Laboratory, Space Physics Program: Secondary Payload Particle Radiation Experiments for Program 622A Satellites, Report TDR62 191, September 1962.

Space Physics Laboratory, ATS-1 Omnidirectional Spectrometer, Report TR-1001 (2260-20)-8, May 1967.

Stassinopoulos, E. G., Exposure of Atmosphere Explorer Satellites to Van Allen Belt Radiation, Missions C, D, and E, NASA-TM-X-65612, July 1971.

Stuhlinger, E., Mesmer, G., The Argus Experiment, Chapter 13 in Space Science and Engineering, 168-175, 202-203, McGraw-Hill Book Company, New York, 1965.

Teague, M. J., The Calibration Constants for the OGO 1 and 3 Electron Spectrometer, NSSDC 70-14, 1970.

Thomas, L., Taylor, R. E., Sporadic E Phenomena Associated with the High Altitude Nuclear Explosions Over Johnston Island, Advances in Upper Atmosphere Research, 45-55, The Macmillan Company, New York, 1963.

Temnyy, V. V., Investigations of the Upper Atmosphere Using the Artificial Earth Satellites Cosmos 3 and Cosmos 5, Space Research IV, Proceedings of the Fourth International Space Science Symposium, Warsaw, Poland, June 4-10, 1963, edited by P. Muller, 582-587, North-Holland Publishing Company, Amsterdam, (Interscience Publishers) John Wiley and Sons, Inc., New York, 1964.

Temnyy, V. V., Special Features of the Distribution of Electrons of About 100 keV Energy at Great Heights Above Sea Level, Cosmic Research, 2, 710-711, 1964, English Translation of Kosmicheskie Issledovaniya.

Temnyy, V. V., Atlas of the Intensity Distributions of Trapped Corpuscles Measured by the "Cosmos-3" and Cosmos-5" Satellites, Space Research V, Proceedings of the Fifth International Space Science Symposium, Florence, May 12-16, 1964, edited by D. G. King-Hele, P. Muller, G. Righini, 489-497, North-Holland Publishing Company, Amsterdam, (Interscience Publishers) John Wiley a Sons, Inc., New York, 1965.

Temnyy, V. V., Spatial Distribution of Different Groups of Trapped Corpuscles Based on Data fron the Satellites "Kosmos-3" and "Kosmos-5", Transactions of the All-Union Conference on Space Physics, 281-287, June 10-16, 1965, NASA TT F-389.

Varnerin, L. J., Comstock, R. L., Dean, W. A., Kordos, R. W., The Satellite Ferrimagnetic Power Limiter, The Bell System Technical Journal, 42, 1817-1828, 1963.

Vakulov, P. V., Gorchakov, Ye., V., Logachev, Yu. I., Radiation Belts of the Earth, FTD-MR-65-417, 1965.

Valerio, J., Protons from 40 to 110 MeV Observed on Injun 3, Journal of Geophysical Research, 69, 4949-4958, 1964.

Vampola, A. L., Recent Measurements of the Inner Zone Electron Life-Times, paper presented at COSPAR, 10th Plenary Meeting, London, England, July 24-29, 1967.

Van Allen, J. A., Spatial Distribution and Time Decay of the Intensities of Geomagnetically Trapped Electrons from the High-Altitude Nuclear Burst of July 1962, SUI-63-11, 1963.

Van Allen, J. A., Lifetimes of Geomagnetically Trapped Electrons of Several MeV Energy, Nature, 203, 1006-1007, 1964.

Van Allen, J. A., Some General Aspects of Geomagnetically Trapped Radiation, Radiation Trapped in the Earth's Magnetic Field, proceedings of the Advanced Study Institute held at the Chr. Michelsen Institute, Bergen, Norway, August 16-September 3, 1965, edited by B. M. McCormac, 65-75, D. Reidel Publishing Company, Dordrecht, Holland, Gordon and Breach Science Publishers, New York, 1966.

Van Allen, J. A., Spatial Distribution and Time Decay of the Intensities of Geomagnetically Trapped Electrons from the High Altitude Nuclear Burst of July 1962, Radiation Trapped in the Earth's Magnetic Field, proceedings of the Advanced Study Institute held at the Chr. Michelsen Institute, Bergen, Norway, August 16-September 3, 2965, edited by B. M. McCormac, 575-592, D. Reidel Publishing Company, Dordrecht, Holland, Gordon and Breach Science Publishers, New York, 1966.

Van Allen, J. A., Frank, L. A., O'Brien, B. J., Satellite Observations of the Artificial Radiation Belt of July 1962, Journal of Geophysical Research, 68, 619-627, 1963.

Van Allen, J. A., Lin, W. C., Fifteen-Month History of the Artificial Radiation Belt Due to the Starfish Nuclear Burst, paper presented at AGU, 45th Annual Meeting, Washington, D.C., April 21-24, 1964.

Van Allen, J. A., McIlwain, C. E., Ludwig, G. H., Radiation Observations with Satellite 1958 (epsilon), Journal of Geophysical Research, 64, 271-286, 1959.

Van Allen, J. A., McIlwain, C. E., Ludwig, G. H., Satellite Observations of Electrons Artificially Injected into the Geomagnetic Field, Journal of Geophysical Research, 64, 877-891, 1959.

Vaysberg, O. L., Shuyskaya, F. K., One Anomaly in Electron Pitch-Distribution, Transactions of the All-Union Conference on Space Physics, 273-276, June 10-16, NASA TT F-389.

Vernov, S. N., Chudakov, A. E., Investigations of Radiations on Man-Made Earth Satellite Cosmos-17, Report FTD-TT-65-263, April 1965.

Vernov, S. N., Nesterov, V. Ye., Pisarenko, N. F., Savenko, I. A., Tverskaya, L. V., Shavrin, P. I., Study of the earth's Outer Radiation Zone at Low Altitudes During Spacecraft-Satellite Flights and the "Kosmos" AES Flights Between 1960 and 1963, Transactions of the All-Union Conference on Space Physics, 588-606, June 10-16, 1965, NASA TT F-389.

Vernov, S. N., Nesterov, V. E., Savenko, I. A., Shavrin, P. I., Sharvina, K. N., Geographical Distribution of Radiation Intensity in the Region of the Brazilian Magnetic Anomaly at an Altitude of about 300 km, Cosmic Research, 2, 417-422, 1964.

Vernov, S. N., Savenko, I. A., Shavrin, P. I., Nesterov, V. E., Pisarenko, N. F., Shavrina, K. N., Investigation of the Earth's Radiation Belts in the Region of the Brazilian Anomaly at Altitudes of 200-400 km, Space Research V, Proceedings of the Fifth International Space Science Symposium, Florence, May 12-16, 1964, edited by D. G. King-Hele, P. Muller, G. Righini, 343-359, North-Holland Publishing Company, Amsterdam, (Interscience Publishers) John Wiley and Sons, Inc., New York, 1965.

Vernov, S. N., Savenko, I. A., Shavrin, P. I., Nesterov, V. E., Pisarenko, N. F., Tel'tsov, M. V., Pervaya, T. I., Erofeeva, V. N., Some Results of Radiation Measurements Carried Out during 1960-1963 at 200-400 km, Cosmic Research, 2, 119-126, 1964, English Translation of Kosmicheskie Issledovaniya.

Waddel, R. C., The Relay I Radiation Effects Experiment, NASA TN-D-3665, 1965.

Walt, M., Overall Analysis of Experiments on Artificial Radiation Belts, Radiation Trapped in the Earth's Magnetic Field, edited by B. M. McCormac, 666-670, D. Reidel Publishing Company, Dordrecht, Holland, Gordon and Breach Science Publishers, New York, 1966.

Walt, M., MacDonald, W. M., The Influence of the Earth's Atmosphere on Geomagnetically Trapped Particles, Reviews of Geophysics, 2, 543-577, 1964.

Warren, C. S., Gill, W. L., Radiation Dosimetry Aboard the Spacecraft of the Eighth Mercury-Atlas Mission, NASA TN D-1862, 1964.

Weber, A. H., Brisken, A. F., Coughlin, M. E., Fennell, J. F., George, J. A., Kottmeyer, W. K., Manson, D. J., Ockersz, J. R. Paikeday, J. M., Further Detailed Analysis of Telemetry Records Obtained by Explorer IV Satellite Concerning Geomagnetically Trapped Radiation, DASA 1889, 1966.

Weber, A. H., Brisken, A. F., Fennel, J. F., George, J. A., Hoverter, R. T., Manson, D. J., Paikeday, J. M., Unidirectional and Omnidirectional Flux Densities of Trapped Particles Injun I and Explorer 4 Satellites, DASA-2052, 1968.

Weber, A. H., Delaney, R. M., Fennell, J. F., George, J. A., Manson, D. J., Ockersz, J. R., Paikeday, J. M., Bock, J. K., Analysis of Argus/Explorer IV Records, DASA 1613, 1965.

Welch, J. A., Jr., Atmospheric and Magnetic Loss Mechanisms for Geomagnetically Trapped Particles, The Upper Atmosphere Above F2-Maximum, papers presented at the Symposium of the Ionospheric Research Committee Agard Avionics Panel, Paris, France (AGARDograph 42), edited by H. Poeverlein, 83-94, NATO-AGARD, Paris, (May 1959).

Welch, J. A., Jr., Kaufmann, R. L., Hess, W. N., Trapped Electron Time Histories for L=1.30, Journal of Geophysical Research, 68, 685-699, 1963.

Welch, J. A., Whitaker, W. A., Theory of Geomagnetically trapped electrons from an artificial source, Journal of Geophysical Research, 64, 909-922, 1959.

West, H. I., Jr., Some Observations of the Trapped Electrons Produced by the Russian High Altitude Nuclear Detonation of October 28, 1962, Radiation Trapped in the Earth's Magnetic Field, edited by B. M. McCormac, 634-662, D. Reidel Publishing Company, Dordrecht, Holland, Gordon and Breach Science Publishers, New York, 1966.

West, H. I., Jr., The Trapped Electron Spectra from the Starfish Detonation and from the Outer Belt in h Fall of 1962, Radiation Trapped in the Earth's Magnetic Field, edited by B. M. McCormac, 663-665, D. Reide' Publishing Company, Dordrecht, Holland, Gordon and Breach Science Publishers, New York, 1966.

West, H. I., Mann, L. G., Bloom, S. D., Spectra and Fluxes of Electrons Trapped in the Earth's Magnetic Field Following Recent High-Altitude Nuclear Bursts, paper presented at AGU, 44th Annual Meeting, Washington, D.C., April 17-20, 1963.

West, H. I., Jr., Mann, L. G., Bloom, S. D., Some Electron Spectra in the Radiation Belts in the Fall of 1962, Space Research V, Proceedings of the 5th International Space Science Symposium, Florence, May 12-16, 1964, edited by D. G. King-Hele, North-Holland Publishing Company, Amsterdam (Interscience Publishers), John Wiuley and Sons, Inc., New York, 423-445, 1965.

White, R. S., Freden, S. C., Mihalov, J. D., Mozer, F. S., Paulikas, G. A., The Artificial Radiation Belts at Low Altitudes, paper presented at AGU, 44th Annual Meeting, Washington, D.C., April 17-20, 1963.

Zinn, J., Hoerlin, H., Petschek, A. G., The Motion of Bomb Debris Following the Starfish Test, Radiation Trapped in the Earth's Magnetic Field, proceedings of the Advanced Study Institute held at the Chr. Michelsen Institute, Bergen, Norway, August 16-September 3, 1965, edited by B. M. McCormac, 671-692, D. Reidel Publishing Company, Dordrecht, Holland, Gordon and Breach Science Publishers, New York, 1966.

APPENDIX A

COMPUTER TAPE DOCUMENTATION

The data tapes were generated on the CDC 6000 series computer system under control of the NOS/BE operating system. The tapes are 9 track 1600 bpi tapes. Data are written to disk using formatted write statements. The tapes are then generated from the disk using the COPYBF utility routine. The tape format is the AFWL standard internal binary format.

The tapes are multifile tapes. The first file is a header file with narrative information. It may be read by using the following FORTRAN read statement.

```
      READ 10, (HEAD(I), I=1, 8)
   10 FORMAT (8 A10)
```

The succeeding files contain data; the number of files and the data type within the files are identified in the header record (Figure A-1 is a copy of a header file).

The data files are written using the following FORTRAN write statement:

```
  100 WRITE(10,100)KYR,IDAY,KHR,TIME,EL,B,XLONG,N,
      ((M(I),FLUX(I),ERROR(I),BKG(I),),I=1,N)
      FORMAT(2I3,I2,F5.2,F6.3,F5.3,F6.1,I2,3(I2,3E10.3),/,
      4(I2,3E10.3)
```

where

KDAY	LAST 2 DIGITS OF THE YEAR
IDAY	DAY OF YEAR JANUARY 1 IS DAY 1
KHR	HOUR OF DAY UNIVERSAL TIME
TIME	MINUTES OF HOUR
EL	MCILWAIN L PARAMETER
B	MAGNETIC FIELD IN GAUSS
XLONG	GEOGRAPHIC LONGITUDE

APPENDIX A

COMPUTER TAPE DOCUMENTATION

The data tapes were generated on the CDC 6000 series computer system under control of the NOS/BE operating system. The tapes are 9 track 1600 bpi tapes. Data are written to disk using formatted write statements. The tapes are then generated from the disk using the COPYBF utility routine. The tape format is the AFWL standard internal binary format.

The tapes are multifile tapes. The first file is a header file with narrative information. It may be read by using the following FORTRAN read statement.

```
     READ 10, (HEAD(I), I=1, 8)
  10 FORMAT (8 A10)
```

The succeeding files contain data; the number of files and the data type within the files are identified in the header record (Figure A-1 is a copy of a header file).

The data files are written using the following FORTRAN write statement:

```
100  WRITE(10,100)KYR,IDAY,KHR,TIME,EL,B,XLONG,N,
     ((M(I),FLUX(I),ERROR(I),BKG(I),),I=1,N)
     FORMAT(2I3,I2,F5.2,F6.3,F5.3,F6.1,I2,3(I2,3E10.3),/,
     4(I2,3E10.3)
```

where

KDAY	LAST 2 DIGITS OF THE YEAR
IDAY	DAY OF YEAR JANUARY 1 IS DAY 1
KHR	HOUR OF DAY UNIVERSAL TIME
TIME	MINUTES OF HOUR
EL	MCILWAIN L PARAMETER
B	MAGNETIC FIELD IN GAUSS
XLONG	GEOGRAPHIC LONGITUDE

```
DATA FOR ARGUS 2 USING THE JASON ROCKETS
  DATA IS FOR THE JASON FLIGHT 2019,2021,2024,2024,2027
  DATA FOR FLIGHT 2027 WAS USED TO DETERMINE THE BACKGROUND
     IT IS INCLUDED TO SHOW BACKGROUND ACCURACY

  ALL DATA FOR THIS EFFORT WAS GIVEN IN TIME SINCE LAUNCH
     AND LAUNCH WAS GIVEN IN TIME SINCE EVENT
     TIME OF EVENT WAS ASSUMED TO BE 03:20 UT, 30 AUGUST 1958
     ABSOLUTE REAL TIME WAS CALCULATED FROM THE THREE DESCRIBED
     TIMES.

  ALL DETECTOR ARE SHIELDED GM TUBES

DATA CHANNELS INCLUDE IN THIS ANALYSIS ARE
  CHANNEL 1    ELECTRONS GREATER THAN .21 MEV
     EFFICIENCY /GEOMETRY FACTOR USED TO GENERATE TAPE IS 2.62
  CHANNEL 3    ELECTRONS GREATER THAN 1.0 MEV
     EFFICIENCY /GEOMETRY FACTOR USED TO GENERATE TAPE IS .719
  CHANNEL 6    ELECTRONS GREATER THAN 4.3 MEV
     EFFICIENCY /GEOMETRY FACTOR USED TO GENERATE TAPE IS 6.09
  CHANNEL 7    ELECTRONS GREATER THAN .44 MEV
     EFFICIENCY /GEOMETRY FACTOR USED TO GENERATE TAPE IS .582
  CHANNEL 8    ELECTRONS GREATER THAN .44 MEV
     EFFICIENCY /GEOMETRY FACTOR USED TO GENERATE TAPE IS 286.

DATA IS WRITTEN ON A SINGLE FILE ACCORDING TO THE FORMAT DESCRIBED
  BELOW:

THE DATA WAS WRITTEN WITH THE FOLLOWING FORMATED WRITE STATEMENT
       WRITE(10,100)KYR,IDAY,KHR,TIME,EL,B,XLONG,N,
       ((M(I),FLUX(I),ERROR(I),BKG(I)),I=1,N)
 100   FORMAT(2I3,I2,F5.2,F6.3,F5.3,F6.1,I2,3(I2,3E10.3),/,
       4(I2,3E10.3))

WHERE**
  KDAY      LAST 2 DIGITS OF THE YEAR
  IDAY      DAY OF YEAR  JANUARY 1 IS DAY 1
  KHR       HOUR OF DAY UNIVERSAL TIME
  TIME      MINUTES OF HOUR
  EL        MCILLWAIN L PARAMETER
  B         MAGNETIC FIELD IN GAUSS
  XLONG     GEOGRAPHIC LONGITUDE
  N         NUMBER OF CHANNELS IN THIS DATA RECORD
  M         CHANNEL NUMBER  SEE DEFINITION ABOVE
  FLUX      BACKGROUND CORRECTED FLUX IN ELECTRONS/CM**2/SEC GREATER
            THAN THE REFERENCE ENERGY
  ERROR     UNCERTAINTY IN THE FLUX
  BKG       BACKGROUND WHICH WAS SUBTRACTED TO GIVE THE FLUX
```

Figure A-1. Copy of Argus Header File

N	NUMBER OF CHANNELS IN THIS DATA RECORD
M	CHANNEL NUMBER SEE DEFINITION ABOVE
FLUX	BACKGROUND CORRECTED FLUX IN ELECTRONS/CM**2/SEC GREATER THAN THE REFERENCE ENERGY
ERROR	UNCERTAINTY IN THE FLUX
BKG	BACKGROUND WHICH WAS SUBTRACTED TO GIVE THE FLUX

Flux values set identically to zero indicate that the data values are for some reason not available. The channel number identification is in all cases the same as that used in the literature.

The following is a listing of tapes available at the AFWL library.

ALOUETTE Russian

TAPE IH99 - This unlabeled tape has four files. A header file for Russian with the Starfish subtract followed by the data file. Then there is another header file for Russian II with the Russian I subtract followed by a data file.

TAPE HF92 - This is a labeled duplicate tape (L = ALOUETTE).

EXPLORER 15 Russian

TAPES GE90 and GE125 are unlabeled tapes with short and expanded data sets of the Russian II and III burst with Russian I subtracted.

TAPES HF93 and IC96 are labeled duplicates (L = EXPLORER 15).

TELSTAR Russian

TAPE GF25 is the unlabeled tape and

TAPE HK78 is the labeled tape (L = TELSTAR)

TELSTAR Starfish

TAPES GG50 and GG144 are the unlabeled tapes and

TAPES HL150 and IA125 are the labeled duplicates (L = TELSTAR).

JASON Argus

TAPE ID112 is an unlabeled tape.

Duplicate is at MDAC

EXPLORER 4 Teak and Orange

TAPE KD12 is an unlabeled tape.

Duplicate at MDAC

EXPLORER 4 Argus

TAPE GB63 is the unlabeled tape and

TAPE ID29 is the labeled duplicate.

INJUN

GK 72 is an unlabeled tape

Duplicate at MDAC

TRAAC

GK71 is an unlabeled tape

Duplicate at MDAC

STARAD

GK64 is an unlabeled tape

Duplicate at MDAC.

APPENDIX B

DRIFT VELOCITY CALCULATIONS

As a part of this effort a MDAC developed B and L program, LDINT, was modified to include the capability to calculate the drift velocity of particles in the earth's magnetic field. The magnetic field used is the Olson/Pfitzer model (Reference B-1). A brief summary of this effort is given below.

Development of the Drift Program

The instantaneous drift velocity at a given point is relatively simple to calculate. However, evaluating the rate of change of field lines, or the effective equatorial drift velocity is considerably more difficult. It requires the evaluation of two integrals having singularities. These singularities are integrable but do generate formidable programming problems. The equations required to calculate the drift velocity are given in the next few paragraphs.

The drift velocity in a static magnetic field in the absence of electric and gravitational field effects are due to gradient and curvature drift. The gradient and curvature drift may be written as

$$\bar{U}_g = \frac{CmV_1^2}{2e} \cdot \frac{\bar{B} \times \bar{\nabla} \bar{B}}{B^3} \tag{B-1}$$

$$\bar{U}_c = \frac{CmV_{11}^2}{e} \cdot \frac{\partial \bar{B}}{\partial s} \quad \frac{\bar{B} \times \hat{Y}}{B^3} \tag{B-2}$$

B-1. Olson, W. P., K. A. Pfitzer and G. J. Mroz, Modeling the Magnetospheric Magnetic Field in Quantitative Modeling of Magnetospheric Processes, Geophysical Monograph 21, AGU publisher, W. P. Olson, editor, 1979.

Where $\bar{U}_g$ is the gradient drift

$\bar{U}_c$ is the curvature drift velocity

C is the velocity of light

e is the charge of the particle

B is the magnetic field

$V_\perp$ is the velocity perpendicular to the magnetic field

V_{11} is the velocity parallel to the magnetic field

$\hat{Y}$ is the unit vector along the principal normal to the magnetic field

$\frac{\partial B}{\partial s}$ is the change in B along the field direction

m is the relativistic mass.

Additional equations useful in the solution of the problem are

$$m = m_0 \gamma$$

where m_0 is the rest mass

γ is the relativistic factor

since

$$\gamma = \frac{1}{\sqrt{1 - V^2/c^2}} \tag{B-3}$$

$$\frac{V^2}{c^2} = 1 - \frac{1}{\gamma^2} \tag{B-4}$$

$$V_\perp^2 = V_0^2 \cdot \frac{B}{B_m} \tag{B-5}$$

$$V_{11}^2 = V_0^2 \left(1 - \frac{B}{B_m}\right) \tag{B-6}$$

where B_m is the magnetic field at the mirror point and V_0 is the magnitude of the velocity.

The total instantaneous drift velocity at a given point along the field line is given by

$$\overline{U} = \overline{U}_g + \overline{U}_c \tag{B-7}$$

If one is interested in the drift velocity of charged particles one generally needs to know the average drift velocity. That is the rate at which particles move around the earth. Since the geographic coordinate system is not aligned with the magnetic field we must determine the drift motion in the minimum B plane.

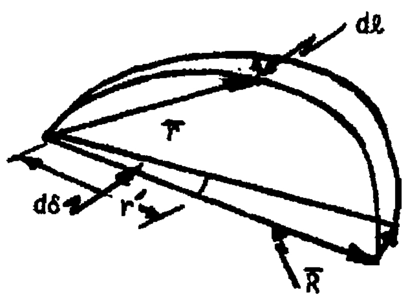

$\overline{r}$ vector to instantaneous drift point
$\overline{R}$ vector to minimum B
$\hat{R}$ unit vector to minimum B
$dl = |U|\ dt$
$r' = \overline{r}\,.\hat{R}$
$dl = r'\ \delta = \overline{r}.\hat{R}d\delta$

Then in a time dt a particle moves a distance Udt perpendicular to the field line plane. The angular motion, dδ, is given by

$$d\delta = \frac{dl}{r'} \qquad \text{where } dl = Udt \tag{B-8}$$

$$d\delta = \frac{|U|\,dt}{\overline{r}.\hat{R}} \tag{B-9}$$

As the particle moves from mirror point to mirror point the total angular displacement, θ, is given by

$$\theta = \int_{t=0}^{t=t_B} \frac{U dt}{\overline{r}.\hat{R}} \quad t_B \text{ is the bounce time} \tag{B-10}$$

The average angular velocity is

$$\omega = \frac{\theta}{t_B} \tag{B-11}$$

$$\langle U \rangle = \omega |R| \tag{B-12}$$

The integration of a particle's motion is parameterized in terms of the distance, s, along the field line such that

$$ds = V_{11} \, dt \tag{B-13}$$

Thus

$$t_B = \int \frac{ds}{V_{11}} \tag{B-14}$$

$$\theta = \int \frac{U ds}{V_{11} \overline{r}.\hat{R}} \tag{B-15}$$

since $V_{11} = V_o \sqrt{1 - \frac{B}{B_m}}$

The average drift velocity, U, can be written as

$$\langle U \rangle = \frac{\displaystyle\int_{B_M}^{B_M} \frac{\overline{U} \cdot |R| \, ds}{\overline{r} \cdot \hat{R} \sqrt{1 - B/B_M}}}{\displaystyle\int_{B_M}^{B_M} \frac{ds}{\sqrt{1 - B/B_M}}} \tag{B-16}$$

Substituting the various functions into the above equation gives

$$\langle U \rangle = \frac{\displaystyle\int \frac{\left[\frac{CmV_{\perp}^2}{2e} \cdot \frac{\overline{B} \times \overline{\nabla} B}{B^3} + \frac{CmV_{11}^2}{e} \left|\frac{\partial B}{\partial s}\right| \frac{\overline{B} \times \hat{Y}}{B^3}\right] |R|}{(\overline{r} \cdot \hat{R}) \sqrt{1 - B/B_M}} \, ds}{\displaystyle\int ds \, / \sqrt{1 - B/B_M}} \tag{B-17}$$

$$\langle U \rangle = \frac{\displaystyle\frac{C^3 m_o}{e} \left(\gamma - \frac{1}{\gamma}\right) \int \frac{|R|^2}{(\overline{r} \cdot \overline{R}) \cdot B} \left[\frac{|\overline{\nabla} R|}{2B_M \sqrt{1 - B/B_M}} + \frac{\sqrt{1 - \frac{B}{B_M}}}{B} \left|\frac{\partial \hat{B}}{\partial s}\right|\right] ds}{\displaystyle\int \frac{ds}{\sqrt{1 - B/B_M}}} \tag{B-18}$$

The current field line integral which is used to determine the second invariant is of the form

$$\int \frac{ds}{\sqrt{1 - B/B_m}} \tag{B-19}$$

Since B_m, the mirror point field is not known until B_{min} is determined, the initial integration along the field lines saves the values of B and the step size ds. Thus in order to evaluate the drift velocity, the values $|\nabla B|$ and $|\partial B/\partial s|$ must also be saved along the integration trajectory. The vector R to minimum B must also be saved. These modifications increased the program array size by 2000 words.

Computer speed decreased by a factor of 3 because of the need for calculating gradients.

A second problem is that the two integrals have a singularity near the end points. This is an integrable singularity, and proper step size control near the end points is required to produce accurate results.

Drift Program Test

The drift program has been found to be a very useful tool. The integral appears to be stable over all the values that we have been able to test. The results, when using only the dipole field, are consistent with Hess (Hess, 1968). There are, however, a number of surprising results. Hess indicates that the drift period increases 50 percent for off-equatorial particles (a decrease in drift velocity). Figures B-1 and B-2 indicate that this is true for very large B/B_o. However, for particles having equatorial pitch angles between 30^o and 90^o, the drift velocity change in a dipole field is less than 10 percent.

The drift velocity is also very model dependent. Even at L=3, the difference in drift velocity between the main field and the main plus external fields is 12 percent. Furthermore, once the external field is included, the B/B_o

dependence becomes much stronger. At L=7, near local midnight (see Figure 3), the change in drift velocity due to the external field is over 30 percent. Figure 3-3 shows the dependence of the drift velocity for the main field and the main field plus dipole fields. This plot is for a longitude of 0^0 and a universal time of 0 hours, and shows the effect on the drift velocity as one approaches the near tail region.

We believe that this drift program will be of general usefulness to the scientific community.

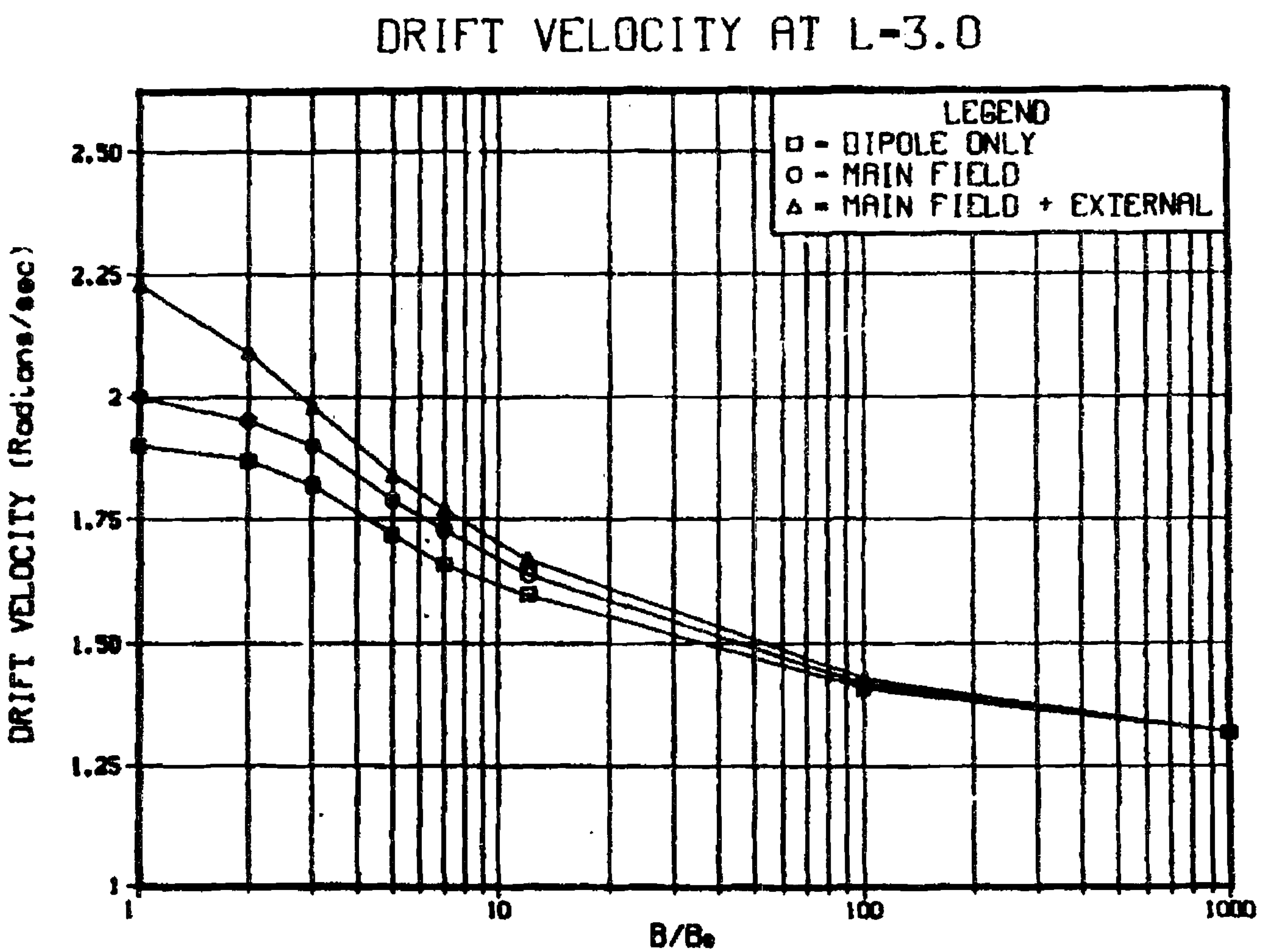

Figure B-1. Drift Velocity at L = 3

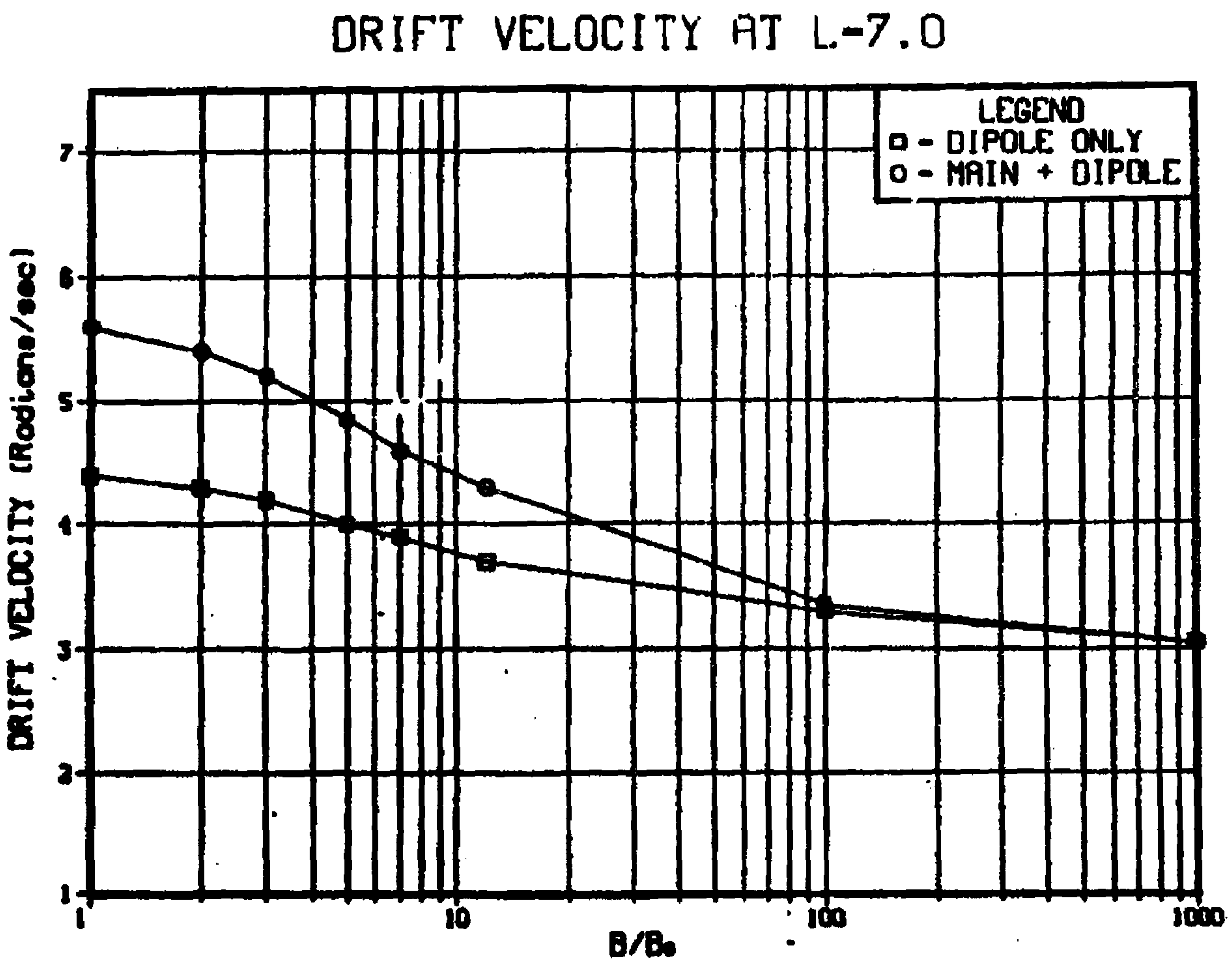

Figure B-2. Drift Velocity at L = 7

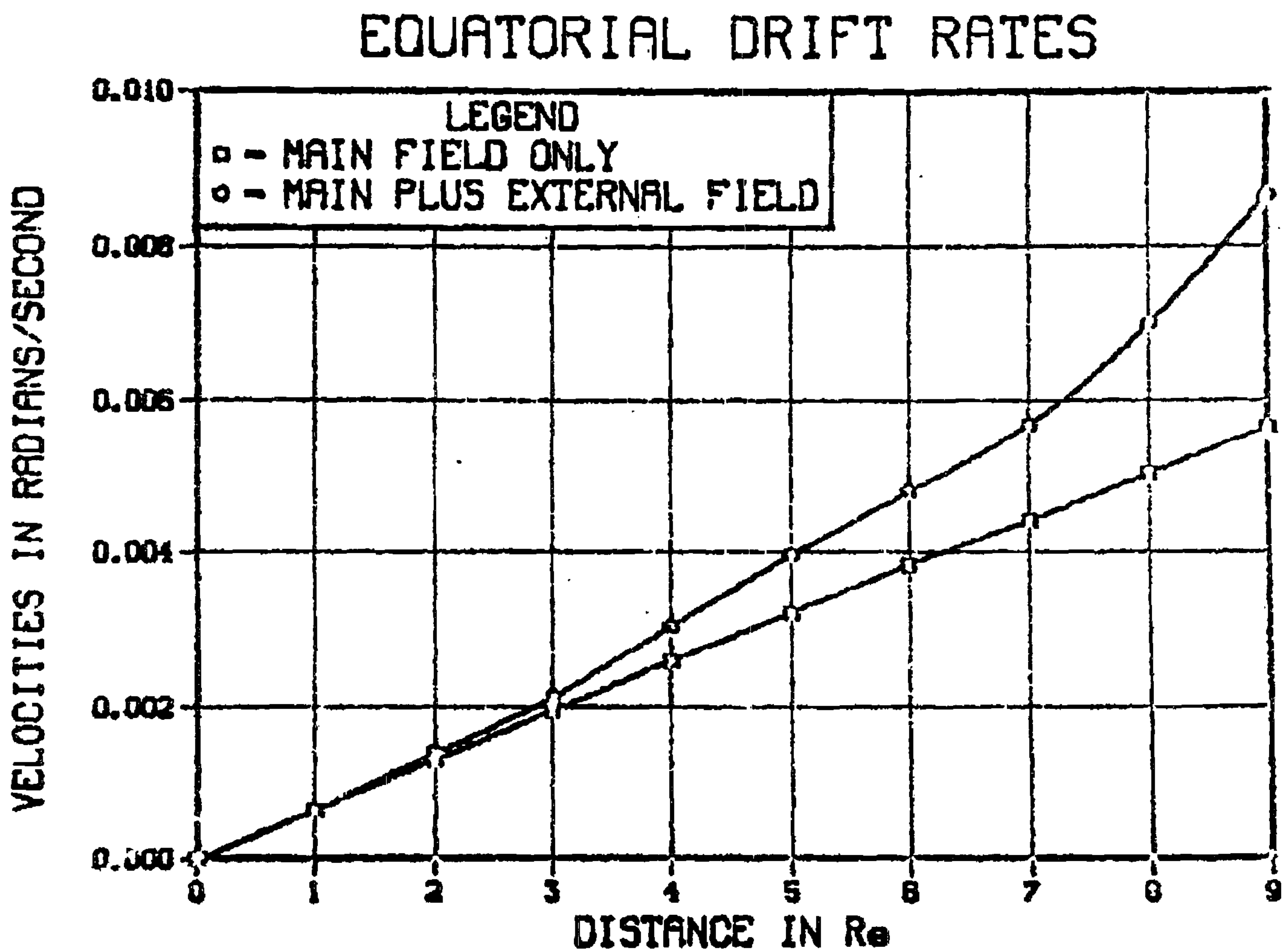

Figure B-3. Equatorial Drift Rates as a Function of L

APPENDIX C

CONVERSION SUBROUTINE FOR STARAD VOLTAGES TO COUNT RATES

```
      SUBROUTINE WLCRM(M1)
C**********THIS PROGRAM CHANGES LCRM VOLTAGES INTO COUNTING RATES
      DIMENSION WEST(6)
      COMMON /CONV/ TEMP(12),OUT(20)
      EQUIVALENCE (WEST(1),OUT(14))
      X = TEMP(2)
      Y = TEMP(1)
      IF(X.GT. 1.25) GO TO 4
      WEST(1) = 4.0*EXP(Y*.52899)
      GO TO 10
    4 IF(X.GT. 2.5) GO TO 6
      WEST(1) = 37.0*EXP(Y*.64992)
      GO TO 10
    6 IF(X.GT. 3.75) GO TO 8
      WEST(1) = 650.*EXP(Y*.63746)
      GO TO 10
    8 WEST(1) = 5000.*EXP(Y*.70941)
   10 CONTINUE
      X = TEMP(4)
      Y = TEMP(3)
      IF(X.GT. 1.25) GO TO 14
      WEST(2) = 4.0*EXP(Y*.55274)
      GO TO 20
   14 IF(X.GT. 2.5) GO TO 16
      WEST(2) = 39.0*EXP(Y*.65708)
      GO TO 20
   16 IF(X.GT. 3.75) GO TO 18
      WEST(2) = 520.0*EXP(Y*.69634)
      GO TO 20
   18 WEST(2) = 4300.0*EXP(Y*.70830)
   20 CONTINUE
      X = TEMP(6)
      Y = TEMP(5)
      IF(X.GT. 1.25) GO TO 24
      WEST(3) = 4.4*EXP(Y*.56825)
      GO TO 30
   24 IF(X.GT. 2.5) GO TO 26
      WEST(3) = 37.*EXP(Y*.63685)
      GO TO 30
   26 IF(X.GT. 3.75) GO TO 28
      WEST(3) = 480.*EXP(Y*.68966)
      GO TO 30
   28 WEST(3) = 5900.*EXP(Y*.62088)
   30 CONTINUE
      X = TEMP(8)
```

```
      Y = TEMP(7)
      IF(X.GT. 1.25) GO TO 34
      WEST(4) = 3.7*EXP(Y*.56247)
      GO TO 40
 34   IF(X.GT. 2.5) GO TO 36
      WEST(4) = 37.*EXP(Y*.57873)
      GO TO 40
 36   IF(X.GT. 3.75) GO TO 38
      WEST(4) = 520.*EXP(Y*.66298)
      GO TO 40
38    WEST(4) = 6100.*EXP(Y*.62087)
40    CONTINUE
      X = TEMP(10)
      Y = TEMP(9)
      IF(X.GT. 1.25) GO TO 44
      WEST(5) = 4.0*EXP(Y*.55274)
      GO TO 50
 44   IF(X.GT. 2.5) GO TO 46
      WEST(5) = 40.*EXP(Y*.63651)
      GO TO 50
 46   IF(X.GT. 3.75) GO TO 48
      WEST(5) = 530.*EXP(Y*.67372)
      GO TO 50
48    WEST(5) = 6000.*EXP(Y*.64864)
50    CONTINUE
      X = TEMP(12)
      Y = TEMP(11)
      IF(X.GT. 1.25) GO TO 54
      WEST(6) = 4.3*EXP(Y*.57315)
      GO TO 60
 54   IF(X.GT. 2.5) GO TO 56
      WEST(6) = 43.*EXP(Y*.64753)
      GO TO 60
 56   IF(X.GT. 3.75) GO TO 58
      WEST(6) = 500.*EXP(Y*.70138)
      GO TO 60
58    WEST(6) = 4300.*EXP(Y*.69891)
60    CONTINUE
100   CONTINUE
      RETURN
      END
```

DISTRIBUTION

DTIC/DDA, Alexandria
DNA, Wash
  (RAAE)
  (RAEV)
AFIT
AFSC/DLWM
AF Test Pilot School
Sandia Nat'l Lab, Albuquerque
NASA/GSFC /Code 601, Greenbelt
Aerospace Corp, Los Angeles
Computer Sciences Corp, Albuquerque
JAYCOR, San Diego
Kaman TEMPO/DASIAC, Santa Barbara
Lockheed Palo Alto Rsch Lab, Palo Alto
Lockheed Missile & Space Co, Palo Alto
McDonnell Douglas Astro Co, Huntington Beach
AFELM/Rand Corp, Santa Monica
AFWL
  (HO)
  (SUL)
  (NTYC)
  (NTN)
  (NTYCE)
Official Record Copy (AFWL/NTY/Capt Greaves)